12 b.s.

(9) TECHNICAL REPORT

(6) # CENSE EXPLOSION TEST PROGRAM.

Report 2.

CENSE 2, EXPLOSIONS IN SOIL.

by

(10) James K. Ingram

(14) WES-TR-N-77-6

Weapons Effects Laboratory
U. S. Army Engineer Waterways Experiment Station
P. O. Box 631, Vicksburg, Miss. 39180

(12) 60 P.

(11) Dec[illegible]77

Report 2 of a Series

Approved For Public Release; Distribution Unlimited

Prepared for Office, Chief of Engineers, U. S. Army
Washington, D. C. 20314

Under R&D Project (16) 4A762719AT40 Task (17) A
Work Unit 018, Ground Shock from Multiple Bursts

038 100 JOB

Destroy this report when no longer needed. Do not return it to the originator.

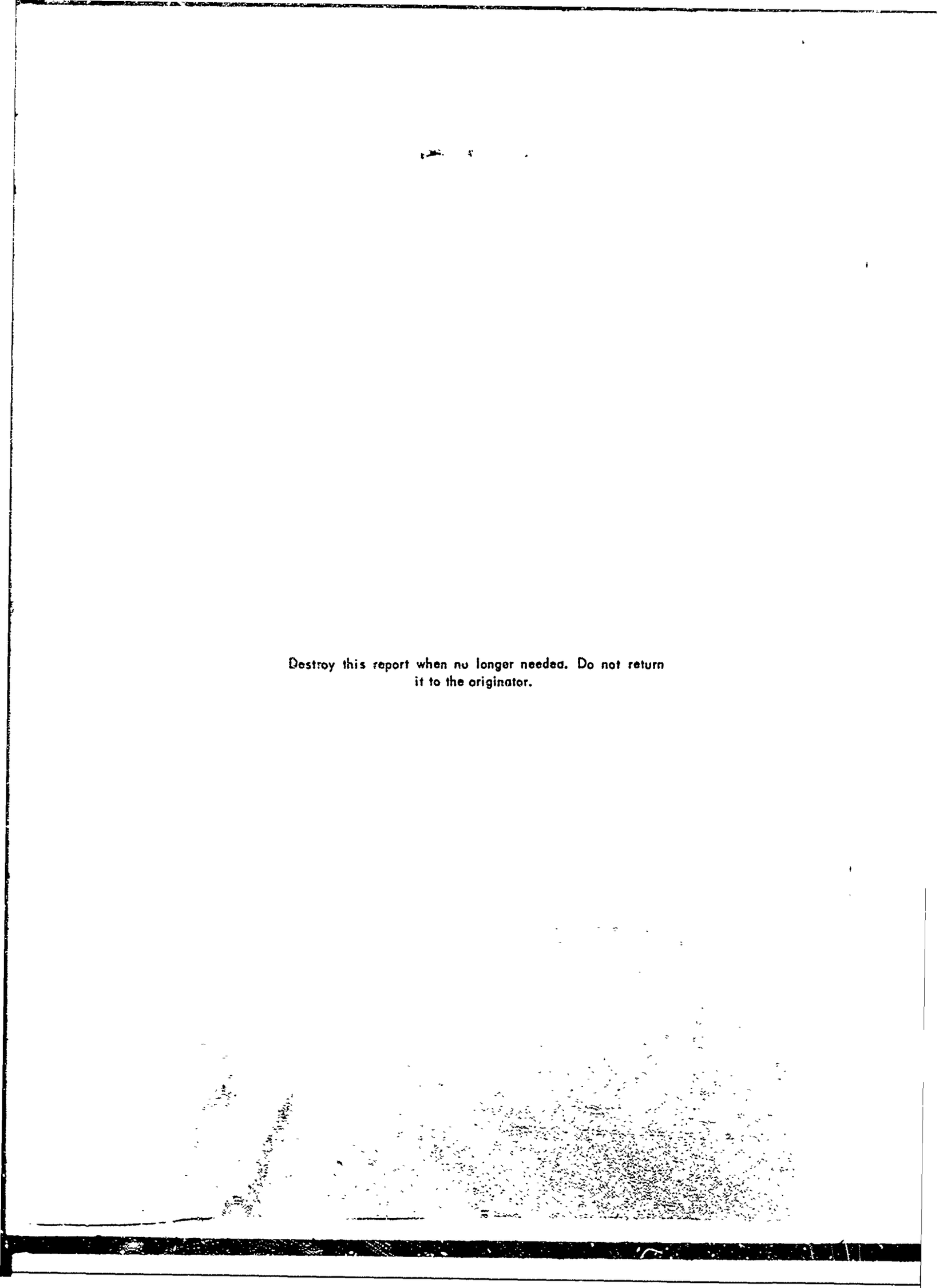

Unclassified

SECURITY CLASSIFICATION OF THIS PAGE (When Data Entered)

REPORT DOCUMENTATION PAGE

READ INSTRUCTIONS BEFORE COMPLETING FORM

1. REPORT NUMBER: Technical Report N-77-6	2. GOVT ACCESSION NO.
3. RECIPIENT'S CATALOG NUMBER	
4. TITLE (and Subtitle): CENSE EXPLOSION TEST PROGRAM; Report 2, CENSE 2, EXPLOSIONS IN SOIL	5. TYPE OF REPORT & PERIOD COVERED: Report 2 of a series
	6. PERFORMING ORG. REPORT NUMBER
7. AUTHOR(s): James K. Ingram	8. CONTRACT OR GRANT NUMBER(s): See Block 18
9. PERFORMING ORGANIZATION NAME AND ADDRESS: U. S. Army Engineer Waterways Experiment Station, Weapons Effects Laboratory, P. O. Box 631, Vicksburg, Miss. 39180	10. PROGRAM ELEMENT, PROJECT, TASK AREA & WORK UNIT NUMBERS
11. CONTROLLING OFFICE NAME AND ADDRESS: Office, Chief of Engineers, U. S. Army, Washington, D. C. 20314	12. REPORT DATE: December 1977
	13. NUMBER OF PAGES: 253
14. MONITORING AGENCY NAME & ADDRESS (if different from Controlling Office)	15. SECURITY CLASS. (of this report): Unclassified
	15a. DECLASSIFICATION/DOWNGRADING SCHEDULE

16. DISTRIBUTION STATEMENT (of this Report)

Approved for public release; distribution unlimited.

17. DISTRIBUTION STATEMENT (of the abstract entered in Block 20, if different from Report)

18. SUPPLEMENTARY NOTES

This research was sponsored by the Office, Chief of Engineers under R&D Project 4A762719AT40, Task A1, Work Unit 018, "Ground Shock From Multiple Bursts"

19. KEY WORDS (Continue on reverse side if necessary and identify by block number)

Airblast-induced ground motion	Explosion effects
Airblast waves	Explosions
Bursting charges	Explosives
CENSE (Test program)	Ground shock
Cratering	Stresses

20. ABSTRACT (Continue on reverse side if necessary and identify by block number)

The objective of CENSE 2 was to study the effects of burst position on ground shock, stress, airblast, and cratering in soil (clayey silt). Nine tests were conducted using 500-pound spherical cast TNT explosive charges. Burst positions ranged from an elevated (airburst, noncratering) charge position of -10.8 feet ~~(1.6 W^1/3)~~ to burial at a depth of +10.8 feet ~~(1.6 W^1/3)~~. Apparent craters were measured on all tests. Surface airblast was measured on Events 1 through 6, but not on the buried events (Events 7 through 9).

(Continued)

DD FORM 1 JAN 73 1473 EDITION OF 1 NOV 65 IS OBSOLETE

Unclassified

SECURITY CLASSIFICATION OF THIS PAGE (When Data Entered)

20. ABSTRACT (Continued).

Near-surface (1.5-foot depth) vertical and horizontal ground motions were measured on Events 1 through 6. Stresses and ground motions were measured directly beneath the explosion on Events 1 through 6. No near-surface motions, stresses, or airblasts were measured on Events 7 through 9. Instead, radial of stress and ground motion measurements were made at burst depth on these buried events.

Data are presented in the form of time histories and amplitude-distance plots.

Previously unpublished results from a smaller scale (2 pounds TNT) pilot study (Pre-CENSE), conducted in 1965 in a highly uniform loess deposit, provided supplementary data from a much smaller energy source and are included in Appendixes A and B of this report.

Additional analysis and data comparisons will be provided in Report 4, "Analysis and Summary of CENSE Data."

THE CONTENTS OF THIS REPORT ARE NOT TO BE USED FOR ADVERTISING, PUBLICATION, OR PROMOTIONAL PURPOSES. CITATION OF TRADE NAMES DOES NOT CONSTITUTE AN OFFICIAL ENDORSEMENT OR APPROVAL OF THE USE OF SUCH COMMERCIAL PRODUCTS.

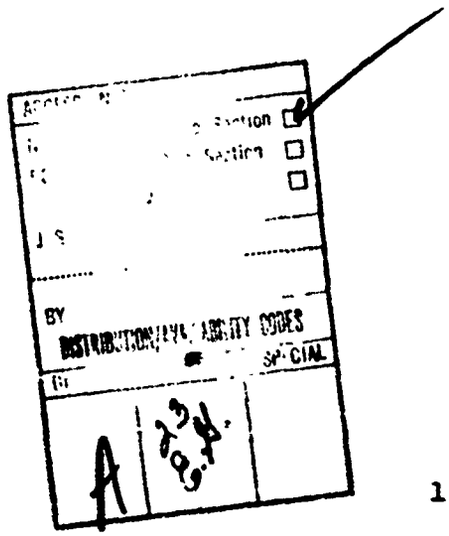

PREFACE

This report is the second of a series of four reports on the Coupling Efficiency of Near-Surface Explosions (CENSE). Reports 1 through 3 are data reports describing tests in sandstone, soil, and a layered soil/sandstone geology, respectively. Report 4 (in preparation) will analyze and summarize the entire test series.

The CENSE series was sponsored by the Office, Chief of Engineers (OCE), under R&D Project 4A762719AT40, Task A1, Work Unit 018, Ground Shock From Multiple Bursts, and conducted by the Weapons Effects Laboratory (WEL), U. S. Army Engineer Waterways Experiment Station (WES). Mr. D. S. Reynolds served as technical monitor for OCE.

The height/depth-of-burst test program was initiated in 1973. The initial phase, CENSE 1, explored the influence of a relatively uniform sandstone formation near the Mixed Company test site, Glade Park, Colorado.

Fieldwork for CENSE 2 was conducted in the fall of 1974 in clayey silt at Camp Shelby, Mississippi National Guard Military Reservation; tests were under the direction of Mr. J. K. Ingram, Project Scientist, Phenomenology and Effects Division (PED), WEL. The site was prepared and instruments were installed by PED personnel: Mr. S. E. Bartlett, Supervisory Technician; and Messrs. T. P. Williams, W. Washington, and J. W. Carson.

Messrs. L. T. Watson and S. Bell of WES Instrumentation Services Division (ISD) provided field instrumentation support, and Messrs. E. P. Leake and E. L. Sadler (ISD) provided instrument calibration.

Field Data computer processing was coordinated by Mr. J. T. Brogan and Mrs. D. W. McAlpin, PED.

The study was under the general supervision of Mr. J. L. Drake, Program Manager, PED; Mr. L. F. Ingram, Chief, PED; and Mr. W. J. Flathau, Chief, WEL.

During these tests, COL G. H. Hilt, CE, and COL J. L. Cannon, CE, were Commanders and Directors of WES. Mr. F. R. Brown was Technical Director.

CONTENTS

TABLES

FIGURES

FIGURES

FIGURES

FIGURES

CONVERSION FACTORS, U. S. CUSTOMARY TO METRIC (SI) UNITS OF MEASUREMENT

U. S. customary units of measurement used in this report can be converted to metric (SI) units as follows:

Multiply	By	To Obtain
inches	2.54	centimetres
feet	0.3048	metres
miles (U. S. statute)	1.609344	kilometres
pounds (mass)	0.4535924	kilograms
pounds (mass) per cubic foot	16.01846	kilograms per cubic metre
pounds per square inch	6894.757	pascals
feet per second	0.3048	metres per second
degrees (angle)	0.01745329	radians

CENSE EXPLOSION TEST PROGRAM

CENSE 2, EXPLOSIONS IN SOIL

CHAPTER 1

INTRODUCTION

1.1 BACKGROUND

Ground shock, stress, cratering, and surface airblast are highly sensitive to burst position for near-surface explosions. Previous high-explosive (HE)[1] tests have indicated large increases in ground shock magnitudes and crater sizes when the height of burst (HOB) or depth of burst (DOB) is varied from slightly elevated to buried configurations. Since Project Mole (Reference 1), (the Mole tests were not adequately instrumented in the regions of interest), no systematic test program has been directed toward documentation of HOB effects. More than a score of large-scale tests have been conducted in recent years, however, wide variations in geology, yield, and burst configuration preclude a quantitative definition of HOB effects. Ground motion measurements on-axis below the explosion were virtually nonexistent. Limited data are available for the Flat Top Series (Reference 2), one point from Middle Gust Event 4 (References 3 and 4), and a few locations from a low-yield nuclear explosion in a granite cavity. Ground shock predictions by large computers are not reliable for near-surface explosions. A more reliable calculational capability exists for airbust configurations in the superseismic regime. Predictions for motions below the explosion normally are determined by assuming an effective reduced energy for contained bursts. Efficiency factors derived from scaled, contained burst data can generally be regarded as an educated guess.

In 1965, a DOB feasibility study (Appendix A) was conducted in a

[1] For convenience, symbols and unusual abbreviations used in this report are listed and defined in the Notation (Appendix C).

uniform loess deposit using 2-pound[1] spherical TNT charges. This study was designated Pre-CENSE (Coupling Efficiency of Near-Surface Explosions) and provided the basis for the CENSE program. CENSE 1 (References 5 and 6) was a systematic empirical study of the HOB/DOB effects on energy coupling and ground motion in a sandstone geology. Spherical 1000-pound liquid nitromethane (NM) charges were used.

CENSE 2 was a complementary experimental study in a uniform clayey-silt geology that employed 300-pound spherical TNT charges. Burst positions for CENSE 2 were selected to cover a broad range of energy loading conditions and ranged from noncratering airbursts to deeply buried, where most of the available explosive energy is directly coupled to the ground. For both CENSE 1 and 2, emphasis was placed on charge positions between contact burst (surface tangent) and partially buried (buried tangent), where the postulated maximum rate of change in energy transfer was expected to occur. Two regions of interest were singled out as most descriptive of energy partitioning. The region directly beneath the explosion, a zone for which empirical data are almost totally lacking, and the region of the near-surface (defined as typically 1.5 to 2 feet deep, extending generally from about the 1000-psi surface overpressure region to the 5- to 10-psi region) from which considerable experimental data are available from numerous past experiments and that conveniently allow for direct comparison. (It must be pointed out that although voluminous data are available from near-surface detonations, most of the detonations were either surface tangent or half buried.) The Pre-CENSE feasibility study (Appendix A), being primarily a conceptual experiment, provided for measurements directly beneath the explosion only.

1.2 OBJECTIVE

The overall objective of the CENSE program was to study the influence of burst position on ground shock, cratering, and airblast in

---

[1] A table of factors for converting U. S. customary units of measurement to metric (SI) units is presented on page 9.

different geologic media. The specific objective of CENSE 2 was to study these effects, including stress propagation, in a relatively uniform deposit of sandy clay. Primary emphasis was placed on measurements of ground shock and stress directly beneath the explosion.

1.3 SCOPE

This report is the second in a series of four reports detailing the results of the CENSE experimental program and presents a summary of the CENSE 2 data along with pertinent observations. A summary of the Pre-CENSE data is presented in Appendix A of this report. Detailed analyses and conclusions will be presented in Report 4 of the series, "Analysis and Summary of CENSE Data."

CHAPTER 2

APPROACH

2.1 DESCRIPTION OF TEST SITE

The CENSE 2 test series was conducted in the DeSoto National Forest (part of the Camp Shelby, Mississippi National Guard Military Reservation) about 6 miles southeast of McLaurin, Mississippi. The site geology consists of a relatively uniform fluviatile deposit of red clayey-silt extending from the surface to a depth of approximately 24 feet. A shift in coloration from red to whitish-purple was observed at this depth and continued to maximum sample depth of 29 feet, Figure 2.1. A stable water table was present at an average depth of 29 feet.

2.2 EXPERIMENTAL PLAN

Three hundred-pound cast spherical TNT charges were detonated at nine burst positions relative to the surface of the soil (Table 2.1, Figure 2.2). Events 1 through 3 were noncratering airbursts; Event 4 was a surface tangent; Event 5 was half buried (half in, half out); Event 6 was buried tangent; and Events 7 through 9 were buried at depths of 3.6, 7.2, and 10.8 feet, respectively. (All burst positions refer to charge center of gravity (CG) relative to the surface of the soil.) Each charge was detonated at its geometric center with a single Reynolds RP-1M exploding bridge wire detonator.

2.3 INSTRUMENTATION LAYOUT

CENSE 2 included stress and acceleration measurements at locations directly beneath the burst point, ground zero (GZ), as well as two component (vertical and horizontal) particle velocity measurements along a single horizontal radial near the ground surface (Figure 2.3(a) and (b)). Surface airblast was measured along this same horizontal radial. Additionally, stresses were measured along a horizontal radial positioned at shot depth for the two deepest detonations, 7.2 and 10.8 feet DOB. No ground motion measurements were made directly beneath the explosion for Events 7, 8, and 9. Instead, the near-surface horizontal sensing

instruments were repositioned at shot depth. No surface airblast or near-surface motion measurements were made on these three shots. Some stress measurements were, however, made beneath the explosions for all events.

Shot points for the experiment were positioned along a 180-deg arc with a 36-deg angle separation between GZ's for the different events (Figure 2.4). This arrangement allowed use of a single cable layout for all events in the testing program. All airbursts (Events 1 through 3) and the surface tangent detonation (Event 4) were conducted over the same GZ, using the same emplaced instruments. All subsequent shots used new GZ's and newly installed instruments.

Ground motion instrument locations are listed in Tables 2.2 and 2.3 and stress gage locations are listed in Tables 2.4 and 2.5. Six constant positions were selected for the near-surface instrument array at horizontal ranges of 13.4, 25, 32, 43, 57, and 67 feet from GZ. These ranges were predicated by the expected maximum ground surface overpressures corresponding to 450, 150, 70, 30, 15, and 10 psi. Surface airblast pressure gages were placed at the same horizontal distances as the motion gages (except for Events 7, 8, and 9, on which no airblast measurements were made), but were offset 3 feet to minimize interference with the ground motion measurements.

No near-surface motion measurements were made on Events 7 through 9. Instead, a horizontal instrument array was placed at charge depth for these detonations.

2.4 TRANSDUCERS

Basic transducers used in this study were of the same type as were used in CENSE 1 (Reference 6) (i.e., standard "off-the-shelf" instruments: Endevco Series 2200 piezoresistive accelerometers; Bytrex AB-200 diaphragm-type airblast gages; and the latest commercially available modification of the Sandia DX velocity gage). Kulite series LQ-080U stress gages (Reference 7), a commercially available version of the SE stress gage developed by the U. S. Army Engineer Waterways Experiment Station (WES) were used.

Several developmental gages were used in addition to the "standard" instruments. A WES-developed passive (Brinell-type) stress gage (Reference 8) was used to measure peak dynamic stresses in the kilobar region near the charge on Events 5, 8, and 9. Ytterbium piezoresistive high-stress gages (Reference 9) and inductive high-range velocity gages (Reference 10), both fielded by Stanford Research Institute (SRI) personnel, were also used on Events 5, 8, and 9 close to the charge (Reference 11).

2.5 GAGE INSTALLATION

Motion instruments were mounted inside protective canisters (Reference 12). Canisters located directly beneath the charges were emplaced as they were for CENSE 1 (Reference 6). Stress gages were prepackaged in plugs of property matching grout before being positioned. Near-surface gages and gages placed along the horizontal radial at shot depth (for Events 7, 8, and 9) were installed in individual augered vertical holes. All motion and stress instruments were grouted in place with property-matching grout, and the boreholes were completely filled with the same grout. Surface airblast gages were flush mounted in the center of 2-by 2- by 1-foot-deep cement pads.

2.6 GROUT

An attempt was made to approximate the native site material with a chemical grout for gage emplacement. A grout mix, E-2D, designed to match a similar site material (Fort Polk, Louisiana) was modified (Designated Mix, E-2D(m)) for use in the CENSE 2 experiments. The grout formula is listed in Table 2.6.

2.7 DATA RECORDING AND REDUCTION SYSTEMS

Signal conditioning systems were standard, i.e., WES-built 3-kHz carrier amplifier-demodulators (Reference 13) were used for the velocity gages and dc-amplifiers were used for the accelerometers and stress and airblast gages. A wide band Sangamo Sabre IV 32-track FM magnetic-tape recorder was used to store the analog data signals. The recording system was activated by a timing control countdown unit via hard-wire link.

Analog-to-digital data conversion was performed with the WES automatic data processing system. All integrations, filtering, baseline shifting, and other processings were performed on the WES GE 635 series computer using various optional software routines developed at WES (References 14 and 15). Final computer output was in the form of analog plots of motions, stress, and pressure versus time. Most of the data presented in this report were baseline-shifted and filtered.

TABLE 2.1 TEST EVENT DESIGNATION.

Event No.	HOB/DOB (-)/(+)[a] Elevation (ft)	$(W^{1/3})$	(R_c)
1	-10.8	-1.61	-12
2	-7.2	-1.07	-8
3	-3.6	-0.54	-4
4	-0.9	-0.13	-1
5	0	0	0
6	+0.9	+0.13	+1
7	+3.6	+0.54	+4
8	+7.2	+1.07	+8
9	+10.8	+1.61	+12

[a] (-) = HOB above soil surface.
(+) = DOB below soil surface.

TABLE 2.2 LOCATION OF GROUND MOTION VERTICAL INSTRUMENTS DIRECTLY BENEATH EXPLOSION.

Events 1-4 Depth from Ground surface (ft)	Event 5 Depth from Charge CG (ft)	Event 6 Depth from Charge CG (ft)	Measurement
6.7	6.4	7.6	AV
10.0	10.9	11.8	AV
13.4	14.3	15.2	AV
16.7	17.6	18.5	AV
20.1	21.0	21.9	AV

TABLE 2.3 LOCATION OF GROUND MOTION NEAR-SURFACE INSTRUMENTS ALONG HORIZONTAL RADIAL.

Range (ft)	Depth from Ground Surface (ft)	Measurement
	Events 1-6[a]	
13.4	0	AB
13.4	1.5	UV,UH
25	0	AB
25	1.5	UV,UH
32	0	AB
32	1.5	UV,UH
43	0	AB
43	1.5	UV,UH
57	0	AB
57	1.5	UV,UH
67	0	AB
67	1.5	UV,UH
	Event 7	
13.4, 25, 32, 43, 57, and 67	3.60	UH
	Event 8	
13.4, 25 32, 43, 57, and 67	7.20	UH
	Event 9	
13.4, 25, 32, 43, 57, and 67	10.8	UH

[a] All ranges, depths, and instruments held constant.

TABLE 2.4 LOCATION OF STRESS GAGE VERTICAL INSTRUMENTS DIRECTLY BENEATH EXPLOSION.

Events 1-4 Depth from Ground Surface (ft)	Event 5 Depth from Charge CG (ft)	Event 6 Depth from Charge CG (ft)	Event 7 Depth from Charge CG (ft)	Measurements
8.7	8.5	3.6	6.4	SV
9.5	9.3	5.6	8.4	SV
10.7	10.5	8.6	11.4	SV
12.7	12.5	12.6	15.4	SV
16.0	15.8	17.6	21.4	SV

TABLE 2.5 LOCATION OF STRESS GAGE INSTRUMENTS ALONG HORIZONTAL RADIAL AT CHARGE CG DEPTH.

Range (ft)	Depth from Ground Surface (ft)	Measurement
	Event 8	
10, 12, 15, 20, and 30	7.20	SH
	Event 9	
10, 12, 15, 20, and 30	10.8	SH

TABLE 2.6 GROUT MIXTURE.

Mix	Constituent	Weight[a] (lb)	Weight (%)
E-2D(m) (fast setting)	Type-I Portland Cement	9.14	5.64
	Cal Seal Gypsum Cement	3.00	3.95
	Bentonite	6.52	5.15
	Barite	18.07	14.26
	Sand (masonry)	61.97	48.91
	Water	28.00	22.10

Note: Grout properties at 7-day cure:
Strength - 150 psi
Density - 127 pcf
Velocity, C_s - 4000 ft/s

[a] Weights to make 1 ft^3 of grout.

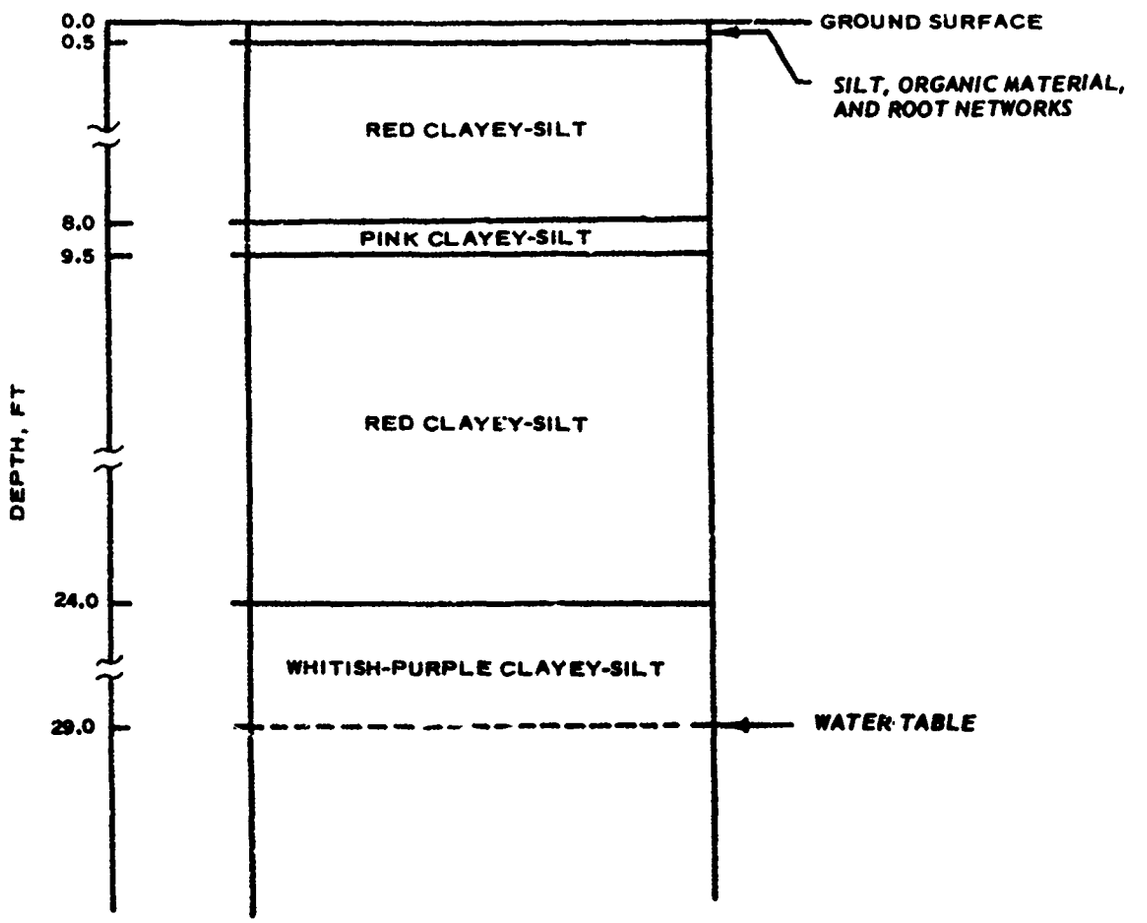

Figure 2.1 Site geology.

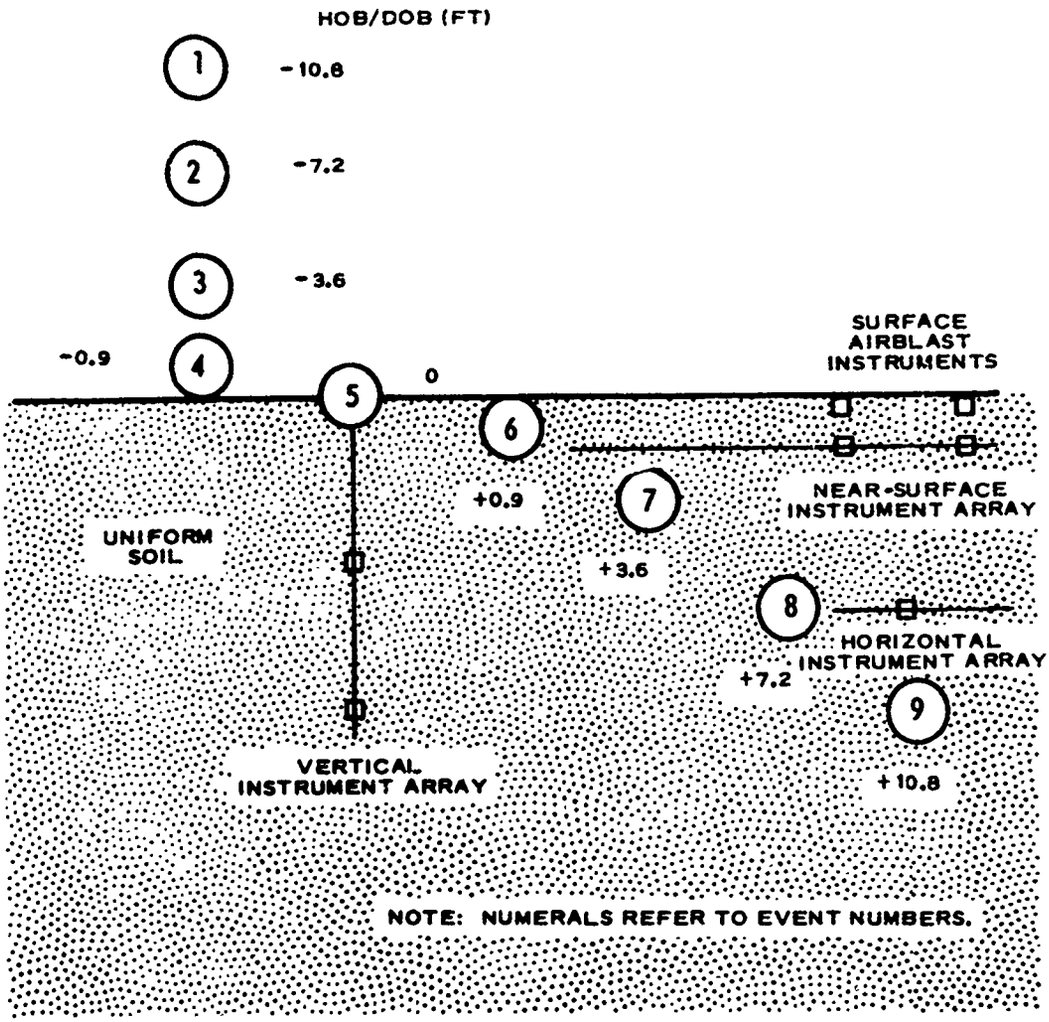

Figure 2.2 CENSE 2 experiment geometry, 300-pound TNT explosive.

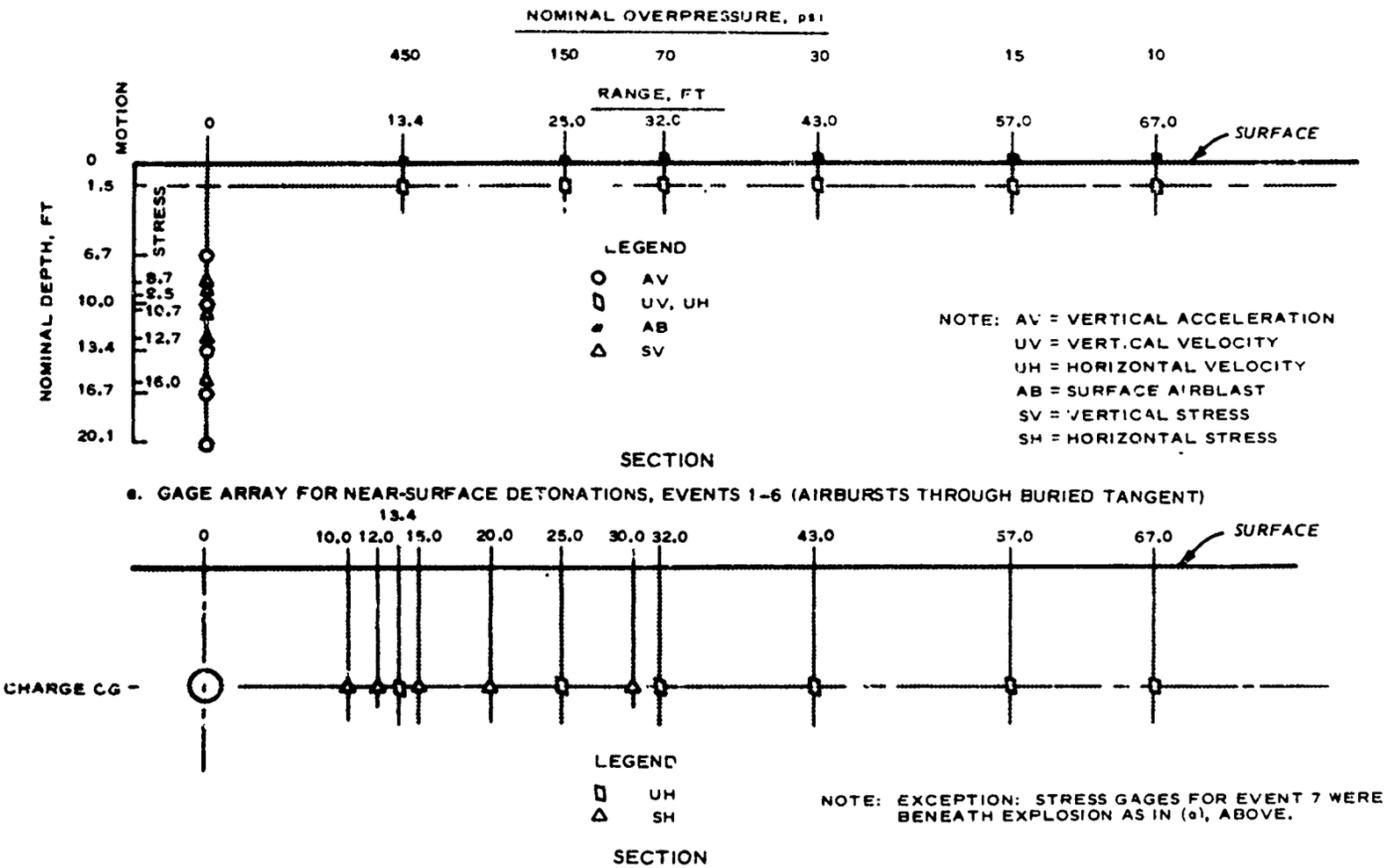

Figure 2.3 Typical CENSE 2 instrument arrays.

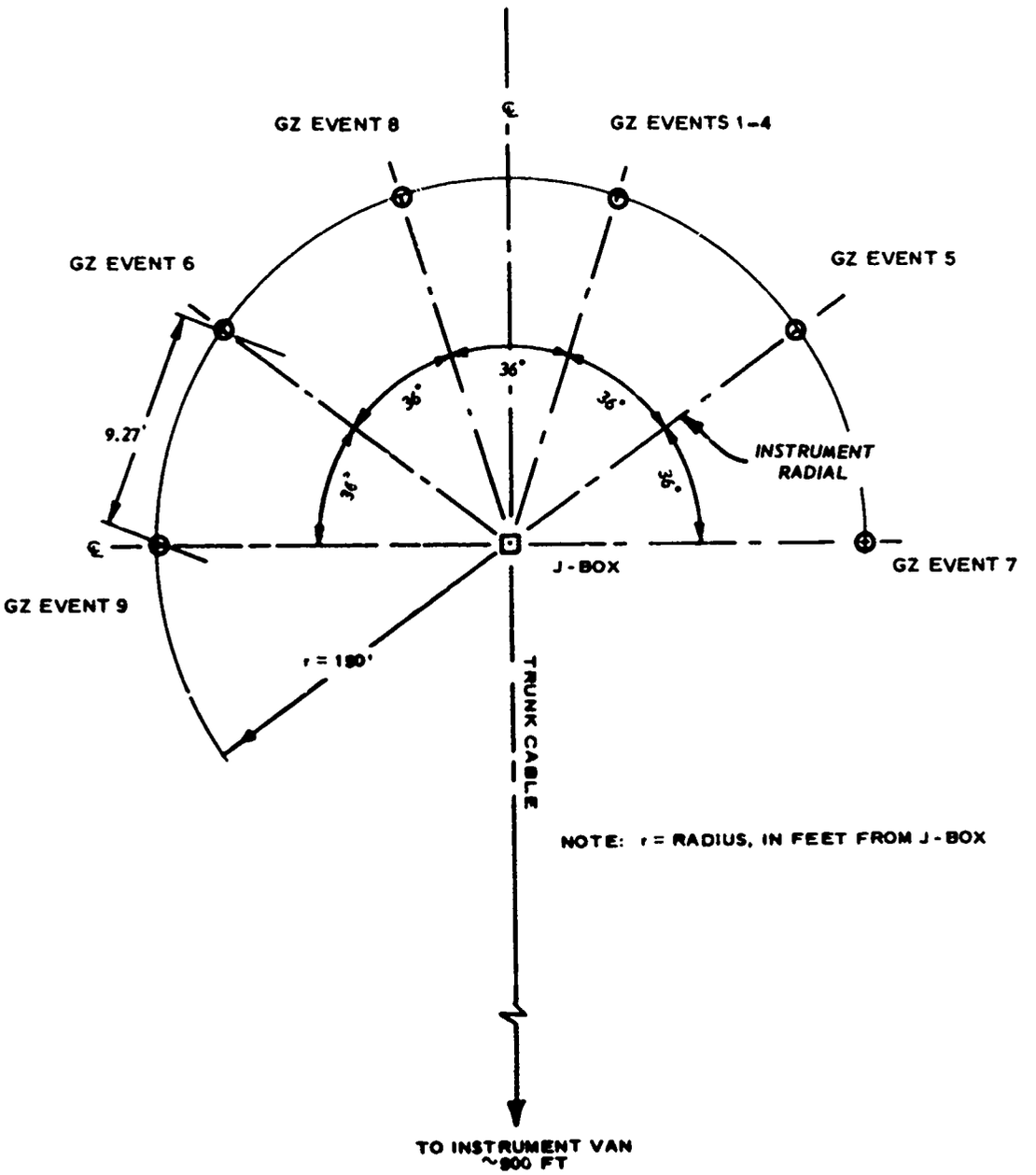

Figure 2.4 CENSE 2 experiment layout.

CHAPTER 3

RESULTS

3.1 CRATERING

Only apparent craters were measured. These measurements are listed in Table 3.1. Figure 3.1 is a composite of the apparent crater profiles. No craters were produced by the aboveground detonations, Events 1, 2, and 3 (HOB = 10.8, 7.2, and 3.6 feet, respectively). Progressively larger apparent craters were produced with increasing charge DOB, beginning with the surface tangent detonation (Event 4). The craters were characteristic for the site material. Apparent crater volumes were divided by the charge weight to derive an index of cratering efficiency. Cratering efficiency as a function of burst position is shown in Figure 3.2. Cratering efficiency increased rapidly to a scaled DOB of 1 $W^{1/3}$ (6.7 feet) and appeared to reach maximum at a scaled depth of 1.75 $W^{1/3}$ (11.7 feet). Cratering efficiency asymptotically approached zero for scaled HOB's greater than -0.13 $W^{1/3}$ (-0.9 feet).

3.2 ARRIVAL TIME

3.2.1 Directly Beneath the Explosion

First motion arrival times directly beneath the explosion for Events 1 through 6 are plotted versus depth in Figure 3.3. Events 1 through 4 were all detonated over the same GZ and fall within a data band that is separated from Events 5 and 6, which were detonated in virgin areas. The slopes of the data from all six events are essentially equal and indicate an average propagation velocity C_s of 3000 ft/s.

3.2.2 Near-Surface Horizontal Radial

Shock front arrival times for surface airblast and near-surface (1.5-foot depth) motion are plotted for Events 1 through 6 in Figure 3.4. Near-surface ground shock propagation was governed by the surface airblast at all ranges instrumented for the elevated and surface tangent detonations (Events 1 through 4), Figure 3.4(a), (b), (c), and (d). Outrunning ground motion was first observed on the half buried

detonation (Event 5), occurring at a range of 50 feet (Figure 3.4(e)). A perturbation was observed in the surface airblast arrival curve for the buried tangent detonation (Event 6) at a range of 35 feet extending to 42 feet, indicating a reduction in velocity (Figure 3.4(f)). The initial propagation velocity resumed beyond the 42-foot range. This propagation anomaly was also experienced in the near-surface soil. The direct transmitted pulse arrived 5 ms after the airblast pulse at the 13.4-foot range, but propagated at a rate 1.5 times faster (2700 versus 1800 ft/s). The directly transmitted arrival curve intersected the transmitted airblast arrival curve at a range of 36 feet, indicating the point of outrunning in the ground.

3.2.3 Horizontal Radial at Charge Depth

First motion arrival times from the buried explosions, Events 7, 8, and 9, are shown in Figure 3.5. The arrival time-distance curves for Events 7 and 8 (DOB = 3.6 and 7.2 feet, respectively) have similar slopes and are bilinear. The initial slopes for both events indicate a propagation velocity of 1500 ft/s. A change in slope occurring at 43 and 36 feet for Events 7 (DOB = 3.6 feet) and 8 (DOB = 7.2 feet), respectively, indicates arrival of refracted energy from an underlying 2700 ft/s layer. This interface occurs at an approximate depth of 14 feet below the ground surface and is due primarily to an increase in water content below this depth. Propagation velocity measured for the deepest detonation of this series, Event 9 (DOB = 10.8 feet), was a constant 2700 ft/s beyond a horizontal range of 13 feet. In the range of 0 to 13 feet the apparent average propagation velocity was 3600 ft/s.

3.3 VERTICAL GROUND SHOCK DIRECTLY BENEATH THE EXPLOSION

3.3.1 Data Recovery

Ground motion and stress data taken in the region directly beneath the explosion were of excellent quality. Only seven data channels were lost for the entire test series. All other data channels yielded full or partial data. Data losses for GZ measurements are summarized in Table 3.2.

3.3.2 Vertical Acceleration

Recorded vertical acceleration-time histories directly beneath the explosions are shown in composite in Figures 3.6-3.8 for Events 1 through 6. The waveforms are generally characterized by an initial downward spike followed by a lower amplitude, longer duration upward pulse. Both peak amplitudes and pulse duration increased with increasing charge burial. Pulse frequencies decreased as the airblast energy fraction decreased.

Scaled peak downward acceleration directly beneath the explosion is plotted versus scaled depth in Figure 3.9. The initial slopes were similar for all data between scaled depths of $1\ W^{1/3}$ (6.7 feet) and $1.49\ W^{1/3}$ (10 feet), i.e., a slope of $R^{-7.97}$, where R is the slope of data with respect to distance. Beyond this distance the curves for all elevated shots (Events 1, 2, and 3) tended to flatten and become bilinear. No tendency toward bilinearity was observed for the surface tangent, half buried, and buried tangent detonations (Events 4, 5, and 6, respectively). Acceleration magnitudes increased progressively with increasing charge DOB. Note, however, that there was virtually no difference between Events 2 and 3.

3.3.3 Particle Velocity

All particle velocity data from the region directly beneath the explosion were derived by numerical integration of the acceleration data. Composited particle velocity waveforms for Events 1 through 6 are shown in Figures 3.10-3.12. The velocity waveforms are similar in overall character to those of the vertical acceleration, namely a sharp initial downward pulse followed by a lower amplitude, longer duration upward pulse. As with the acceleration counterpart, the vertical velocity exhibited increasing amplitudes and pulse durations with increasing charge DOB. The velocity waveforms at the 6.7-foot depth for Events 1 through 4 show a relatively constant baseline offset after arrival of the peak velocity. This is not a physical phenomenon, rather a result of the integration technique where the acceleration signal was submerged in the basic system noise.

Peak radial particle velocity directly beneath (Events 1 through 6) and horizontally on-axis with the explosion (Events 7, 8, and 9) versus scaled distance is plotted in Figure 3.13. The response curve for Events 1, 2, and 3 (elevated charge positions) tended to be bilinear. The initial decay rate (between scaled depths of 1 and 1.49 $W^{1/3}$) was $R^{-5.26}$, decreasing to $R^{-0.57}$ beyond a scaled depth of 1.49 $W^{1/3}$. Peak radial particle velocity for Events 4 through 9 attenuated uniformly at a rate of $R^{-2.58}$. Peak velocity increased with increasing charge burial. Significant increases occurred between Events 3 and 4, 4 and 5, and 5 and 6, indicating the highest velocity sensitivity to burst position occurring in this region. Data from the elevated shots (Events 1 through 3) were tightly clustered, as were the data from the buried shots (Events 7 through 9). Peak velocity increased by 3.5 times from the lowest elevated shot (Event 3, HOB = -3.6 feet) to the surface tangent (Event 4); 2.6 times from the surface tangent to half buried (Event 5); and 1.9 times from half buried to buried tangent (Event 6). A velocity "jump" or enhancement (factor of 5) was observed at a scaled distance of 10 $W^{1/3}$ (67 feet) for the three buried detonations (Events 7, 8, and 9). This enhancement is probably associated with development of end interaction with a surface wave at this distance. Beyond a scaled distance of 10 $W^{1/3}$, the velocity attenuated at the same rate as the initial portion, i.e., as $R^{-2.58}$. Close-in particle velocity data measured by SRI (Reference 11) for Events 8 and 9 attenuated at a rate similar to the WES data but were an order of magnitude lower than values from the projected WES data.

3.3.4 Displacement

Displacements directly beneath the explosion were all derived by doubly integrating the acceleration-time histories. Considerable error is always inherent with progressive time in any integration routine, especially when the original operator signal approaches or lies within the system noise. The problem is further compounded when a double integration is attempted. The result is a signal with highest validity near zero time with accuracy progressively decreasing with increasing time.

In spite of this handicap, exceptionally good displacement waveforms were generated for all but the shallowest (6.7-foot depth) gage location. Data from this location are considered to be of low reliability. Composited displacement waveforms from Events 1 through 6 are presented in Figures 3.14-3.16. Displacement waveforms generally exhibited an oscillatory character for the elevated burst positions (Events 1 through 4). However, the displacement maintained a downward permanent displacement for the half buried (Event 5) and buried tangent (Event 6) detonations. Maximum displacements were recorded for Event 6, Figure 3.16. The effect of burst position on the shape of the displacement waveform is clearly seen in Figure 3.17, which is a comparison of waveforms from the-10.8 foot HOB (Event 1) to +0.9 foot DOB (Event 6) burst positions at a common gage depth (nominally 14 feet). The initial rise time, peak amplitude, and pulse duration increased with increasing charge DOB.

Scaled peak radial transient displacement (downward or outward) directly beneath (for Events 1 through 6) and horizontally on-axis (for Events 7 through 9) is plotted versus scaled distance in Figure 3.18. Only minor differences were present in peak downward displacements from three elevated shots (Events 1 through 3). The slope of the data was relatively flat for Event 1, as $R^{-0.33}$, and progressively steepened to Event 4 (surface tangent). The initial slopes (between scaled distances of 1.5 to 4.5 $W^{1/3}$) were equal for Events 4 through 9, as $R^{-3.16}$. Displacement data from the buried detonations (Events 7 through 9) decreased in slope between scaled distances of 4.5 and 8.5 $W^{1/3}$. As was noted for the velocity data in Section 3.3.3, the displacement data experienced a "jump" at a scaled distance of 10 $W^{1/3}$ (67 feet). Between this distance and a scaled distance of 1.49 $W^{1/3}$ (100 feet), the displacement attenuated with distance at approximately the same slope as the initial portion of the data, i.e., as $R^{-3.16}$.

3.3.5 Stress

A composite of the measured stress waveforms is presented in order of increasing distance from the explosive charge for Events 1 through 9 in Figures 3.19-3.23. The waveforms for Events 1 through 4,

(Figures 3.19 and 3.20) exhibit a slight negative stress following the initial compressive peak. This effect is caused by relief of the static overburden stress (on the order of a few pounds/square inch) associated with gage installation but not associated with the dynamic response of the soil. Stress pulse amplitudes and durations progressively increased in order with increasing charge burial.

On Event 7, gages were positioned both directly beneath the charge and along a horizontal radial located at charge depth (+3.6 feet). Direct comparison was possible between the vertical and horizontal vectors at distances of 11.4 and 21 feet from the charge CG (Figure 3.22). The stress waveforms were markedly different along the two vectors. The vertical waveforms exhibited higher amplitudes, steeper decay of the initial pulse, and a tendency to develop a secondary peak as compared to the horizontal waveforms.

Peak radial stresses measured directly on-axis with the explosion are displayed as functions of distance and burst position in Figure 3.24. Peak stresses from the elevated shots (Events 1, 2, and 3) show only a slight dependence on burst position. The effect of burst position on measured stresses was significant between the elevated shots and surface tangent (Event 4) detonations; stress levels increased by a factor of 3.5. A factor of 2 increase in stress level was observed by moving the charge from half buried to buried tangent (Event 6). The buried events (Events 6 through 9) generally showed an increase in stress level with increasing charge burial. An exception was Event 7 (DOB = +3.6 feet), whose stresses were of the same order of magnitude as those for the half buried detonation. This is probably due to slight changes in site geology and/or a slight irregularity in gage placement. Peak stresses from all events appear to have similar rates of attenuation with distance (approximately as the -4.33 power of distance).

3.4 NEAR-SURFACE GROUND MOTION

3.4.1 Data Recovery

Excellent data recovery was made along the near-surface instrument

radial and along the horizontal radial at shot depth (Events 7, 8, and 9). Only one measurement was lost for the entire test series, measurement 13.4-1.5 UV[1] for Event 1, a gage malfunction.

3.4.2 Horizontal Particle Velocity

Near-surface horizontal particle velocity waveforms at a common range (32 feet) are composited for all events in Figure 3.25. Complete waveforms are shown in Appendix B. The gages for Events 1 through 6 were positioned at a constant 1.5-foot depth below the ground surface, whereas, the gages for Events 7, 8, and 9 were located at shot depth (i.e., 3.6, 7.2, and 10.8 feet, respectively, see Figure 2.3). The waveforms produced by Events 1 through 6 reflect complex driving forces. The initial outward going pulses were produced by the surface airblast. A considerably longer duration secondary outward peak produced by the cratering action was present in the waveforms from Events 4, 5, and 6, but was noticeably absent from the velocity signatures from the non-cratering events (Events 1, 2, and 3). Velocity waveforms produced by the buried shots (Events 7, 8, and 9), where the instruments were placed at shot depth, had a very simple signature: a single outward-going initial pulse caused by the cratering action, followed by a lower amplitude, longer duration inward-going pulse. The cratering-induced motion is detailed in Figure 3.25 by a labeled dashed line. As the airblast energy fraction diminished (i.e., as charge burial increased), high-frequency content of the waveforms decreased.

Peak horizontal particle velocities as a function of scaled distance are shown in Figure 3.26. Although the gages for the three buried events (Events 7, 8, and 9) were positioned at charge depth, these data are included with the near-surface (1.5-foot depth) data for comparison. Only minor differences are apparent in the horizontal particle velocity maxima for the three elevated detonations (Events 1, 2, and 3). Data from the surface tangent (Event 4) detonation fell very near those from the elevated shots beyond a horizontal range of 25 feet ($3.73\ W^{1/3}$).

---

[1] Refer to Appendix B for explanation of measurement numbers.

However, at a scaled distance of $2\ W^{1/3}$ (13.4 feet), horizontal velocity measured from the surface tangent detonation (Event 4) was over 4 times greater than for the elevated shots. The average slope of the horizontal velocity data between scaled distances of $2\ W^{1/3}$ (13.4 feet) and $4\ W^{1/3}$ (32 feet) for all detonations, except the elevated shots, was $R^{-2.58}$. A consistent enhancement in peak outward particle velocity was observed at a scaled distance of $10\ W^{1/3}$ (67 feet) for Events 6 through 9. This phenomenon is associated with formation of a surface wave as previously discussed in Section 3.3.3.

Apart from the primary experiment, velocity gage placement effects were casually studied on Events 7 and 8. At a horizontal range of 43 feet, two additional matched gage canisters were installed adjacent to and on either side of the primary instrument package. The primary measurement was denoted by the label C preceding the measurement number (meaning center), while the auxiliary gages were labeled R and L for right and left positions, respectively, with respect to the primary gage. The primary gage canister was grouted to the surface of the borehole with soil matching grout. The right-hand canister was grouted in its borehole with only the bottom 2 inches of canister grouted; 1 foot of sand was added; and the remainder of the borehole was left open. The left-hand canister was grouted in the same manner as the right-hand canister; however, the remainder of this borehole was left completely unfilled. These three emplacement conditions were thought to represent a reasonable range of placement methods. The recorded waveforms (Figure 3.27) showed identical gage response, indicating that for tests where airblast effects are minimum, hole backfilling may not be critical as long as the base of the canister is firmly coupled to the base of the borehole and the loading pulse is transverse to the borehole axis.

3.4.3 Vertical Particle Velocity

Near-surface vertical particle velocity waveforms at a common range (32 feet) are composited for Events 1 through 6 in Figure 3.28 (see Appendix B for complete time histories). From this figure maximum

velocity is seen to have been downward, except for Event 6 (buried tangent), and was produced by the surface airblast (or "airslap"). The upward, direct-induced motion was of higher amplitude for Event 6. A trailing, secondary downward velocity pulse present in the velocity waveforms from Events 4, 5, and 6 was produced by impact from surface fallback.

Peak downward airslap-driven velocity (Figure 3.29(a)) plotted as a function of scaled distance shows no significant variance in velocity response between the elevated shots (Events 1 through 3). Peak downward velocities measured on the surface tangent shot (Event 4) were slightly lower than those from the elevated detonations but attenuated at a similar rate ($R^{-1.58}$) beyond a scaled horizontal distance of $3.7\ W^{1/3}$ (25 feet). At this distance the downward velocity from the half buried burst position was only 55 percent of that produced by the surface tangent detonations but exhibited less of an attenuation with distance, i.e., $R^{-1.09}$ versus $R^{-1.58}$ for the shallower burst positions. The velocity curves converged at a scaled distance of $12\ W^{1/3}$ (80 feet). Velocity curves for all six events flattened (slope decreased) at scaled distances less than $3.7\ W^{1/3}$. The velocity-distance curve for the buried tangent (Event 6) burst position was unique. Downward velocity amplitudes increased slightly out to a scaled distance of $3.7\ W^{1/3}$, then decreased at a severe rate (approximately R^{-7}), reaching a minimum value at a scaled distance of $6.4\ W^{1/3}$ (43 feet). At this range a reversal in slope occurred ($R^{+6.3}$), indicating a substantial rate of increase in the peak downward velocity with increasing range.

Upward, direct-induced particle velocities (Figure 3.29(b)) exhibited a response similar to the downward, airslap conterpart (Figure 3.29(a)), except that the order of the curves reversed (i.e., magnitudes progressively increased with increasing charge DOB). The tendency of the upward velocity curves to flatten at scaled distances less than 3.7, manifested in the downward airslap pulse (Figure 3.29(a)) for all burst positions, was observed only for the elevated burst positions in the upward, direct-induced pulse. Upward particle velocity

attenuation could be approximated by single slopes for Events 4 and 5; however, point-to-point connection was plotted to show up the actual data trends, a repetitive undulation. Upward velocity maxima measured on the buried tangent detonation (Event 6) defined a U-shaped curve, with minimum response occurring at a scaled distance of $6.4\ W^{1/3}$ (43 feet), which was consistent with the downward airslap velocity.

3.4.4 Horizontal Displacement

Both horizontal and vertical near-surface displacement waveforms at a common distance (32 feet) are composited for Events 1-6 in Figure 3.30. No vertical motions were measured on Events 7-9. Horizontal displacement waveforms from the three elevated shots (Events 1, 2, and 3) are identical in character and, for all practical purposes, in amplitude. Two complete cycles of motion are present, begining with an initial outward going surface airblast-driven displacement pulse. Horizontal displacement response from the surface tangent (Event 4) detonation clearly defines the transition in loading modes from primarily airblast to one that is crater induced. For detonation below buried tangent (Event 6), with the horizontal gage array position at charge depth, the horizontal displacement waveforms show no influence from airblast loading, i.e., all motion is derived directly from the cratering phenomena.

Scaled peak outward near-surface horizontal displacement versus scaled distance is shown in Figure 3.31 for surface tangent (Event 4), half buried (Event 5), and buried tangent (Event 6) burst positions. Outward displacement increased proportionally with increasing DOB. Data from both surface tangent and half buried attenuated at the same rate (as $R^{-3.29}$); however, displacement amplitudes were three times higher for the half buried detonation. Peak displacements from the buried tangent (Event 6) shot were only slightly higher than those produced by Event 5 between scaled distances of $2\ W^{1/3}$ (13.4 feet) and $4.78\ W^{1/3}$ (32 feet) but progressively increased at greater distances. Horizontal displacements from the buried tangent detonation appeared to be bilinear with the transition point near a scaled distance of

$4.78\ W^{1/3}$ (32 feet). This bilinearity was probably the result of relative phasing of the airblast and cratering energy fractions.

3.4.5 Vertical Displacement

Downward airslap dominated the vertical displacement on Events 1 through 4 (surface tangent), as shown in Figure 3.30. Upward crater driven displacement dominated for charges half buried (Event 5) and deeper (see Appendix A for individual displacement waveforms.)

Scaled peak downward airslap-driven near-surface vertical displacement is plotted versus scaled distance in Figure 3.32 for surface tangent, half buried tangent, and buried tangent (Events 4, 5, and 6, respectively) burst positions. Considerable scatter was observed in the data. To simplify comparison, parallel slopes were fitted to the data for all three events. Based on these assigned curves a decrease factor of 1.6 resulted from moving the burst position from surface tangent to half buried. An additional decrease factor of 2.6 was obtained by increasing the DOB from half buried to buried tangent. Overall, the downward airslap-driven displacement decreased by a factor of 4.2 between surface tangent and buried tangent burst positions.

3.5 SURFACE AIRBLAST PRESSURE AND IMPULSE

3.5.1 Data Recovery

Only three surface airblast gages failed to produce data on this experiment. Specific data losses are shown below:

Event No.	Measurement No.	Comment
1	57-0-AB	Faulty gage response
2	13.4-0-AB	Defective gage, removed preshot
3	25-0-AB	Faulty gage response

The gage used at the 13.4-foot range position was found to be defective and was replaced after Event 1. A number of the gages experienced ringing, an adverse feature characteristic of the gage model used.

3.5.2 Airblast Pressure

Measured peak surface airblast pressures are shown as functions of scaled distance and burst position in Figure 3.33. The slopes of the data are essentially the same for the elevated shots through the half buried detonation (Events 1 through 5). The slope was flattened in the buried tangent (Event 6) data along with a significant reduction in peak pressure. Airblast pressure produced by the buried tangent detonation was suppressed by a factor of 7 from that produced by the airbursts (Events 1 through 3) and by a factor of 4.6 from the surface tangent (Event 4) detonation at a scaled distance of $5\ W^{1/3}$ (33.5 feet). Airblast pressure was only minimally suppressed (about 11 percent) by moving the burst position from the surface tangent (Event 4) to half buried (Event 5). A pressure reduction of about 45 percent occurred when the HOB was moved from the -3.6 foot elevated position (Event 3) to the surface tangent (Event 4).

3.5.3 Airblast Impulse

Peak surface airblast impulse is plotted as a function of scaled horizontal distance for Events 1 through 6 in Figure 3.34. Impulse values were essentially identical for the three elevated detonations (Events 1, 2, and 3). The impulse-distance curve for the surface tangent detonations (Event 4) was slightly lower than, but similar in shape to, the elevated shot results. A noticeable reduction in impulse occurred when the burst position was moved from surface tangent (Event 4) to half buried (Event 5). A drastic reduction in peak impulse occurred from the buried tangent (Event 6) detonation (on the order of 34 times at a scaled distance of $2\ W^{1/3}$).

TABLE 3.1 APPARENT CRATER PARAMETERS.

Shot Identification				Apparent Crater Parameter				Cratering Efficiency
Event No.	HOB/DOB $W^{1/3}$	R_c	(ft)	Radius ra (ft)	Depth da (ft)	Lip Height h (ft)	Volume va (ft)	$v_a/_W$ (ft^3/lb)
1	-1.61	-12	-10.8	0		0	0	0
2	-1.07	-8	-7.2	0	0	0	0	0
3	-0.54	-4	-3.6	0	0	0	0	0
4	-0.13	-1	-0.9	5.65	3.60	0.35	149.9	0.50
5	0	0	0	9.10	5.00	0.68	500.0	1.67
6	+0.13	+1	+0.9	10.80	6.50	1.58	908.6	3.03
7	+0.54	+4	+3.6	12.70	7.50	1.45	1547.3	5.16
8	+1.07	+8	+7.2	14.80	9.75	2.12	2588.0	8.63
9	+1.61	+12	+10.8	16.70	9.30	2.20	3080.6	10.27

TABLE 3.2 DATA CHANNELS LOST, GZ MEASUREMENTS.

Event No.	Data Channel No.	Measurement No.	Comment
1	26	0-20.1-AV[a]	Defective gage, deleted preshot
2	27	0-20.1-AV[a]	Defective gage, deleted preshot
	21	13.4-0-AB	Gage damaged by shot
3	27	0-20.1-AV[a]	Defective gage, deleted preshot
4	12	0-6.7-AV[a]	Gage damaged by shot
	27	0-20.1-AV[a]	Defective gage, deleted preshot
6	14	0-7.6-AV	Gage damaged by shot
	15	0-21-AV	Defective gage, deleted preshot
7	17	0-15.4-SV	Gage damaged by shot

[a] Same gage; Events 1 through 4 were repeat shots on same GZ and instrument array.

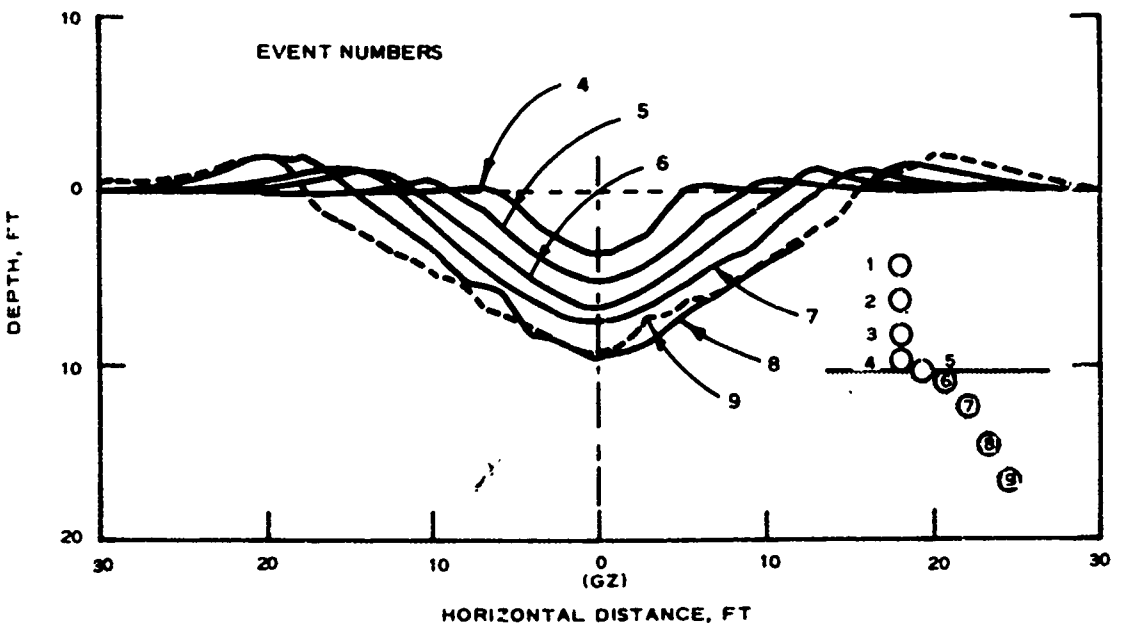

Figure 3.1 Apparent crater profiles.

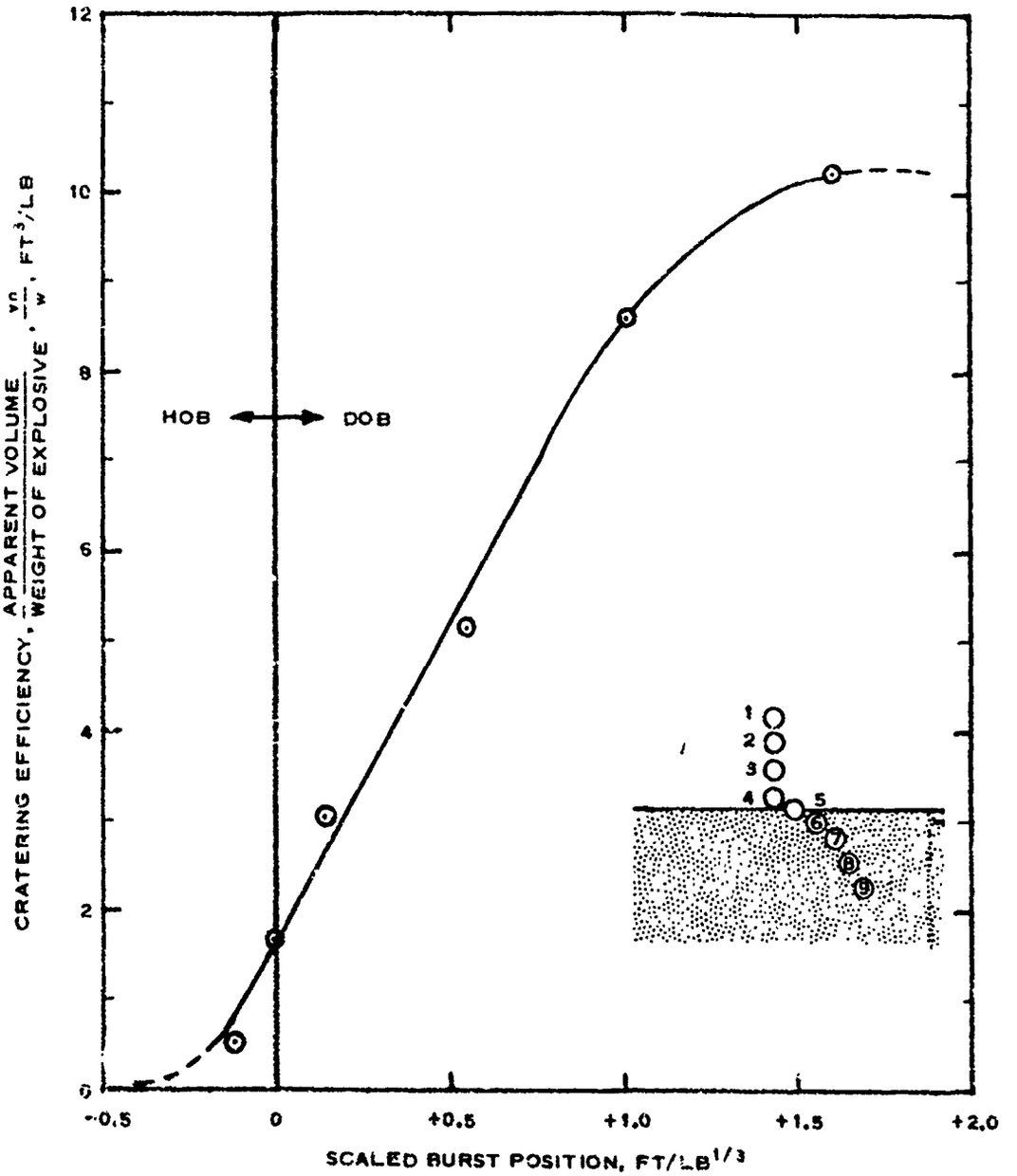

Figure 3.2 Cratering efficiency as a function of charge burst position.

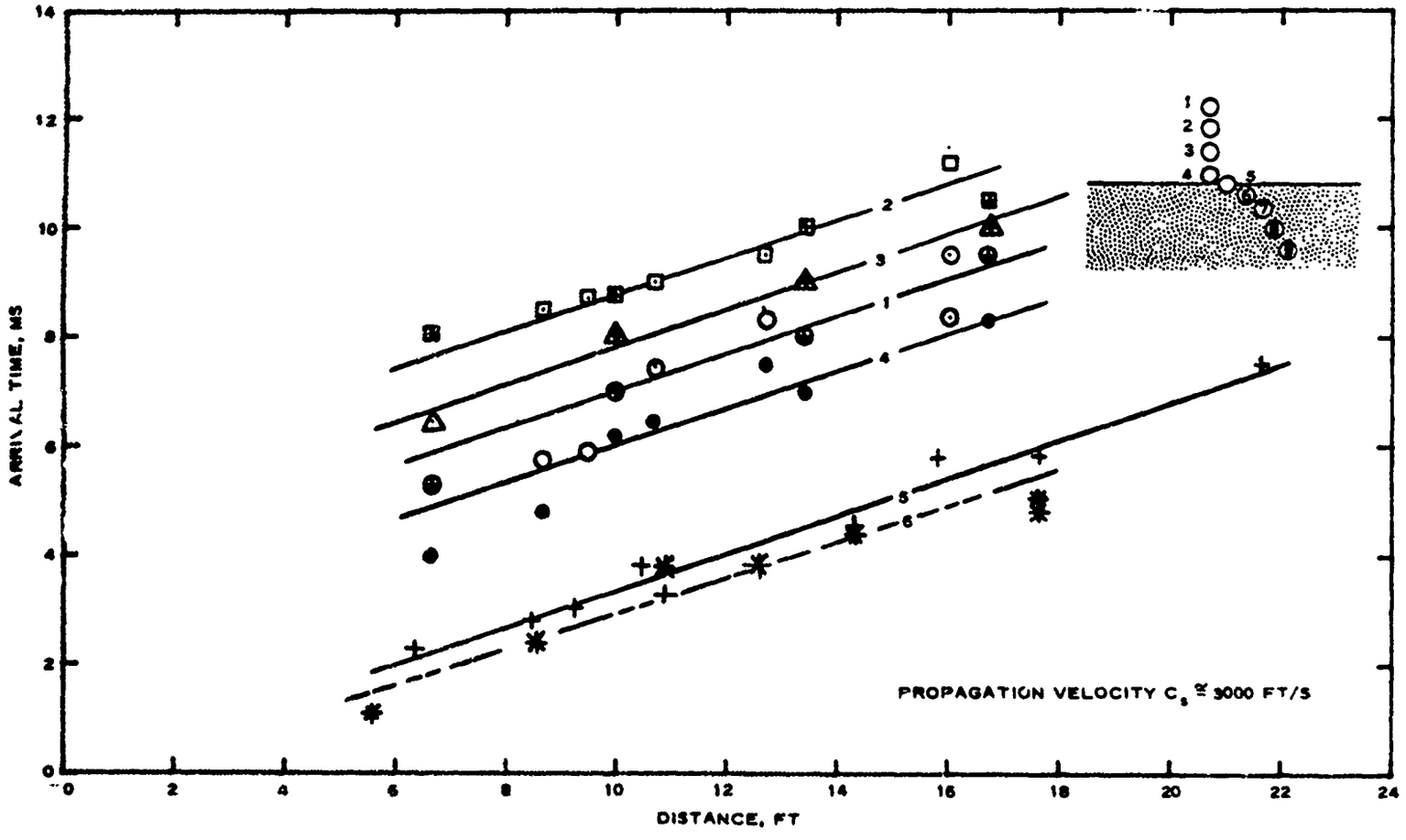

Figure 3.3 First motion arrival times directly beneath the explosion versus depth.

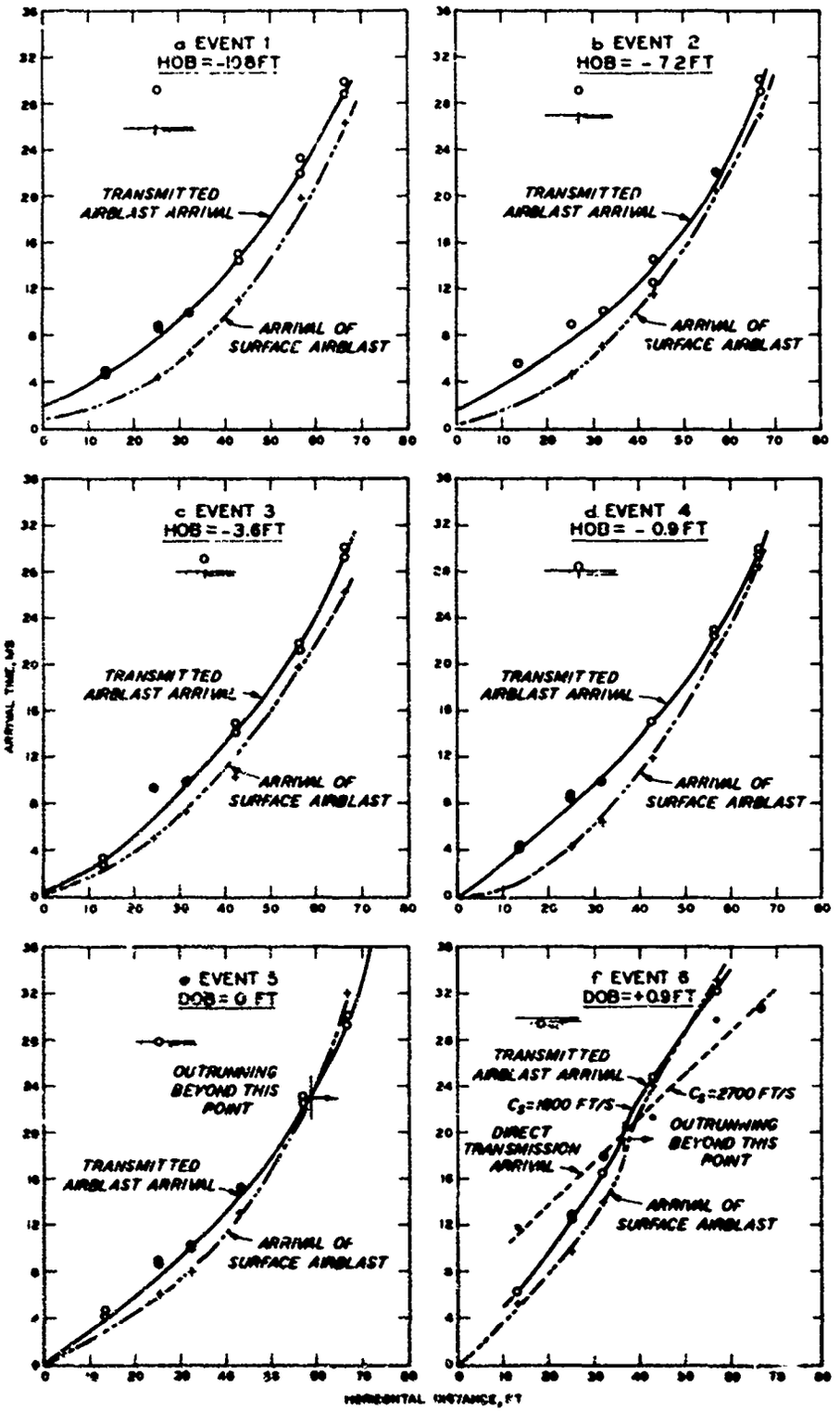

Figure 3.4 First motion arrival times along the near-surface horizontal instrument radial versus horizontal distance, Events 1-6.

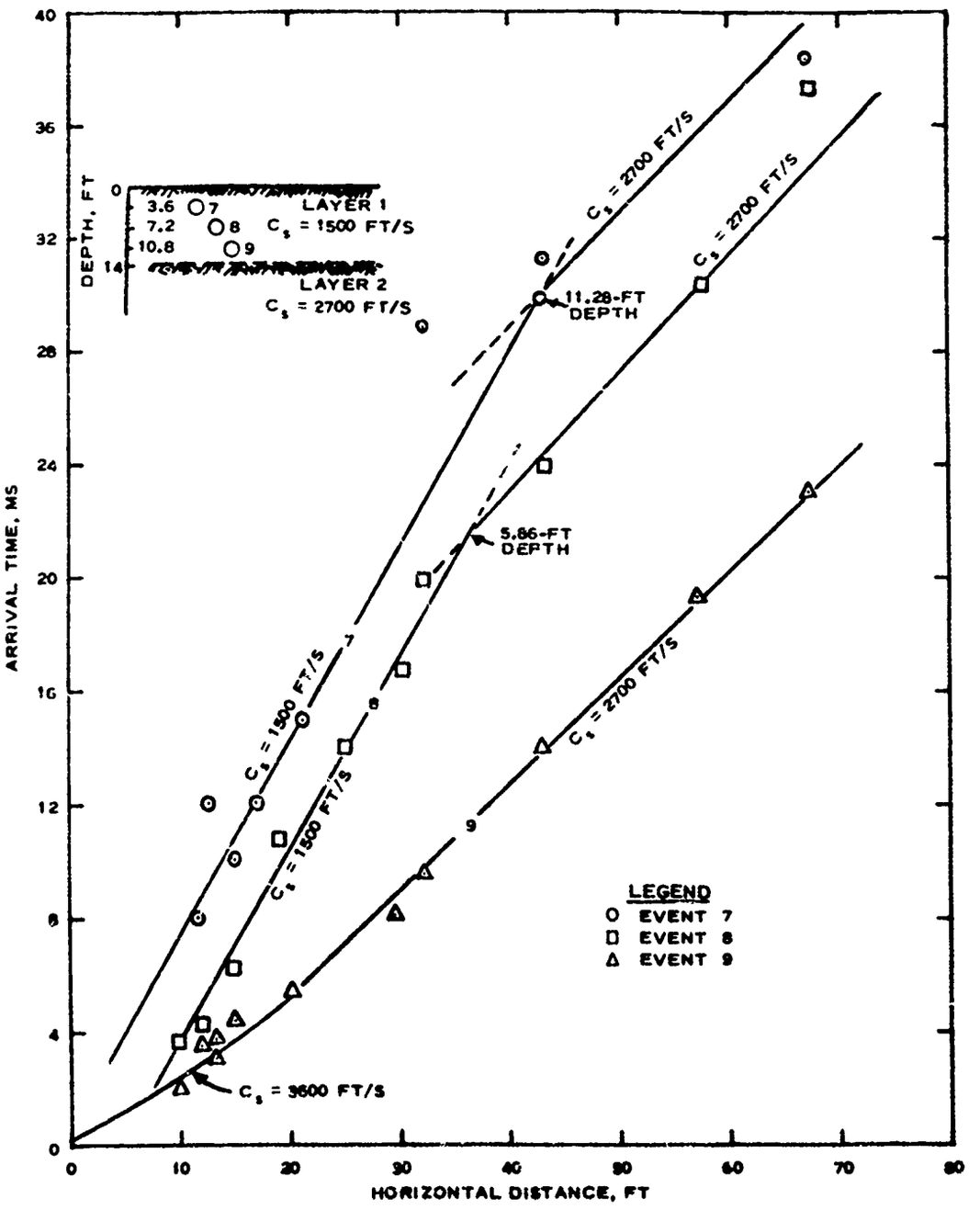

Figure 3.5 First motion arrival times along the horizontal instrument radial versus horizontal distance, Events 7, 8, and 9.

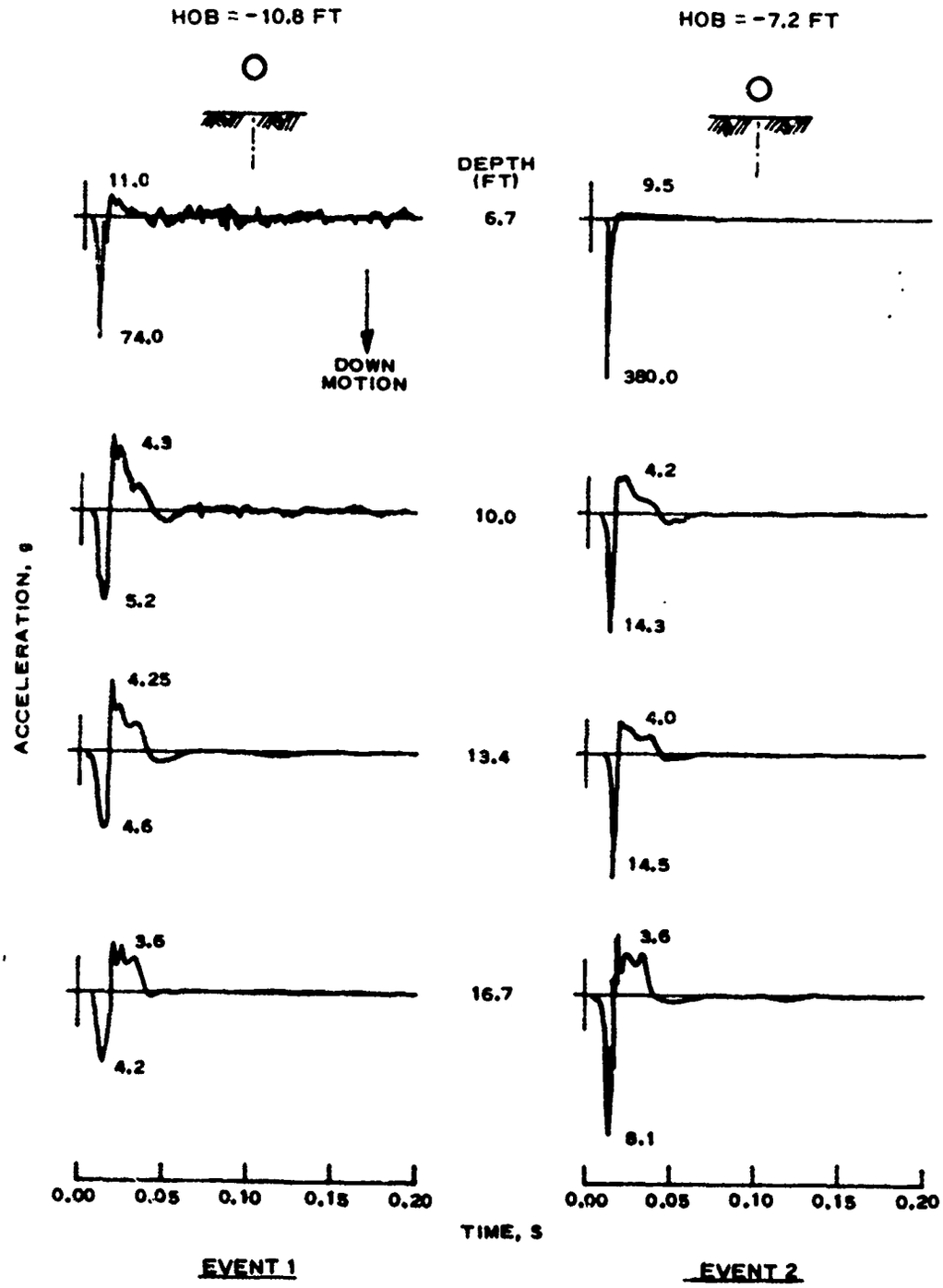

Figure 3.6 Comparison of acceleration waveforms along the vertical radial directly beneath the explosion, Events 1 and 2.

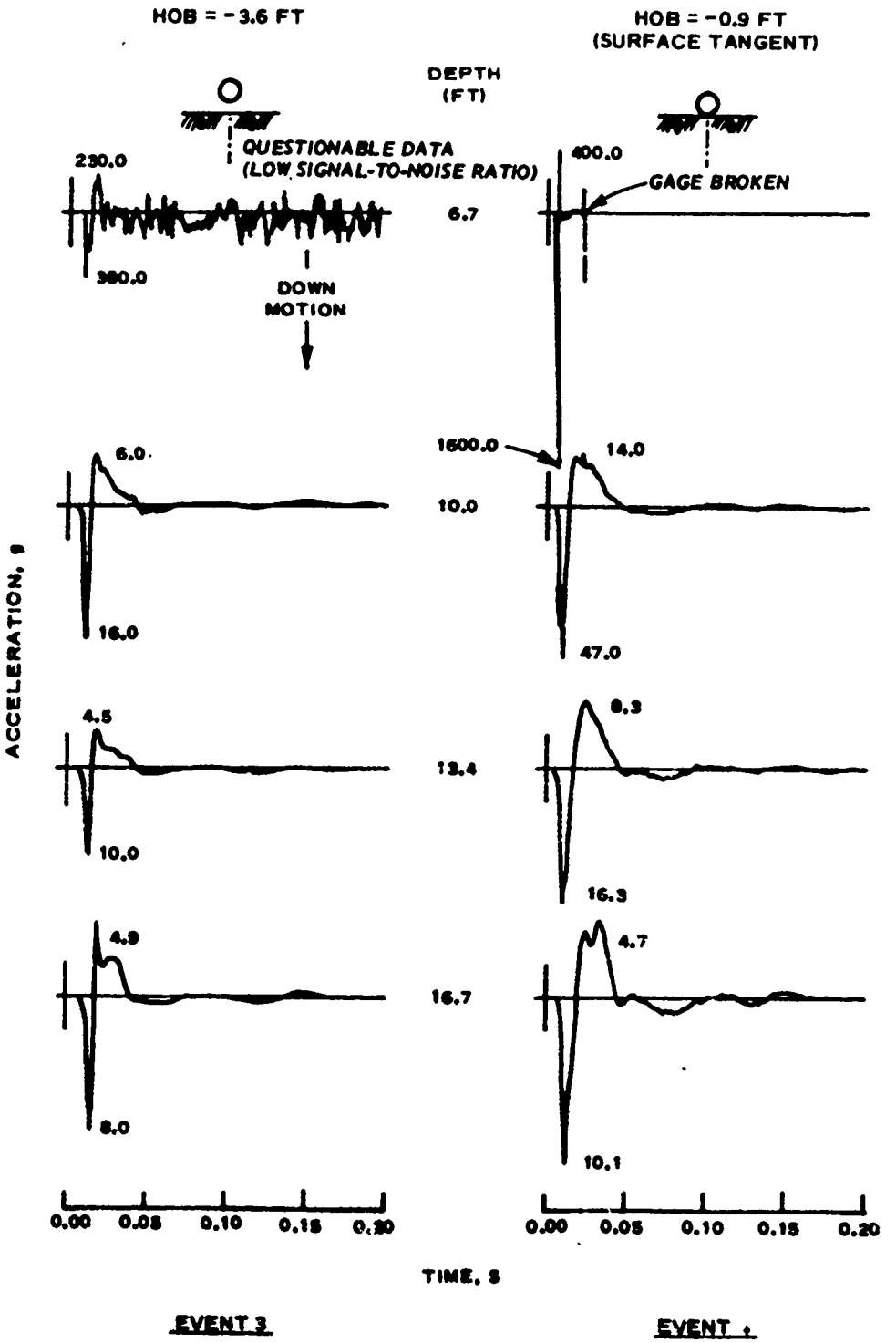

Figure 3.7 Comparison of acceleration waveforms along the vertical radial directly beneath the explosion, Events 3 and 4.

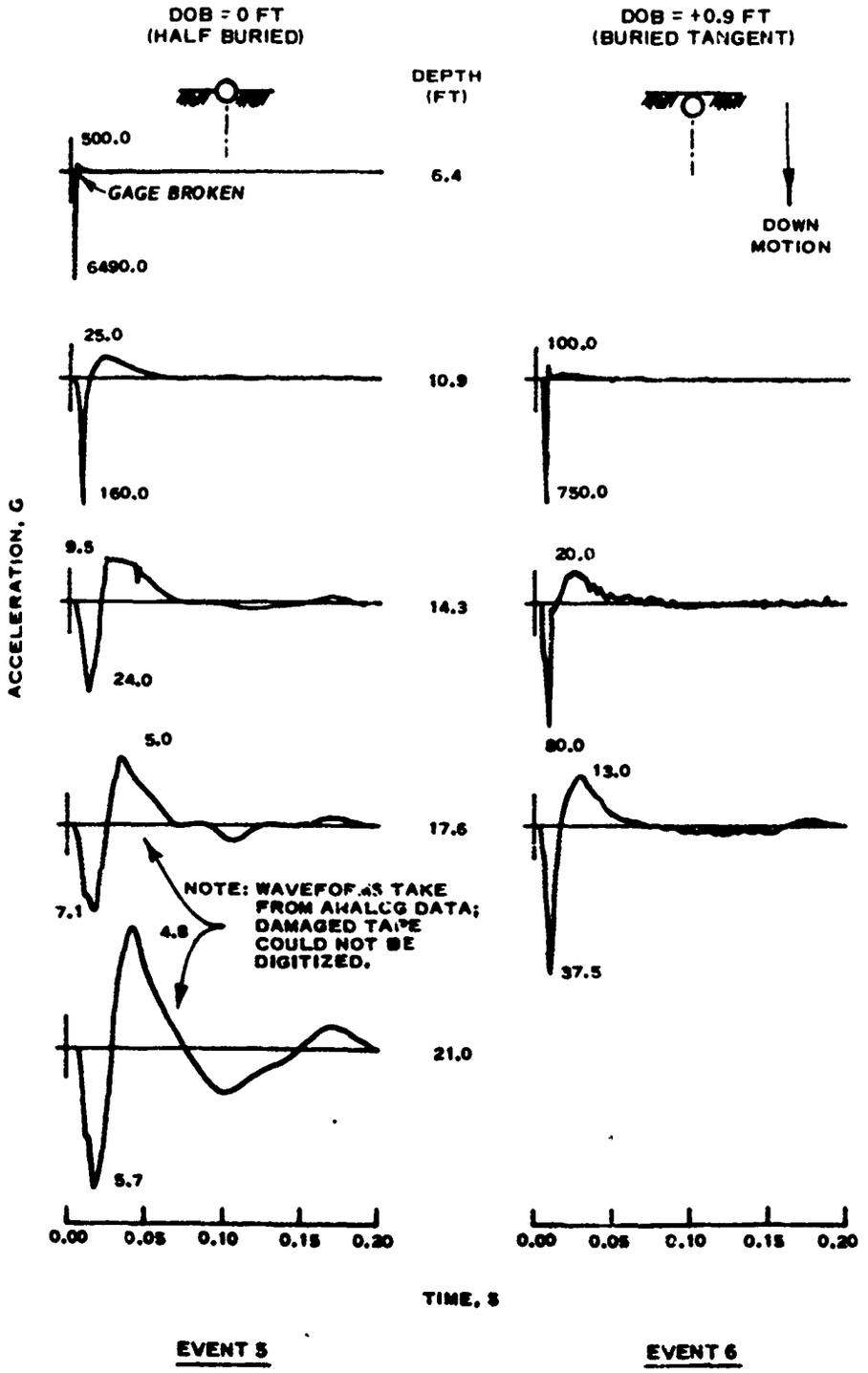

Figure 3.8 Comparison of acceleration waveforms along the vertical radial directly beneath the explosion, Events 5 and 6.

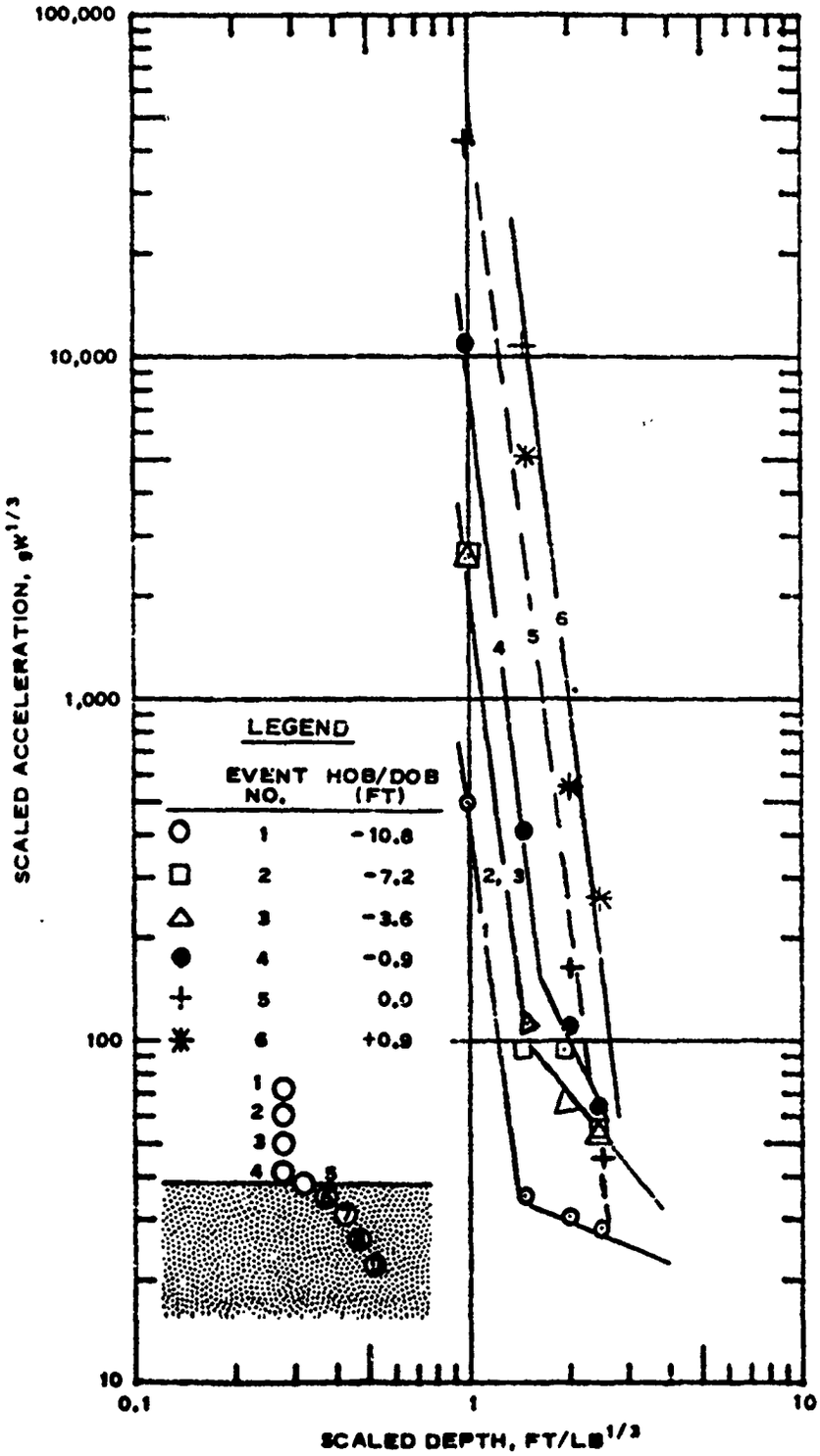

Figure 3.9 Scaled peak downward acceleration along the vertical radial directly beneath the explosion versus scaled depth.

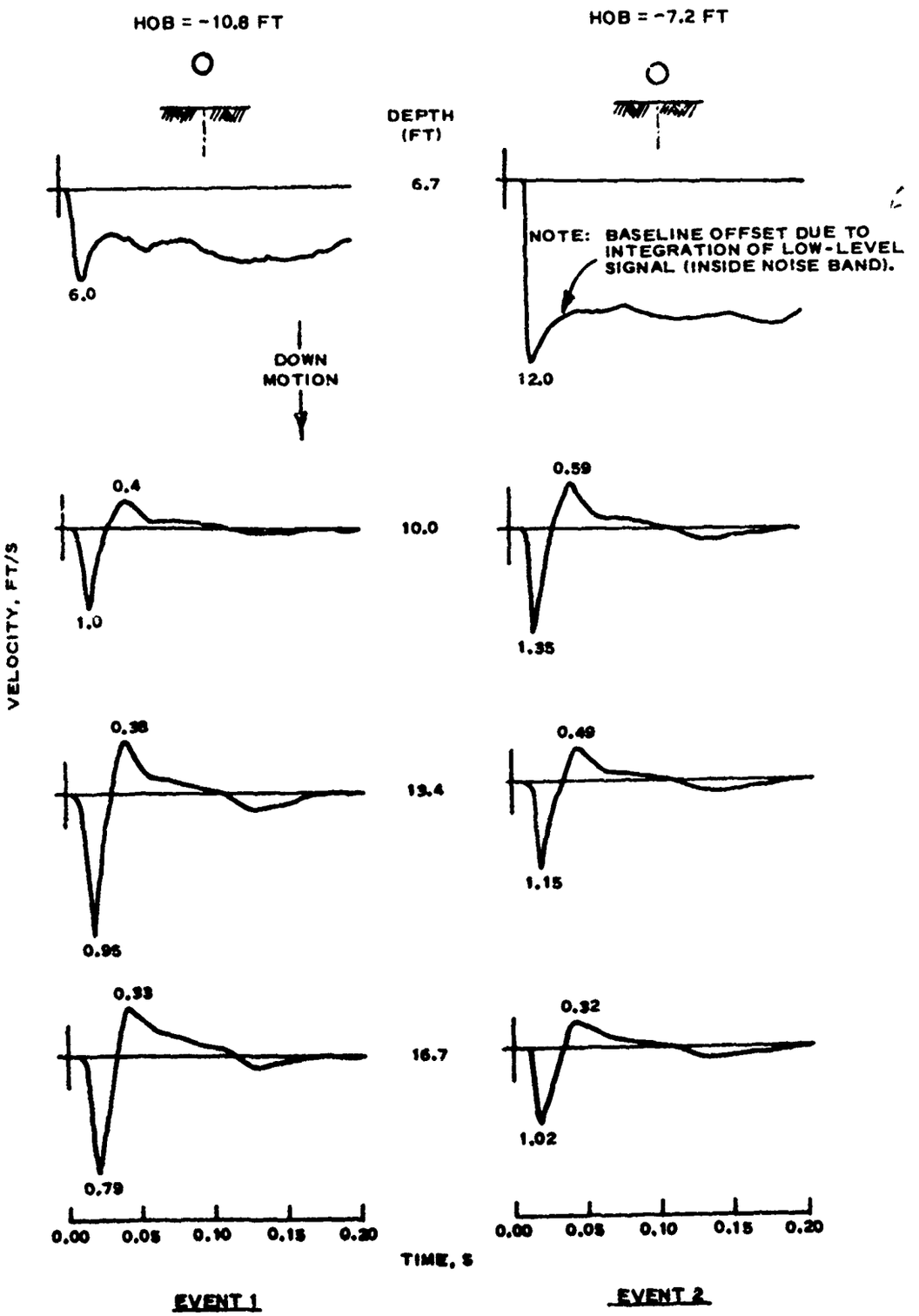

Figure 3.10 Comparison of velocity waveforms along the vertical radial directly beneath the explosion, Events 1 and 2.

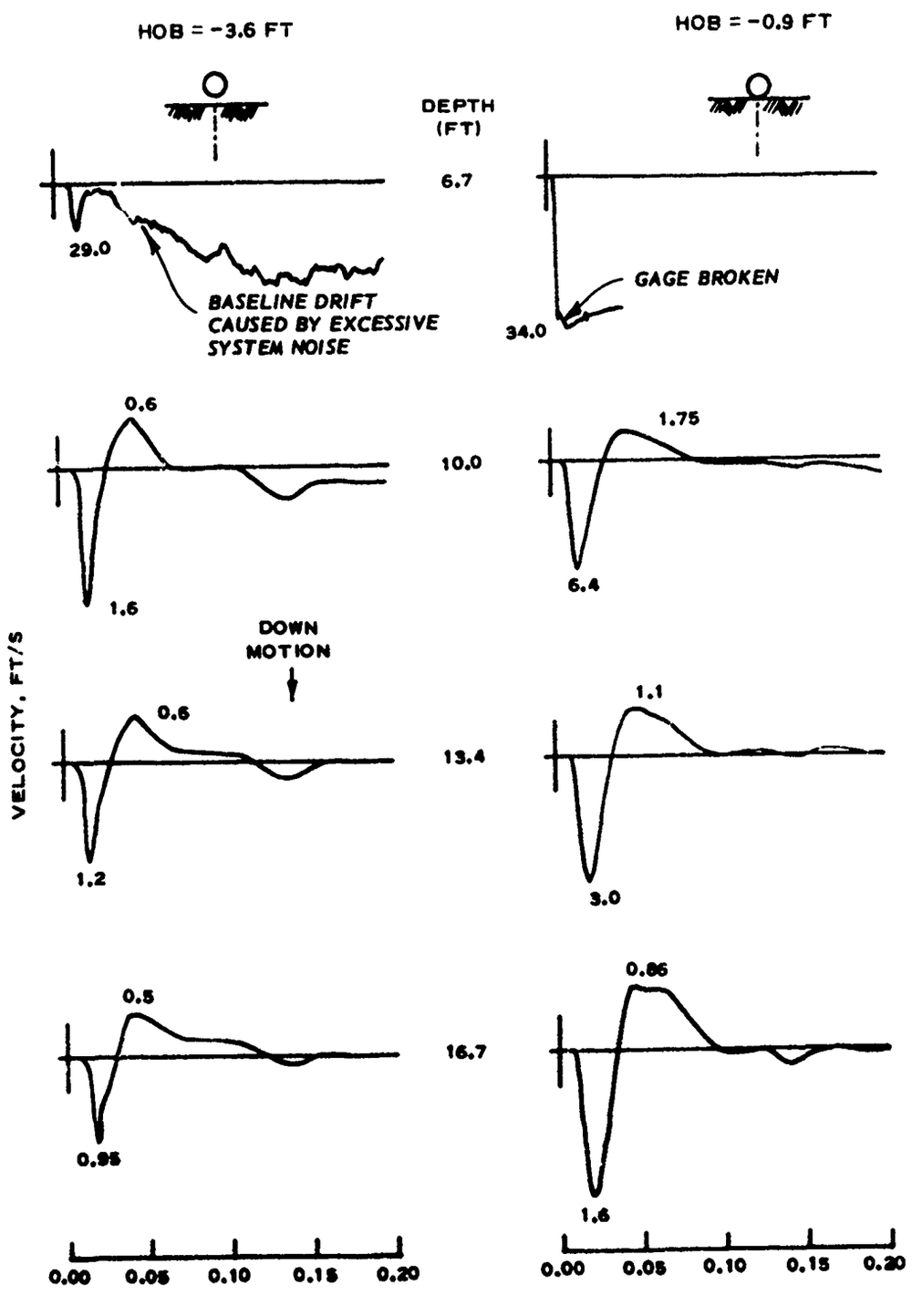

Figure 3.11 Comparison of velocity waveforms along the vertical radial directly beneath the explosion, Events 3 and 4.

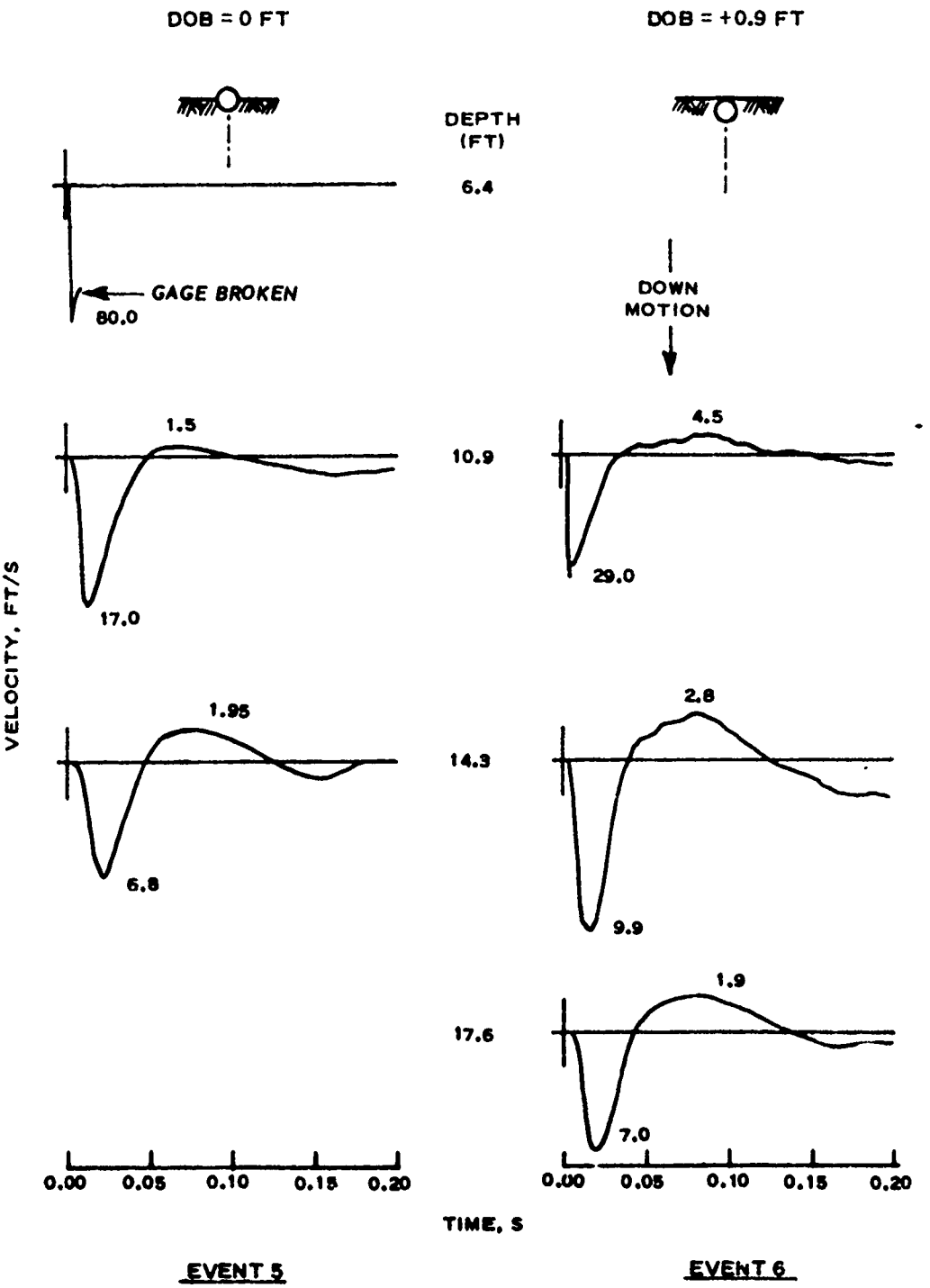

Figure 3.12 Comparison of velocity waveforms along the vertical radial directly beneath the explosion, Events 5 and 6.

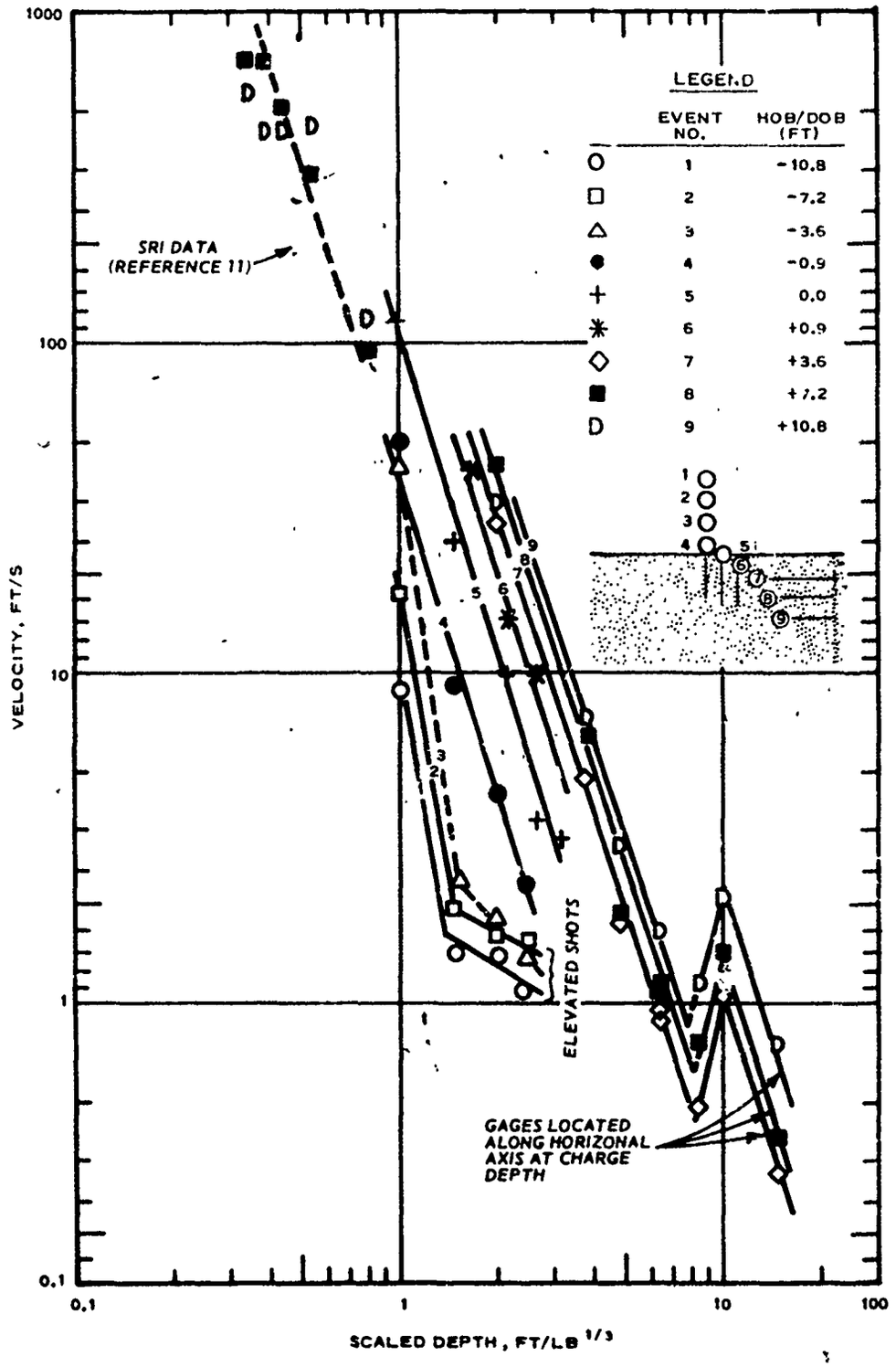

Figure 3.13 Peak radial particle velocity directly beneath and horizontally on-axis with the explosion as a function of scaled depth.

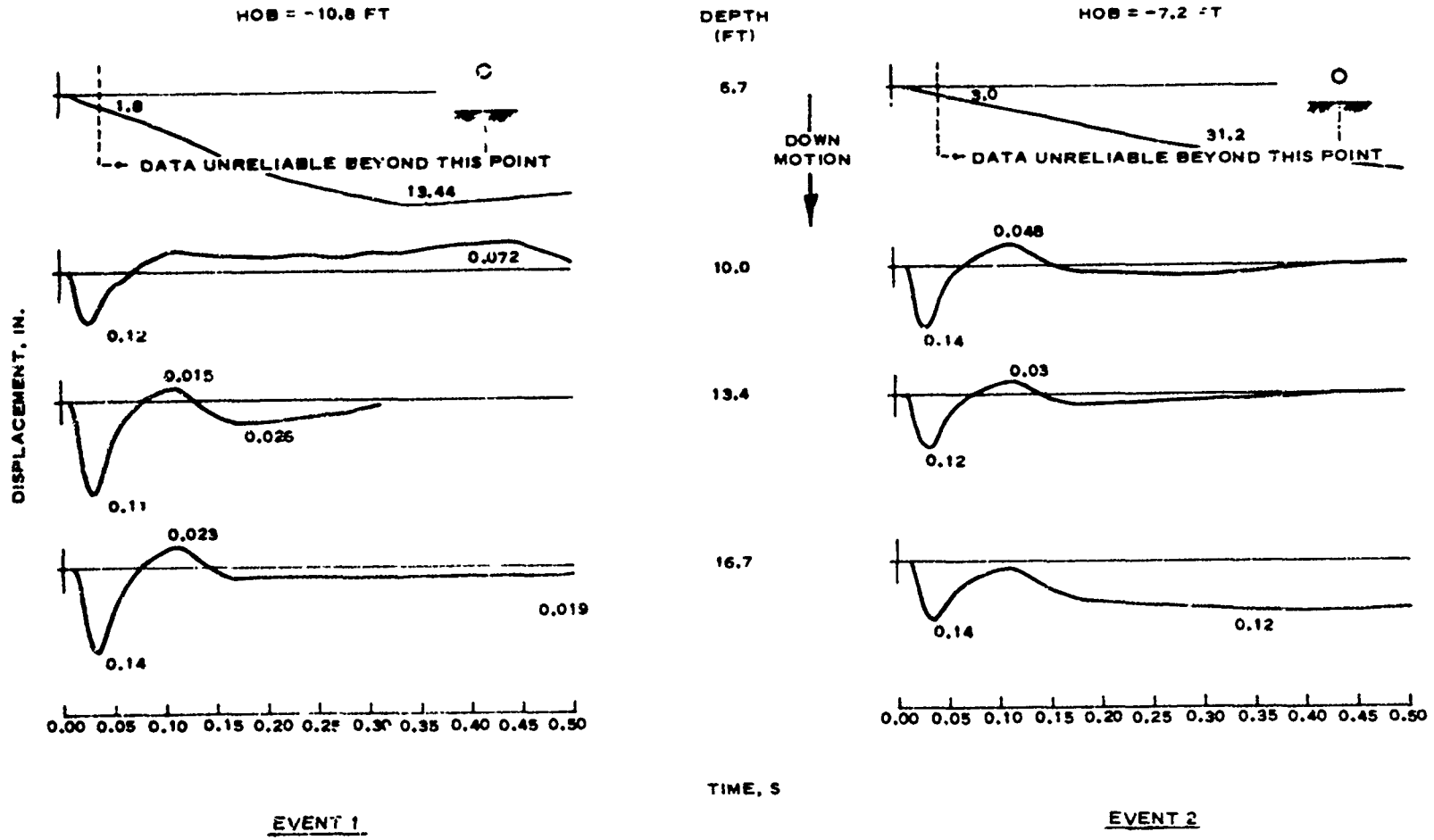

Figure 3.14 Comparison of displacement waveforms along the vertical radial directly beneath the explosion, Events 1 and 2.

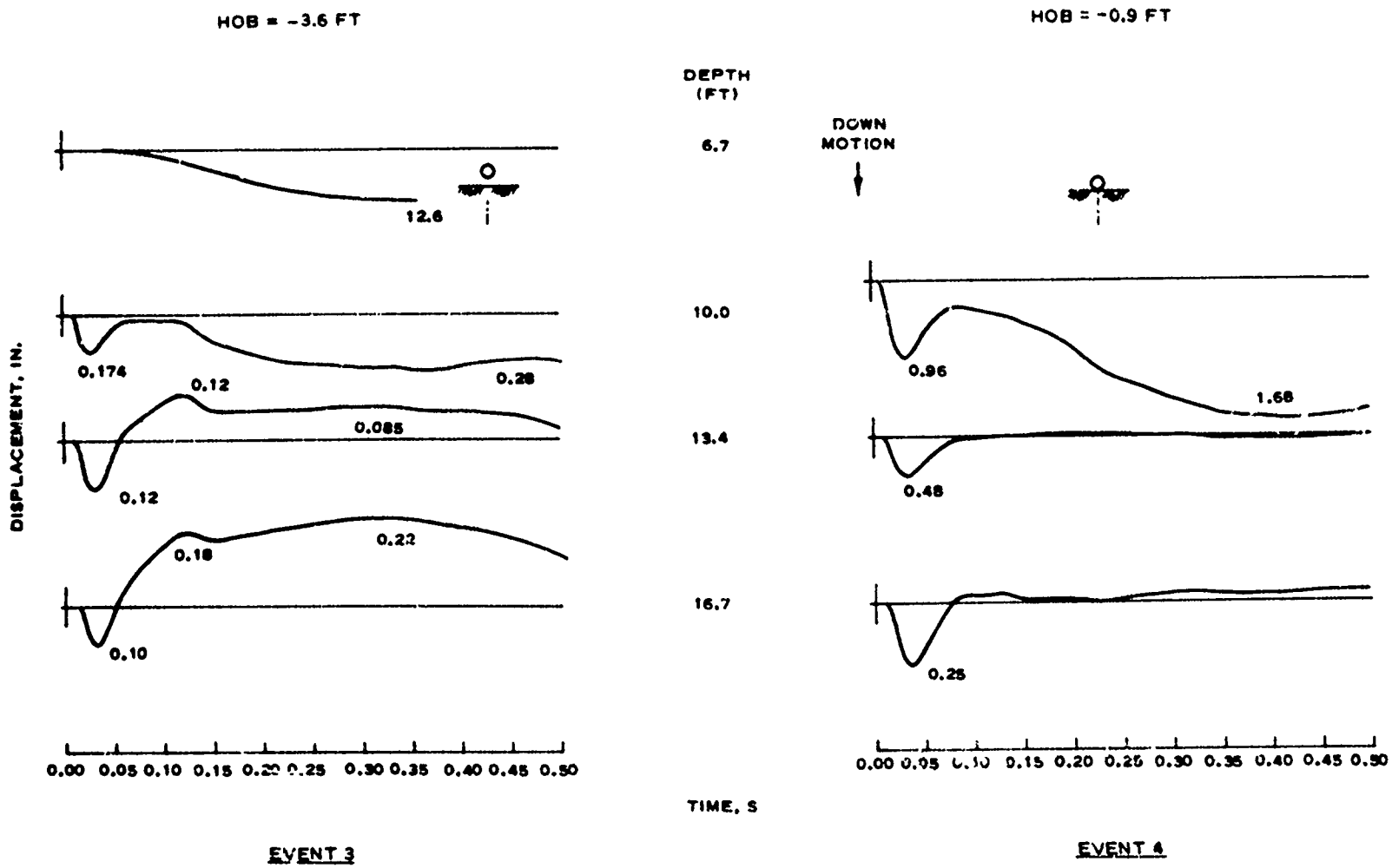

Figure 3.15 Comparison of displacement waveforms along the vertical radial directly beneath the explosion, Events 3 and 4.

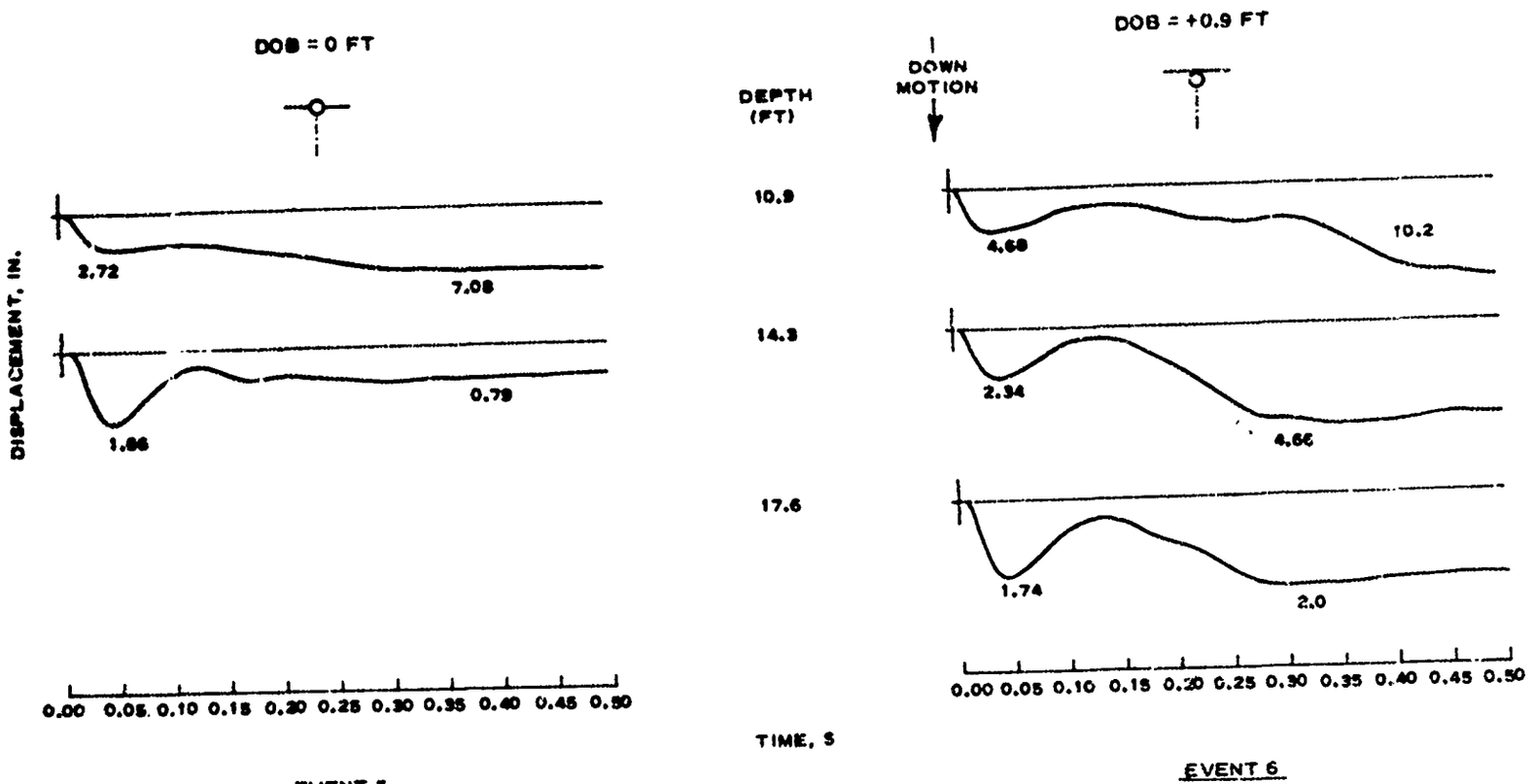

Figure 3.16 Comparison of displacement waveforms along the vertical radial directly beneath the explosion, Events 5 and 6.

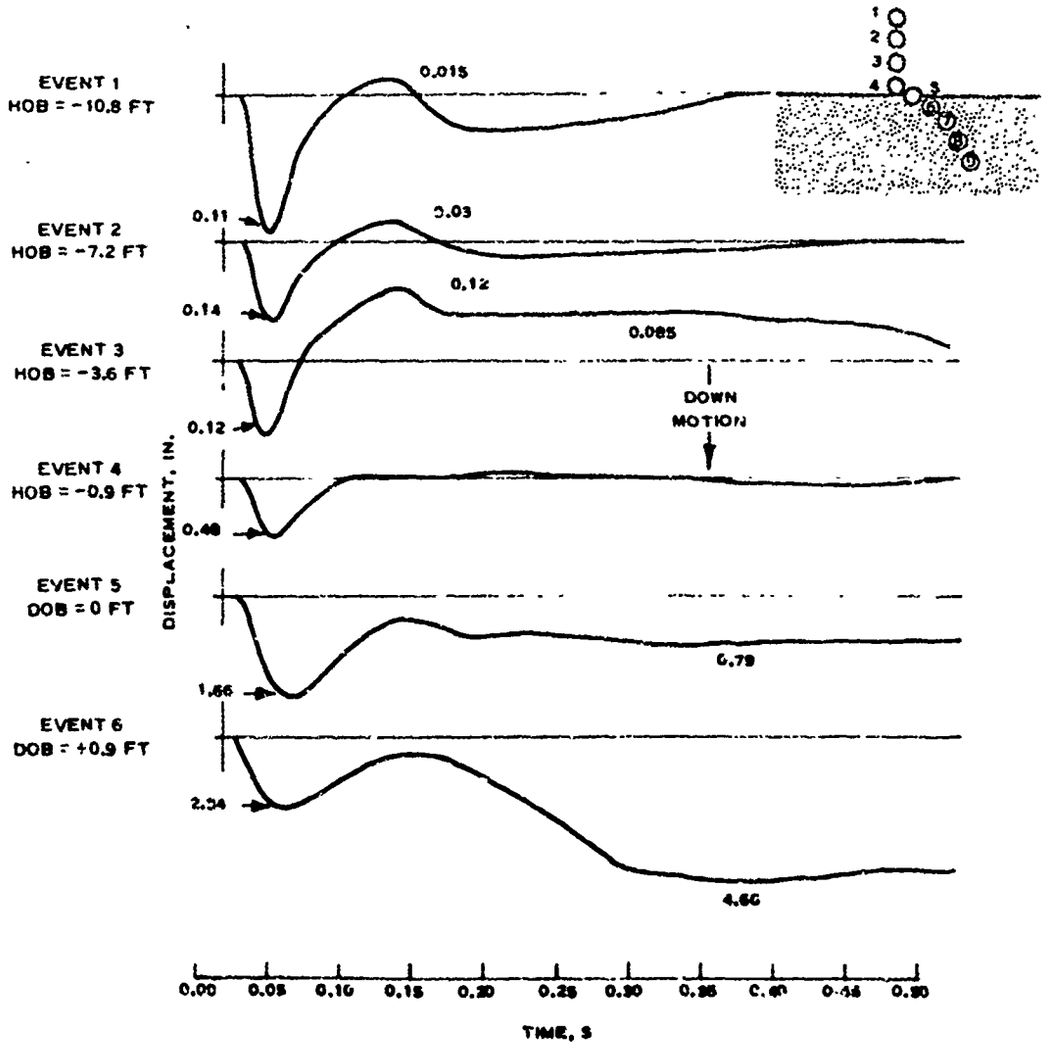

Figure 3.17 Comparison of vertical displacement waveforms at a common depth (nominally 14 ft) directly beneath the explosion.

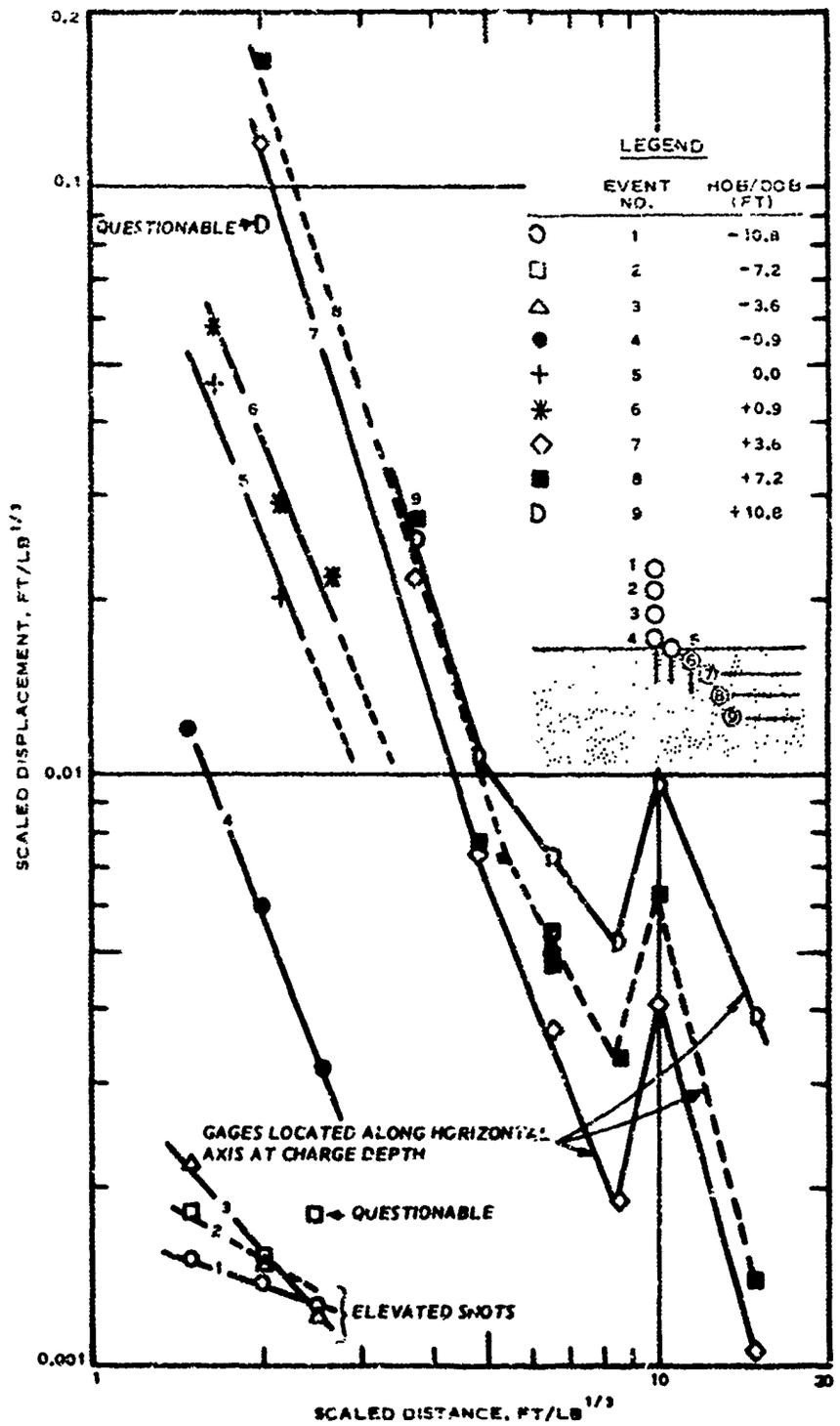

Figure 3.18 Scaled peak radial transient displacement directly beneath and horizontally on-axis with the explosion as a function of scaled distance.

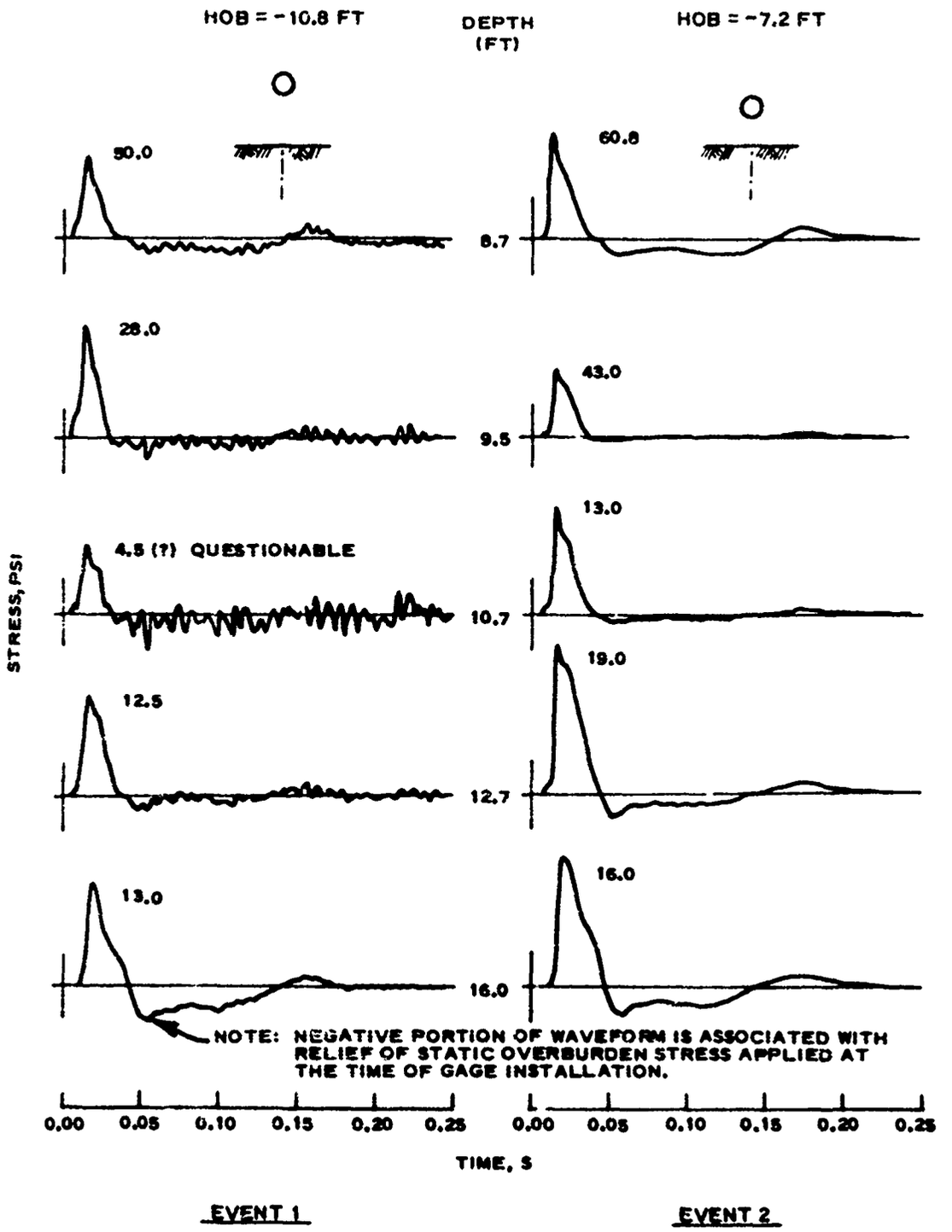

Figure 3.19 Comparison of stress waveforms along the vertical radial directly beneath the explosion, Events 1 and 2.

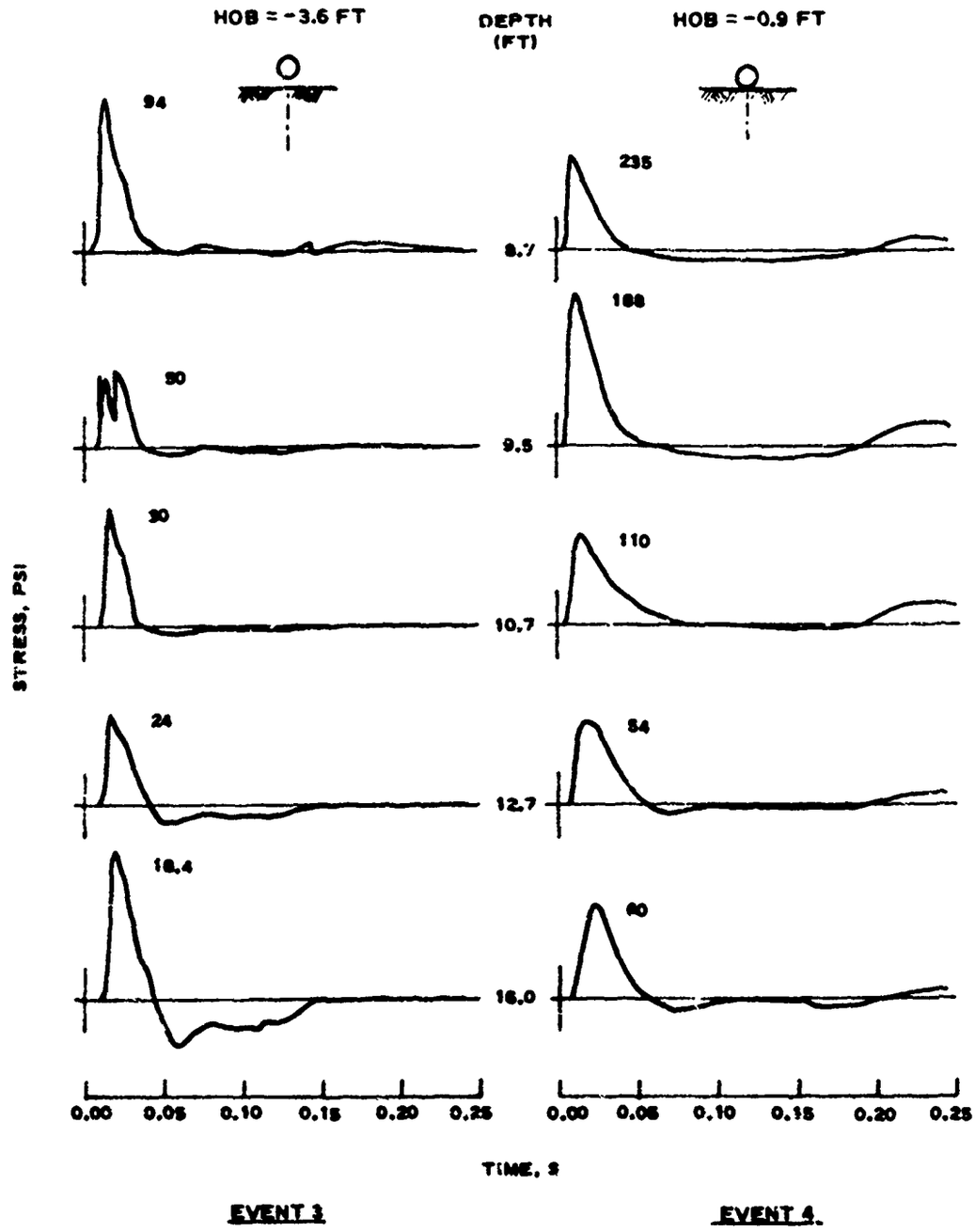

Figure 3.20 Comparison of stress waveforms along the vertical radial directly beneath the explosion, Events 3 and 4.

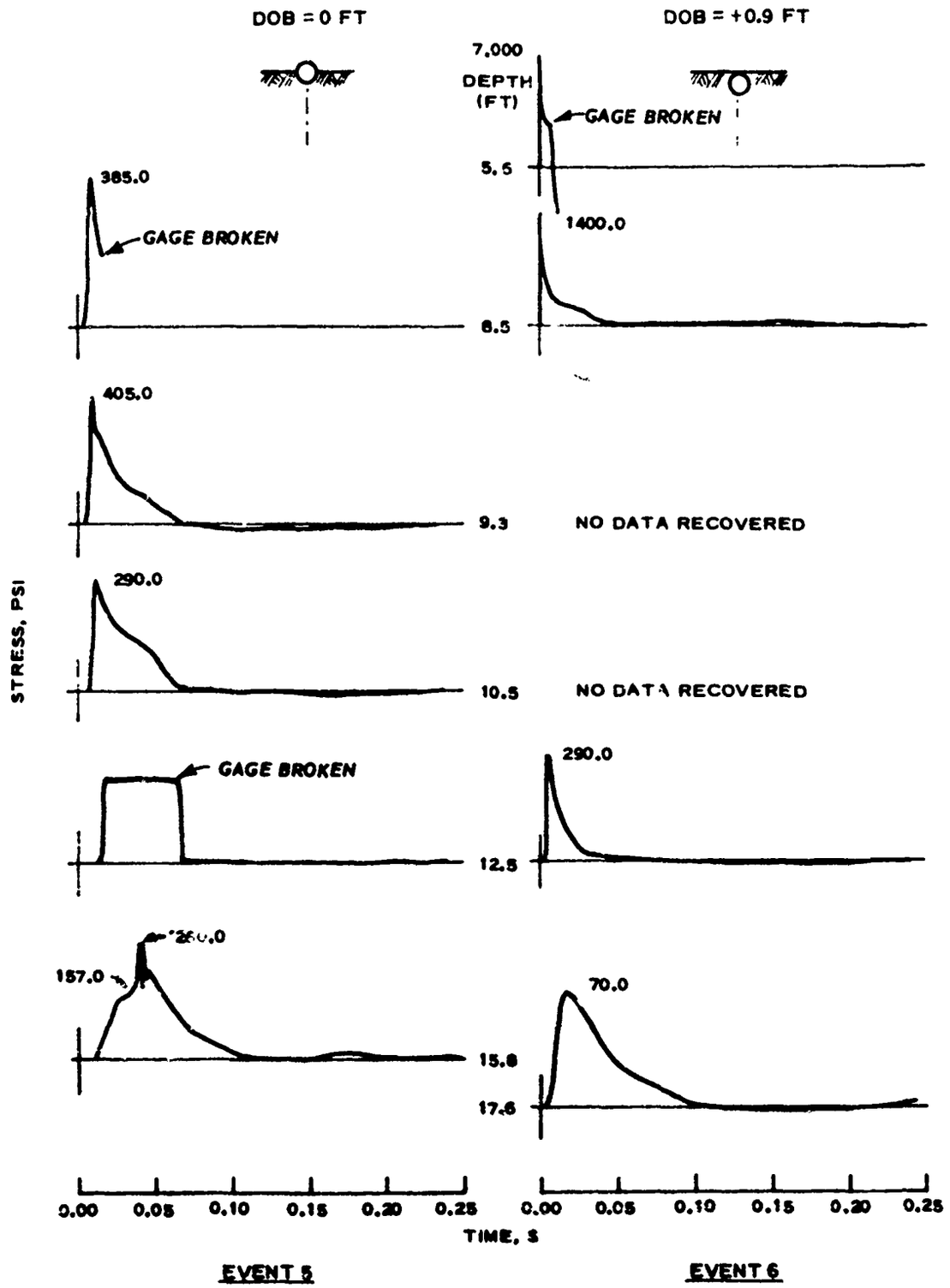

Figure 3.21 Comparison of stress waveforms along the vertical radial directly beneath the explosion, Events 5 and 6.

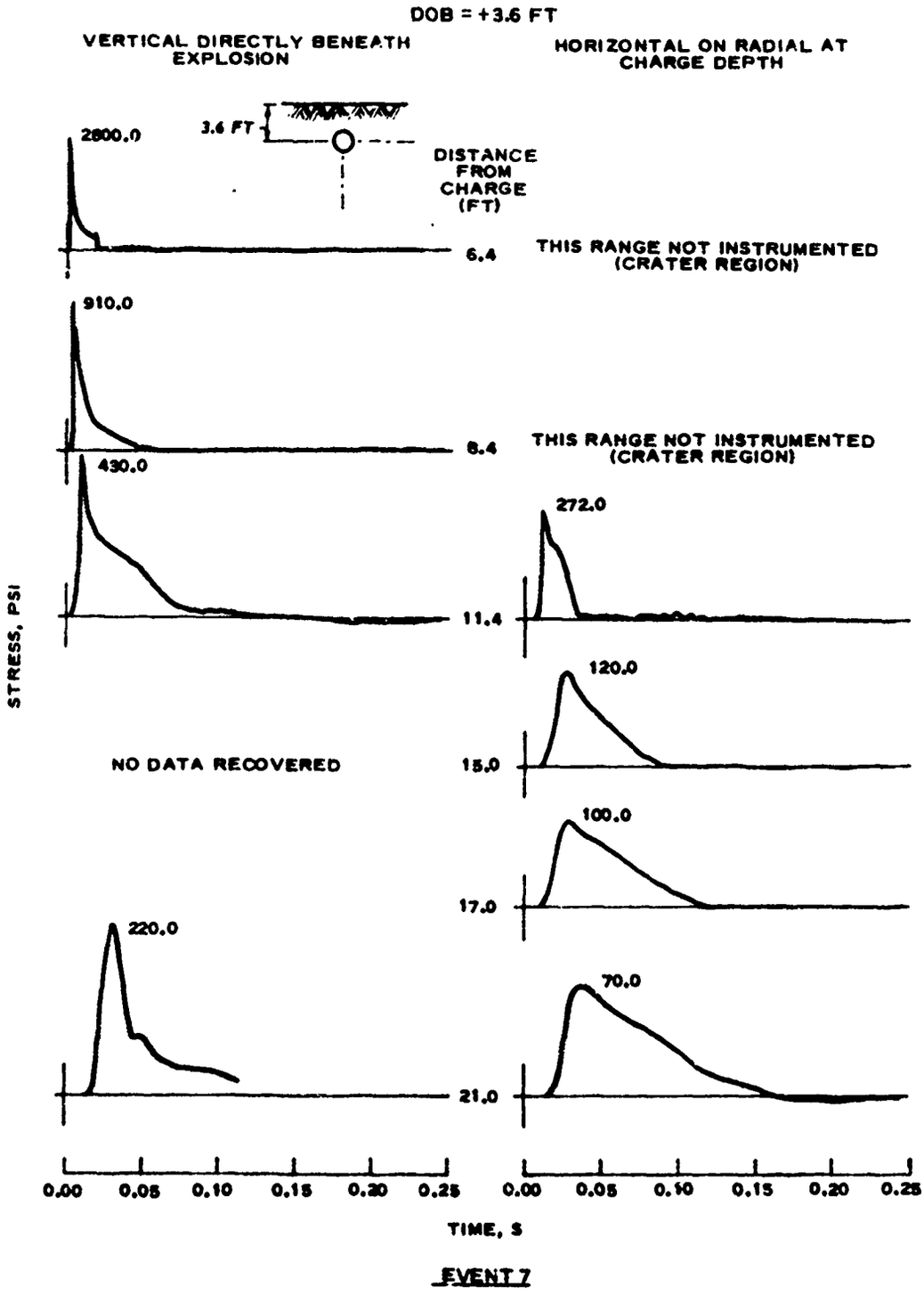

Figure 3.22 Comparison of stress waveforms on vertical axis directly beneath the explosion and along horizontal radial at charge depth, Event 7.

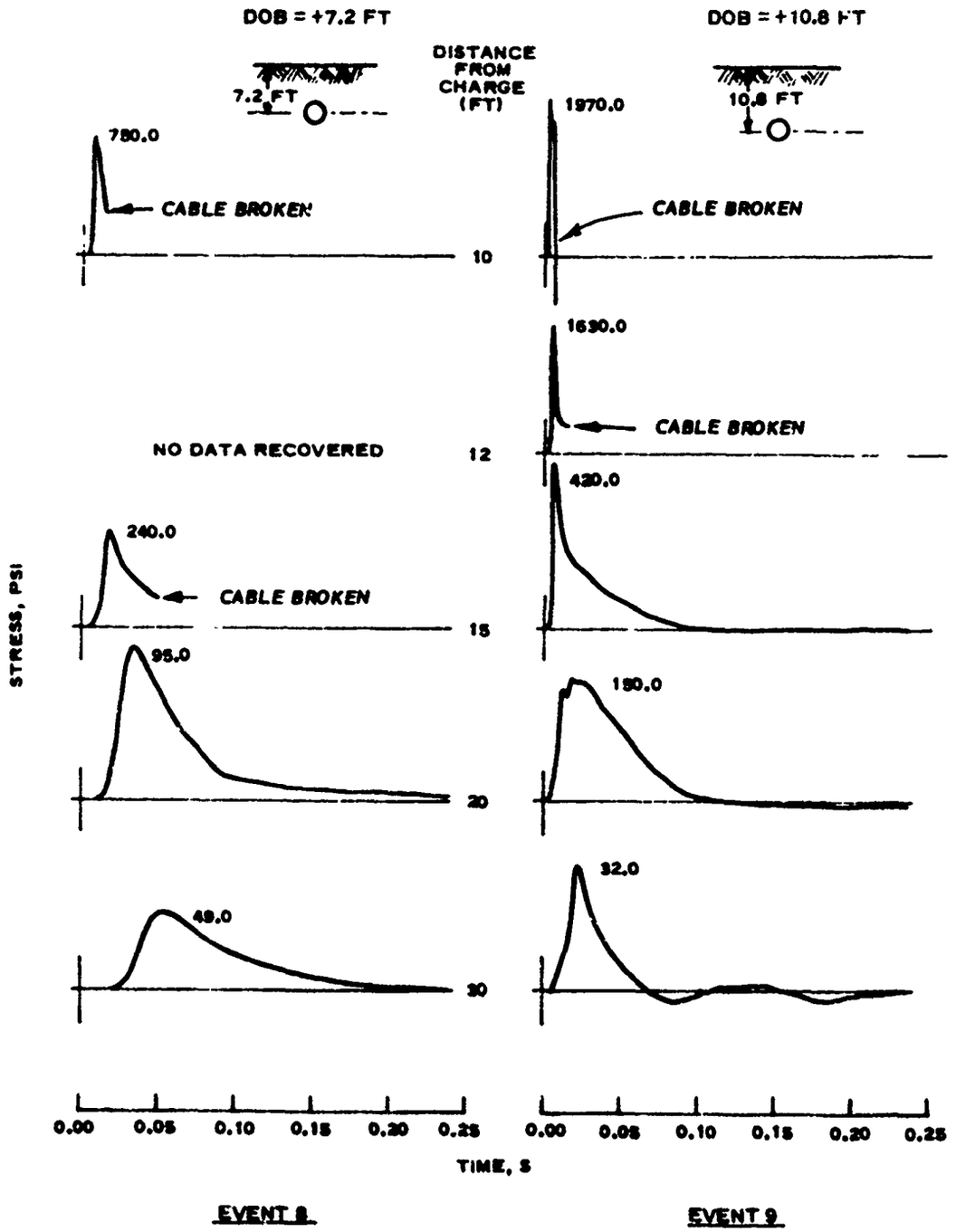

Figure 3.23 Comparison of stress waveforms along the horizontal radial at charge depth, Events 8 and 9.

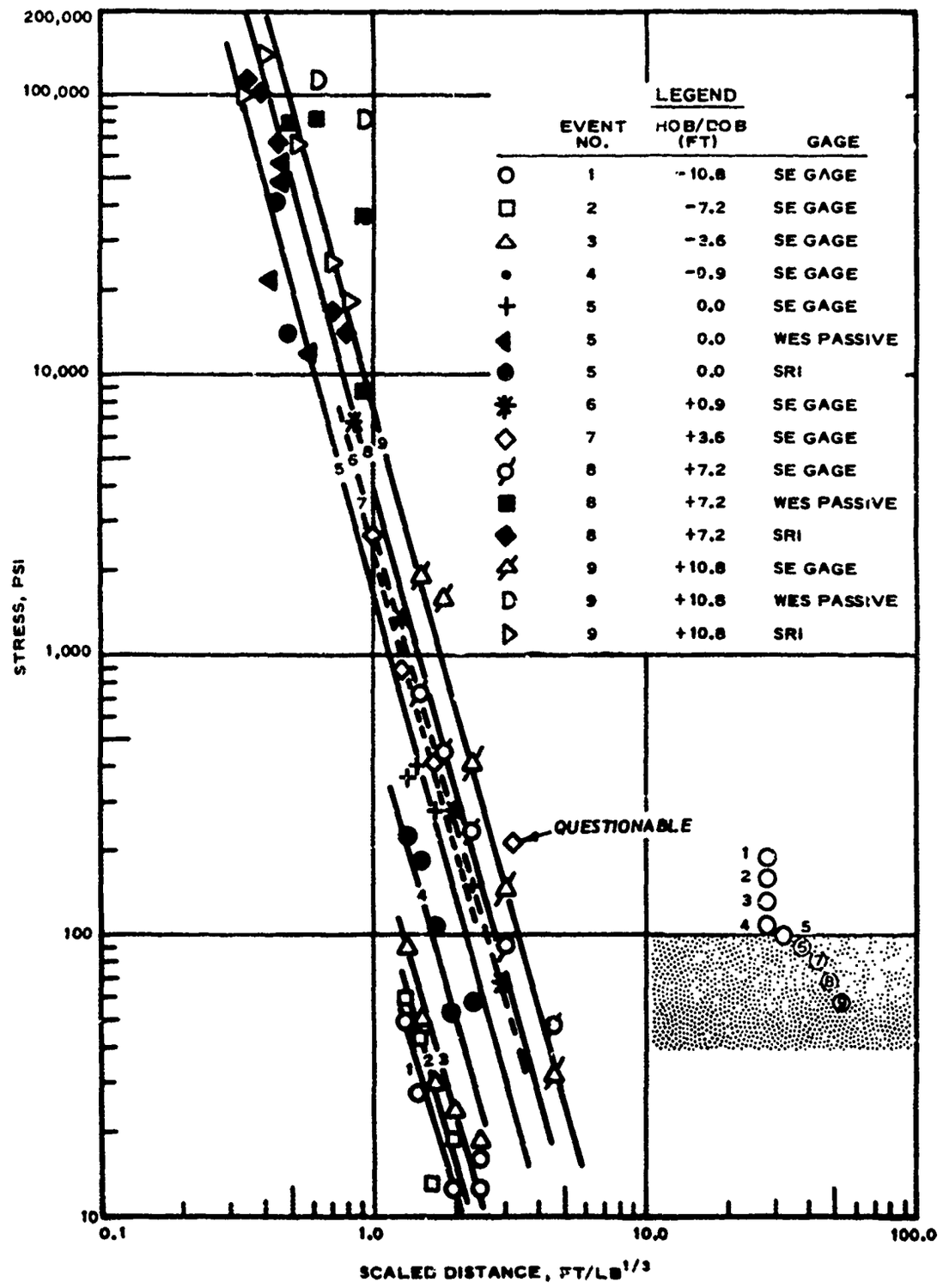

Figure 3.24 Peak radial stress as a function of scaled distance and burst position.

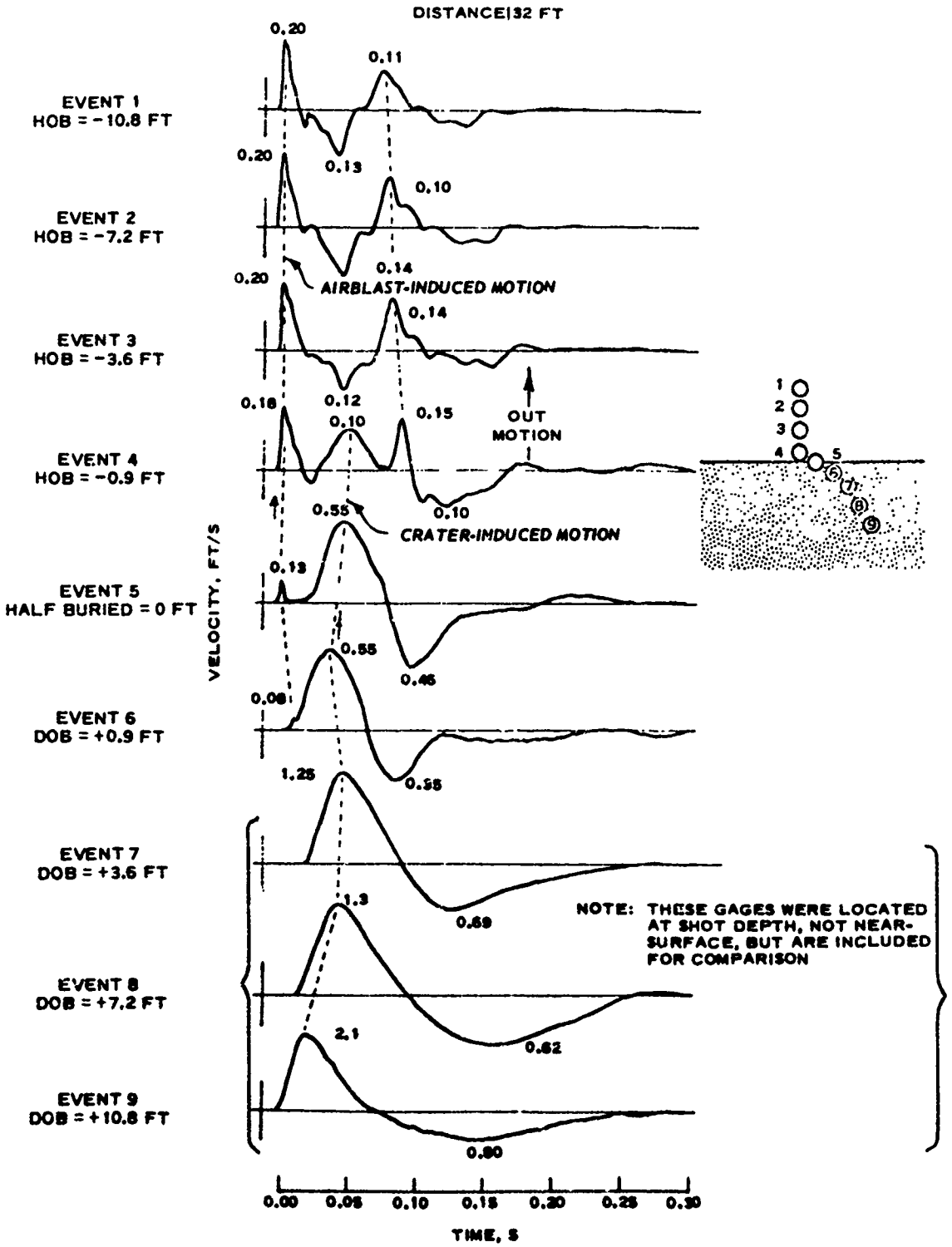

Figure 3.25 Near-surface horizontal particle velocity waveforms at 32-foot range.

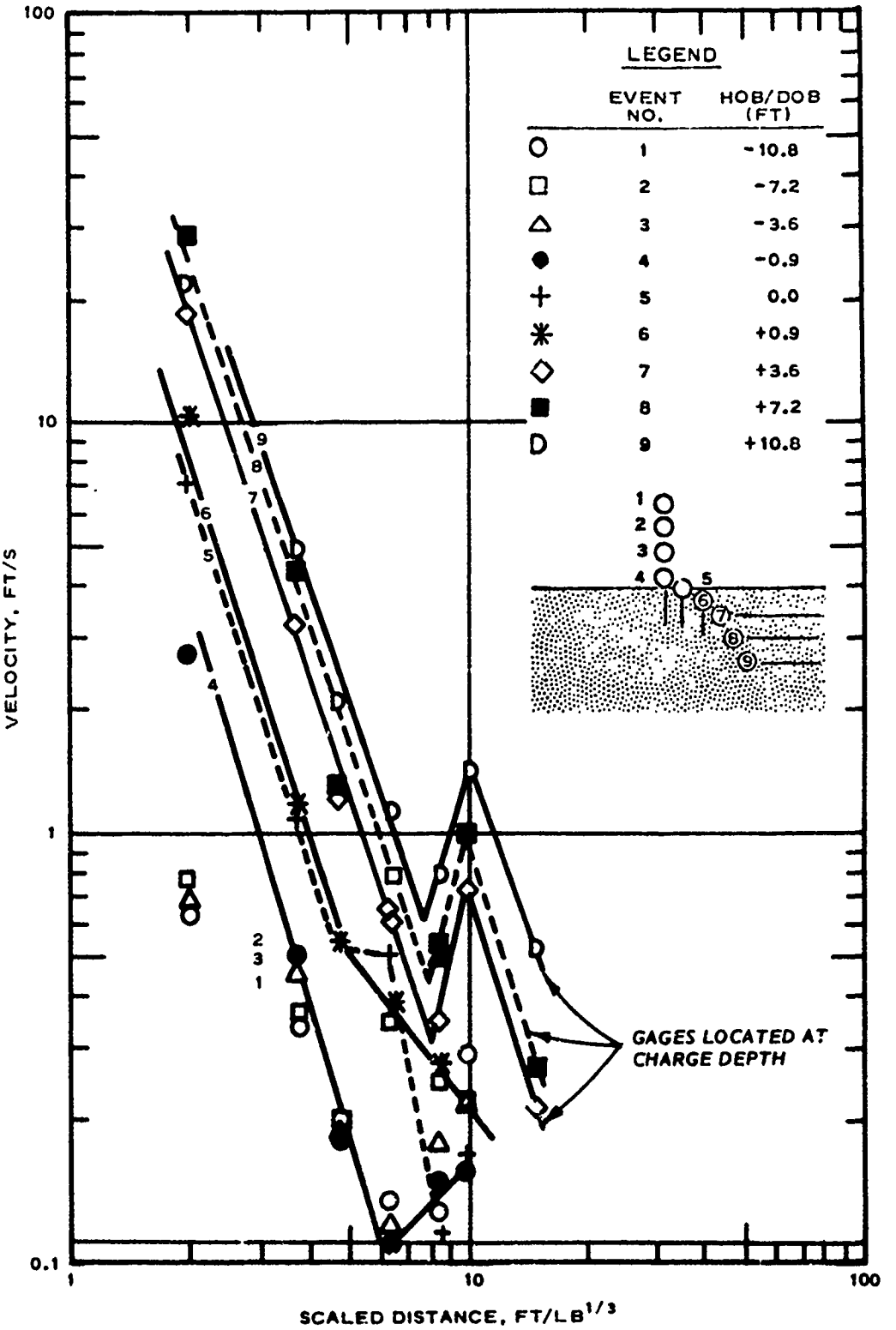

Figure 3.26 Peak outward near-surface horizontal particle velocity as a function of scaled distance.

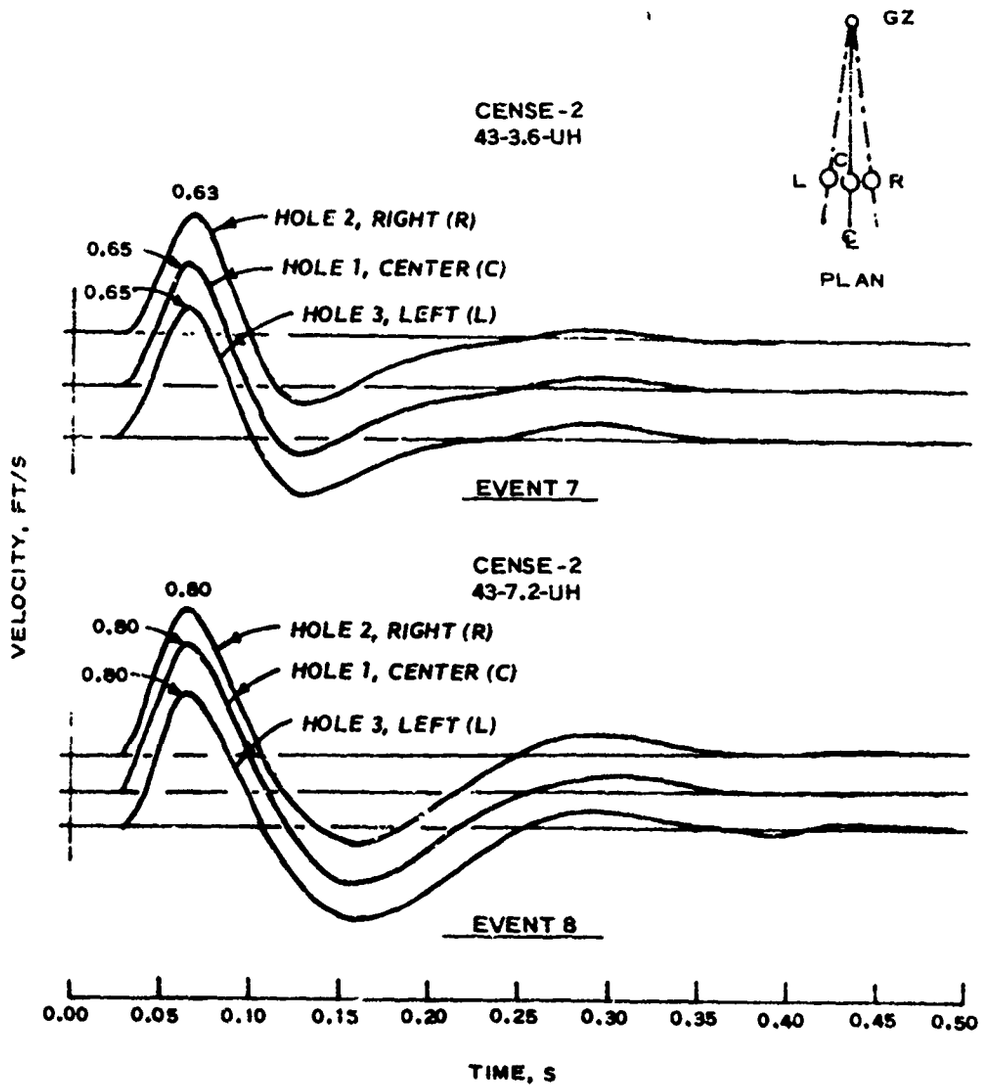

NOTE: HOLE 1 – CANISTER GROUTED TO TOP OF BOREHOLE WITH SOIL MATCHING GROUT.

HOLE 2 – CANISTER GROUTED IN BOTTOM OF HOLE, ONLY BOTTOM 2 IN. OF CANISTER GROUTED. ONE-FOOT SAND BACKFILL. REMAINDER OF INSTRUMENT HOLE LEFT OPEN.

HOLE 3 – CANISTER GROUTED IN BOTTOM OF HOLE, ONLY BOTTOM 2 IN. OF CANISTER GROUTED. NO BACKFILL MATERIAL. HOLE LEFT OPEN.

Figure 3.27 Placement effect study.

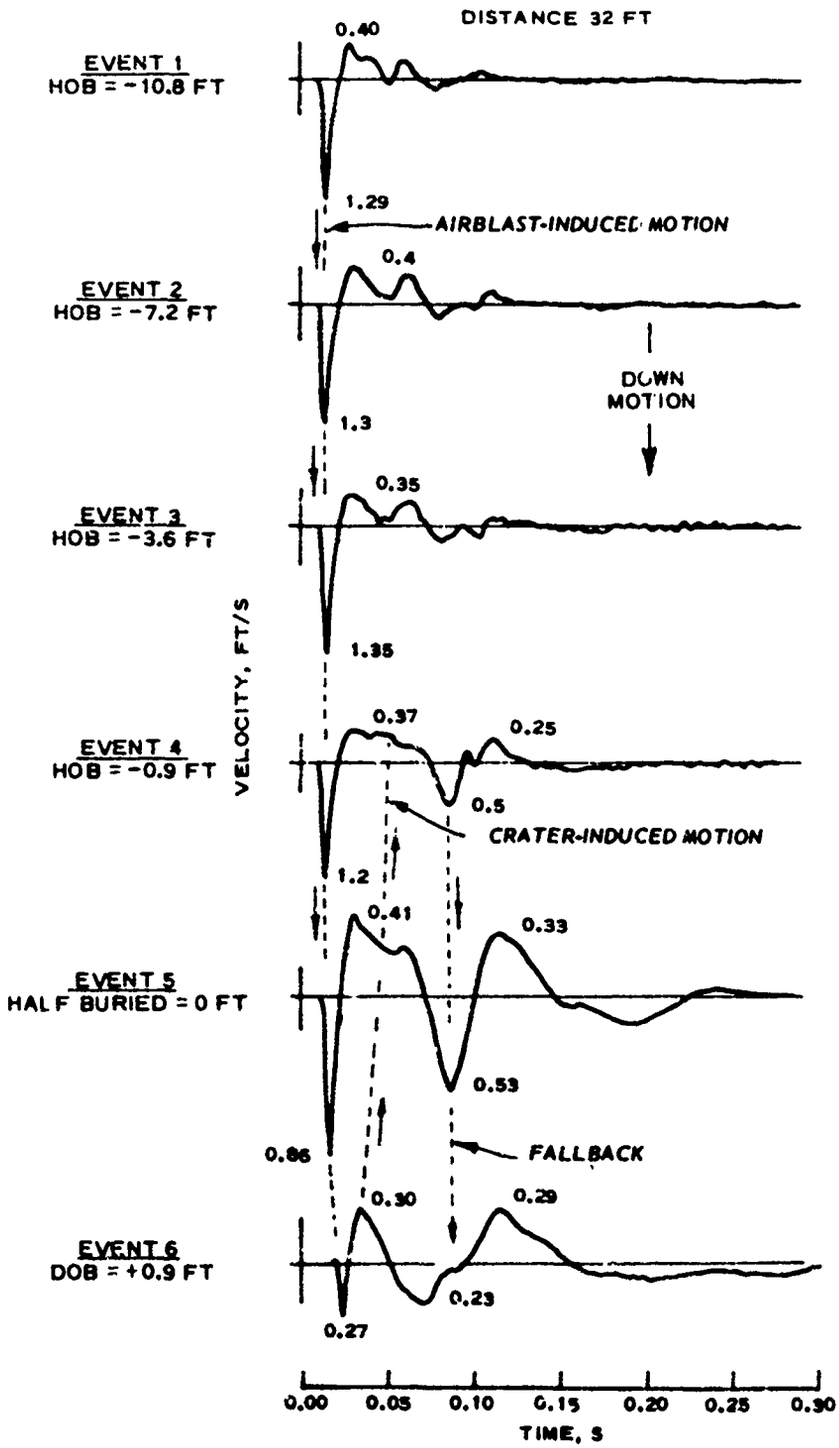

Figure 3.28 Near-surface vertical particle velocity waveforms at 32-foot range.

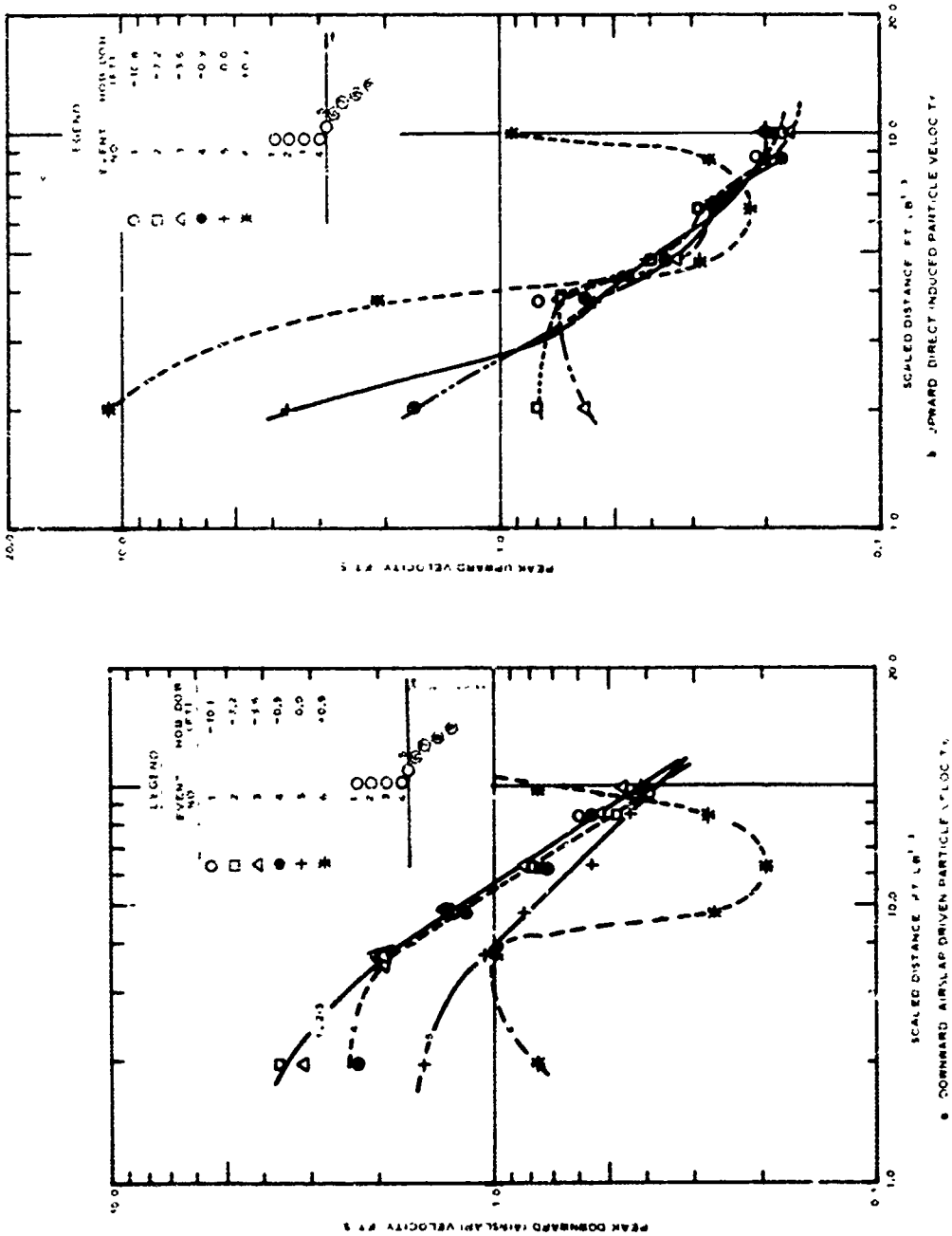

Figure 3.29 Peak vertical near-surface particle velocity as a function of scaled distance and burst position.

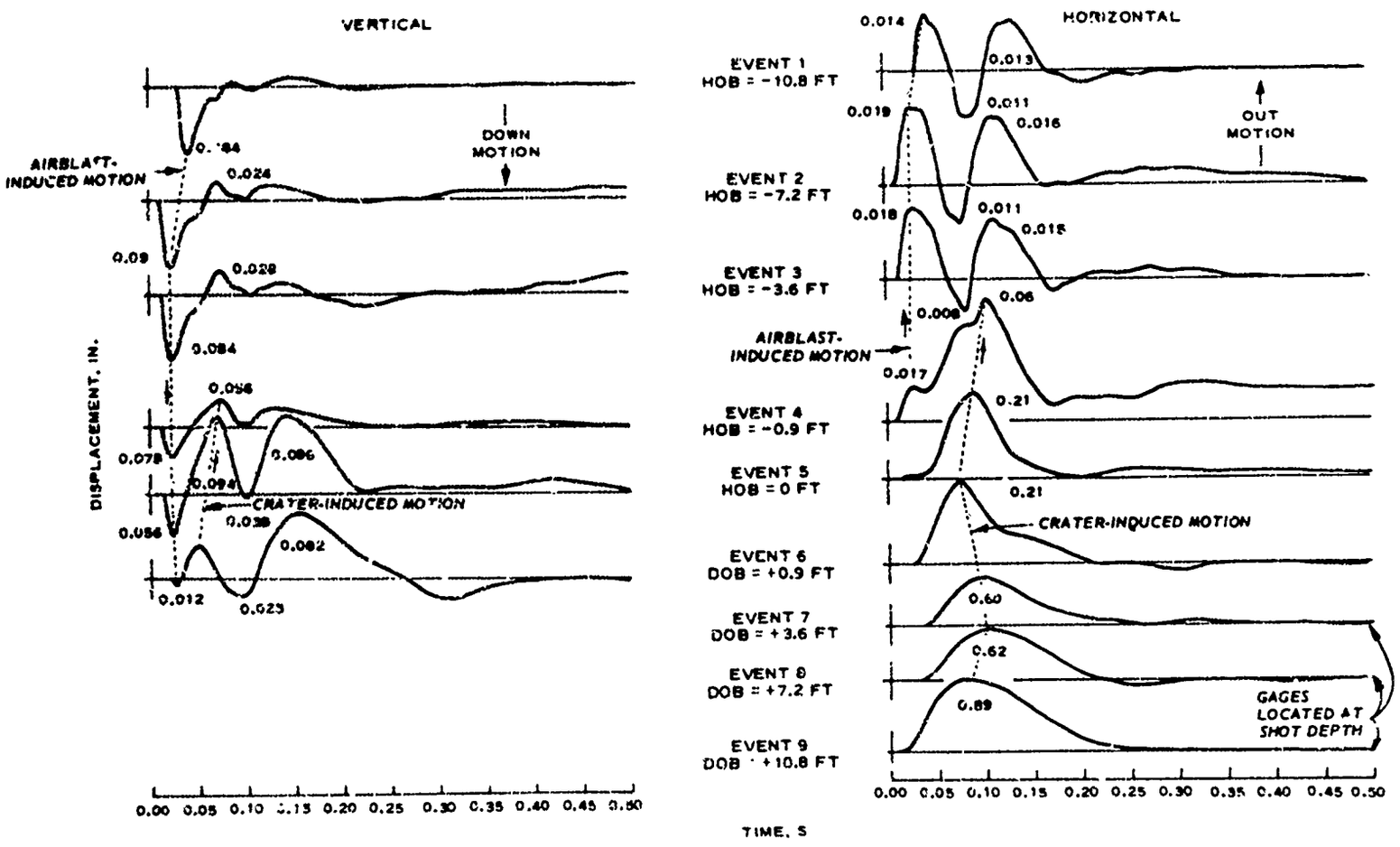

Figure 3.30 Near-surface vertical and horizontal displacement waveforms at 32-foot range.

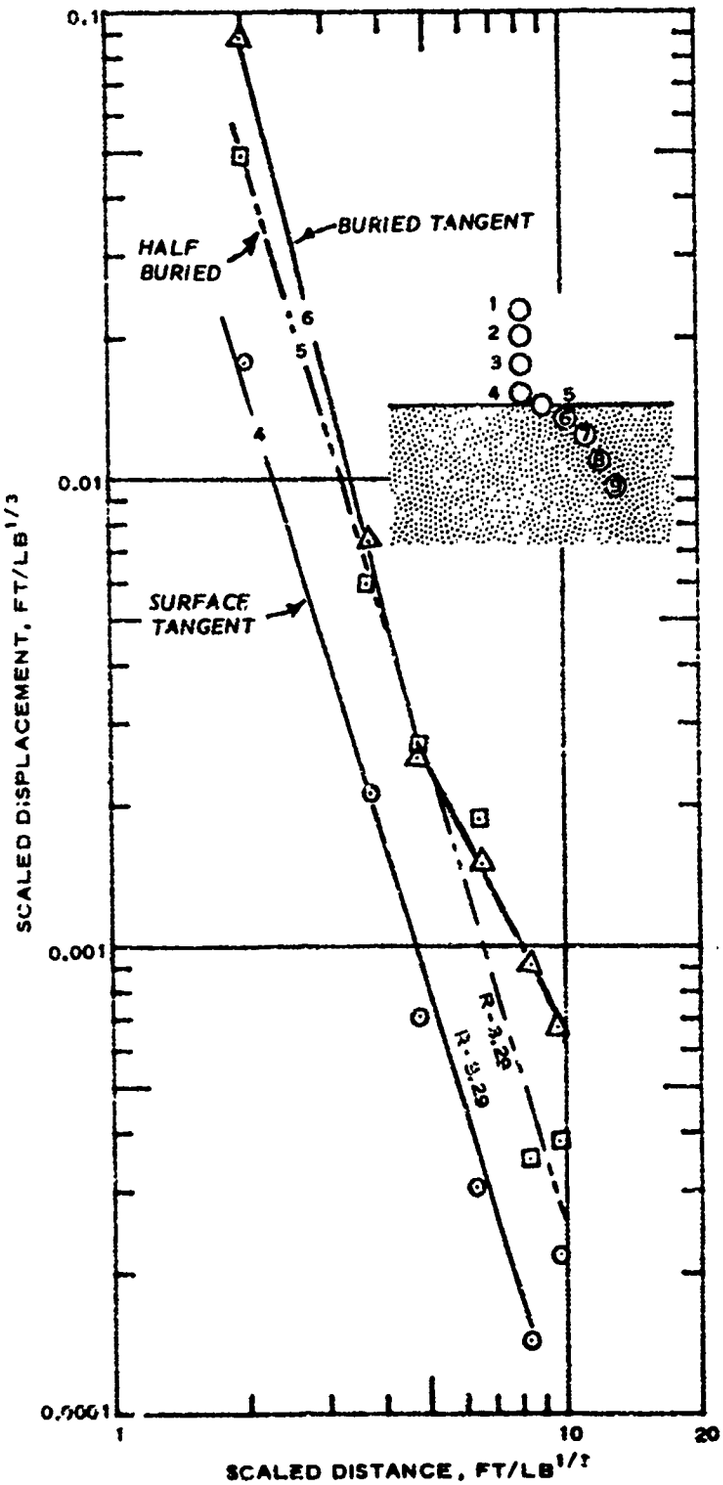

Figure 3.31 Scaled peak outward near-surface horizontal displacement versus scaled distance as a function of burst position, Events 4, 5, and 6.

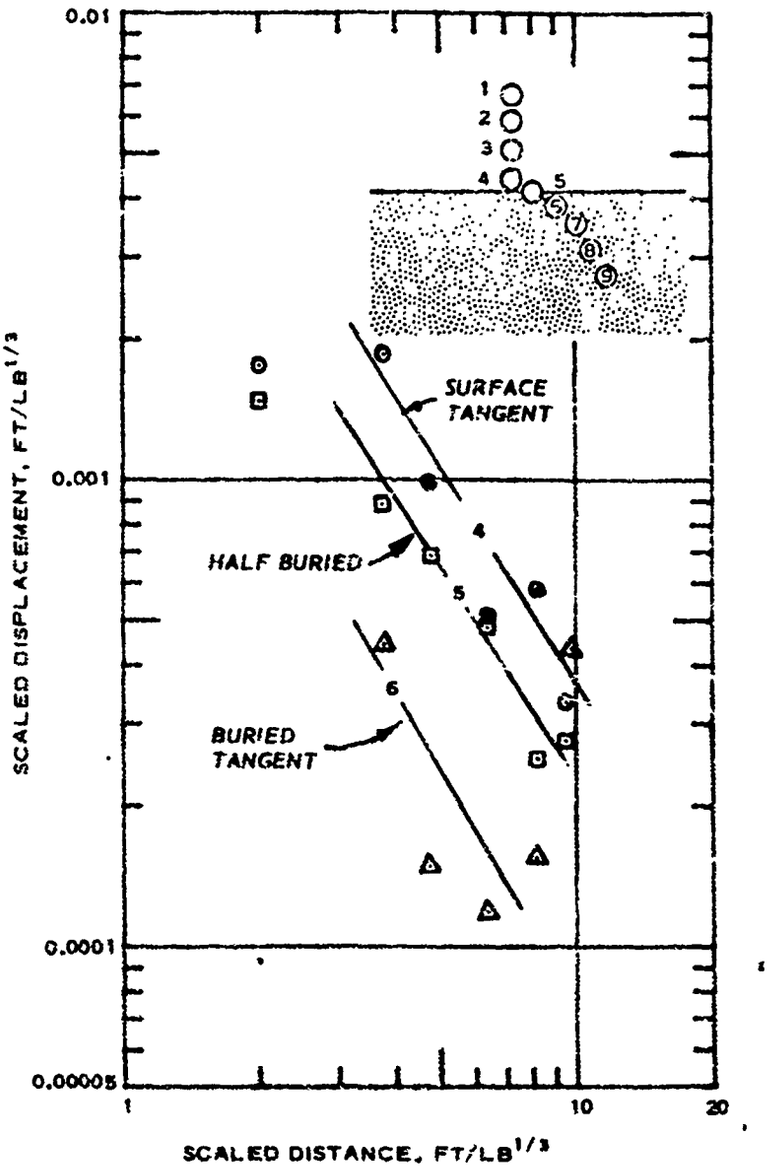

Figure 3.32 Scaled peak downward airslap-driven near-surface vertical displacement versus scaled distance as a function of burst position, Events 4, 5, and 6.

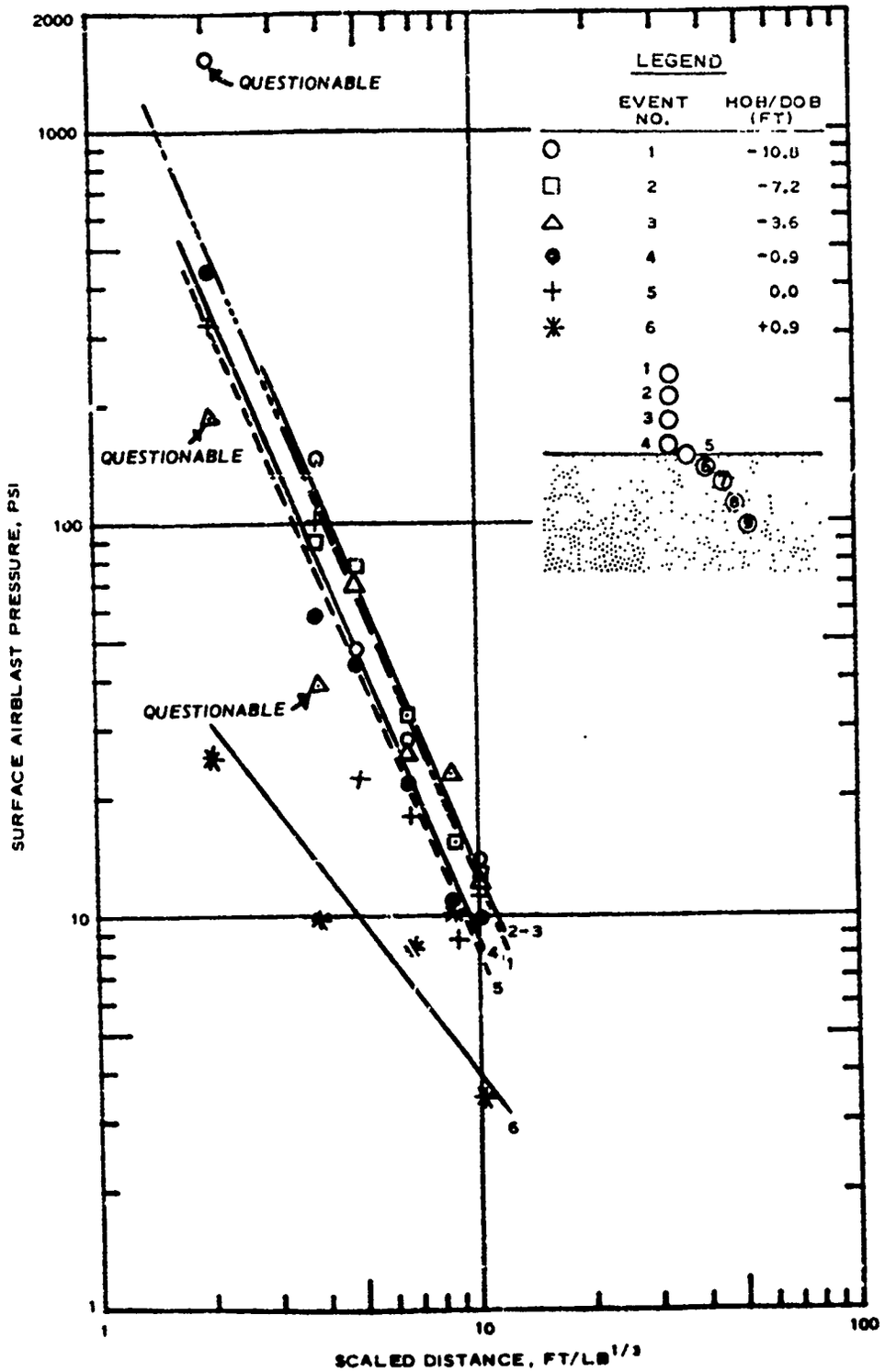

Figure 3.33 Peak surface airblast pressure versus scaled distance.

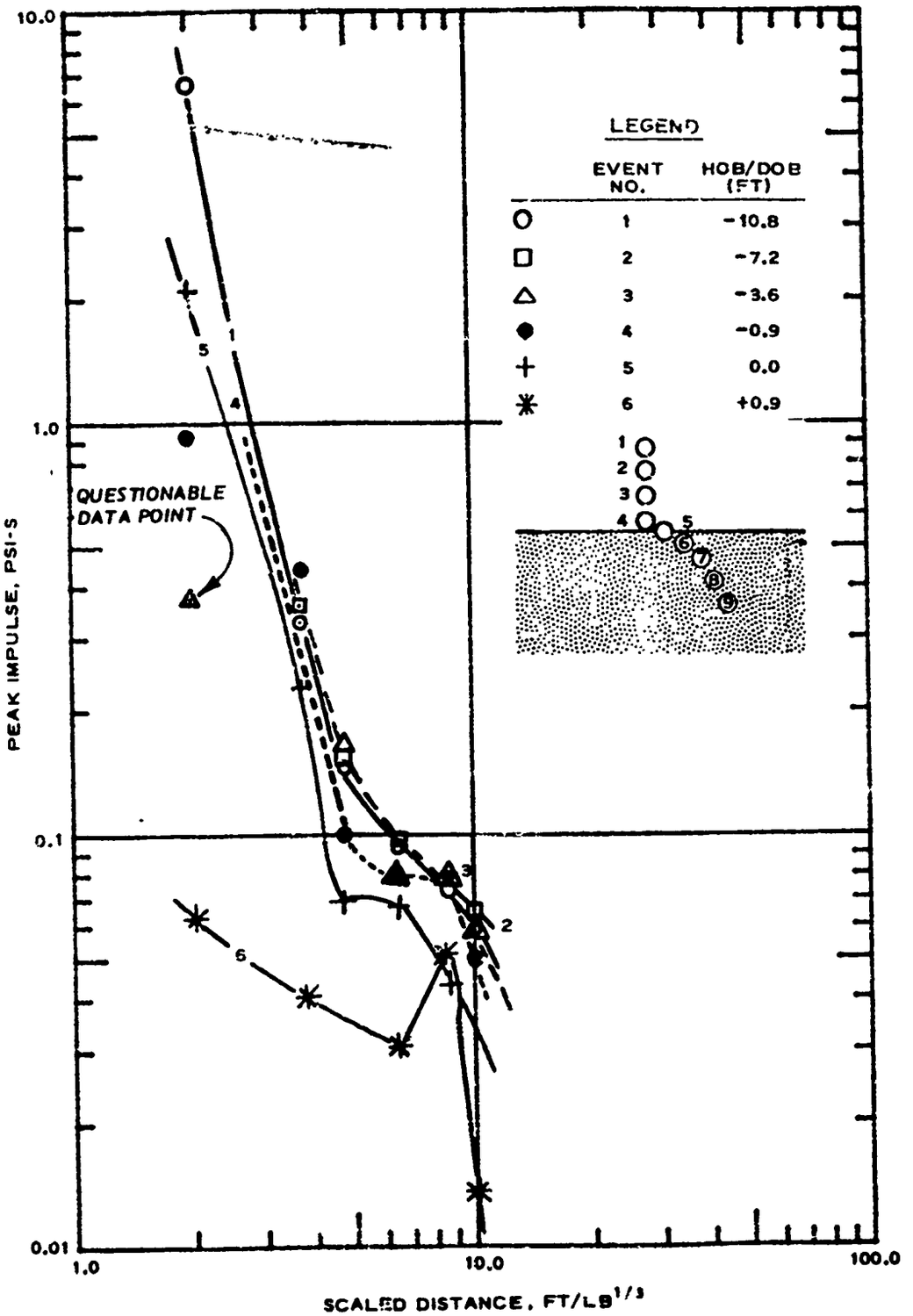

Figure 3.34 Peak surface airblast pressure impulse versus scaled distance.

CHAPTER 4

OBSERVATIONS AND RECOMMENDATIONS

4.1 OBSERVATIONS

This chapter presents pertinent observations from the CENSE 2 experiment. Detailed conclusions will be appropriately treated in Report 4 of this series, "Analysis and Summary of CENSE Data."

The primary objective of the CENSE 2 program was to determine the influence of burst position on ground shock and stress in a uniform soil. Airblast and cratering were of secondary interest. Particular emphasis was placed on measurements directly beneath the explosion and horizontally on-axis at charge depth. The objectives were achieved. Excellent quality ground motion and stress data were recorded.

The CENSE HOB/DOB experiment concept has provided critical insight into the shock physics and wave propagation in the region directly beneath an explosion detonated in both rock and soil. The information retrieved has already had major impact on weapons effects tests design and hardness assessments.

4.1.1 Cratering

No craters were produced by the airbursts, Events 1, 2, and 3. Only apparent craters were measured. The apparent craters behaved in a consistent fashion with size increasing with DOB. Although the optimum DOB was not achieved in this test series, it is believed to occur at a scaled depth of approximately $1.75\ W^{1/3}$ (11.7 feet), where the apparent cratering efficiency is estimated to be at least 10.3 ft^3/lb. A comparison of the apparent cratering efficiencies shows about 12 percent of optimum for the surface burst (half buried) and 3.8 percent for the tangent sphere (surface).

4.1.2 Airblast

The airblast suppression (enhancement) was strongly influenced by the burst position in the region HOB = $3.6\ W^{1/3}$ to DOB = $0.45\ W^{1/3}$.

For HOB's higher than $3.6\ W^{1/3}$, the enhancement asymptotically approached a maximum value 2.4 times the value of the free-air condition. Suppression was substantial and increased almost linearly for burst positions from surface tangent to buried tangent.

4.1.3 Ground Shock

4.1.3.1 WAVE SPEED. The compressional wave propagated downward directly beneath the explosion at a velocity of 3000 ft/s. Propagation speed along the near-surface horizontal radial averaged 1800 ft/s. Outrunning ground motion was first observed on the half buried detonation (Event 5), at a horizontal range of 58 feet. The initial compression wave propagated at an average velocity of 1500 ft/s along the horizontal radial located at shot depth for the buried detonations (Events 7, 8, and 9). A break in the slopes of the arrival time curves for these shots indicated a reflected wave from a higher seismic layer located approximately 14 feet below the ground surface and propagating at a velocity of 2700 ft/s. The higher seismic velocity of the deep layer is attributed primarily to an increase in water content.

4.1.3.2 ACCELERATION MEASUREMENTS. Burst position significantly influenced acceleration measured directly beneath the explosion. Peak amplitudes increased rapidly with increasing charge DOB. Peak downward acceleration from the buried tangent detonation was 36 times that from the surface tangent detonation.

4.1.3.3 PARTICLE VELOCITY. Significant increases in particle velocity directly beneath the explosion occurred for progressive charge burial within the soil. Maximum particle velocity directly beneath the explosion was measured on the buried tangent (Event 6) detonation, which was some 4.9 times greater than that produced from the surface tangent detonation. Although no motion measurements were made directly beneath the explosion for the deeper buried shots (Events 7, 8, and 9), measurements were made along a horizontal radial at shot depth. These measurements are believed to have been deep enough to have been free from surface effects at scaled distances less than $10\ W^{1/3}$ (67 feet) and,

therefore, can be compared with the measurements directly beneath the explosions. Measured particle velocities attenuated at the same rate for both data sets and showed a progressive increase in velocity. Maximum particle velocities from the deepest detonation (10.8 feet) were 11 times greater than those from the surface tangent detonation. A velocity "jump" or enhancement (factor of 5) was observed on these shots at a scaled distance of $10\ W^{1/3}$ (67 feet). This enhancement is thought to be associated with development of, and interaction with, a surface wave at this distance. No significant differences were observed in the shape of the velocity waveforms.

Near-surface horizontal particle velocity was dominated by the surface airblast for the elevated and surface tangent detonations. Direct-induced energy dominated the horizontal velocity for all deeper buried detonations. Peak horizontal particle velocity from the buried tangent detonation was 2.3 times greater than that from the surface tangent detonation. Horizontal velocity from the deepest detonation (10.8 feet) was 17 times greater than that from the surface tangent detonation.

Surface airblast dominated the near-surface vertical particle velocity for the elevated through half buried detonations (Events 1 through 5), except the 13.4-foot distance position on Event 5. Upward, direct-coupled energy dominated the near-surface vertical velocity on the buried tangent shot (Event 6). No vertical measurements were made on the buried shots (Events 7 through 9). Peak downward velocity decreased with decreasing HOB. This reduction was most apparent at scaled distances less than $3.5\ W^{1/3}$. Beyond this distance the curves tended to converge. Upward velocity showed a similar effect but with amplitudes increasing with decreasing HOB. Vertical velocity response from the buried tangent detonation was unique. Both downward and upward velocity-distance curves reached minima at a scaled distance of $6.4\ W^{1/3}$ (43 feet), with amplitudes increasing beyond this distance.

4.1.3.4 DISPLACEMENT. Vertical displacement directly beneath the explosion was greatly influenced as was the vertical particle velocity. Maximum downward displacement produced by the buried tangent detonation

was 6.6 times that from the surface tangent detonation. Maximum displacement (along the horizontal axis) was measured at the deepest buried shot, Event 9 (10.8 feet), which was 30 times that from the surface tangent detonation.

Near-surface downward vertical displacement decreased by a factor of 4.2 by moving the burst position from surface tangent to buried tangent.

Outward near-surface displacement was 3 times greater for the half buried detonation than for the surface tangent distance. Only a slight increase in outward displacement was gained by increasing the DOB to the buried tangent.

4.1.4 Stress

Peak stress, measured directly beneath the explosion, increased with DOB. Stress produced from the buried tangent detonation was 4 times greater than for the surface tangent detonation. Maximum stress was produced by the deepest detonation (10.8 feet) and was 15 times greater than that produced by the surface tangent detonation.

4.2 RECOMMENDATIONS

Ground shock response to burst position has been investigated in two media. CENSE 1 addressed the shock response in rock (sandstone) and CENSE 2 addressed the response in soil (clayey silt). These two materials represent near extremes for real earth materials. However, in the 'real world' simple, single material sites are seldom encountered. Most geologies vary in complexity from relatively simple two-layered systems to highly complex multilayered systems or near heterogeneous masses. To date only analytical studies and a few limited, small-scale laboratory tests have been performed to define the propagation modes and shock transmission characteristics of layered systems. A few large, single detonations have been conducted on complex geologies (i.e., Middle Gust and Mixed Company). A number of acute questions must be resolved for layered systems in order to provide adequate protection for planned or in-place military structures and installations. Some of these are:

a. Mitigation effects of soft soil layer overlaying a higher velocity layer.

b. Shock energy focusing or enhancement by shallow, high-velocity layer(s).

c. Effects of shear along the geologic interface(s).

The efficacy of the CENSE technique, using a series of small HE detonations has been proven. A third phase of the CENSE program (CENSE 3) is recommended to investigate the effects of layer thickness on shock propagation in a two-material system. A soil over sandstone geology would provide a representative model. Burst position would be fixed at the surface tangent configuration with the soil layer being reduced in thickness for each subsequent test. The bare rock would serve as a data reference base.

REFERENCES

1. D. C. Sachs and L. M. Swift; "Small Explosion Tests, Project Mole"; Final Report AFSWP-291, Vols. I and II, Dec 1955; Stanford Research Institute, Menlo Park, Calif.

2. F. M. Sauer and C. T. Vincent; "Ferris Wheel Series, Flat Top Event, Project Officer's Report, Project 1.2/1.3a; Earth Motion and Pressure Histories"; POR-3002 (WT-3002), 12 Apr 1967; Stanford Research Institute, Menlo Park, Calif.

3. E. E. Jaramillo and R. G. Pozega; "Middle Gust Free-Field Data Analysis"; AFWL TR-73-251, Apr 1974; Air Force Weapons Laboratory, Air Force Systems Command, Kirtland Air Force Base, N. Mex.

4. D. W. Murrell; Middle Gust Series, Ground Motion Measurements" (in preparation); U. S. Army Engineer Waterways Experiment Station, CE, Vicksburg, Miss.

5. J. K. Ingram, J. L. Drake, and L. F. Ingram; "Influence of Burst Position on Airblast, Ground Shock, and Cratering in Sandstone"; Miscellaneous Paper N-75-3, May 1975; U. S. Army Engineer Waterways Experiment Station, CE, Vicksburg, Miss.

6. J. K. Ingram; "CENSE Explosion Test Program; CENSE 1, Explosion in Sanistone"; Technical Report N-77-6, Report 1, Sep 1977: U. S. Army Engineer Waterways Experiment Station, CE, Vicksburg, Miss.

7. "Kulite Series LQ-080U Stress Gage Specification Bulletin"; Sep 1974; Kulite Semiconductor, Inc., Ridgefield, N. Y.

8. A. Peekna; "Development of the Brinell Sandwich Passive Transducer"; Army Science Conference Proceedings 22-25 June 1976, Vol. III.

9. M. J. Ginsbert and others; "Effects of Stress on the Electrical Resistance of Ytterbium and Calibration of Ytterbium Stress Transducers"; DNA 3577F, Aug 1973; Stanford Research Institute, Menlo Park, Calif.

10. C. W. Smith and others; "Constitutive Relations from In-Situ Lagrangian Measurements of Stress and Particle Velocity"; DNA Report 28831, Jan 1972; Defense Nuclear Agency, Washington, D. C.

11. C. W. Smith and J. T Rosenberg; "In Situ Constitutive Relations of Soils and Rocks"; Monthly Progress Report No. 4, 28 Feb 1975; Stanford Research Institute, Menlo Park, Calif.

12. A. Peekna; "Ground Motion Canister Design and Evaluation" (in preparation); U. S. Army Engineer Waterways Experiment Station, CE, Vicksburg, Miss.

13. F. P. Hanes; "Signal Conditioning System for Velocity Gages, Instrumentation for Nuclear Weapons Effects Simulation Symposium, Shock Effects"; Technical Report AFSWC TR-70-5, Vol. II, Mar 1970; Air Force Special Weapons Center, Kirtland Air Force Base, N. Mex.

14. H. D. Carleton; "Digital Filters for Routine Data Reduction"; Miscellaneous Paper N-70-1, Mar 1970; U. S. Army Engineer Waterways Experiment Station, CE, Vicksburg, Miss.

15. H. D. Carleton; "Digital Filters for Explosion Effects Analysis"; Technical Report N-71-7, June 1971; U. S. Army Engineer Waterways Experiment Station, CE, Vicksburg, Miss.

APPENDIX A

PRE-CENSE EXPERIMENT

A.1 EXPERIMENTAL PLAN

In 1965 a low budget, depth-of-burst (DOB) feasibility study was conducted in a uniform loess deposit at the U. S. Army Engineer Waterways Experiment Station (WES) in Vicksburg, Mississippi. The material of the test site consisted of a natural deposit of claycy loess, extending to depths ranging from approximately 20 to 40 feet. The material dry density was approximately 100 pcf at a water content of 22 percent. Boring log data are given in Table A.1.

The in-place seismic velocity was measured to be 1100 ft/s. Pre-CENSE was a conceptual experiment using 2-pound cast spherical TNT explosive charges. Burst positions ranged from half buried to a scaled depth of 1 $W^{1/3}$ (1.26 feet). Table A.2 lists the experimental nonmenclature.

Although the Pre-CENSE geometry has been idealized in Figure A.1 for comparison with that of CENSE 2, the actual tests were conducted along a horizontal plane (i.e., the charges were detonated in the face of a vertical cut with instruments placed along radials via vertical boreholes (Figure A.2)). Each shot was made in virgin soil. Particle velocity and stress were the principal parameters measured, although a few measurements of accelerations were also made. Only motions and stresses along the radial plane were measured. DX-type horizontal velocity gages, SE-type stress gages, and Endevco piezoelectric accelerometers were used.

The primary region of interest for this study extended from about 1.26 to 5.67 feet from the center of the charge. Because of the small distances involved, severe restrictions were placed on the instrument canister size, as well as placement and orientation. In lieu of bulky metal canisters, a technique was devised for grouting the particle motion gages in a cylindrical soil plug, roughly 3-3/4 inches in diameter

by 4 inches high. A silicone rubber mold was made in which a soil (loess-cement mixture) could be cast around the gages, Figure A.3.

The mixture found to be most satisfactory for duplicating native deposit strength, density, and water content was manufactured from the following proportions: 57.2 percent loess, 19.0 percent sand, 9.5 percent cement, 9.5 percent plaster of paris, 0.3 percent calcium chloride, and 4.5 percent water. All percentages are by weight.

A.2 MOTION MEASUREMENTS

A.2.1 Acceleration

Accelerations were measured on Events 1, 4, and 5 (DOB = 0, 0.94, and 1.26 feet, respectively). Scaled peak radial acceleration is plotted versus scaled distance in Figure A.4. Accelerations measured from the half buried burst position (Event 1) attenuated as the -8.46 power of distance. Data from the 0.94- and 1.26-foot (Events 4 and 5, respectively) depth burst positions had equal slopes ($R^{-3.66}$), attenuating less rapidly than for the 0 DOB detonation. A sixfold increase in acceleration was obtained by moving the DOB from 0.94 to 1.26 feet.

A.2.2 Particle Velocity

Particle velocity waveforms from the half buried detonations are shown for various radial distances in Figure A.5. The velocity signatures were characterized by an initial outward going peak that decreased in amplitude and increased in duration with increasing distance from the charge. The secondary inward going peak increased in proportion to the initial peak with increasing distance as the response of the soil became more nearly elastic. Peak outward radial particle velocity for all burst positions is plotted versus scaled distance in Figure A.6. A progressive increase in peak particle velocity occurred as the DOB increased. Velocity slopes were equal for all DOB's greater than half buried, i.e., $R^{-2.47}$. Velocity from the half buried detonation appeared to attenuate more rapidly (as was also observed in the acceleration data) at a rate of $R^{-2.78}$. Maximum velocity increases occurred between burst positions of half buried and 0.32 and 0.63 feet, increases of 2 and 1.7 times,

respectively. No significant difference was noted between DOB's of 0.63 and 0.94 feet. Highest particle velocities were obtained for the deepest burst position, 1.26 feet. An overall peak velocity enhancement of 4.2 times was achieved by moving the burst position from half buried to 1.26 feet.

A.3 STRESS

Typical measured stress waveforms (Event 5, DOB = 1.26 feet) are shown in Figure A.7. Figure A.8 is a plot of peak radial stress versus scaled distance for all burst positions. Data slopes for all events were similar, with a tendency to flatten (decrease in rate of attenuation) with increasing distance from the explosion. Both Events 1 and 2 (DOB = 0 and 0.32 feet, respectively) attenuated at a rate of $R^{-2.96}$ between scaled distances of 1.4 and 4.5 $W^{1/3}$. The slope for Events 3, 4, and 5 over the same scaled distance was $R^{-3.26}$. The maximum increase in stress was attained by moving the charge position from half buried to 0.32 feet, an increase of 2.4 times. A 1.9 times increase occurred between DOB's of 0.32 and 0.63 feet. No significant differences in measured stresses were noted for Events 4 and 5 (DOB = 0.94 and 1.26 feet, respectively) out to a scaled distance of 4.5 $W^{1/3}$ (5.67 feet). Beyond this distance the curves tended to diverge. An overall stress increase of about 5 times was attained by moving the burst position from half buried to 1.26 feet.

A.4 DATA PRESENTATION

Data are presented in the form of selected time histories and parameter-distance plots. Available motion- and stress-time histories are presented in Figures A.9-A.17. Figure A.9 is not complete with all data plots since a number of stress-time histories were lost in the interim since the experiment was conducted.

A.5 OBSERVATIONS

A.5.1 Ground Motion

Acceleration data were limited on this test series. However, some

observations can be made. Acceleration levels were strongly influenced by burst position, increasing proportionally with DOB. Acceleration increased by a factor of 6 by increasing the DOB from 0.94 to 1.26 feet (scaled depth of 0.75 and 1 $W^{1/3}$, respectively).

Radial particle velocity also increased with DOB. Velocity measured from the detonation buried at a scaled depth of 1 $W^{1/3}$ (1.26 feet) was almost 3 times that from the surface (half buried) detonation. Little enhancement in particle velocity was achieved for DOB's greater than 0.94 feet (0.75 $W^{1/3}$).

A.5.2 Stress

Stress, as with acceleration and particle velocity, increased with charge DOB. The maximum relative increase in stress occurred between half buried and 0.32-foot burst positions, an increase of 1.7 times. Maximum stress was produced by the deepest detonation (1.26 feet), which was 5 times that produced by the half buried shot. Stress levels tended to be asymptotic with distances beyond a scaled distance of 5 $W^{1/3}$ (6.3 feet).

TABLE A.1 PRE-CENSE BORING LOG DATA.

Sample No.	Depth (ft)	Dry Density (pcf)	Water Content (percent)	Material
1	0-0.5	86.2	24.1	Organic material
2	0.5-1.5	95.3	23.1	Organic material/loess
3	1.5-2.5	98.4	22.7	Loess
4	2.5-3.5	101.1	22.3	Loess
5	3.5-4.0	100.4	22.3	Loess
6	4.0-6.0	100.1	22.2	Loess
7	6.0-7.0	102.2	22.1	Loess
8	12.5-12.9	83.0	21.6	Clayey-loess
9	13.3-13.7	83.4	21.0	Clayey-loess

TABLE A.2 PRE-CENSE TEST EVENT DESIGNATION.

Event No.	DOB		
	(ft)	($W^{1/3}$)	(R_c)
1 (3 shots)	0	0	0
2	+0.32	+0.25	+2
3	+0.63	+0.50	+4
4 (2 shots)	+0.94	+0.75	+6
5 (2 shots)	+1.26	+1.00	+8

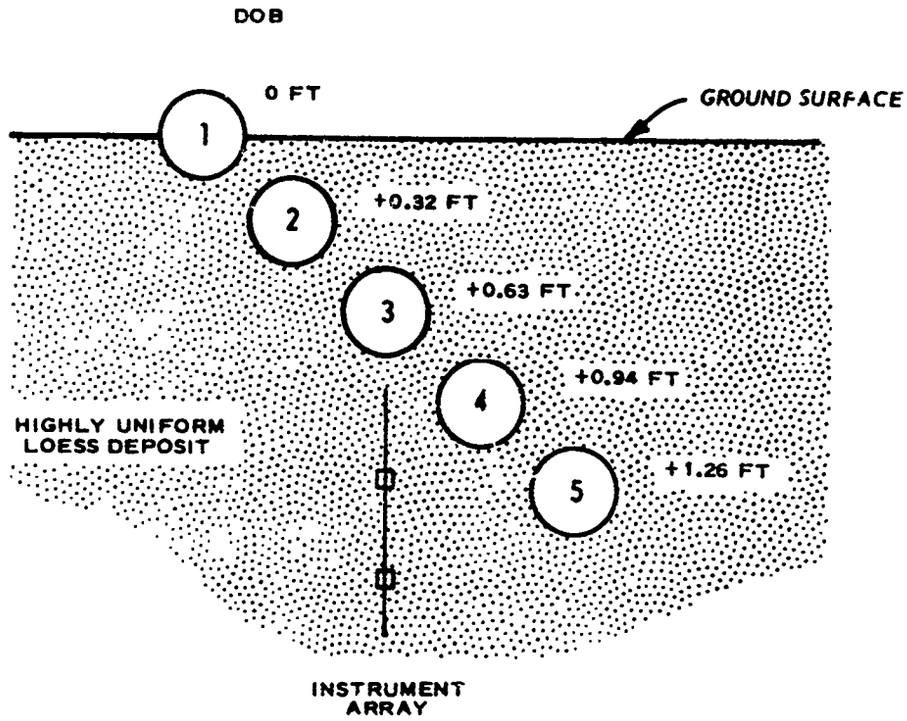

NOTE: NUMERALS REFER TO SHOT NUMBER.

Figure A.1 Idealized Pre-CENSE experiment geometry, 2-pound cast spherical TNT explosive.

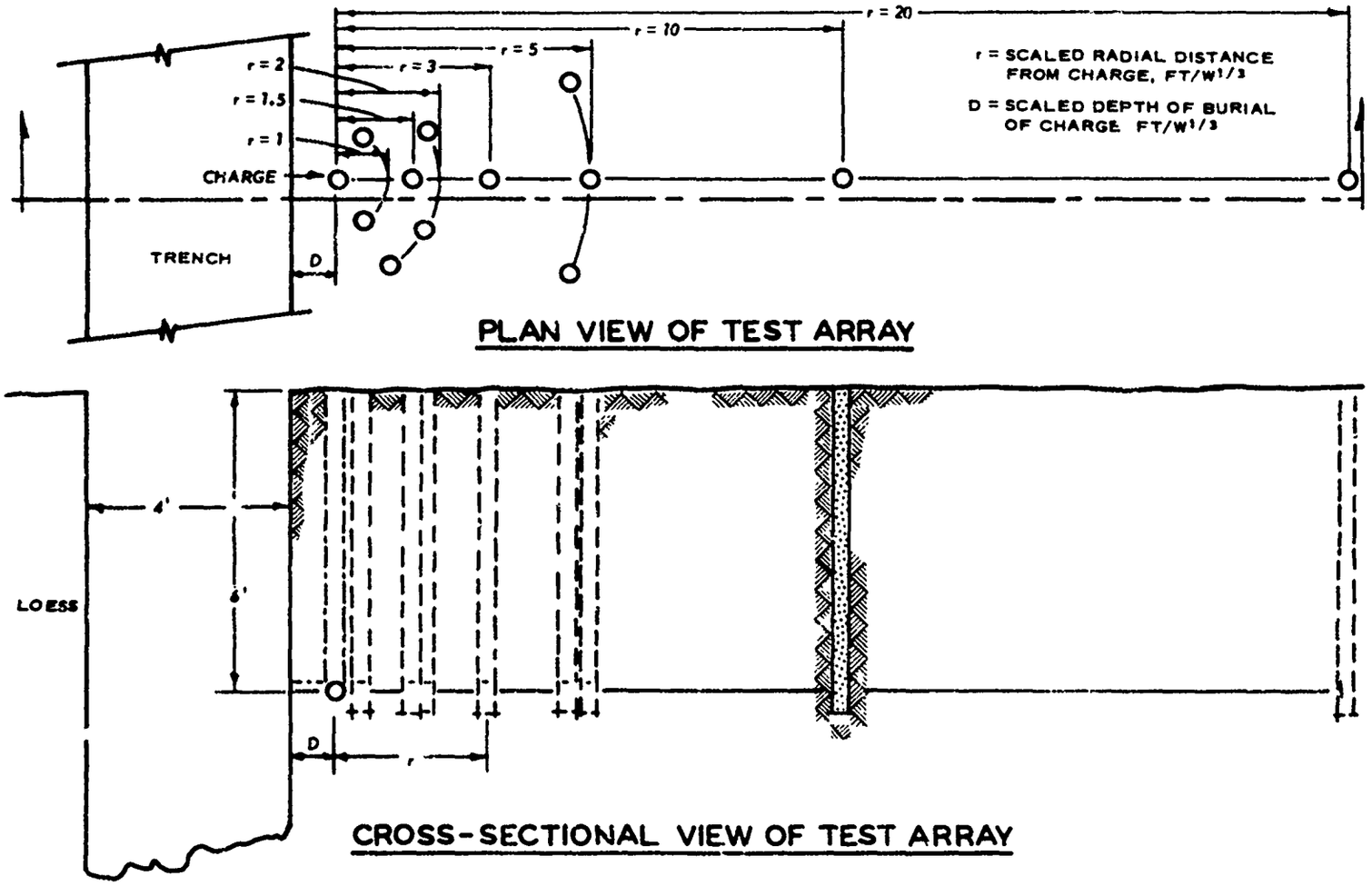

Figure A.2 Actual test configuration for Pre-CENSE.

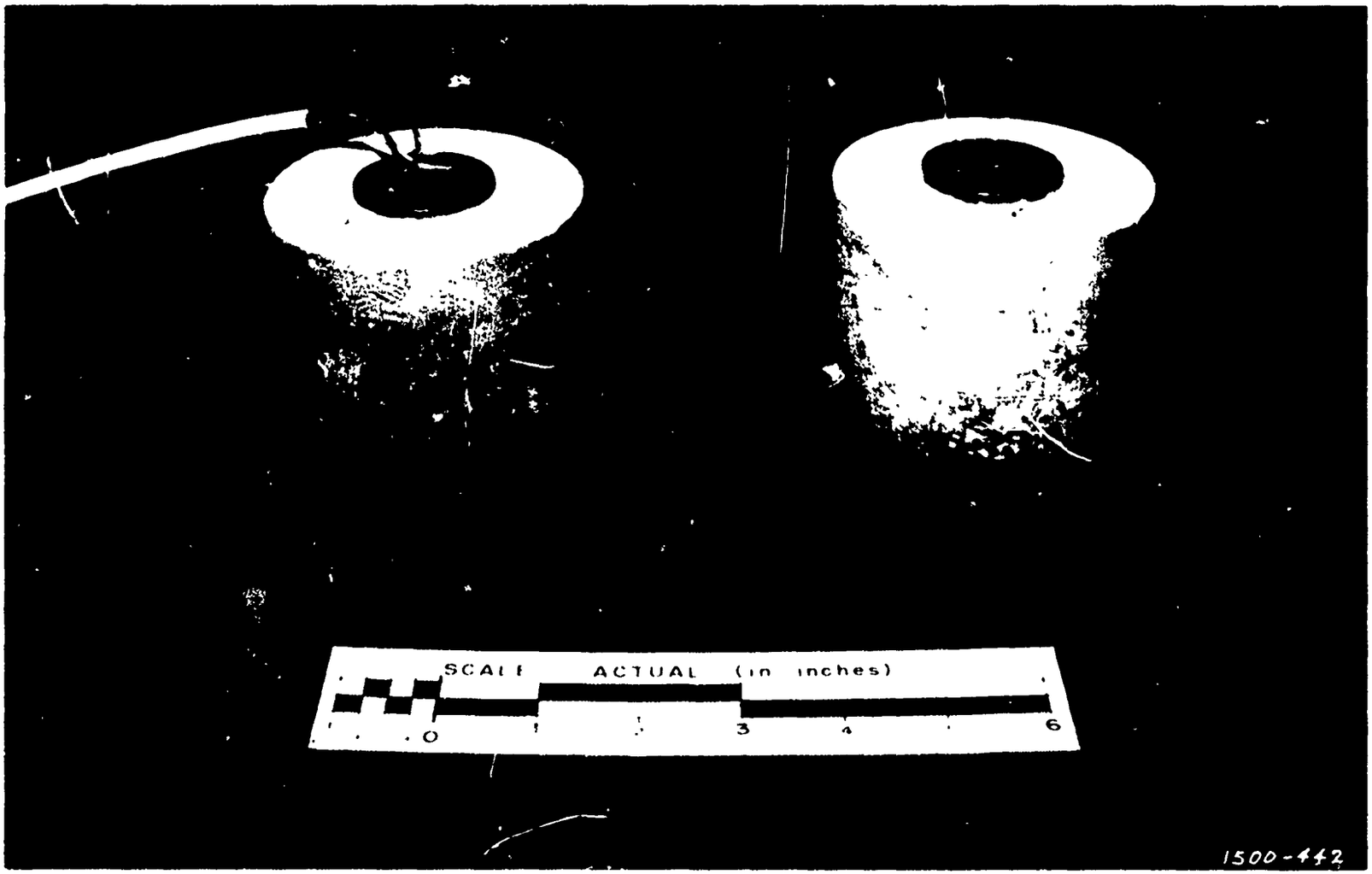

Figure A.3 DX model particle velocity gage mounted in soil cement grout plug.

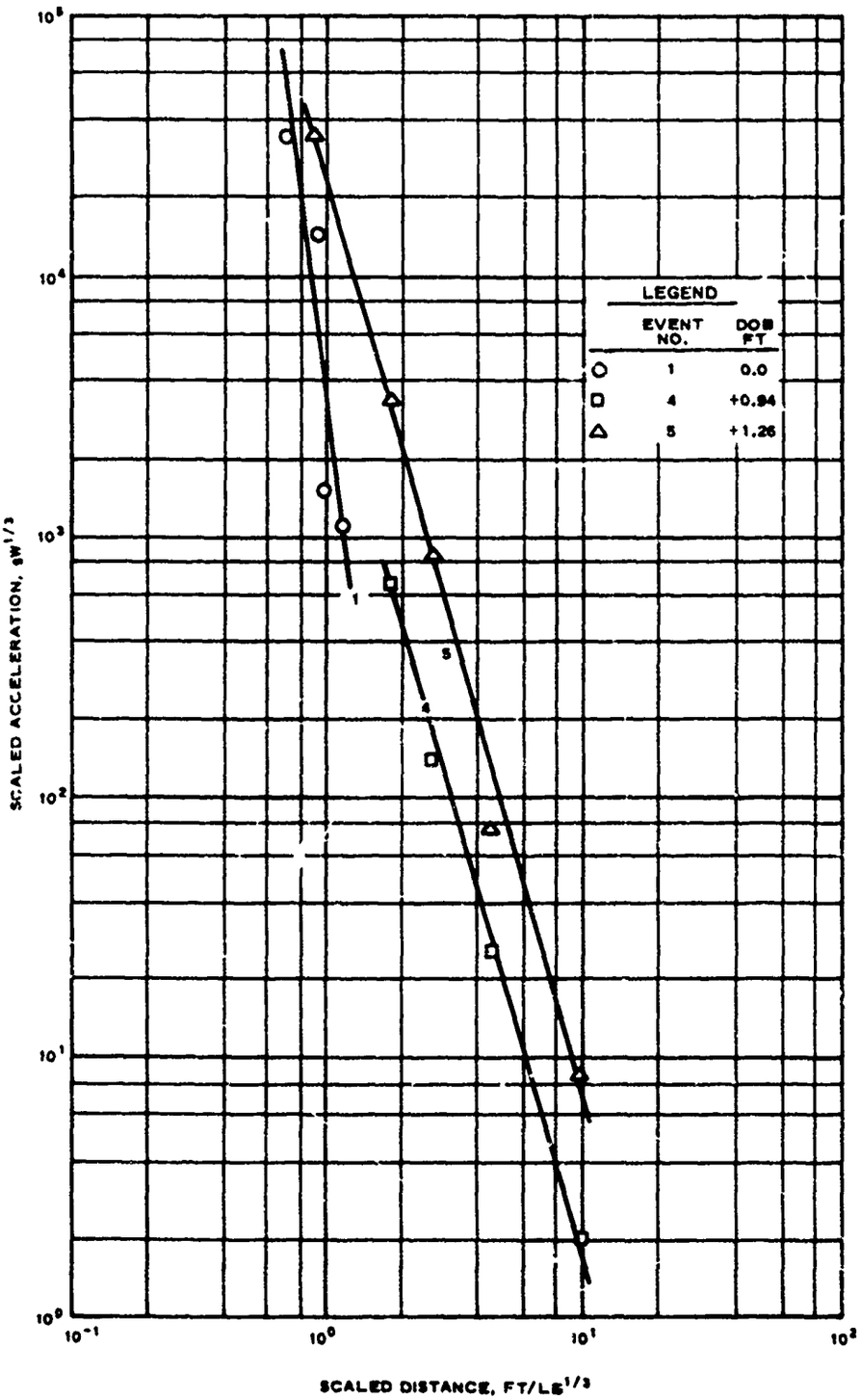

Figure A.4 Scaled peak outward radial acceleration versus scaled distance as a function of burst position.

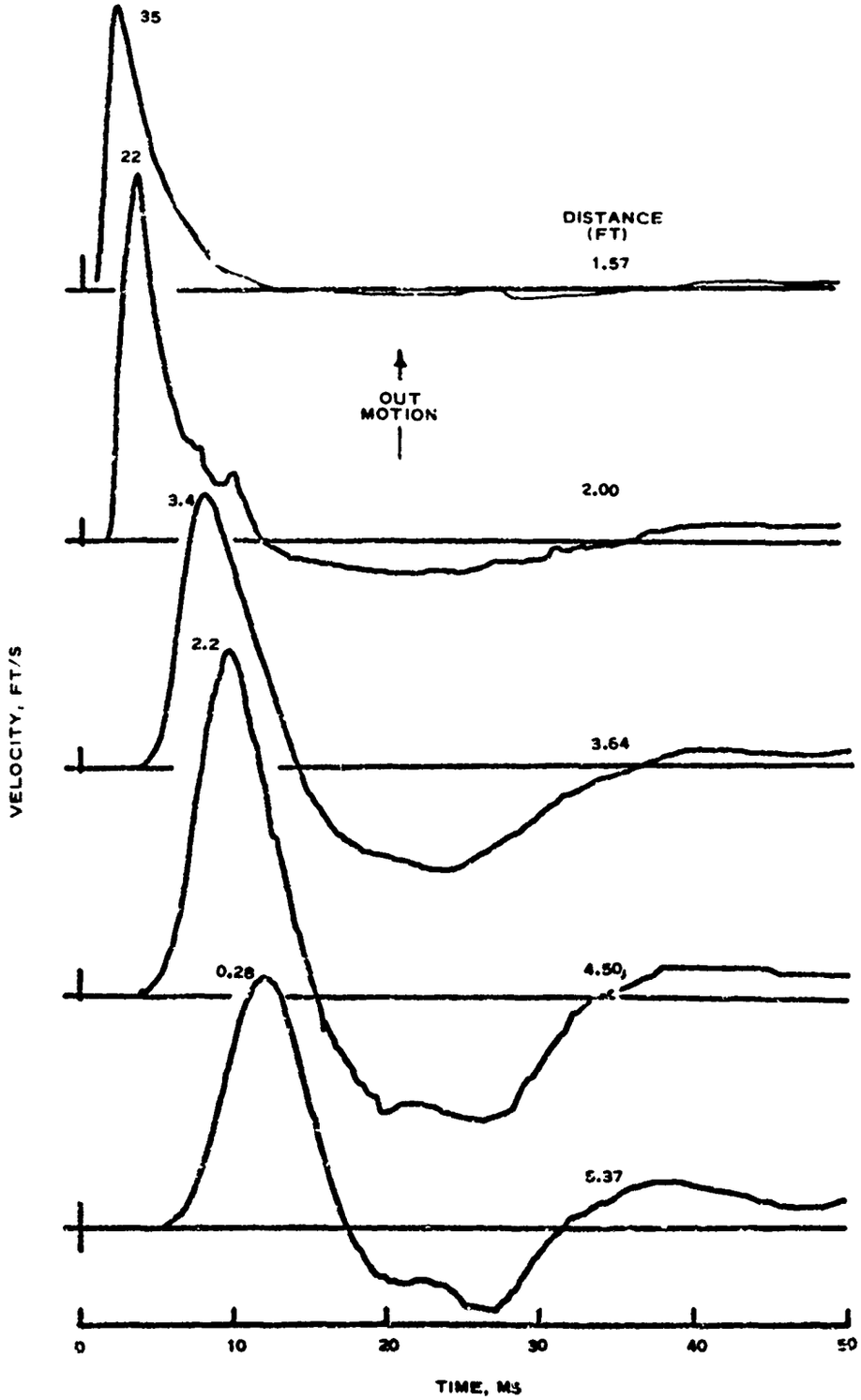

Figure A.5 Velocity waveforms, Event 1 (DOB = 0 foot).

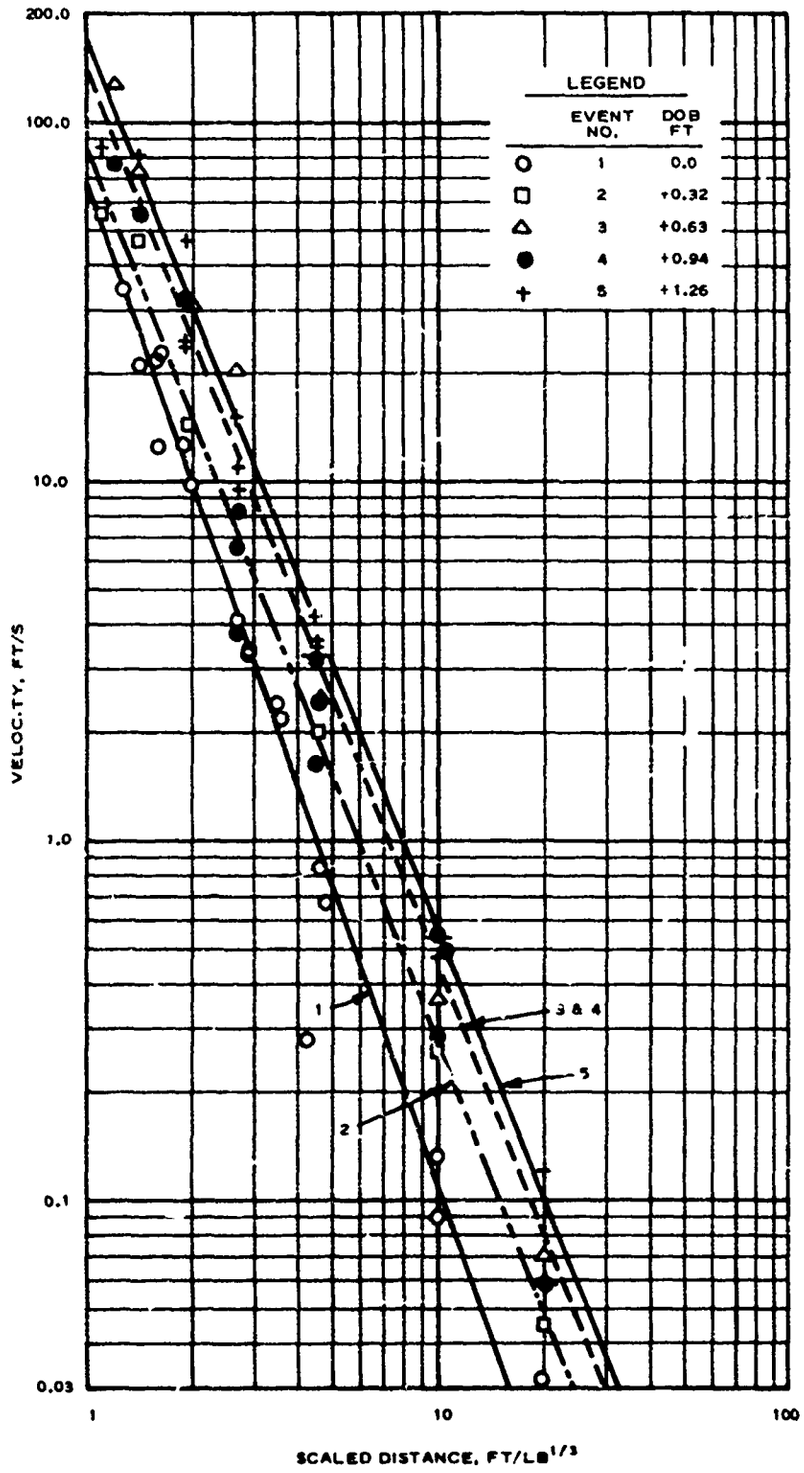

Figure A.6 Peak outward radial particle velocity versus scaled distance as a function of burst position.

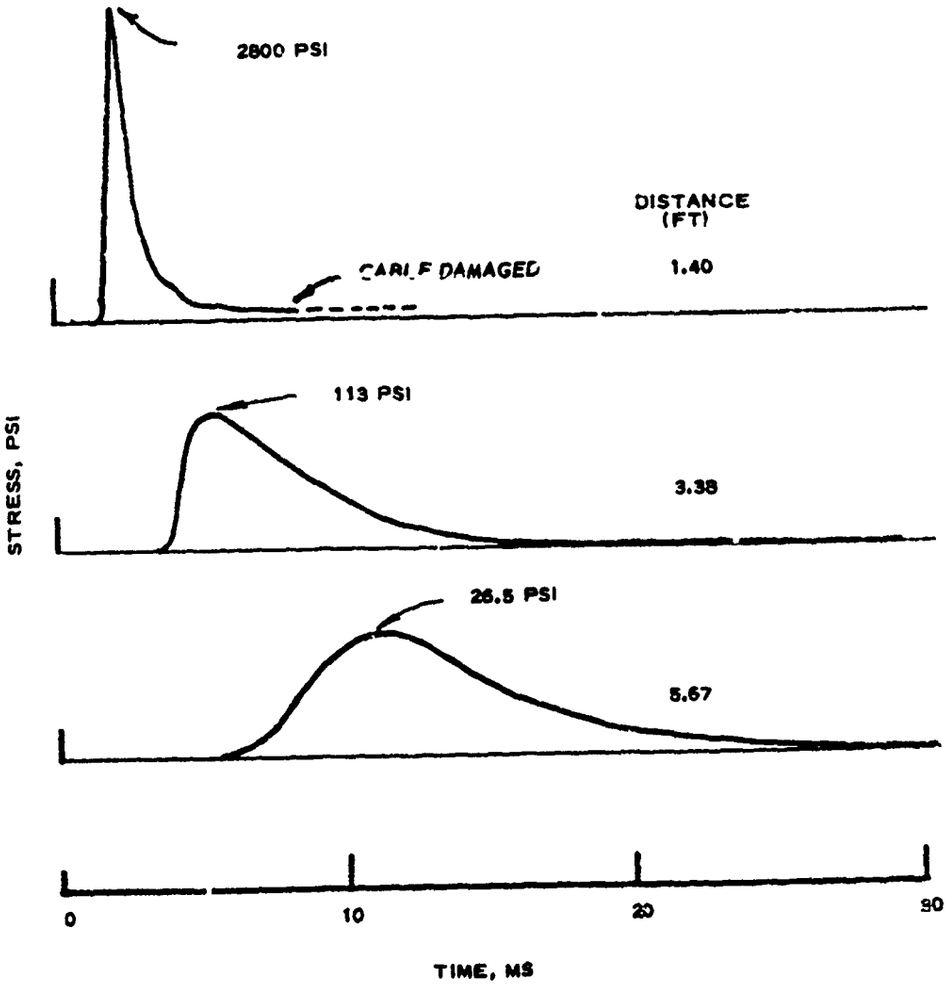

Figure A.7 Stress waveforms, Event 5 (DOB = 1.26 feet).

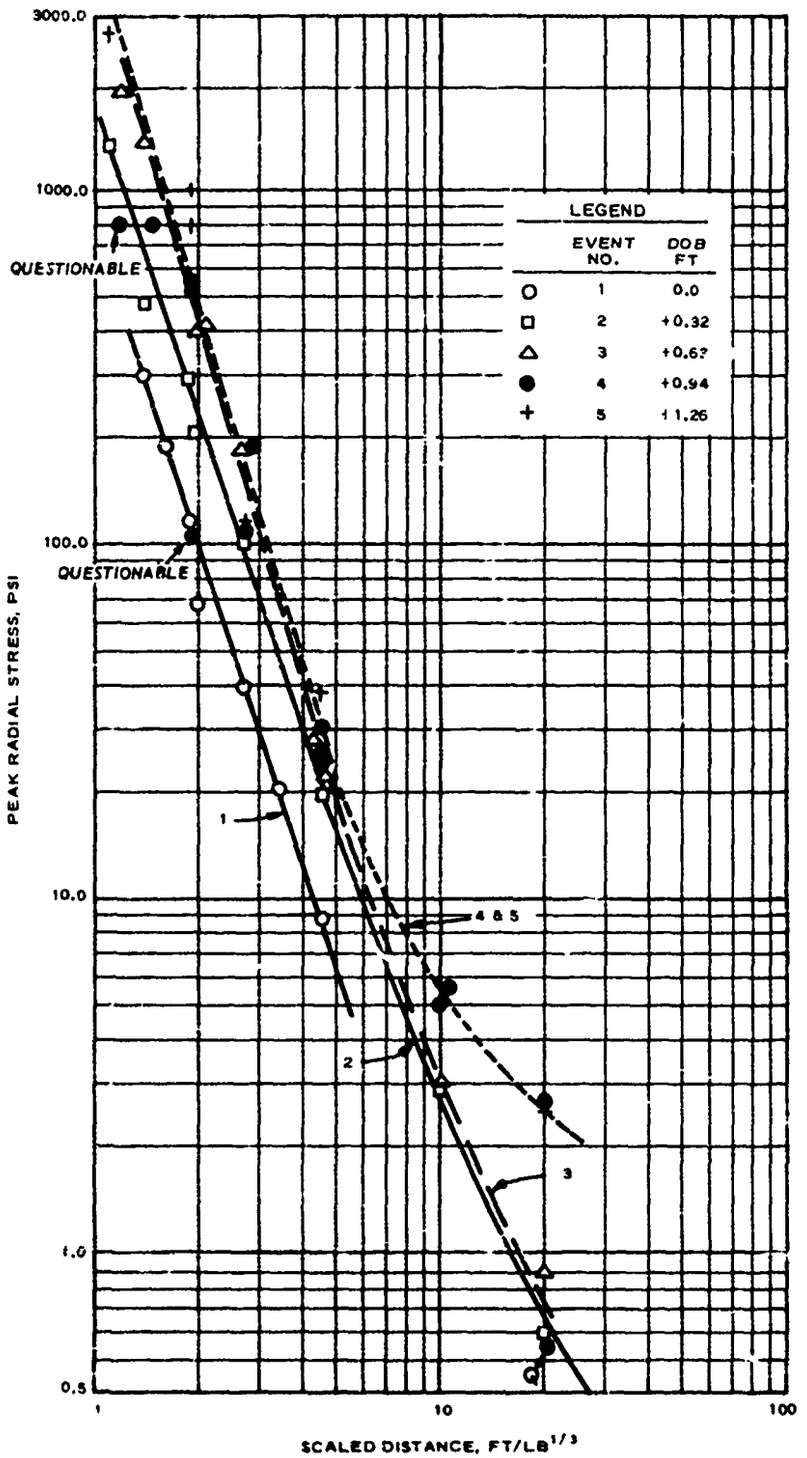

Figure A.8 Peak radial stress versus scaled distance as a function of burst position.

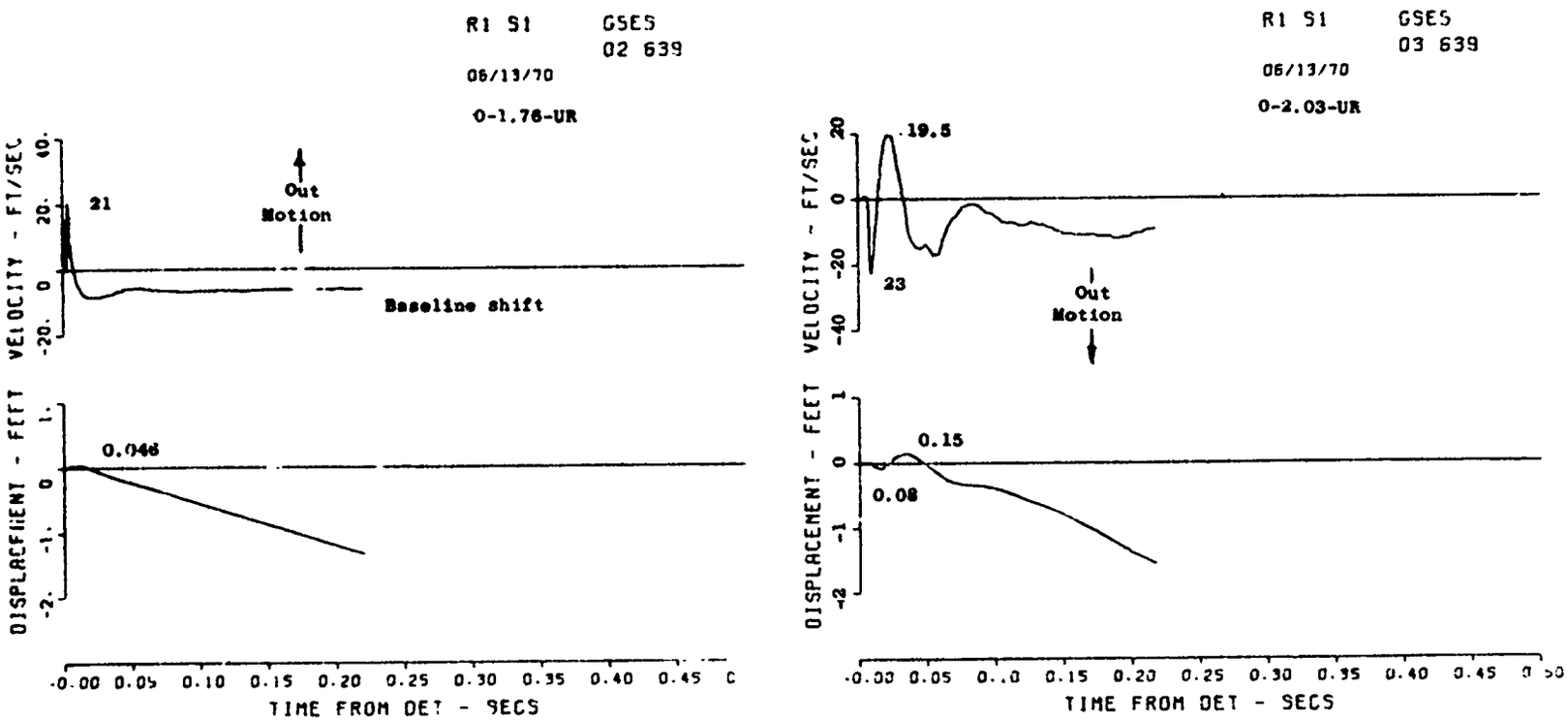

Figure A.9 Event 1, shot 1, half buried, 0 $W^{1/3}$ (0 foot); Pre-CENSE ground motion- and stress-time histories (sheet 1 of 4).

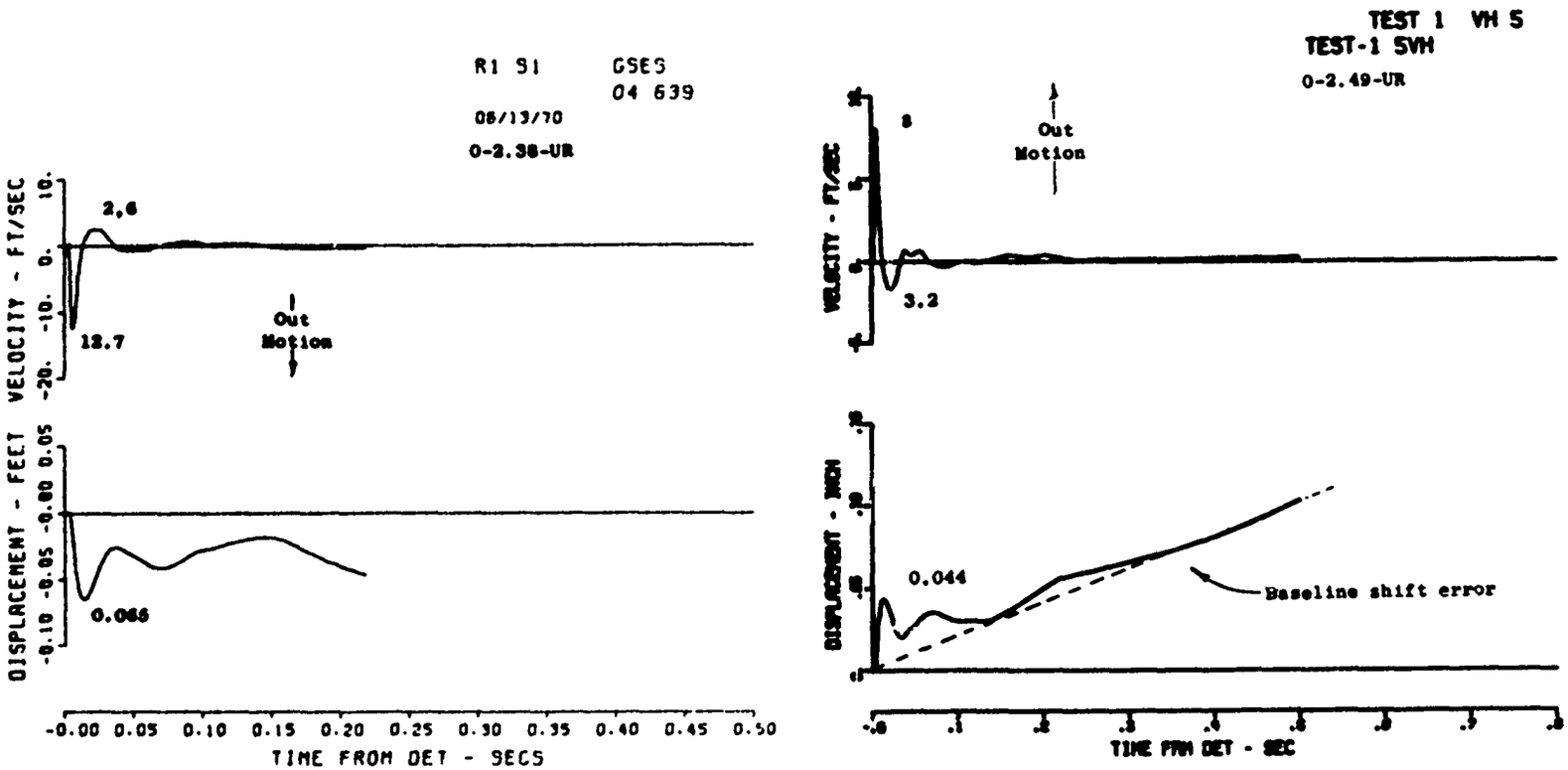

Figure A.9 (sheet 2 of 4).

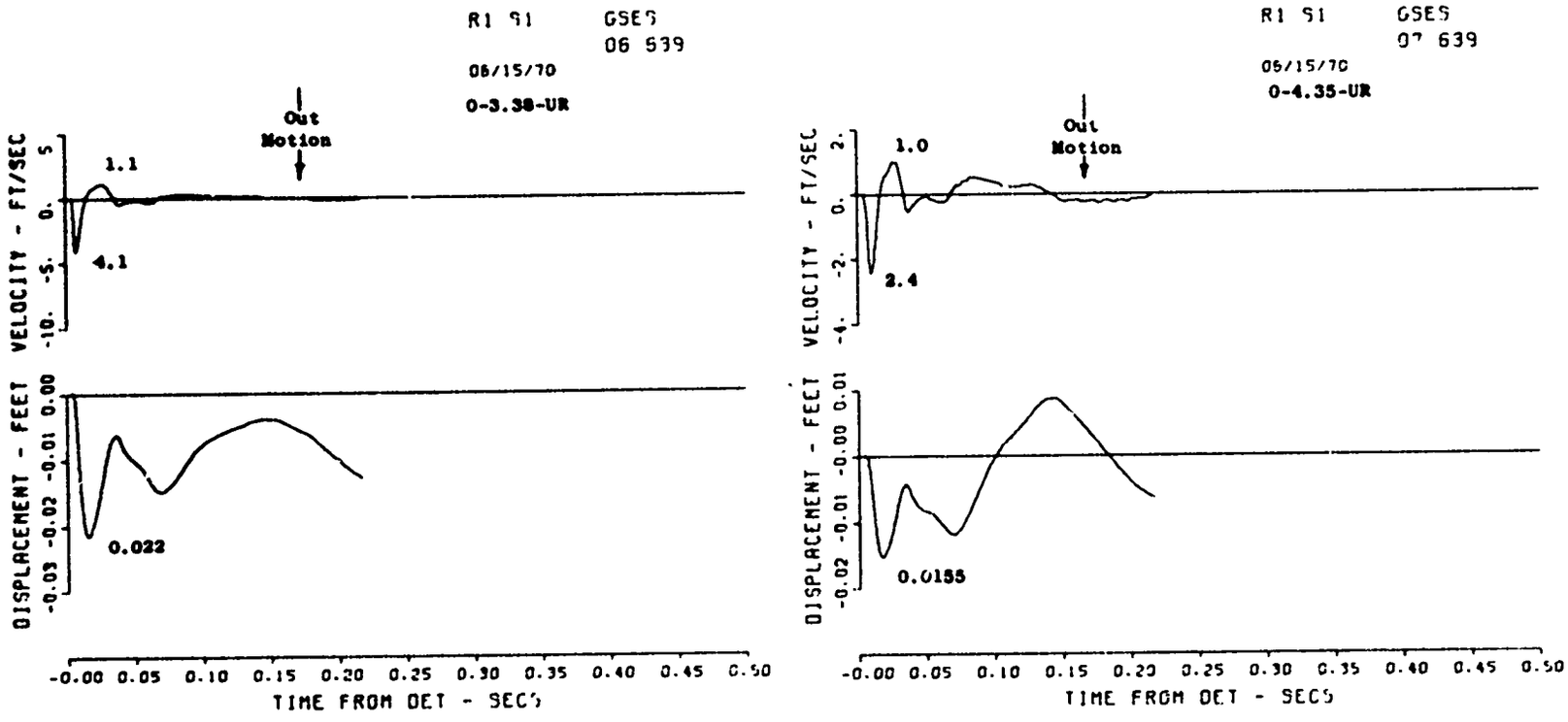

Figure A.9 (sheet 3 of 4).

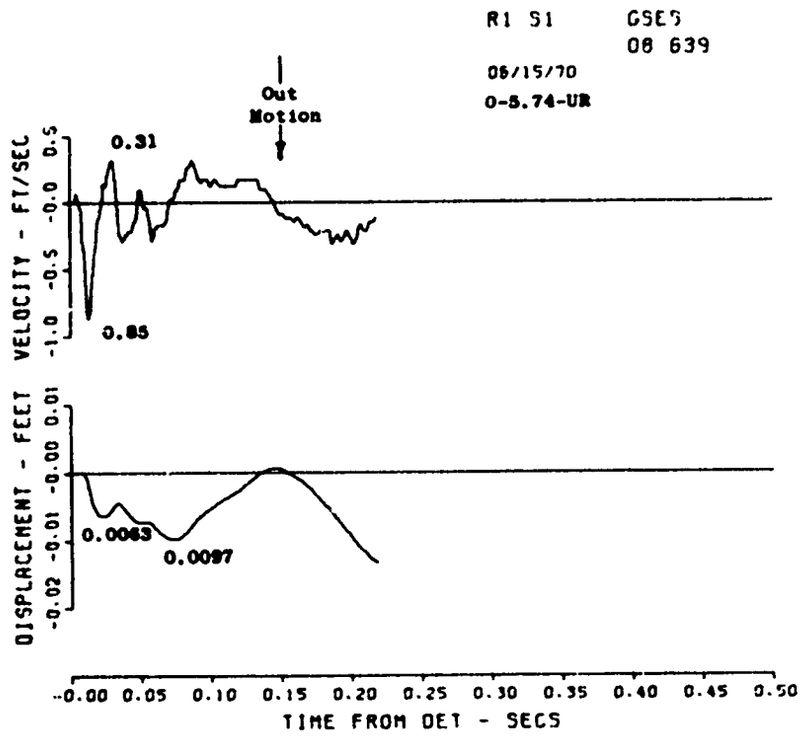

Figure A.9 (sheet 4 of 4).

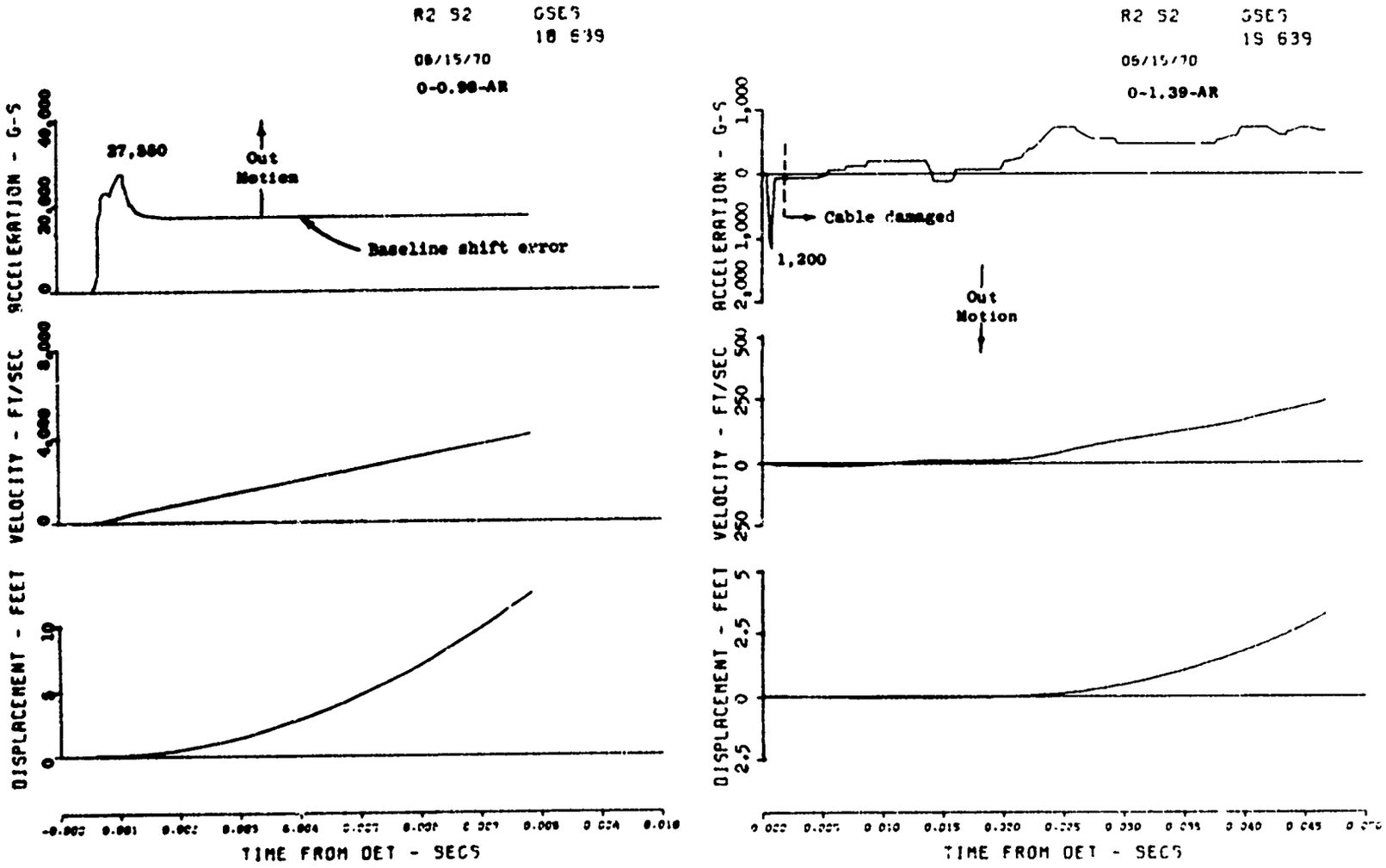

Figure A.10 Event 1, shot 2, half buried, 0 $W^{1/3}$ (0 foot) (sheet 1 of 4).

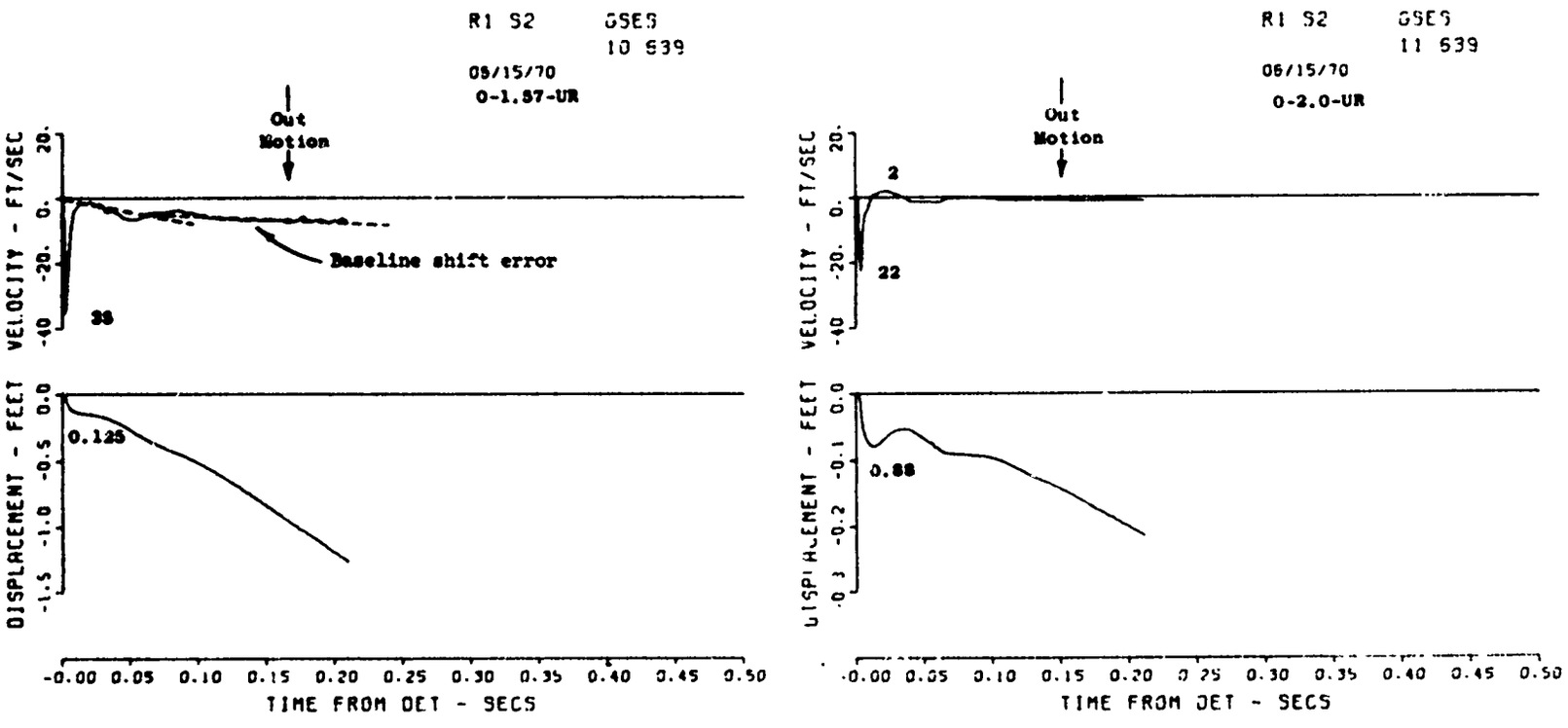

Figure A.10 (sheet 2 of 4).

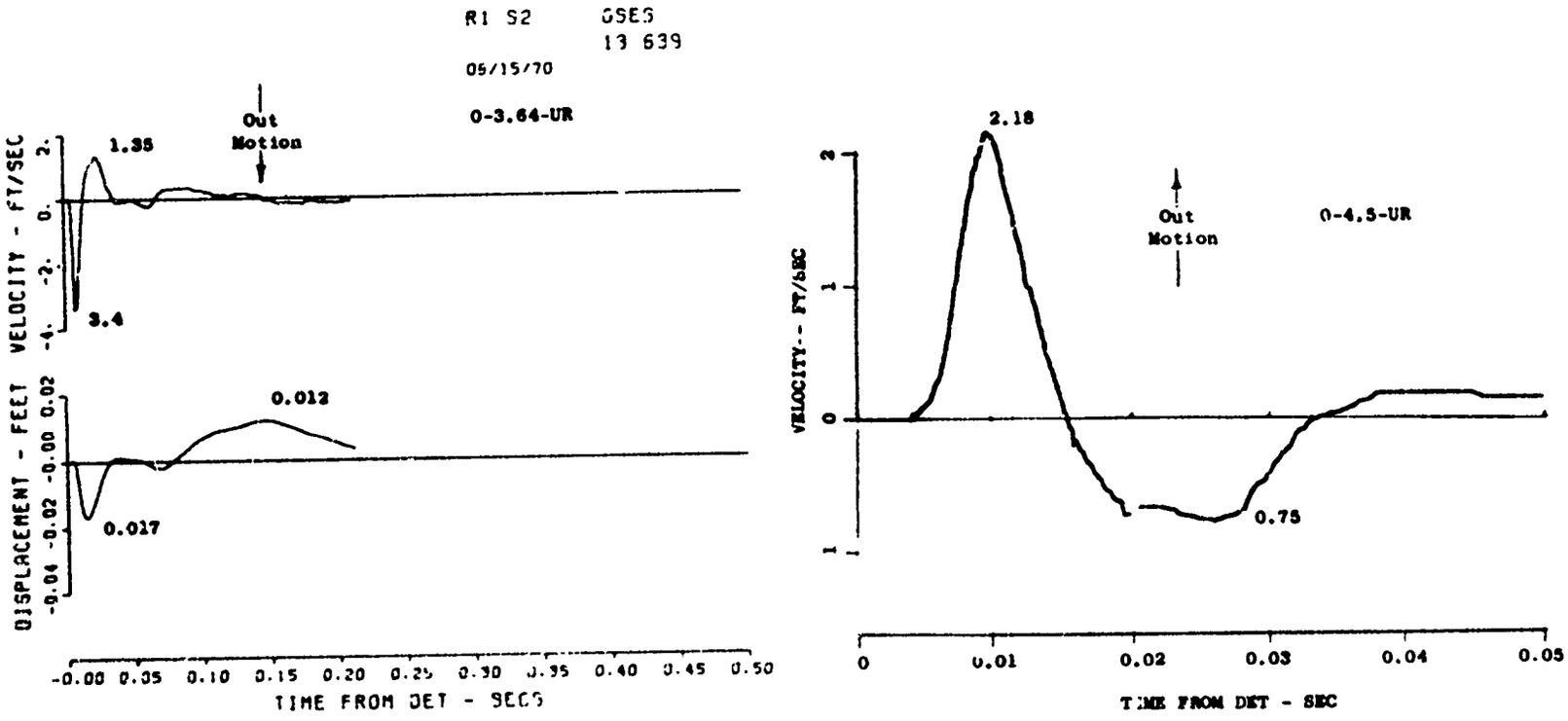

Figure A.10 (sheet 3 of 4).

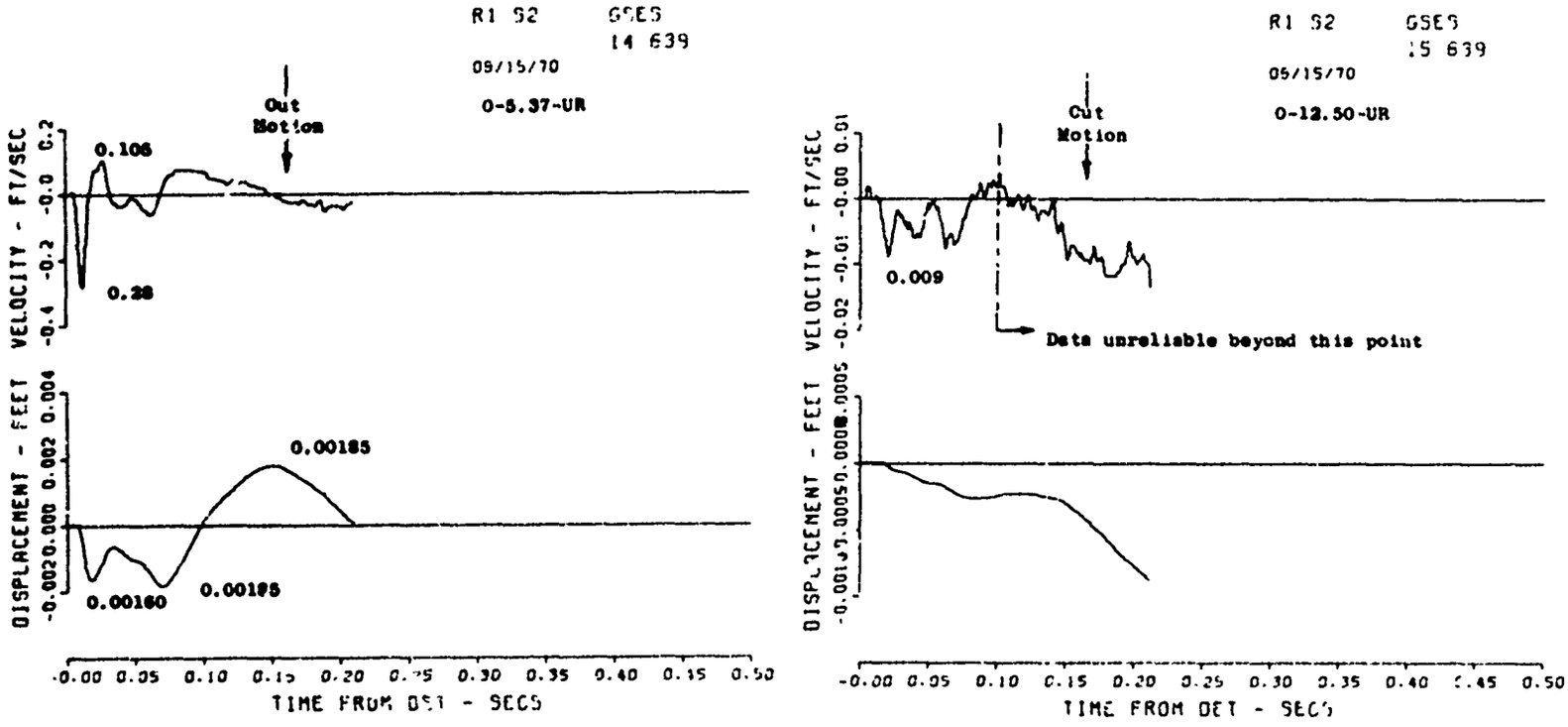

Figure A.10 (sheet 4 of 4).

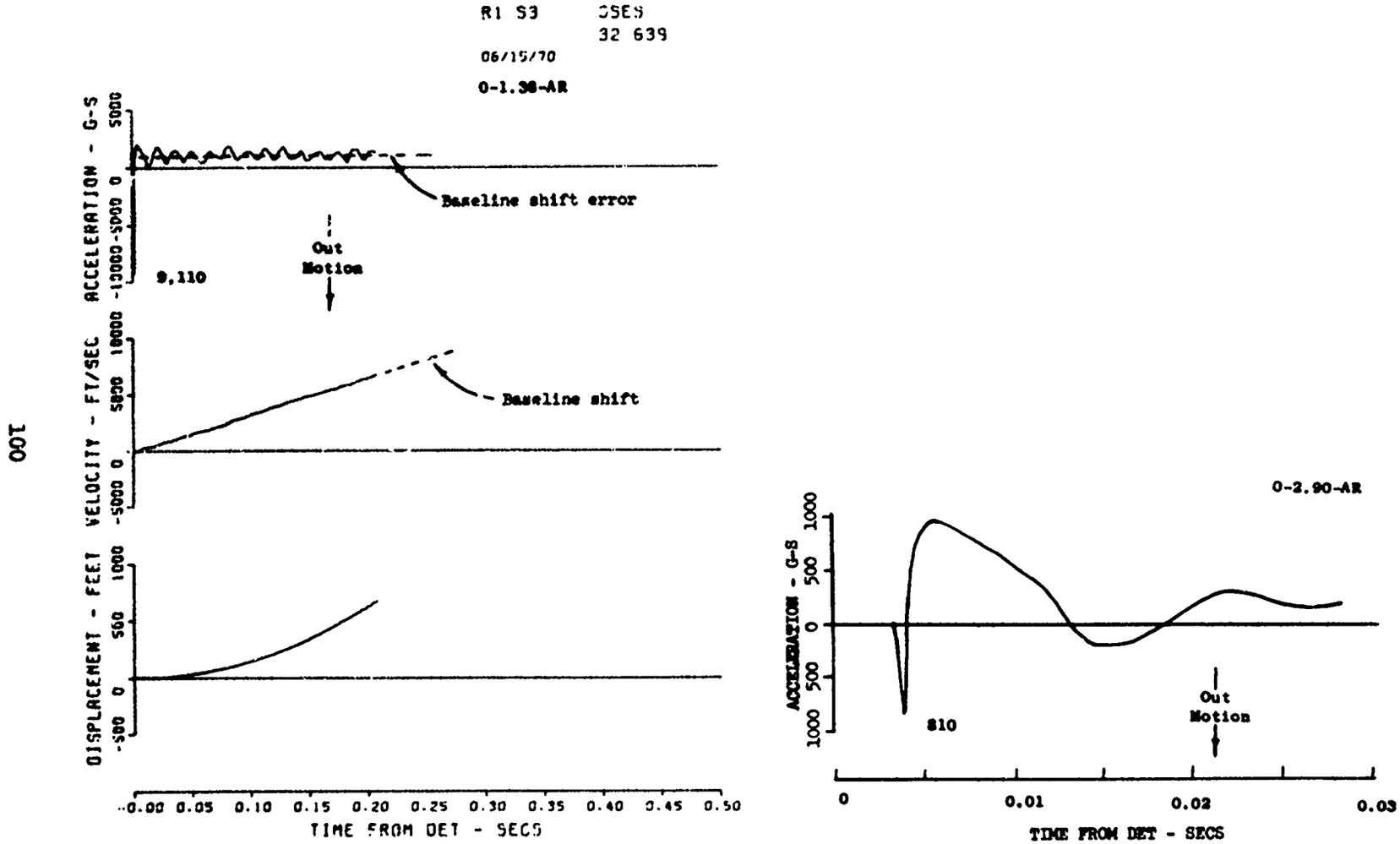

Figure A.11 Event 1, shot 3, half buried, 0 $W^{1/3}$ (0 foot) (sheet 1 of 5).

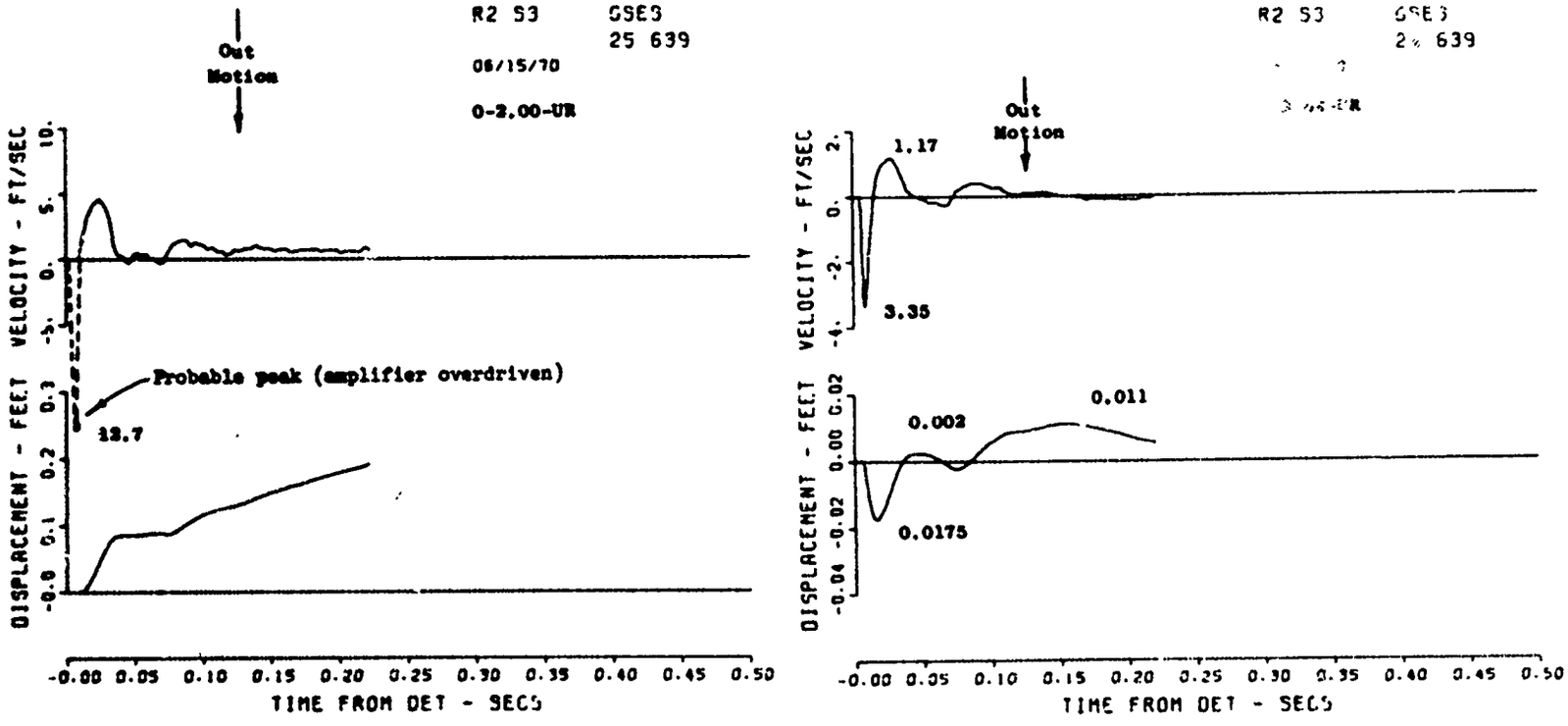

Figure A.11 (sheet 2 of 5).

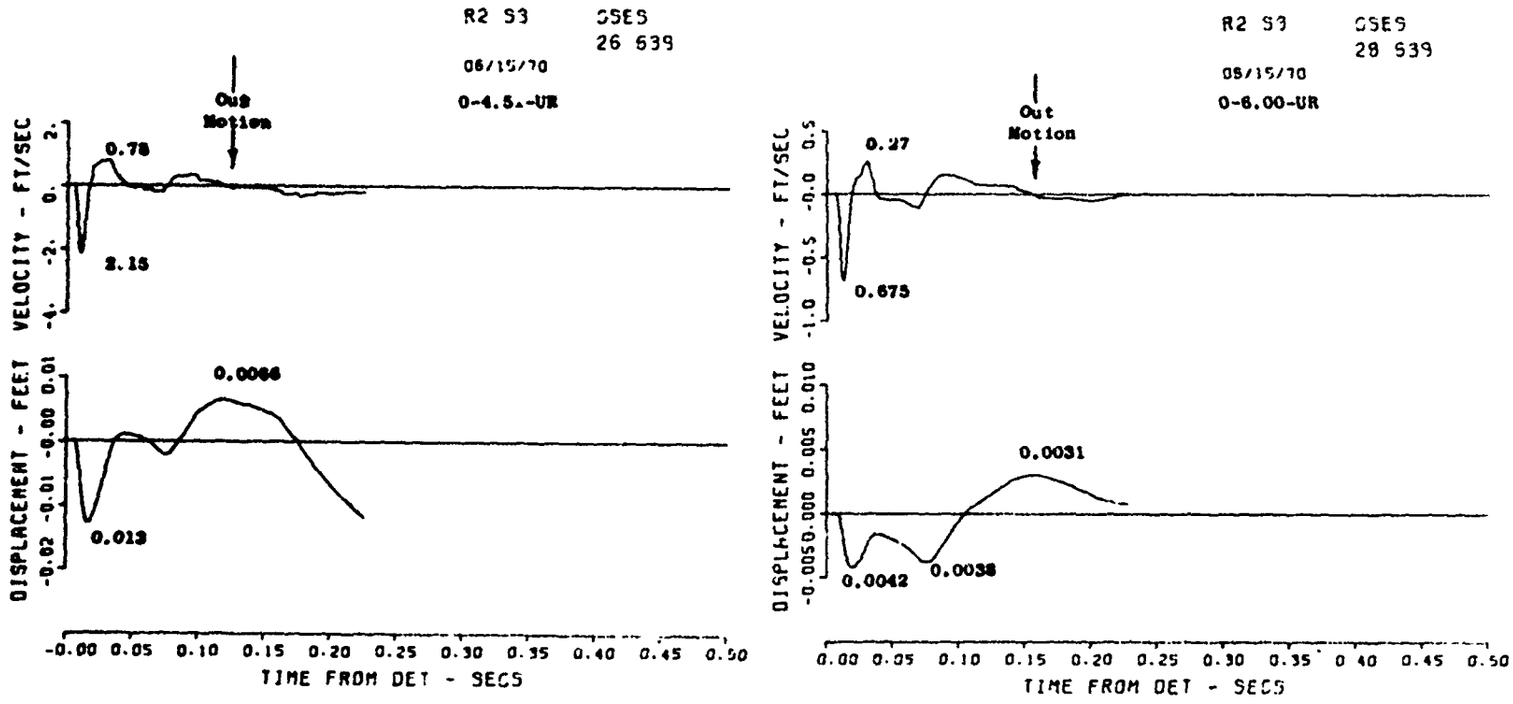

Figure A.11 (sheet 3 of 5).

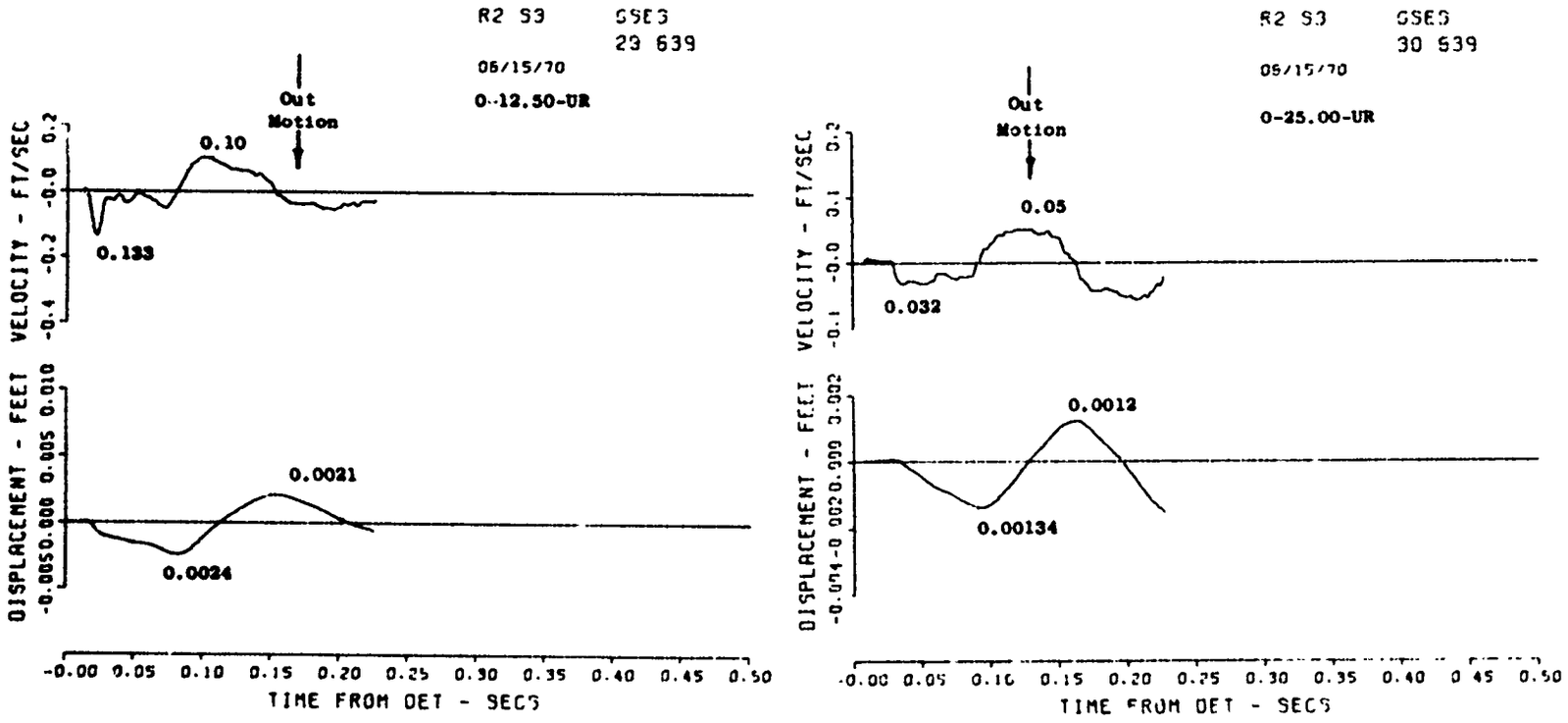

Figure A.11 (sheet 4 of 5)

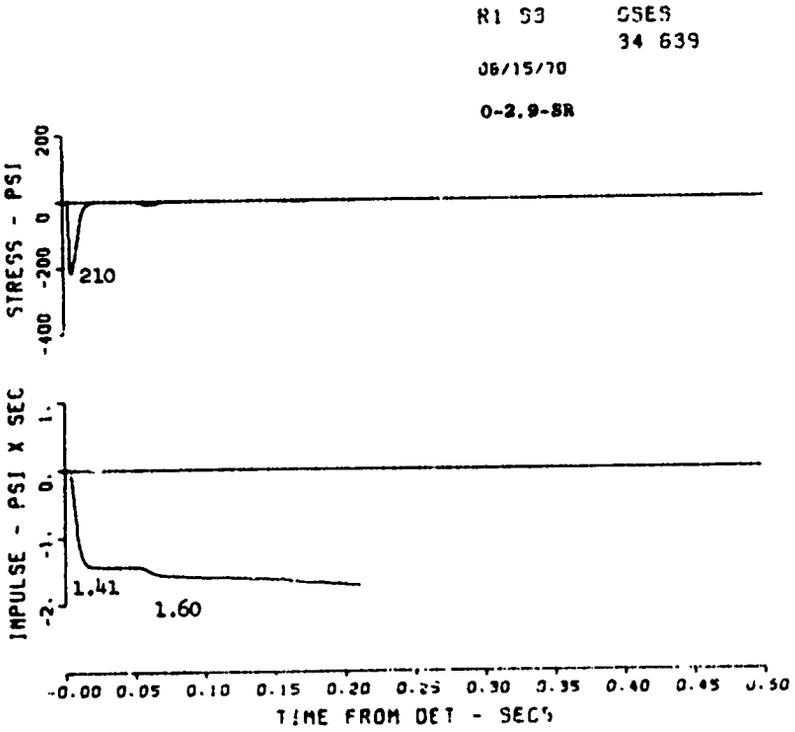

Figure A.11 (sheet 5 of 5).

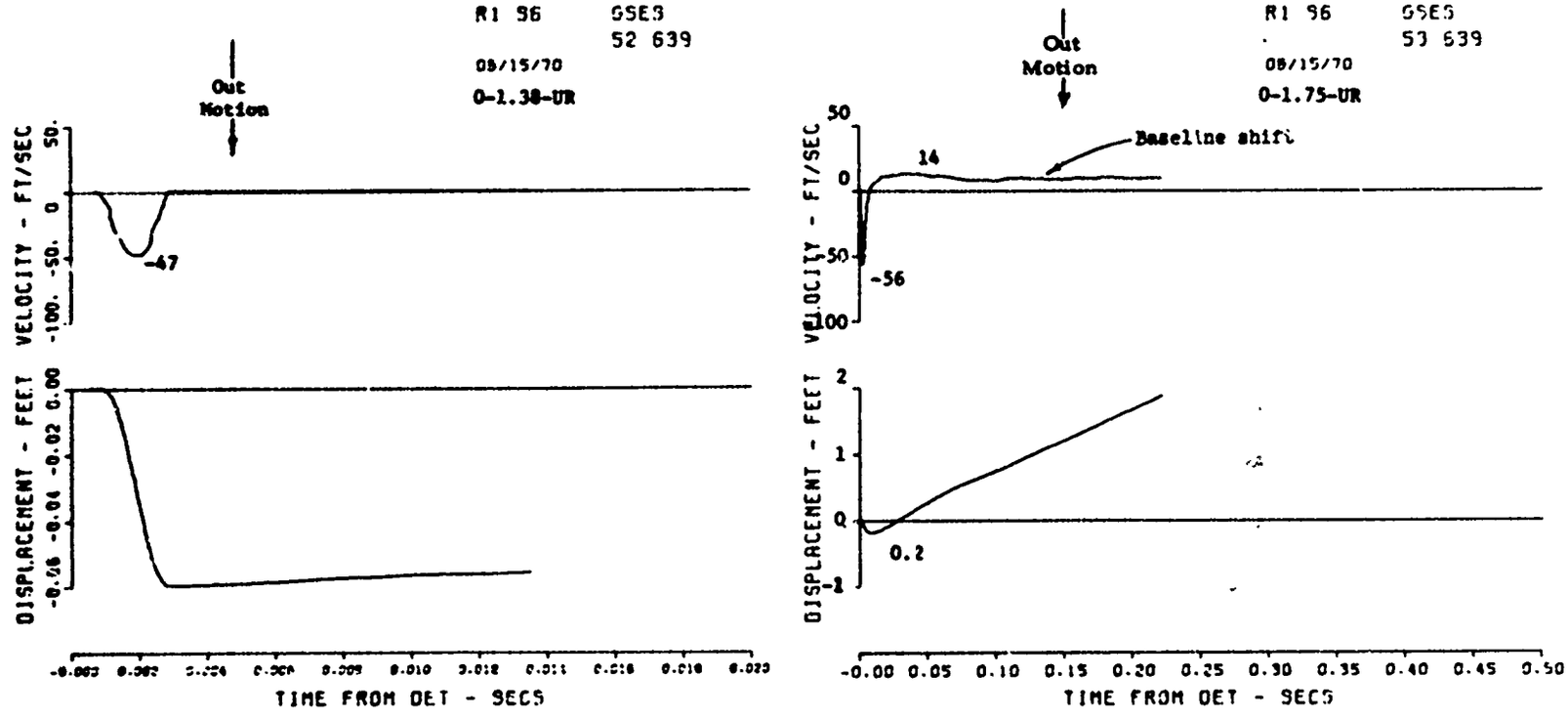

Figure A.12 Event 2, buried, +0.25 $W^{1/3}$ (+0.32 foot) (sheet 1 of 5).

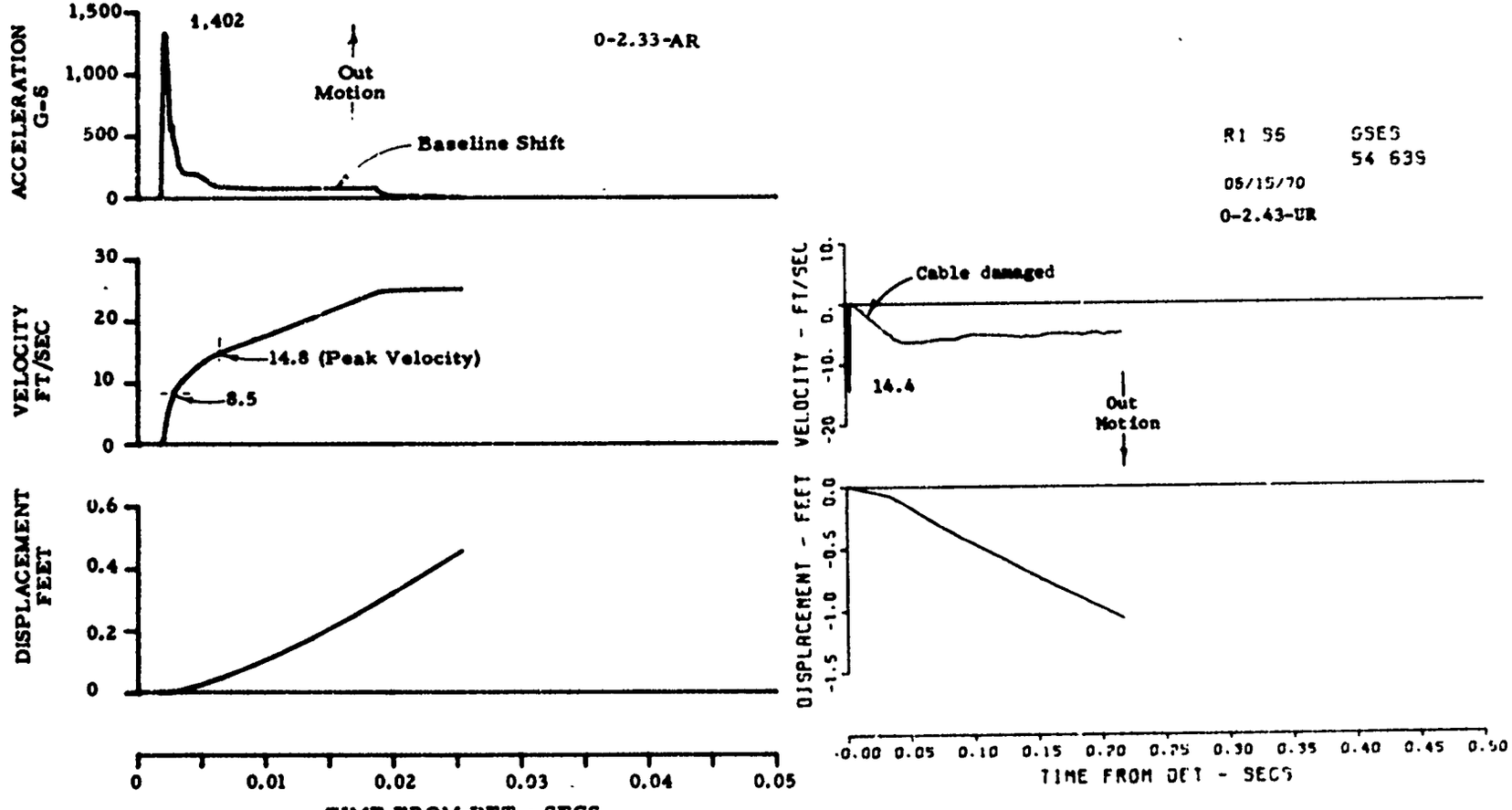

Figure A.12 (sheet 2 of 5).

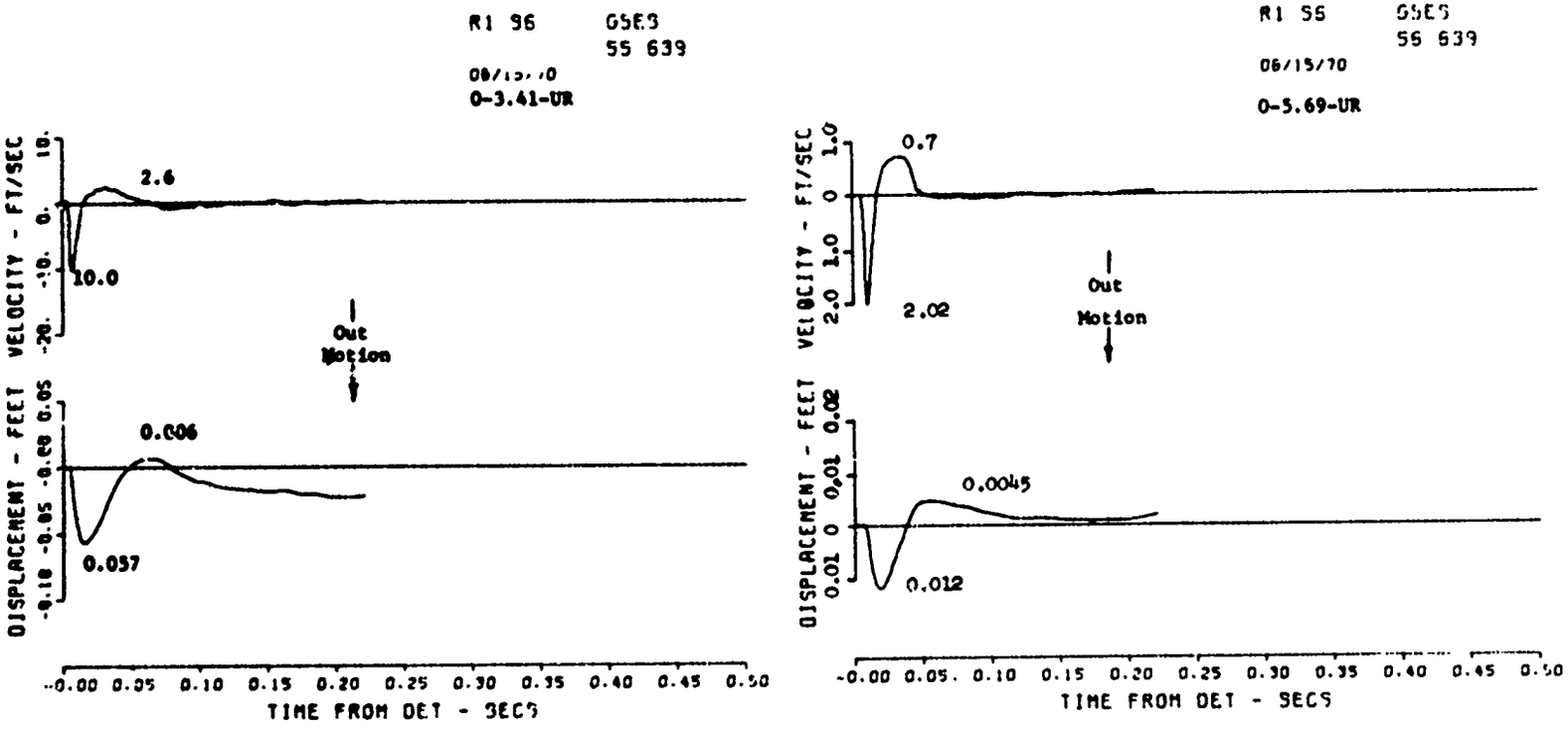

Figure A.12 (sheet 3 of 5).

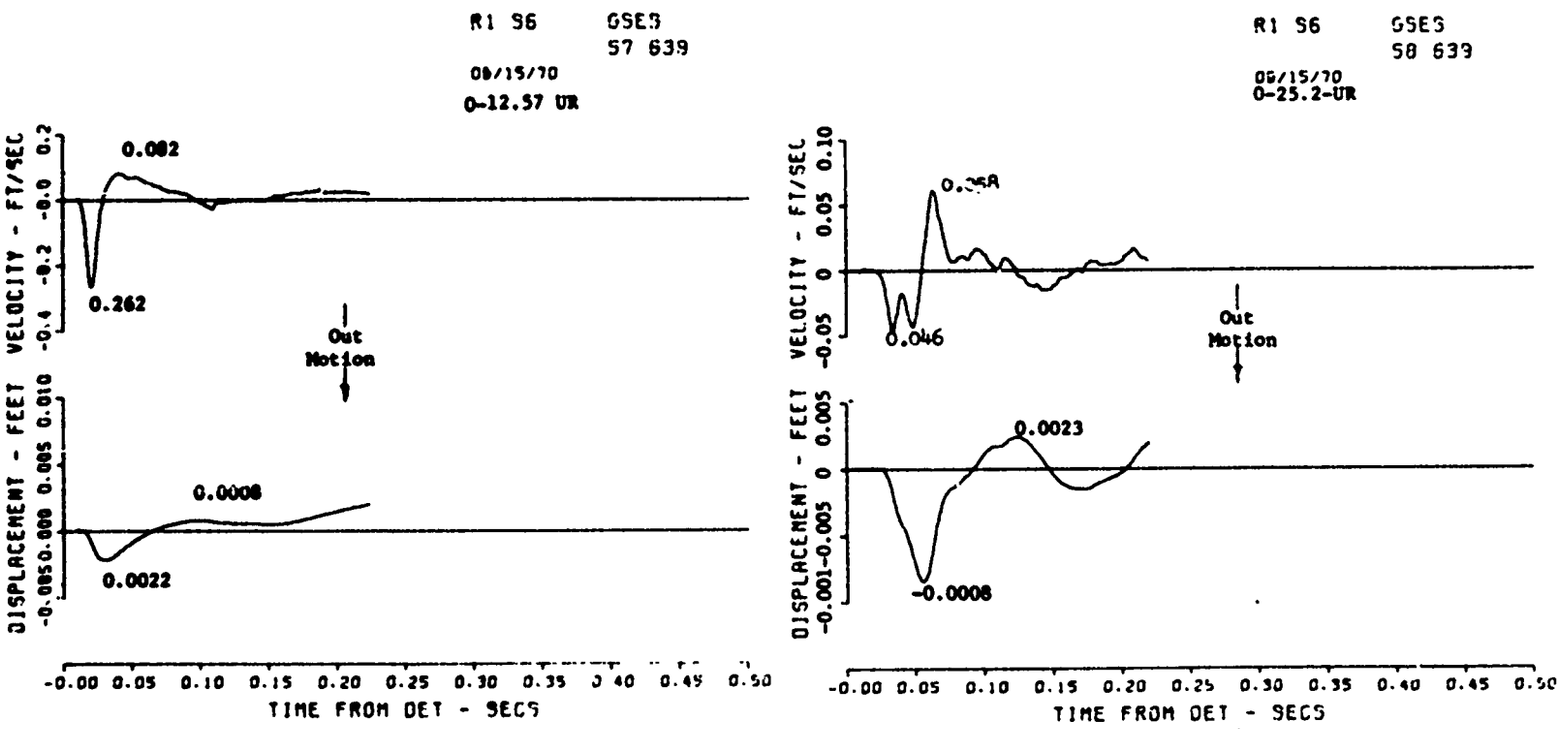

Figure A.12 (sheet 4 of 5).

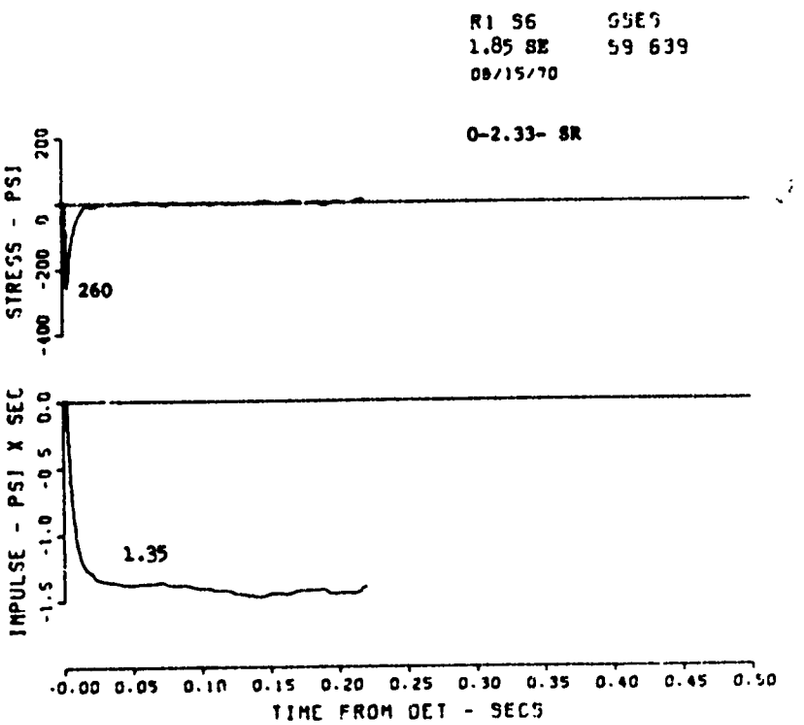

Figure A.12 (sheet 5 of 5).

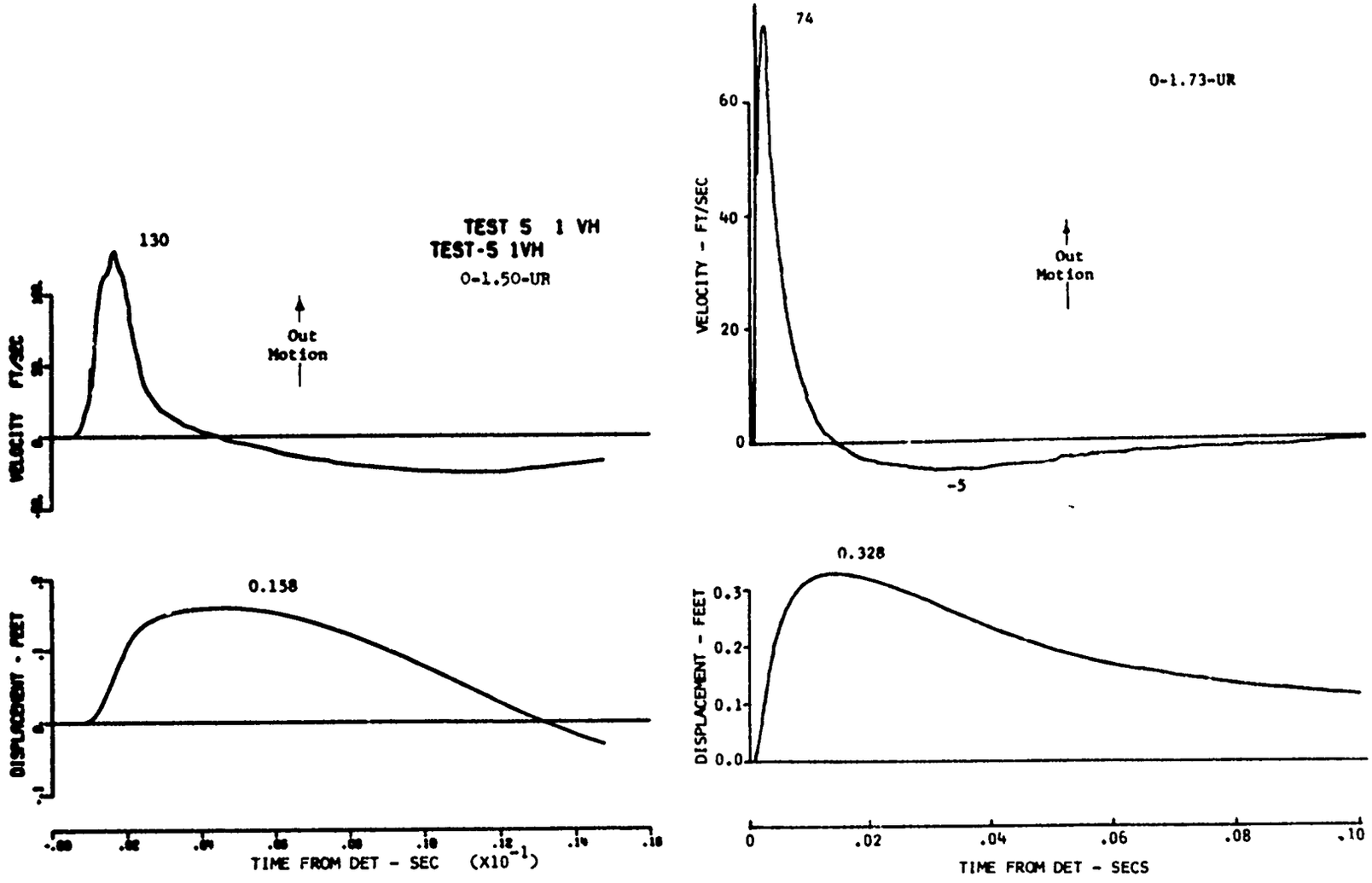

Figure A.13 Event 3, buried, +0.50 $W^{1/3}$ (+0.63 foot) (sheet 1 of 5).

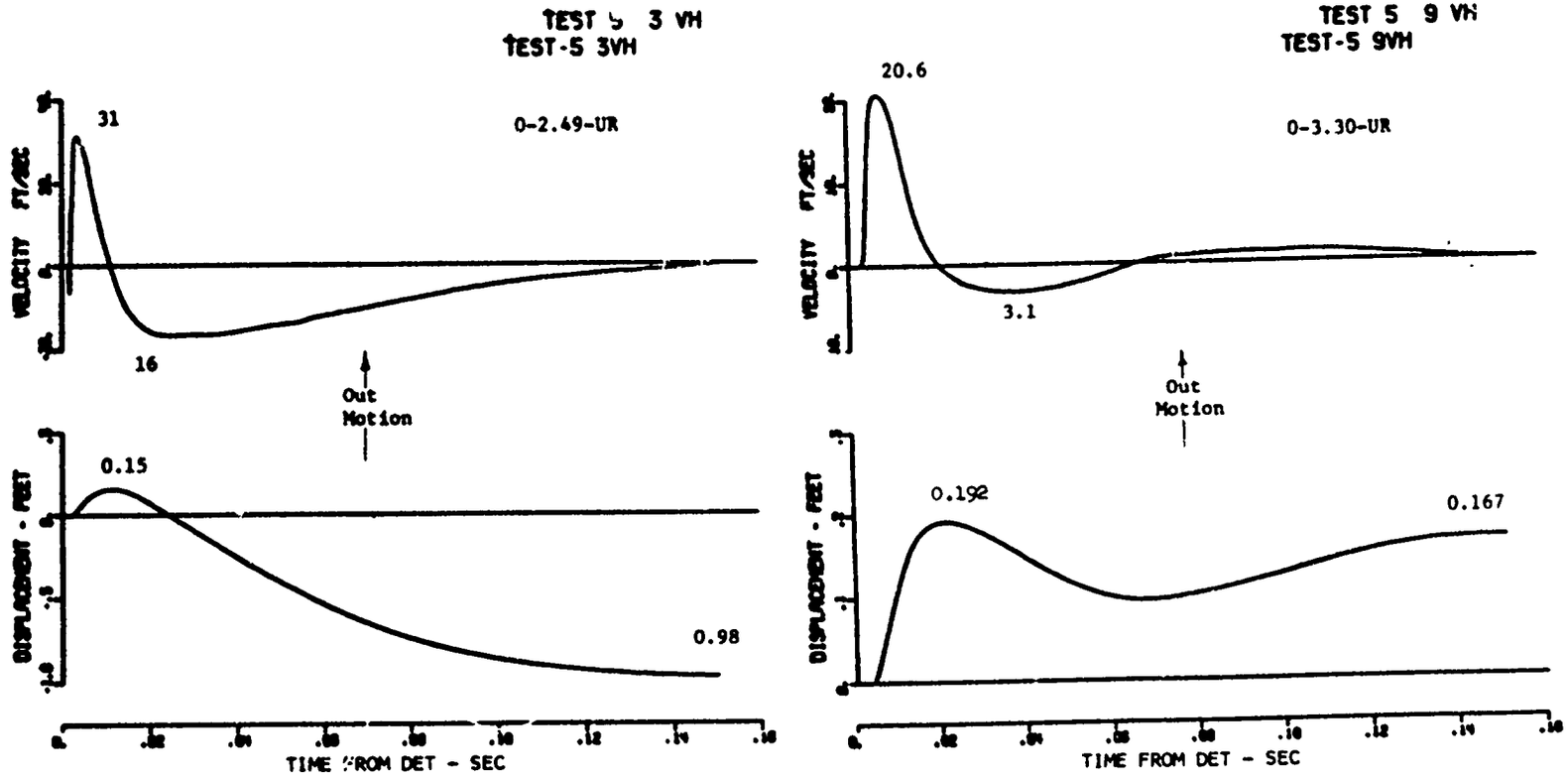

Figure A.13 (sheet 2 of 5).

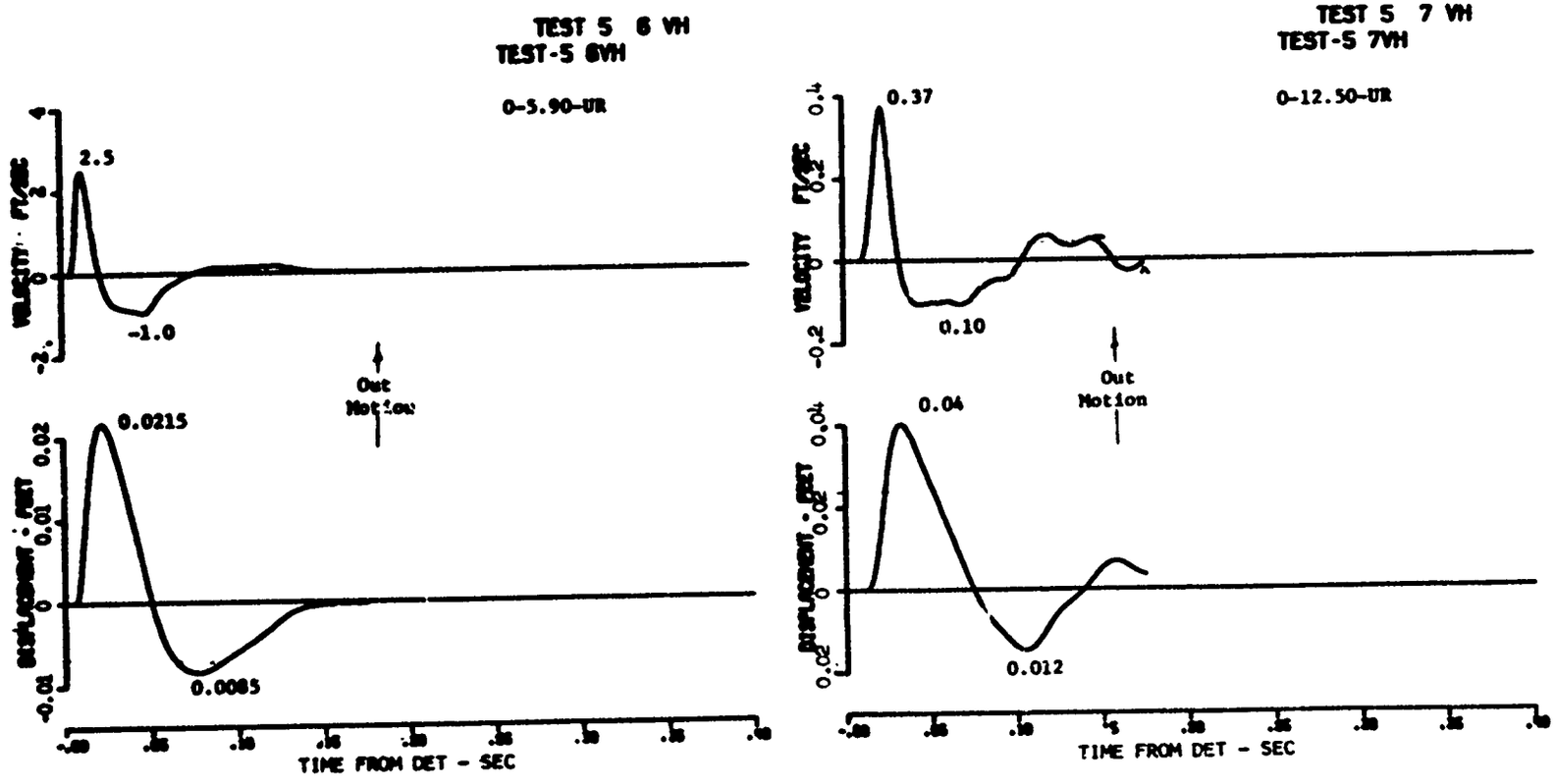

Figure A.13 (sheet 3 of 5).

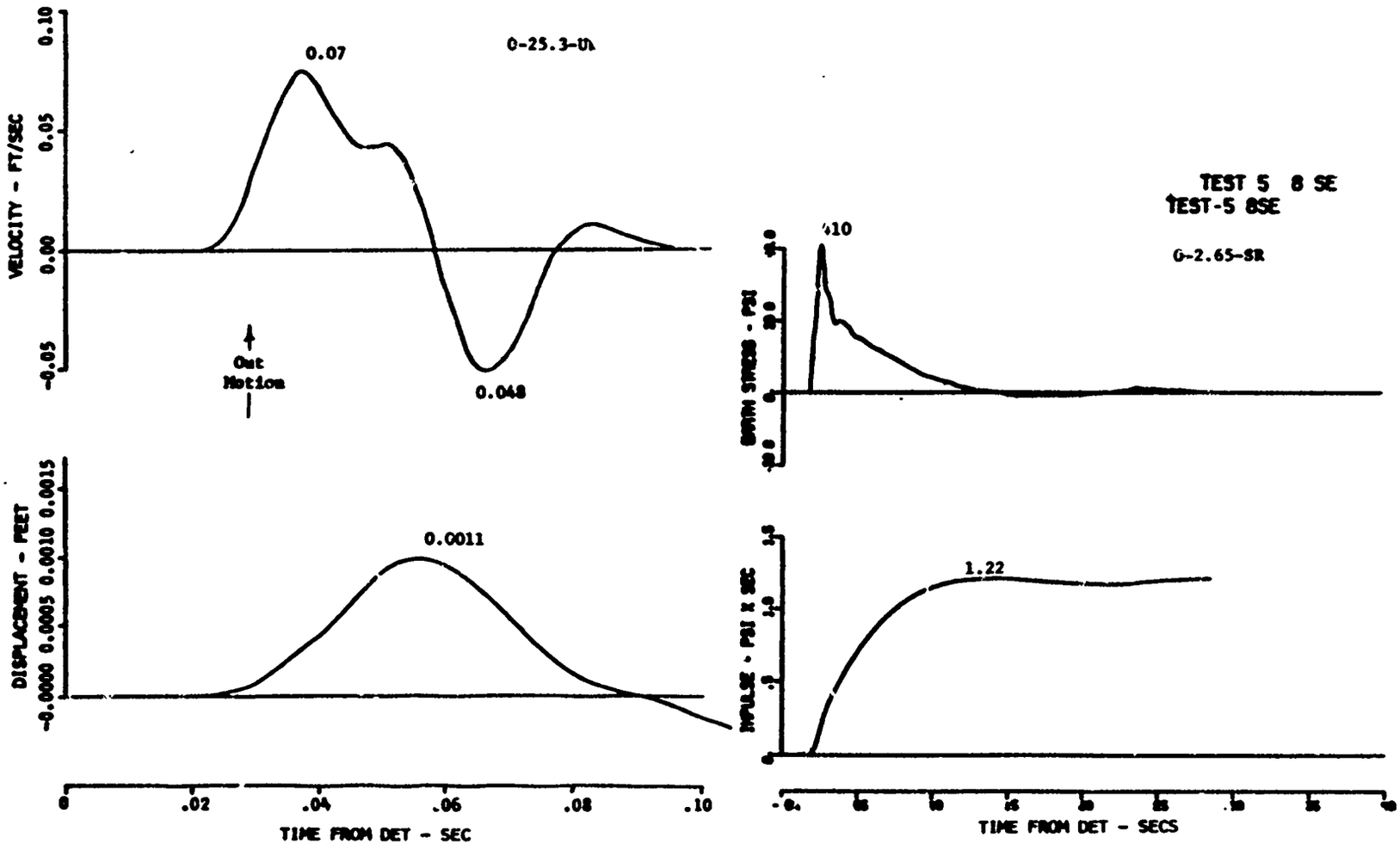

Figure A.13 (sheet 4 of 5).

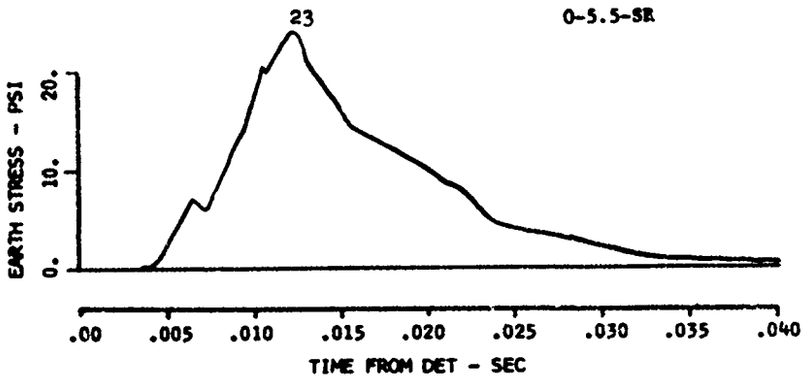

Figure A.13 (sheet 5 of 5).

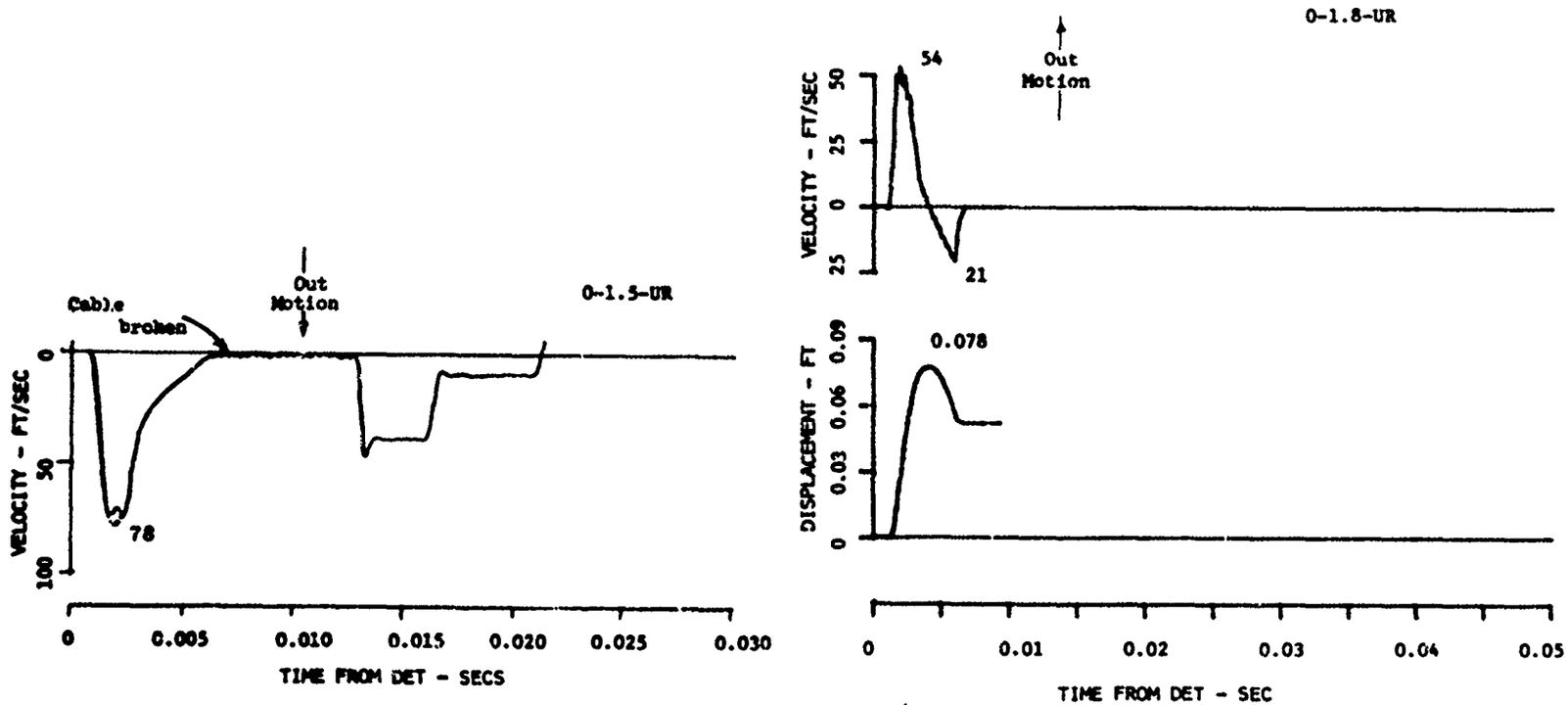

Figure A.14 Event 4, shot 1, buried, +0.75 $W^{1/3}$ (+0.94 foot) (sheet 1 of 6).

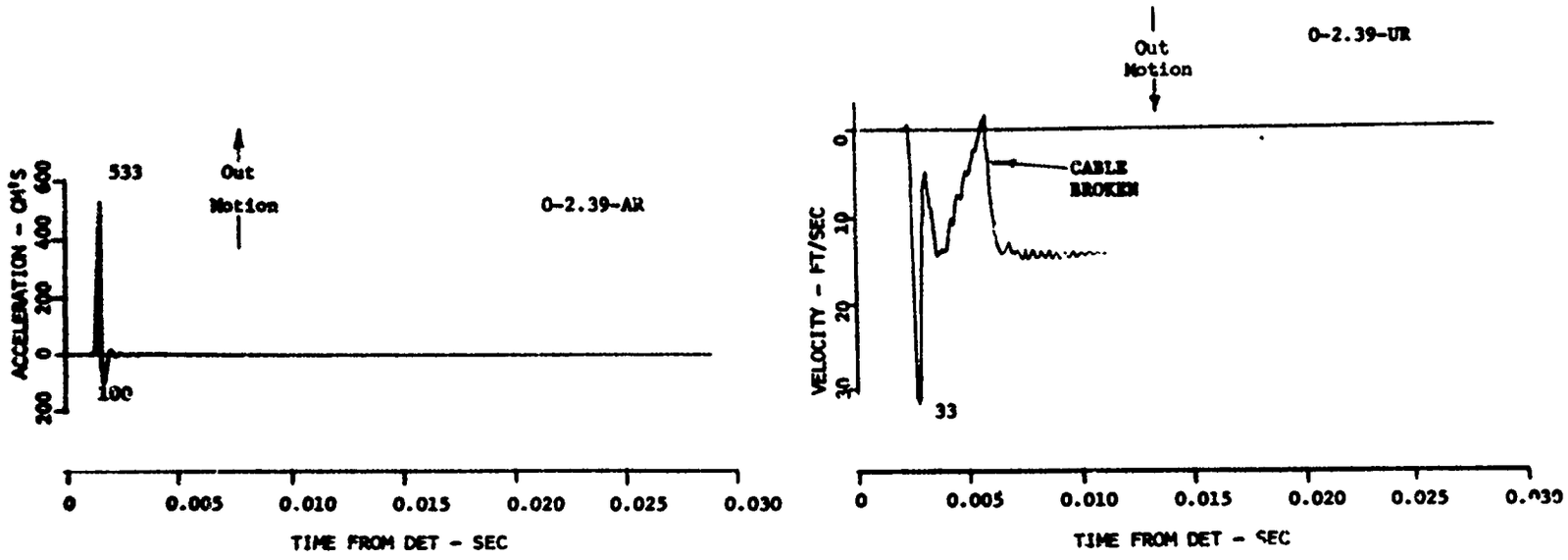

Figure A.14 (sheet 2 of 6).

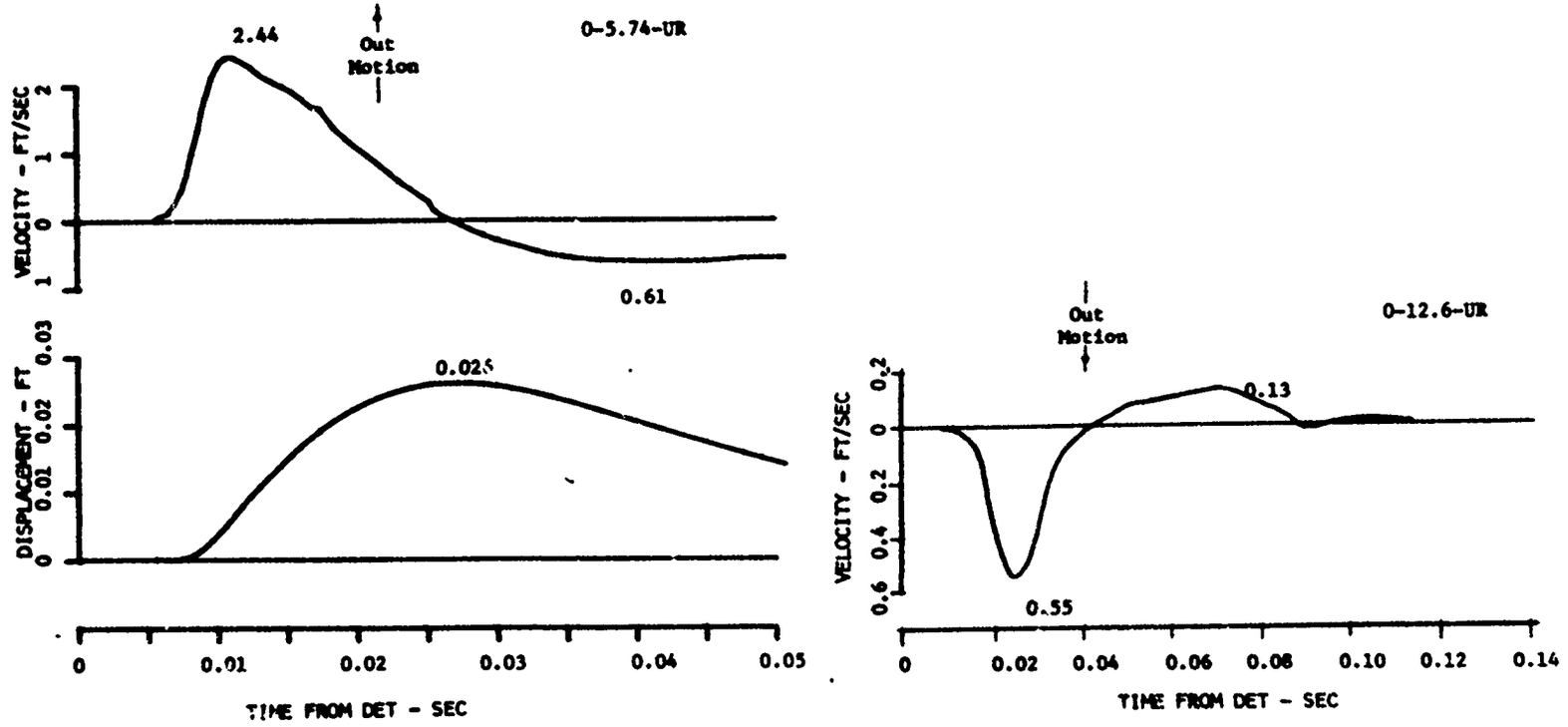

Figure A.14 (sheet 3 of 6).

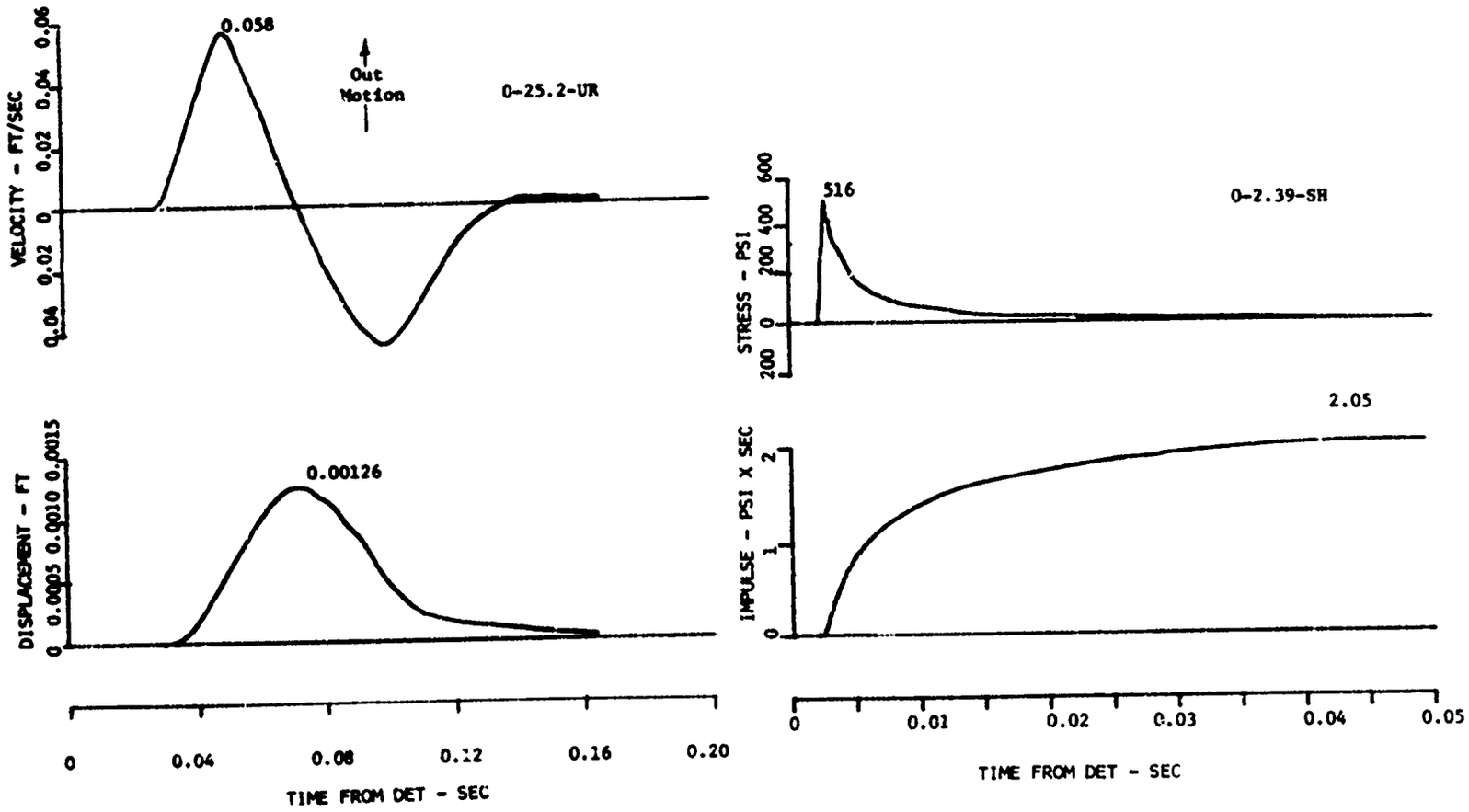

Figure A.14 (sheet 4 of 6).

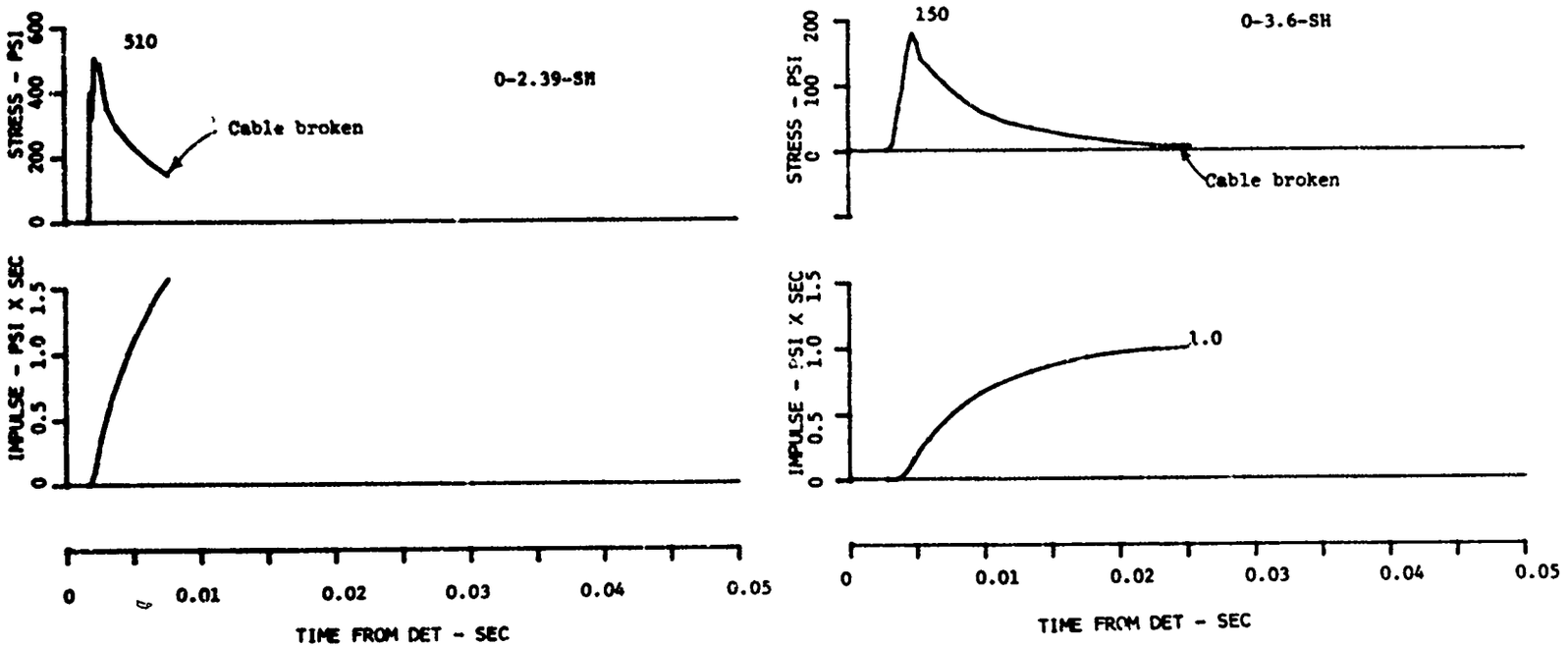

Figure A.14 (sheet 5 of 6).

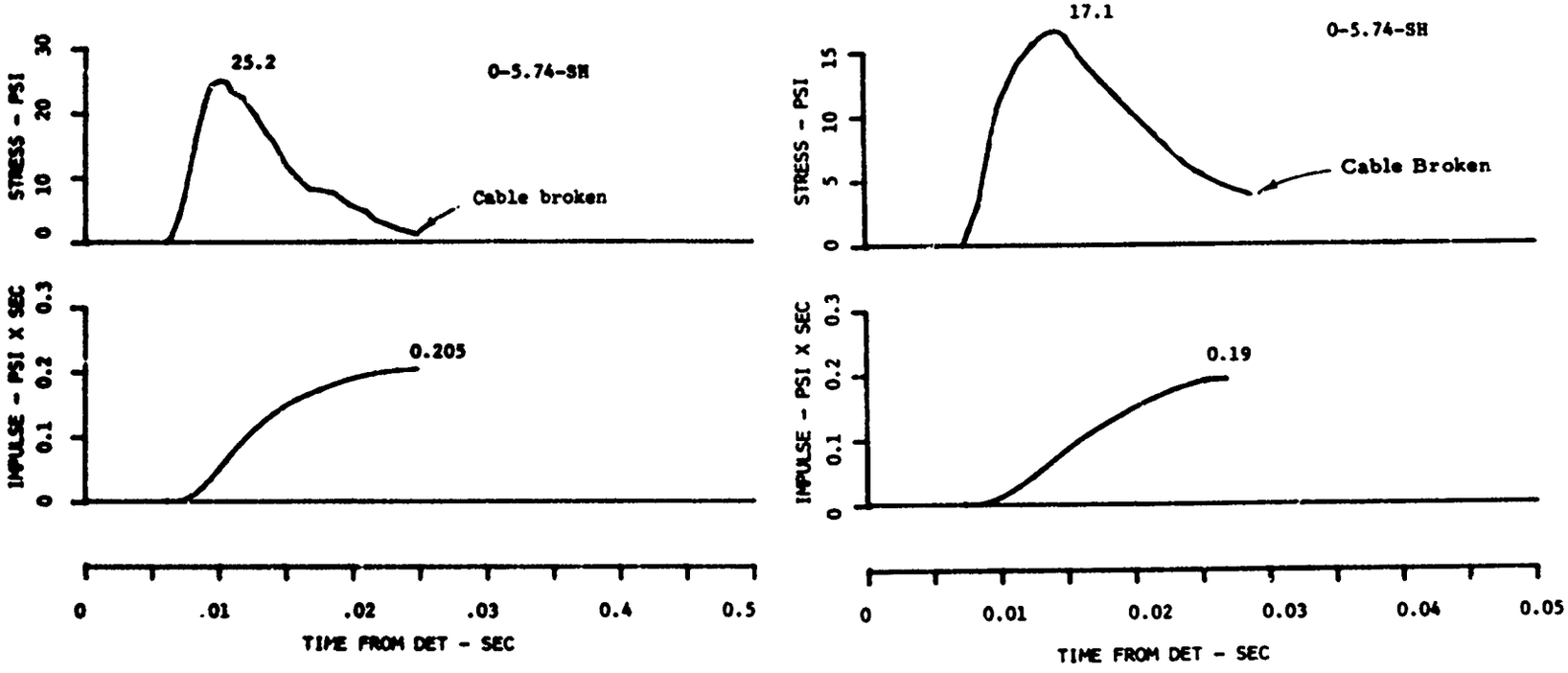

Figure A.14 (sheet 6 of 6).

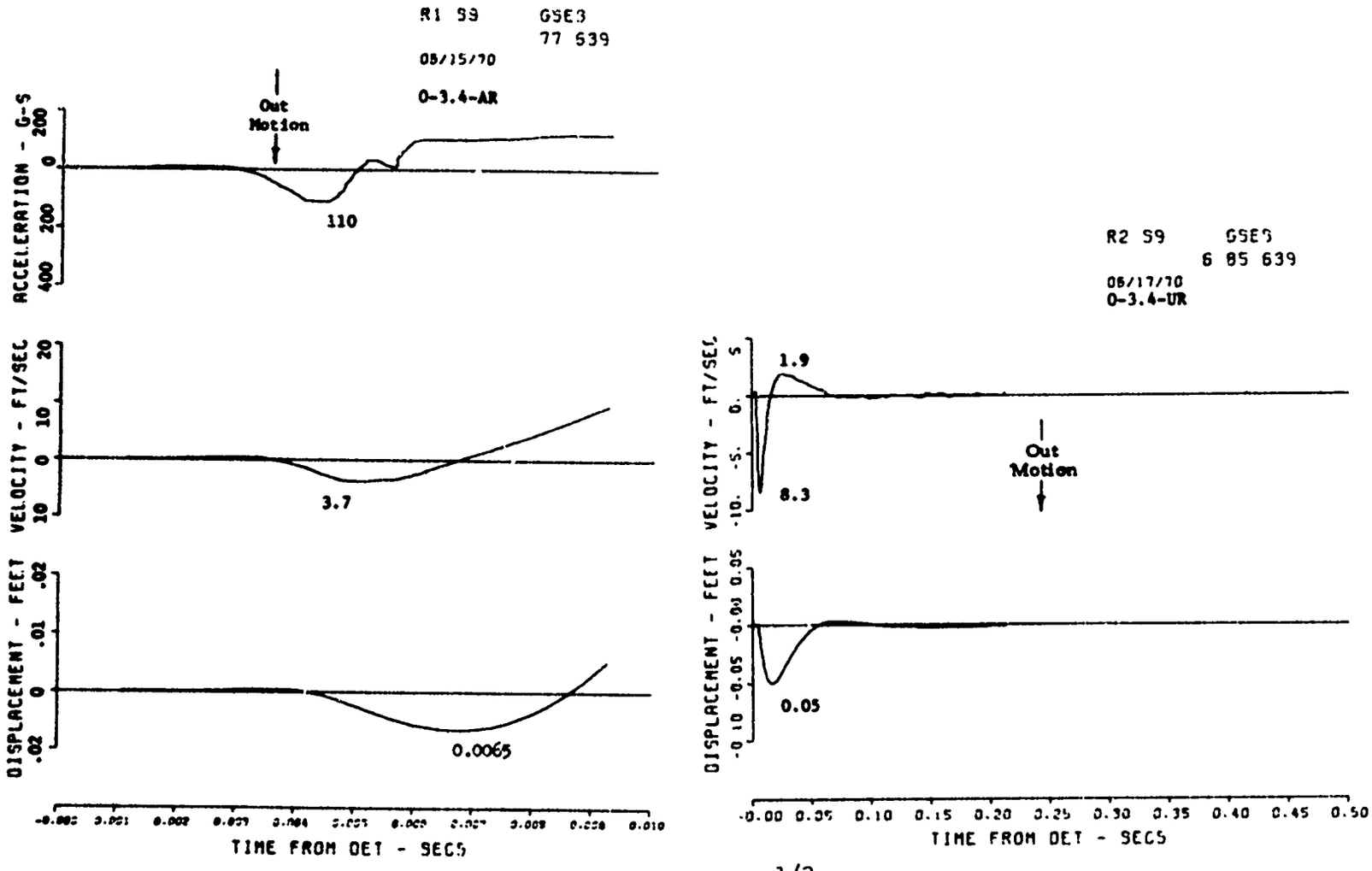

Figure A.15 Event 4, shot 2, buried, +0.75 $W^{1/3}$ (+0.94 foot) (sheet 1 of 6).

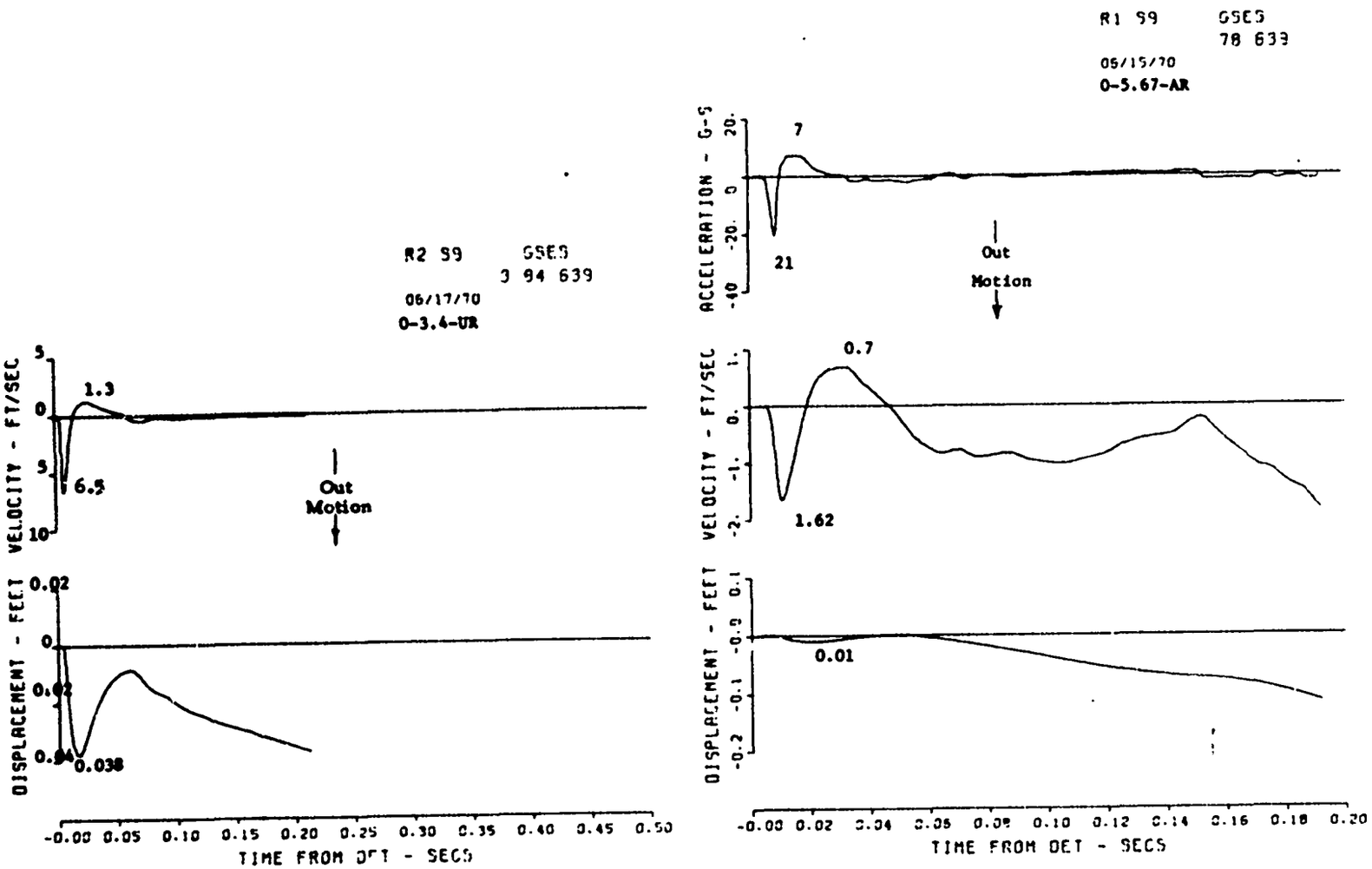

Figure A.15 (sheet 2 of 6).

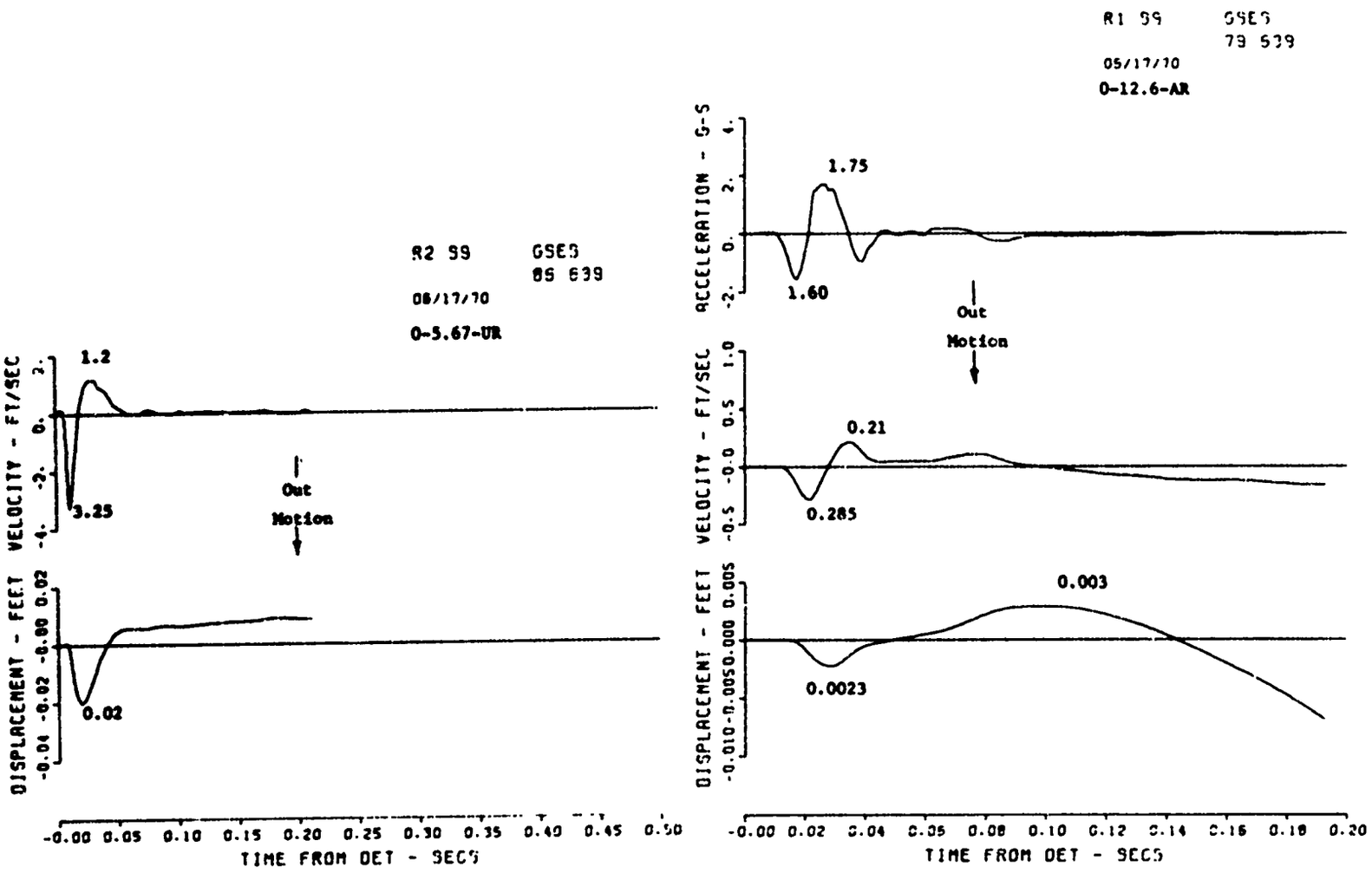

Figure A.15 (sheet 3 of 6).

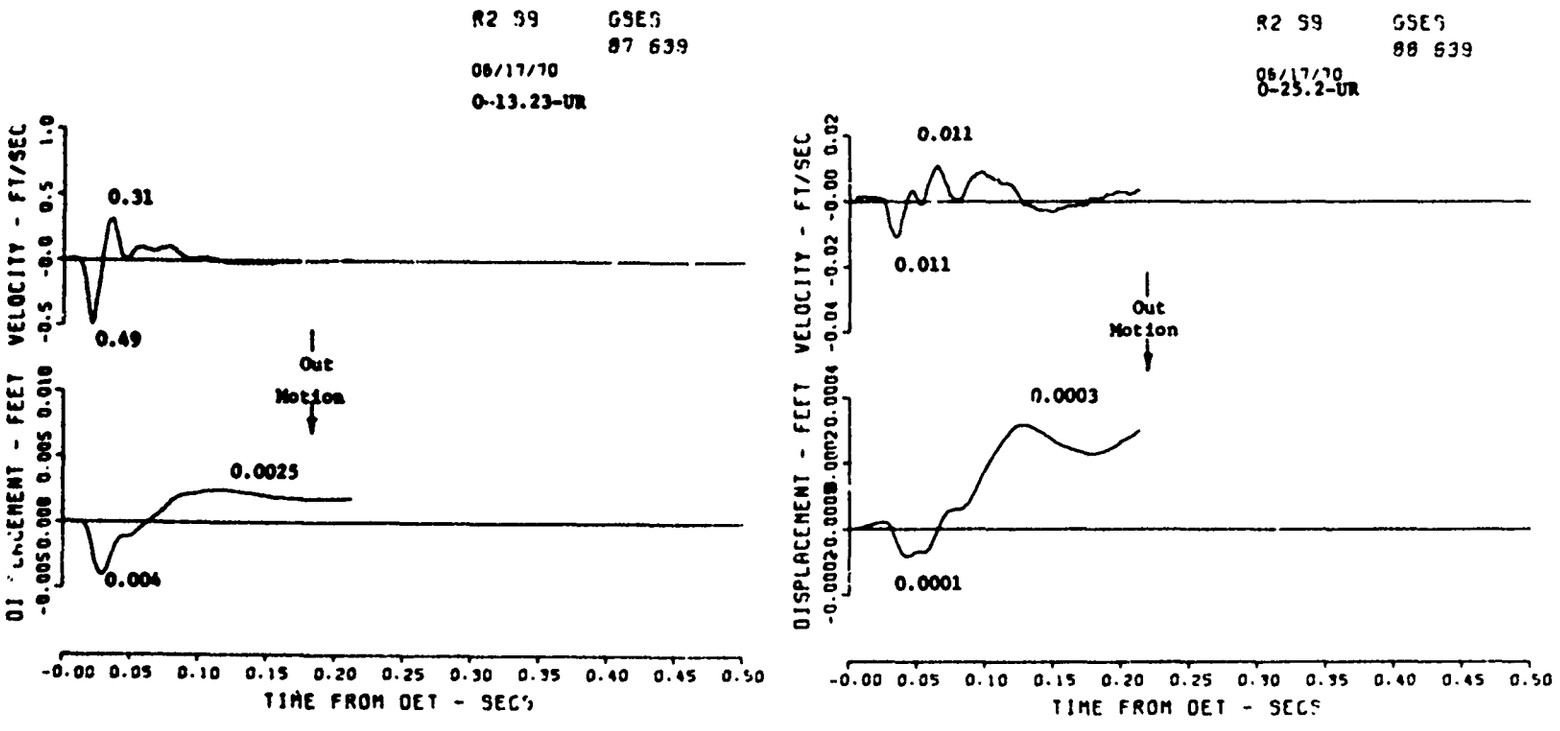

Figure A.15 (sheet 4 of 6).

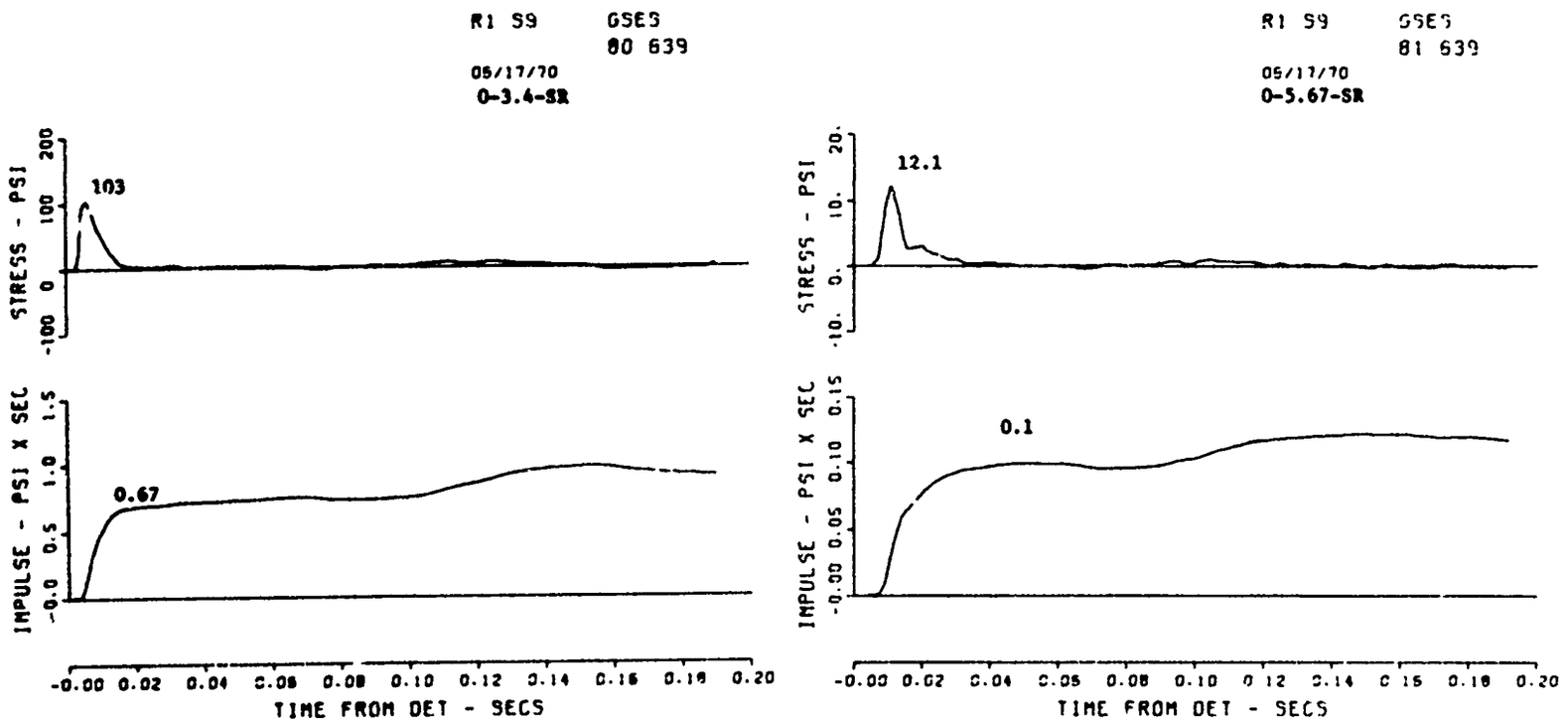

Figure A.15 (sheet 5 of 6)

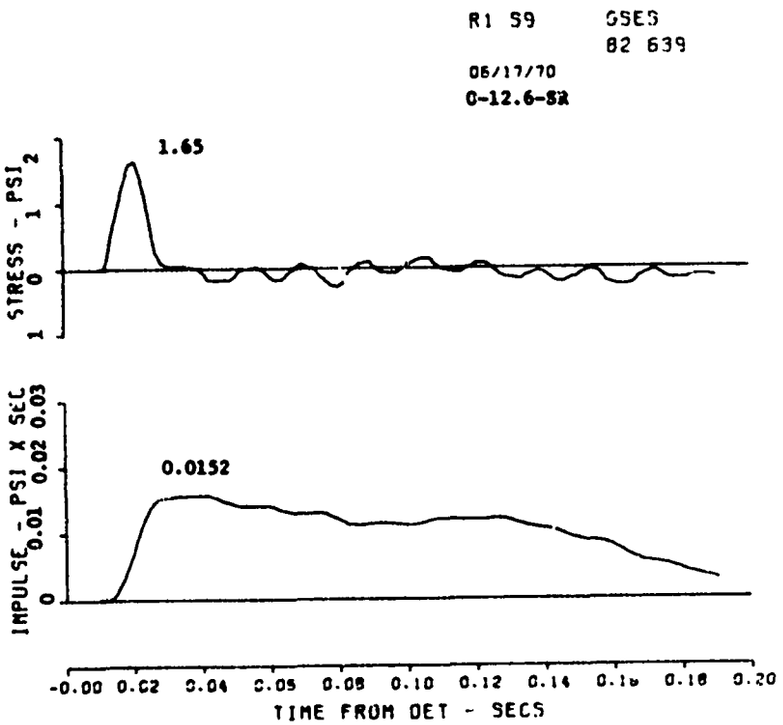

Figure A.15 (sheet 6 of 6).

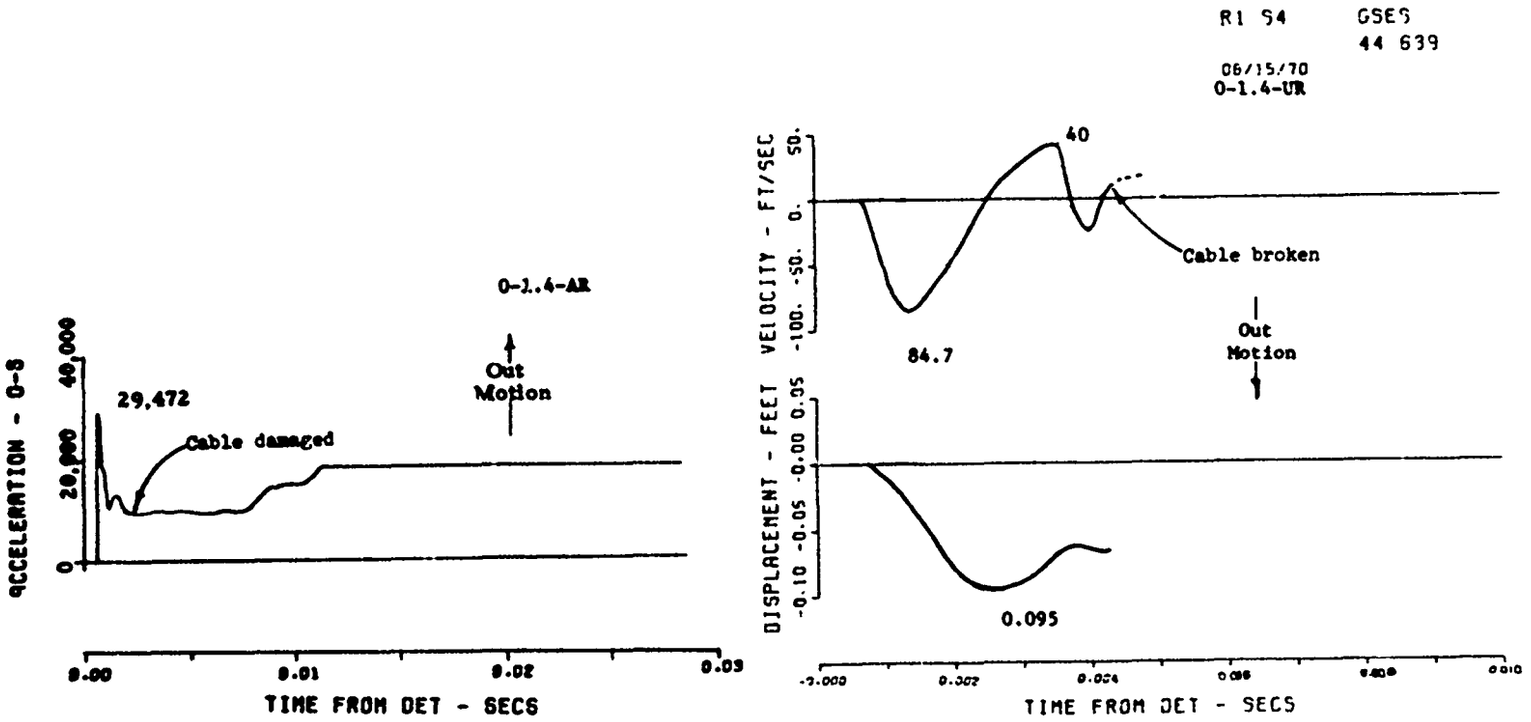

Figure A.16 Event 5, shot 1, buried, +1.00 $W^{1/3}$ (+1.26 feet) (sheet 1 of 5).

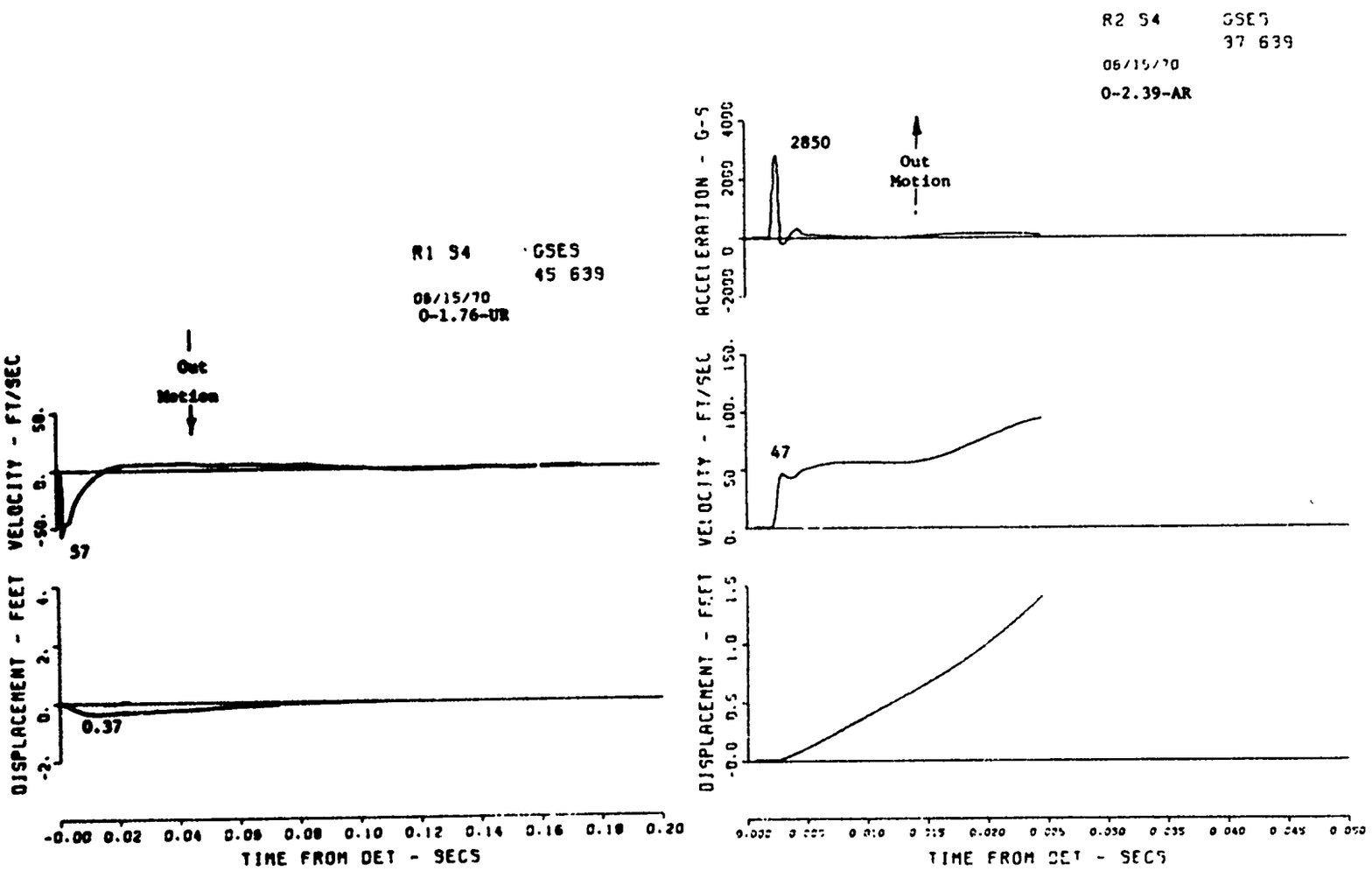

Figure A.16 (sheet 2 of 5).

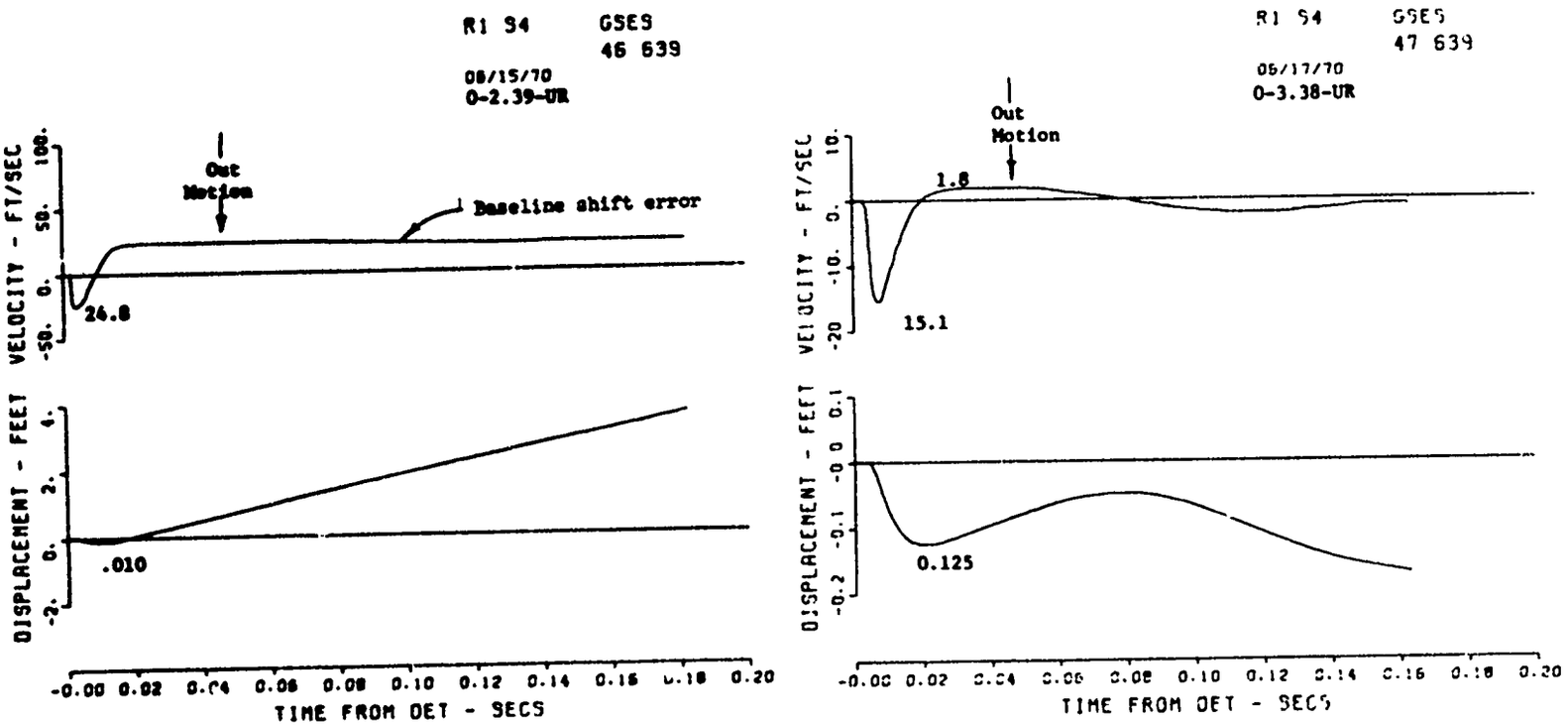

Figure A.16 (sheet 3 of 5).

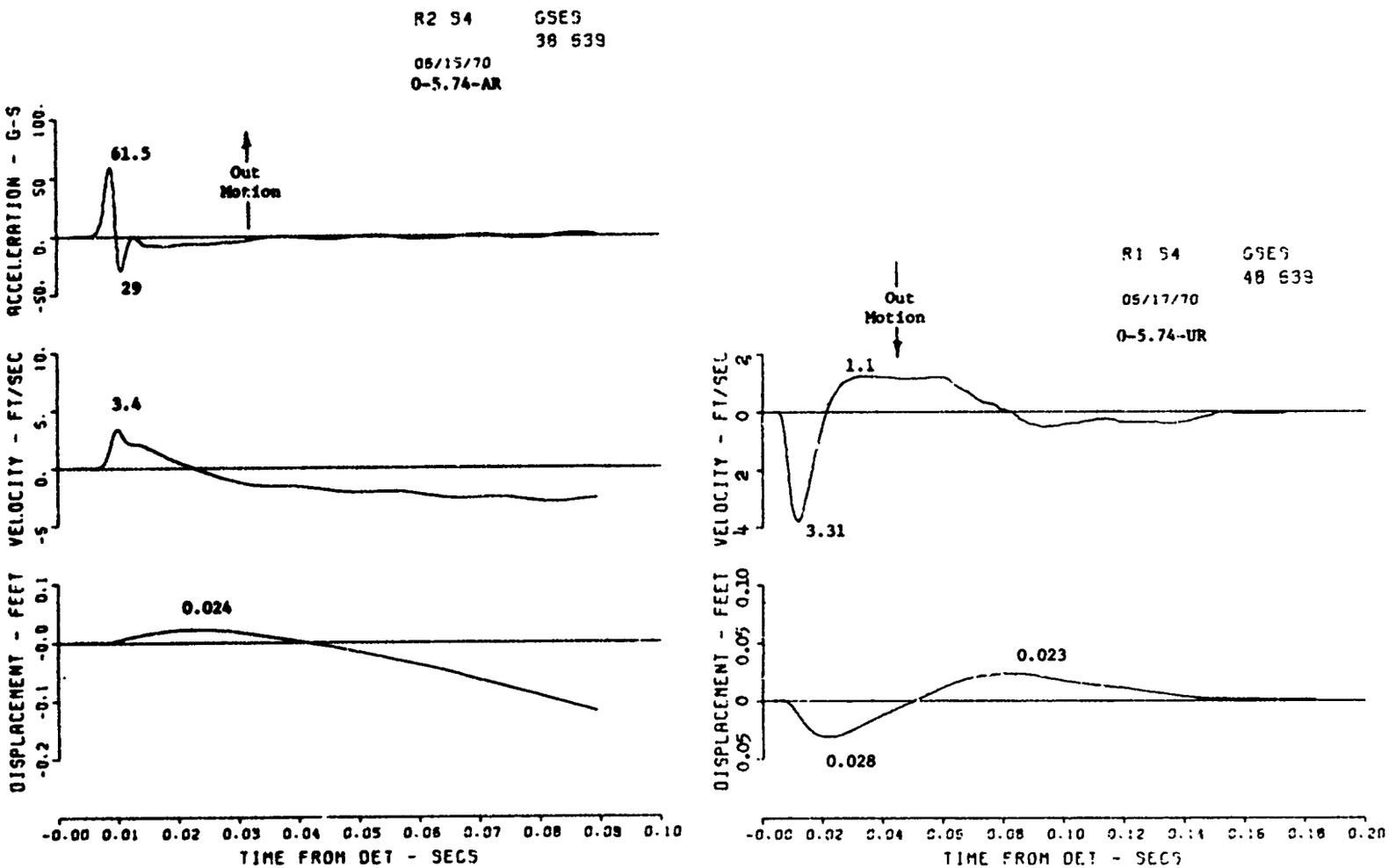

Figure A.16 (sheet 4 of 5).

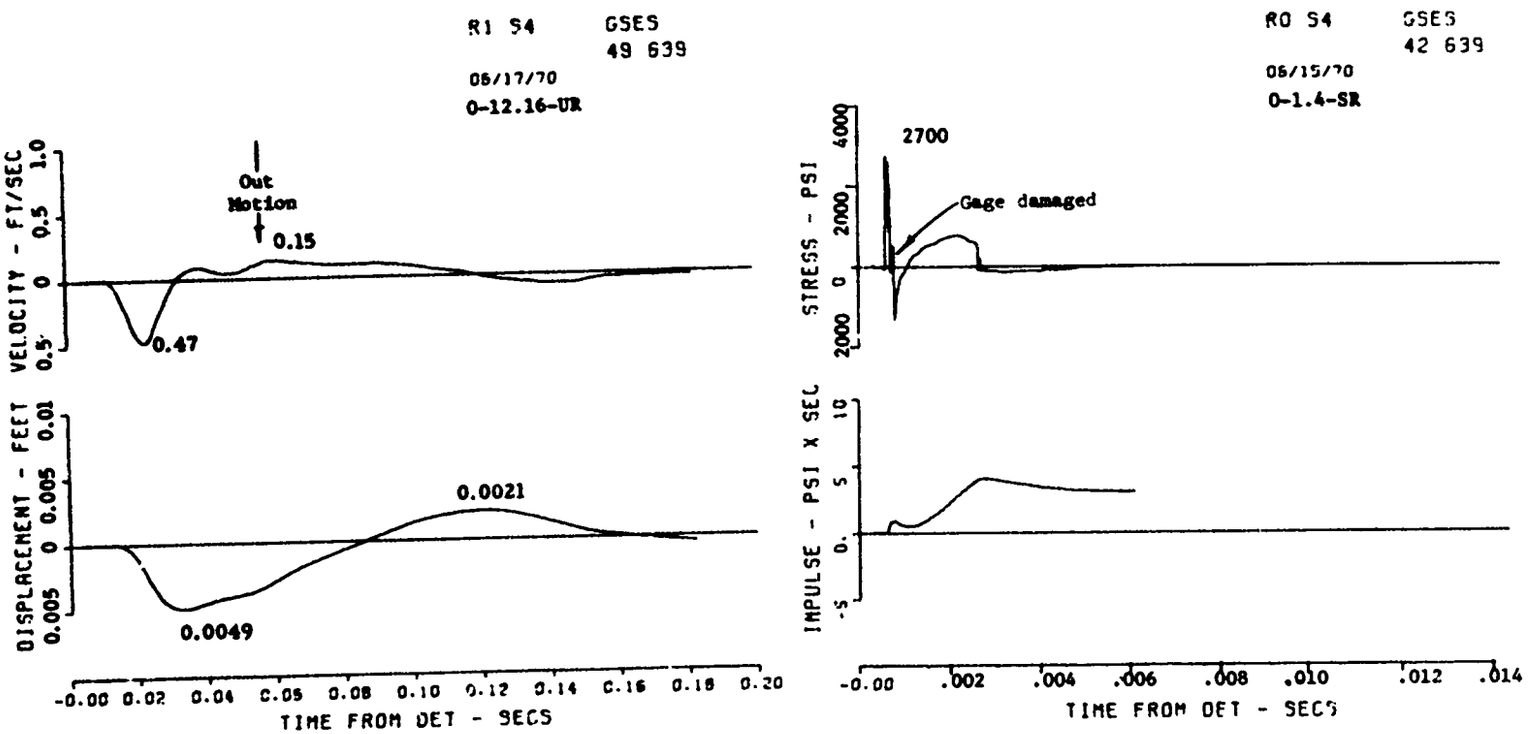

Figure A.16 (sheet 5 of 5).

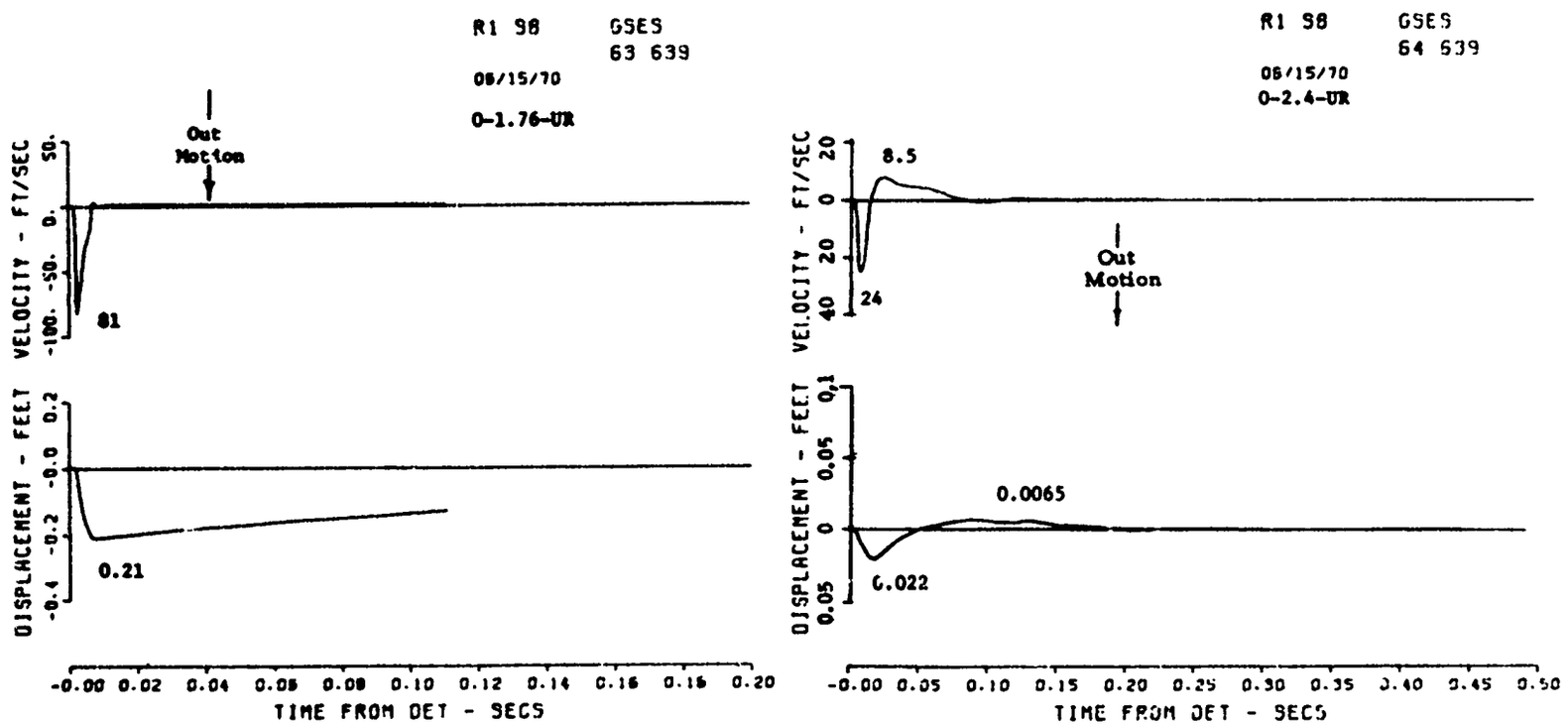

Figure A.17 Event 5, shot 2, buried, +1.00 $W^{1/3}$ (+1.26 feet) (sheet 1 of 6).

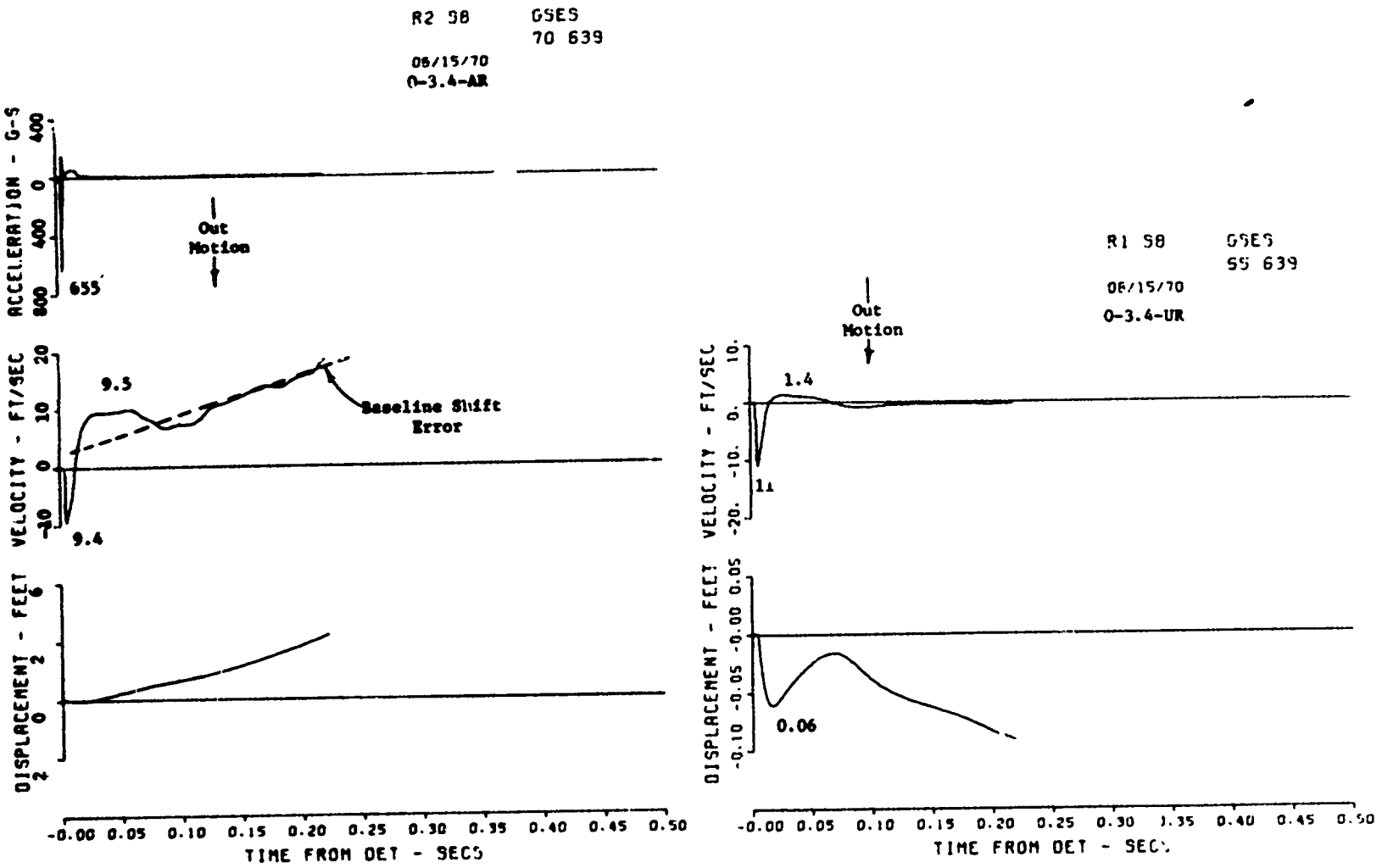

Figure A.17 (sheet 2 of 6).

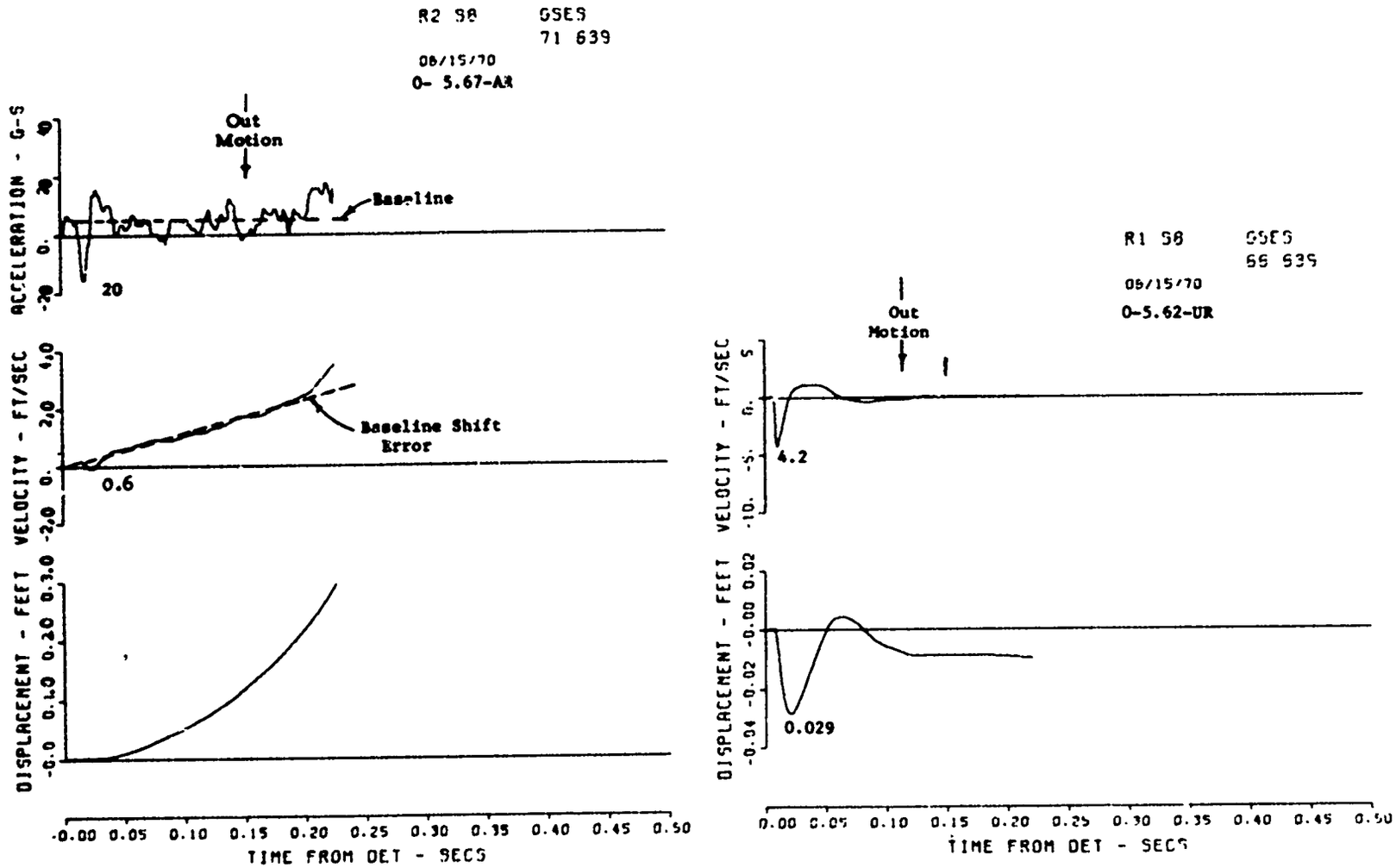

Figure A.17 (sheet 3 of 6).

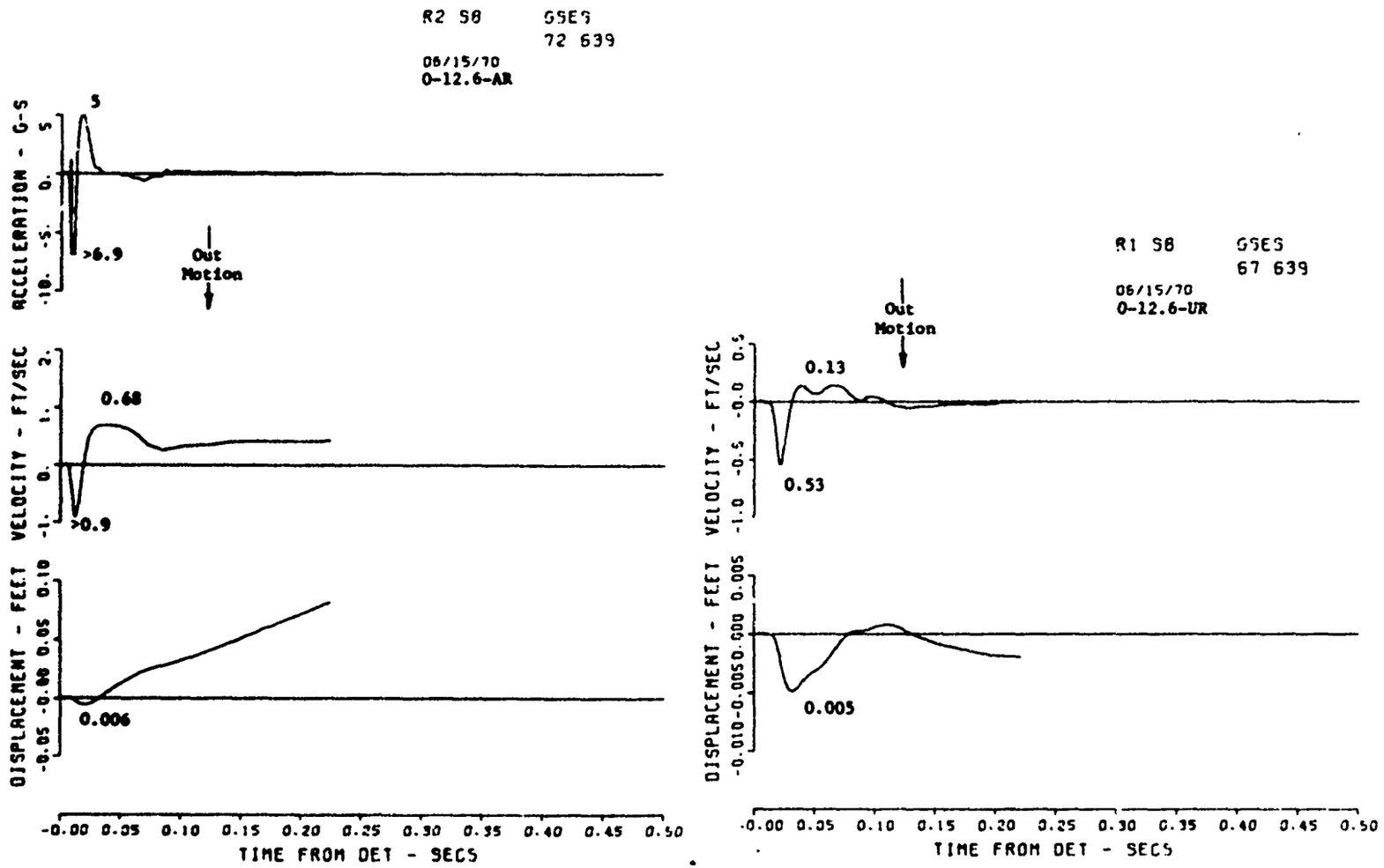

Figure A.17 (sheet 4 of 6).

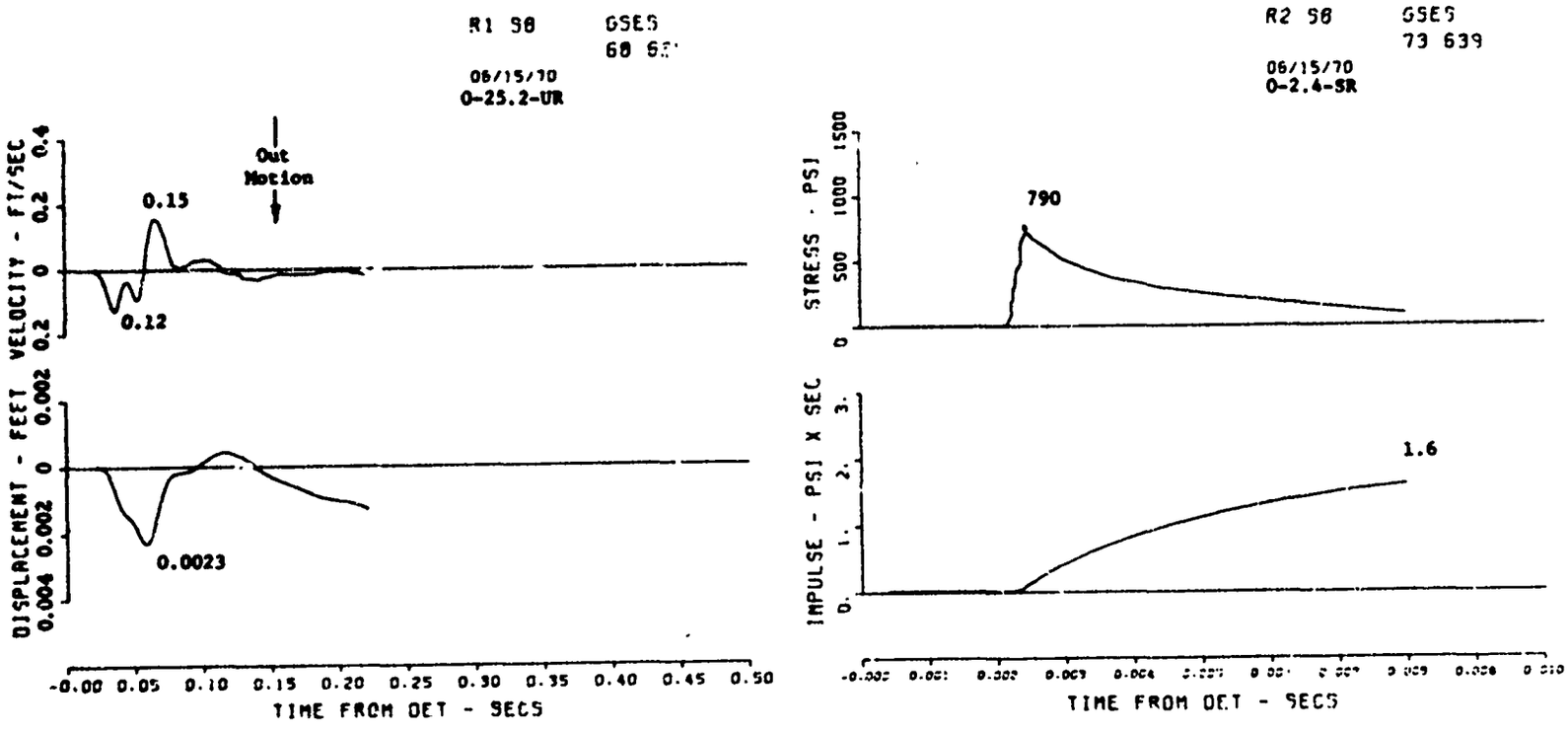

Figure A.17 (sheet 5 of 6).

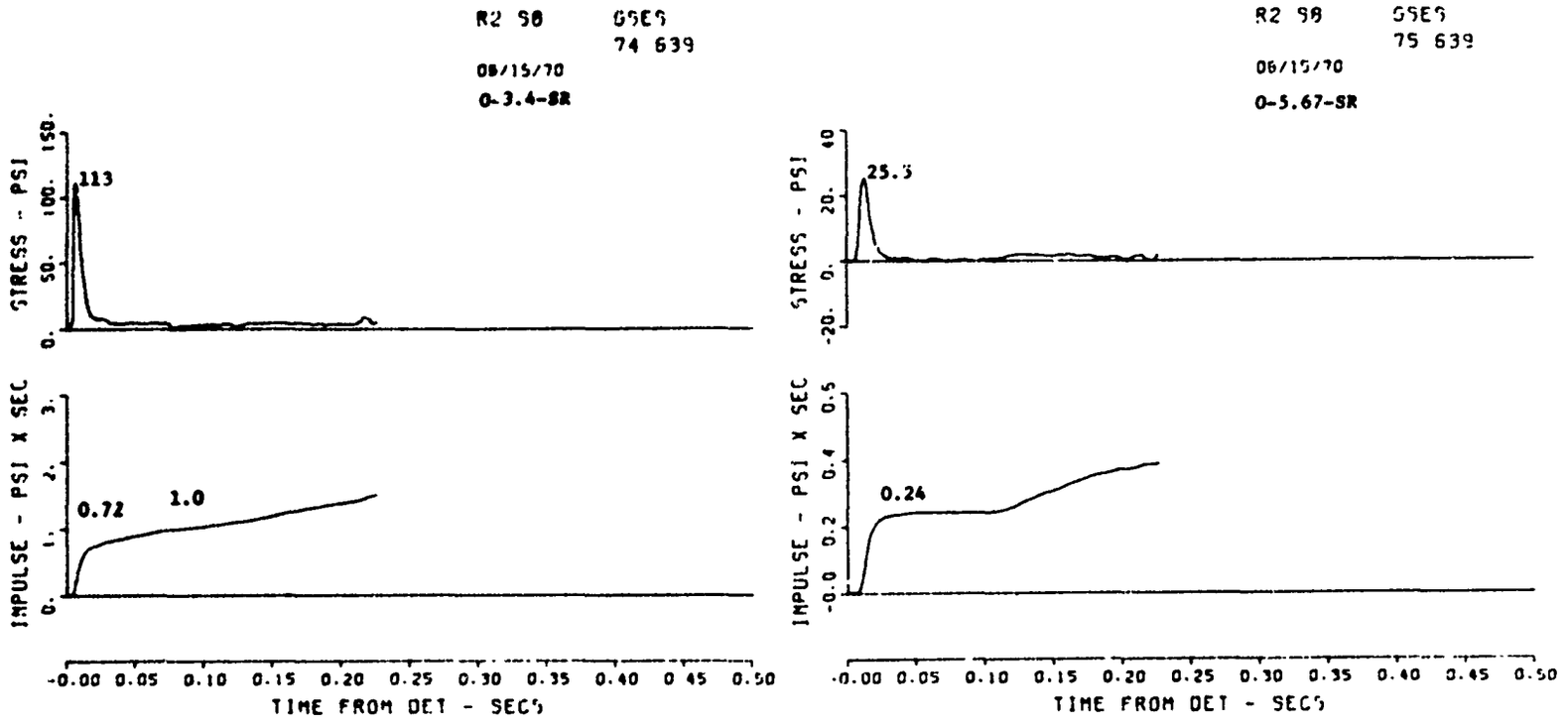

Figure A.17 (sheet 6 of 6).

APPENDIX B

CENSE 2 GROUND MOTION, STRESS, AND SURFACE AIRBLAST-TIME HISTORIES

B.1 DATA TREATMENT

The original analog tapes were digitized and processed on the U. S. Army Engineer Waterways Experiment Station (WES) computer. Various subroutines were used as needed to make corrections for temperature effects on the velocity gage records (Reference 8)[1], filtering, and baseline shifting (References 10 and 11), especially where single and double integrations were performed. Table B.1 lists digital bandpass frequencies. Figure B.1 provides a graphical explanation of the various baseline correction techniques used.

B.2 TIME HISTORIES PRESENTATION

Time histories in Figures B.2-B.23 are presented such that upward motion, outward motion (away from ground zero (GZ)), and compression are upward (positive) on the plots. Conversely, downward motion and inward motion are downward (negative) on the plots. Insert figures on the plots are uncorrected data shown in the "as recorded" condition.

Identification labeling on the plots is formatted as follows:

Location: Upper right-hand corner of plot.

First Line: Experiment, event number.

Second Line: Gage identifier, i.e., distance from GZ in feet, depth in feet, parameter, orientation, and analog tape number, track.

Third Line: Digitizing rate, Hz

Fourth Line: Filter option

Fifth Line: Date, digital tape reel numbers

[1] Reference numbers refer to similarly numbered items in the list of References at the end of the main text.

EXAMPLE:

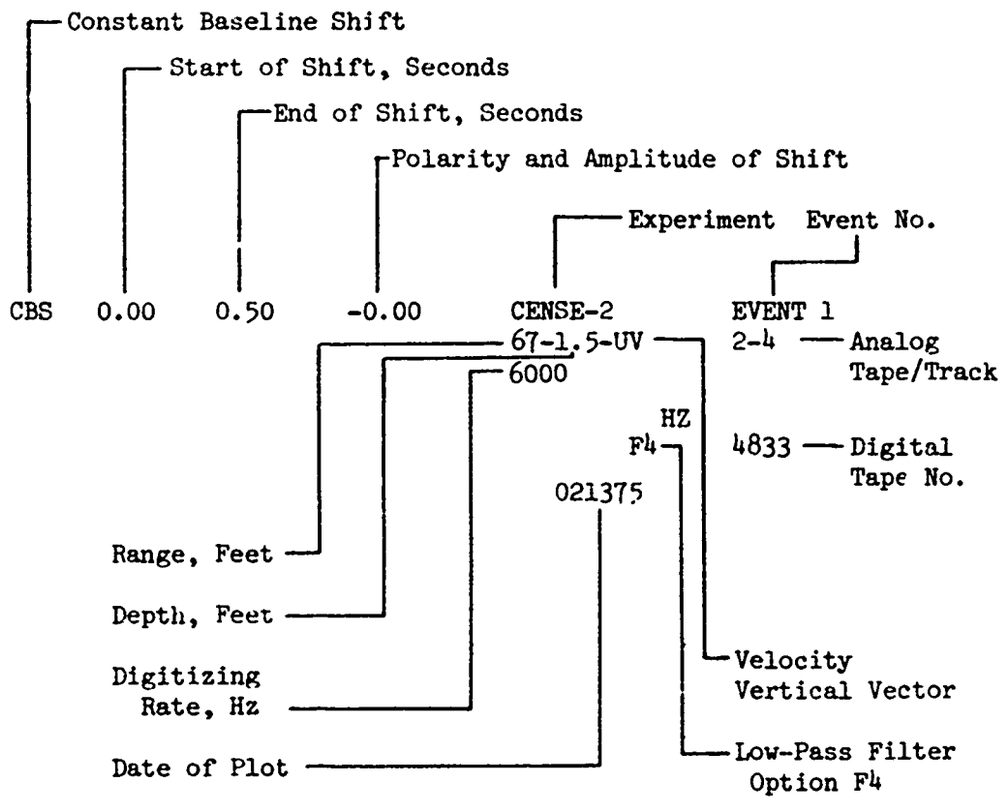
Constant Baseline Shift
Start of Shift, Seconds
End of Shift, Seconds
Polarity and Amplitude of Shift
Experiment
Event No.
CBS
0.00
0.50
-0.00
CENSE-2
EVENT 1
67-1.5-UV
2-4
Analog Tape/Track
6000
HZ
F4
4833
Digital Tape No.
021375
Range, Feet
Depth, Feet
Digitizing Rate, Hz
Date of Plot
Velocity Vertical Vector
Low-Pass Filter Option F4

TABLE B.1 DIGITAL FILTER BANDPASS FREQUENCIES.[a]

Filter Option	Digital Filter Bandpass Frequencies, Hz, at Indicated Digital Sample Rates															
	1000		2000		4000		6000		12,000		24,000		48,000		96,000	
	All Pass	No Pass	All Pass	No Pass	All Pass	No Pass	All Pass	No Pass	All Pass	No Pass	All Pass	No Pass	All Pass	No Pass	All Pass	No Pass
F1	115	243	230	486	460	972	690	1460	1380	2920	2760	5840	5520	11,700	11,040	23,400
F2	50	120	100	240	200	480	300	720	600	1440	1200	2880	2400	5,760	4,800	11,520
F3	40	80	80	160	160	320	240	480	480	960	960	1920	1920	3,840	3,840	7,680
F4	32	60	63	120	125	240	190	360	380	720	760	1440	1520	2,880	3,040	5,760

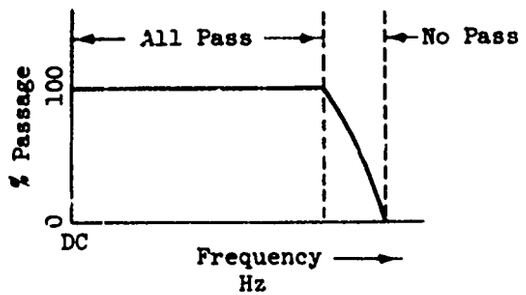

[a] References 10 and 11.

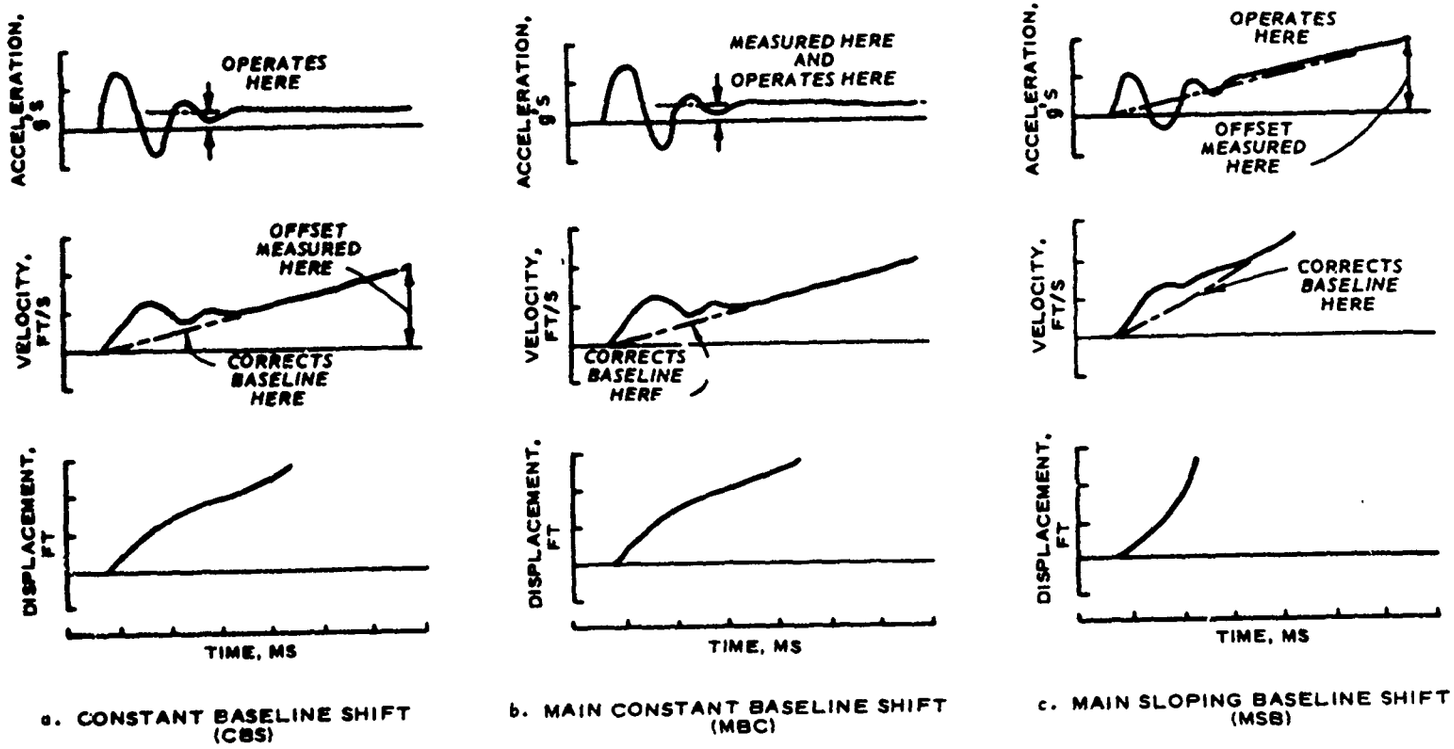

Figure B.1 Baseline correction techniques (shifts are exaggerated for illustration purposes).

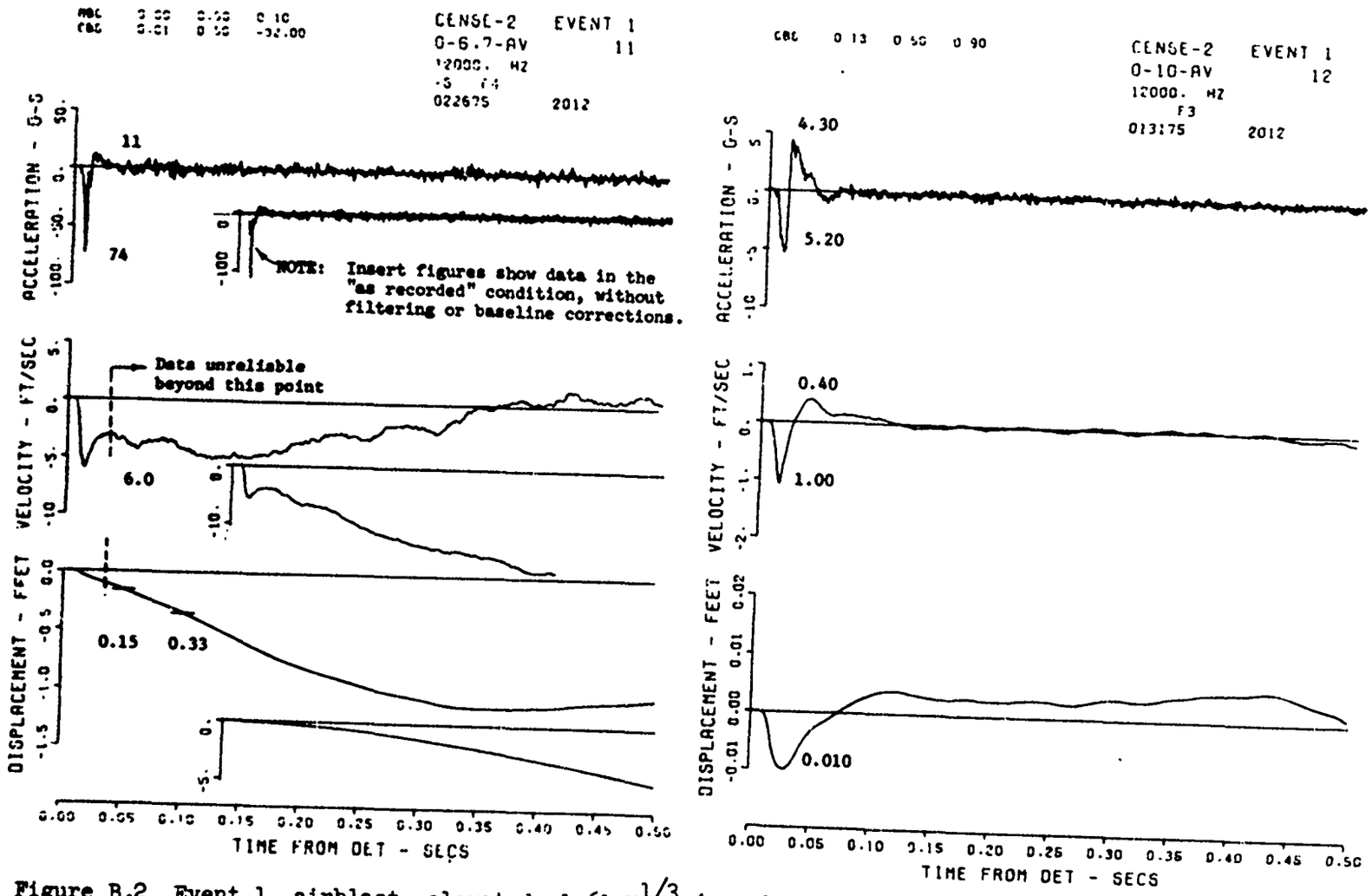

Figure B.2 Event 1, airblast, elevated -1.61 $W^{1/3}$ (-10.8 feet); motion- and stress-time histories along the vertical radial directly beneath the explosion (sheet 1 of 5).

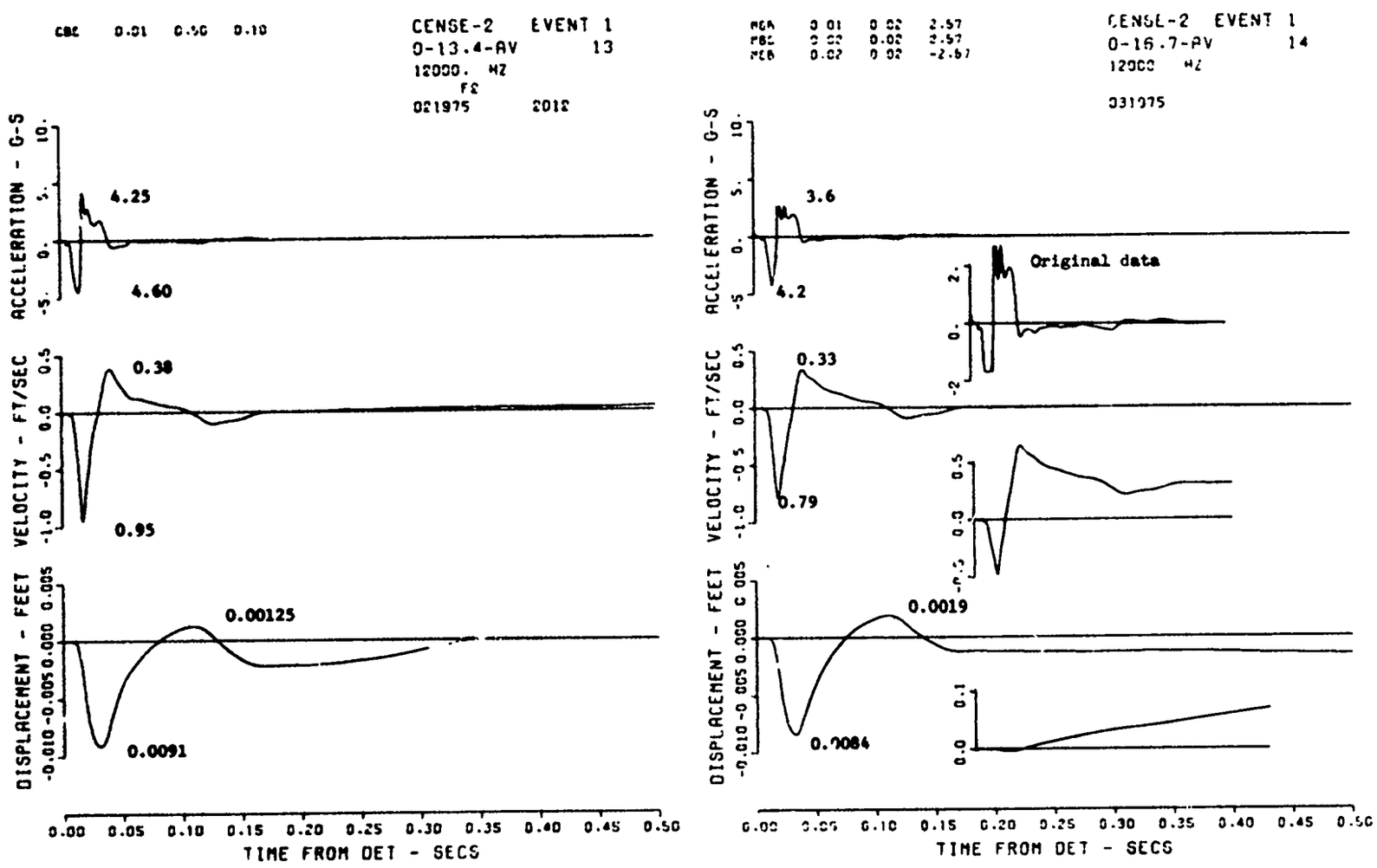

Figure B.2 (sheet 2 of 5).

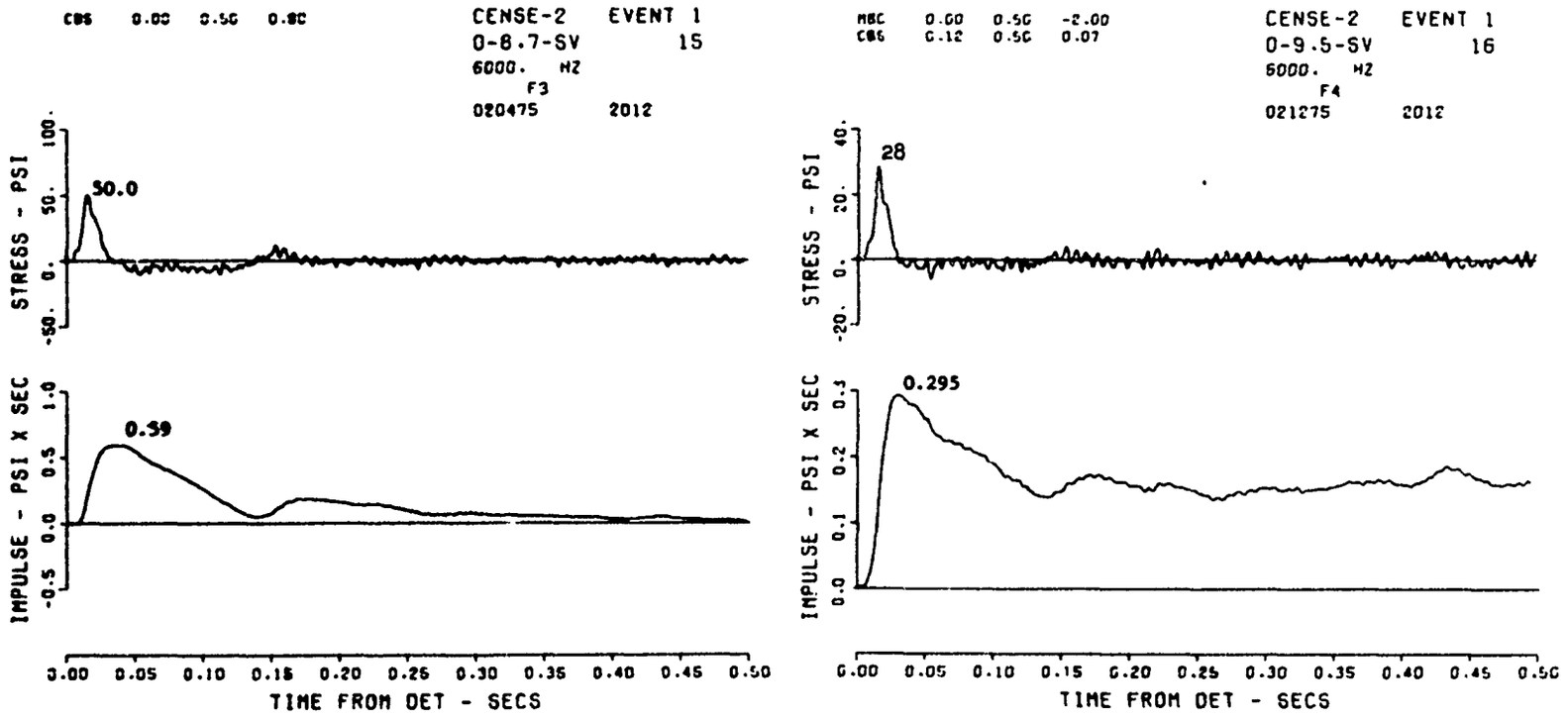

Figure B.2 (sheet 3 of 5).

CENSE-2 EVENT 1
0-20.1-AV

NO DATA RECOVERED
(GAGE SCRATCHED PRESHOT)

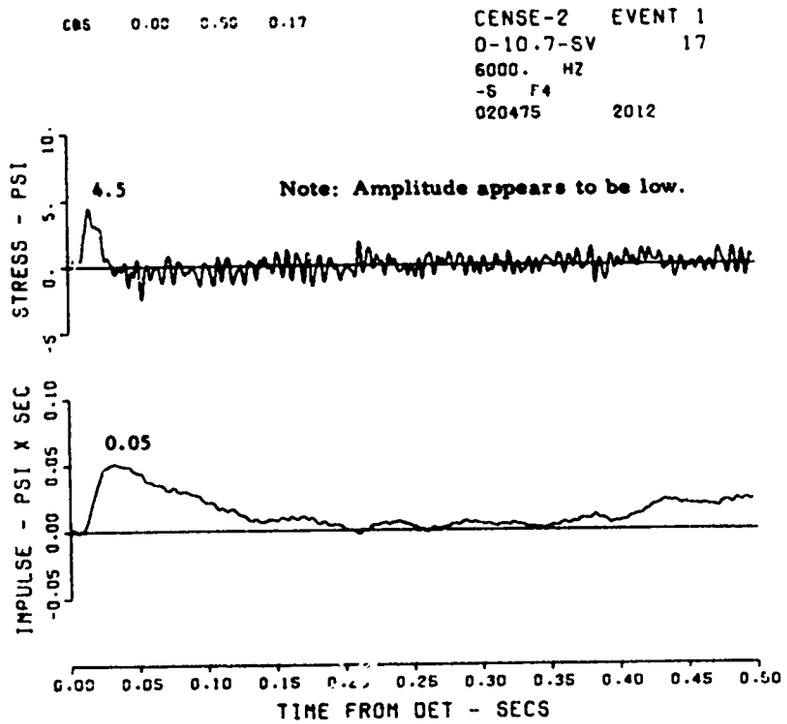

Figure B.2 (sheet 4 of 5).

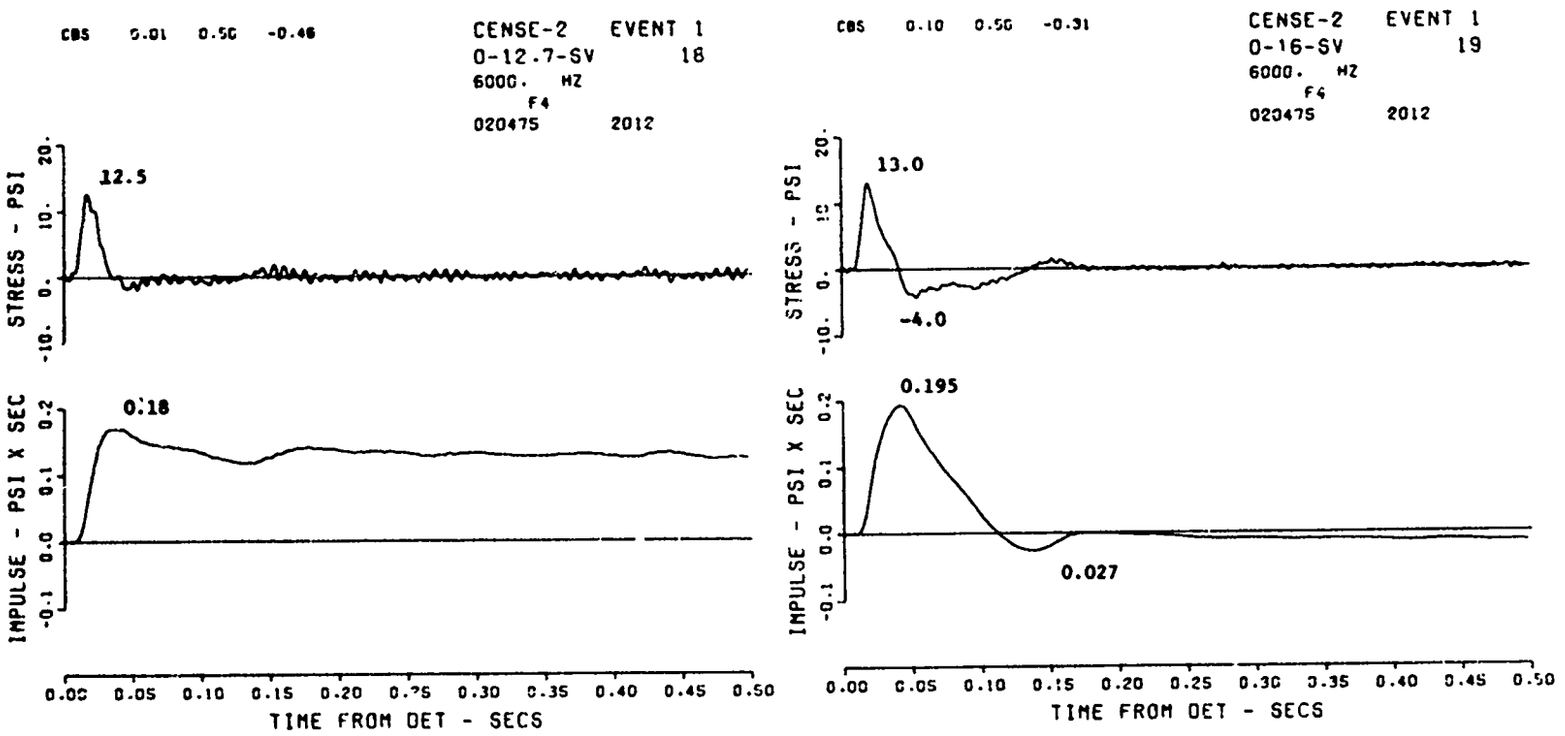

Figure B.2 (sheet 5 of 5).

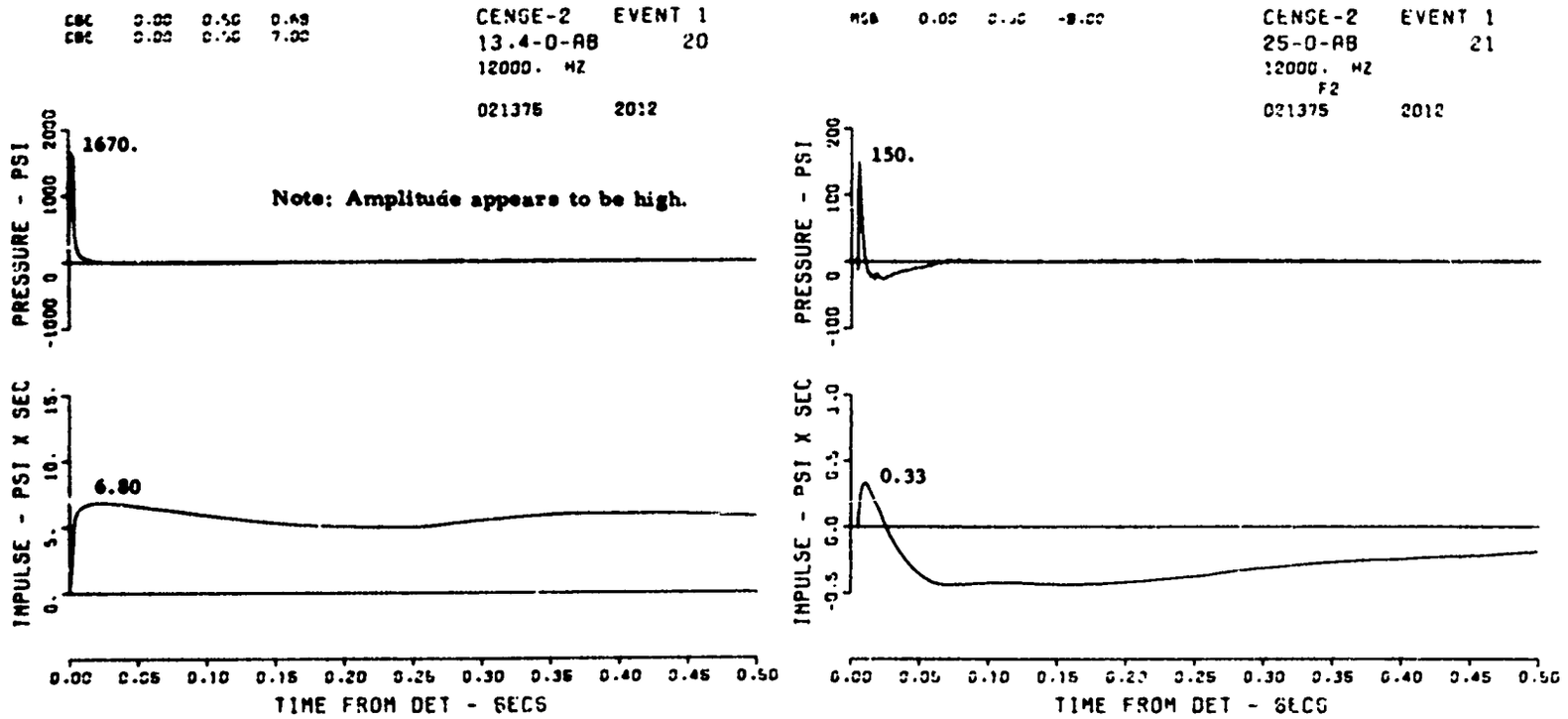

Figure B.3 Event 1, airblast, elevated, $-1.61\ W^{1/3}$ (-10.8 feet); surface airblast-time histories (sheet 1 of 3).

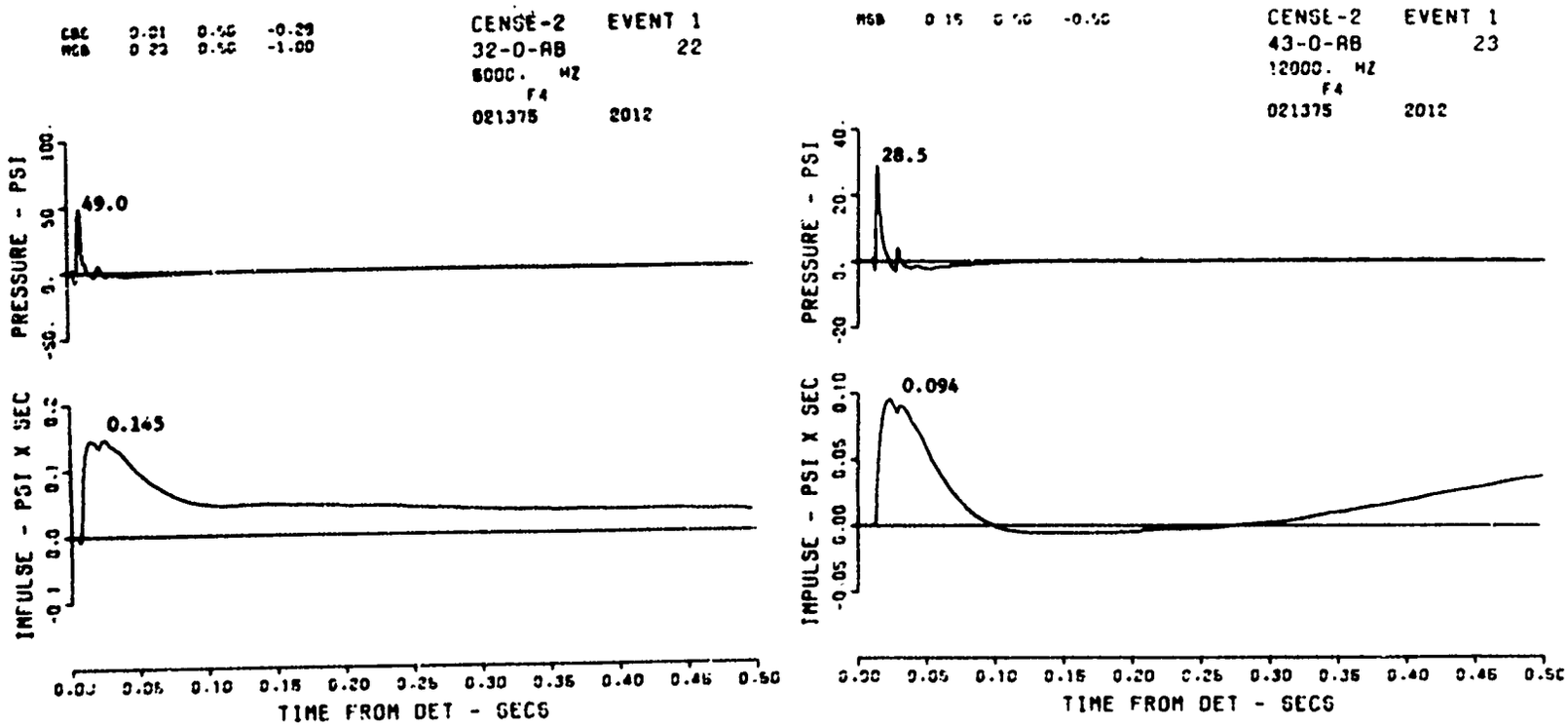

Figure B.3 (sheet 2 of 3).

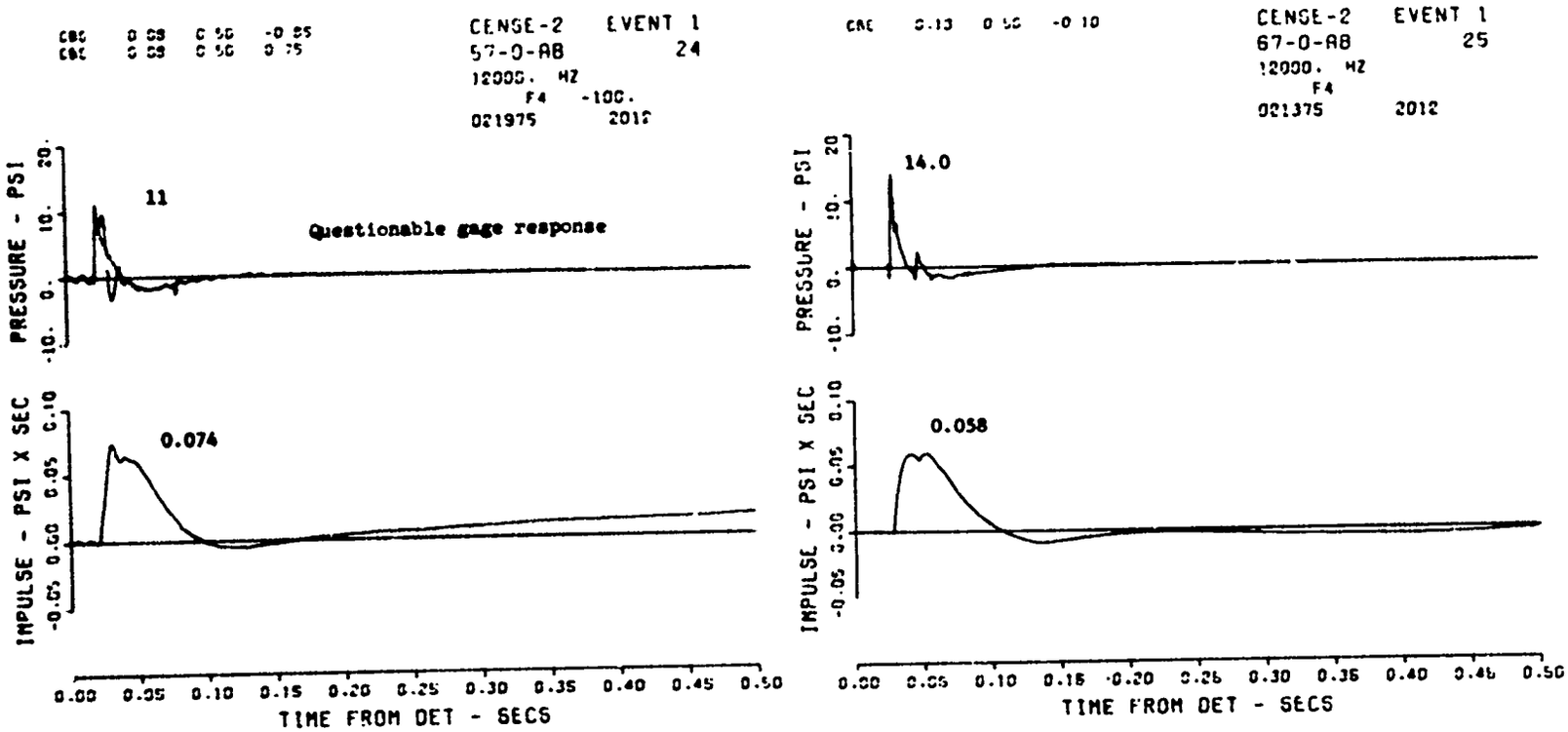

150

Figure B.3 (sheet 3 of 3).

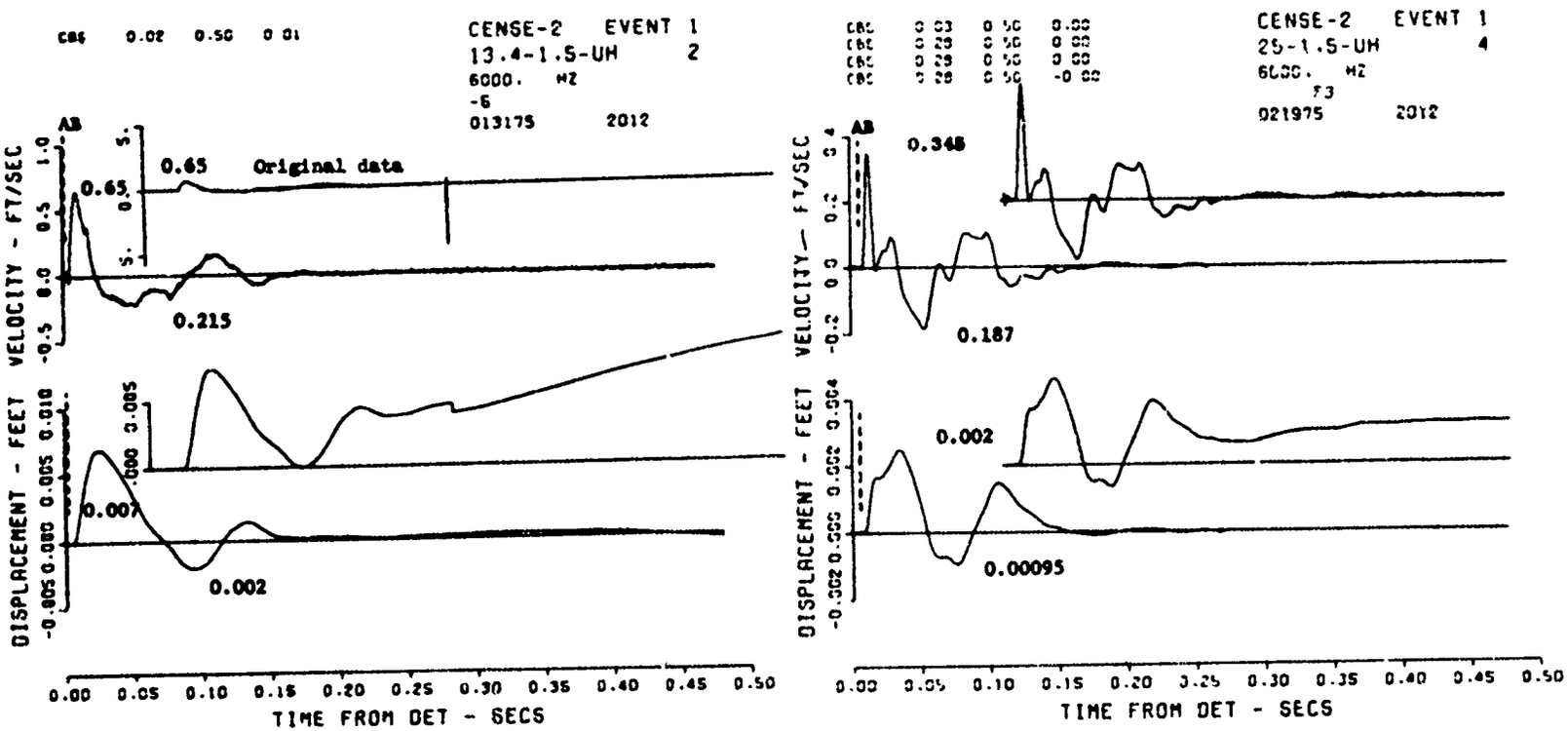

Figure B.4 Event 1, airblast, elevated, $-1.61\ W^{1/3}$ (-10.8 feet); near-surface motion-time histories (sheet 1 of 6).

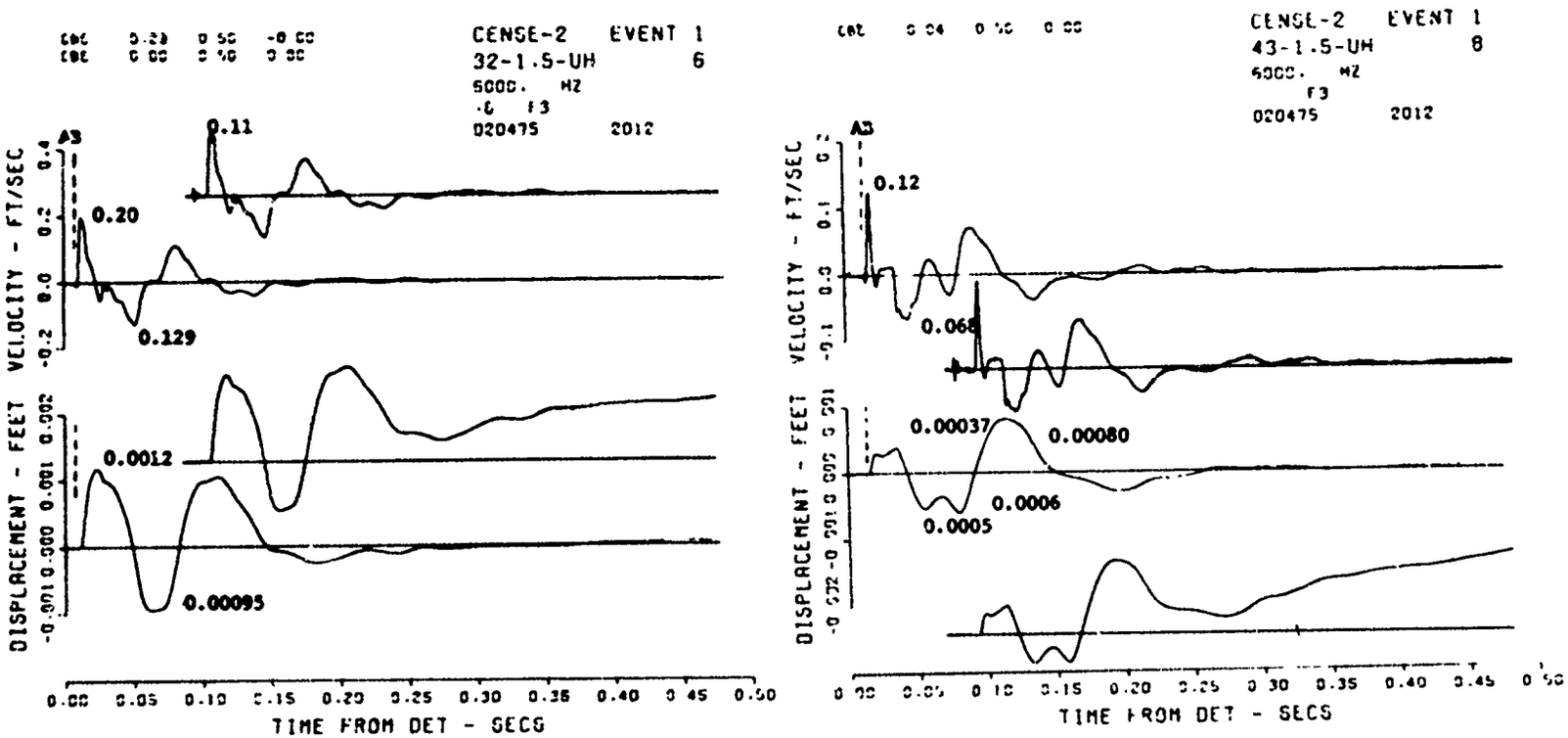

Figure B.4 (sheet 2 of 6).

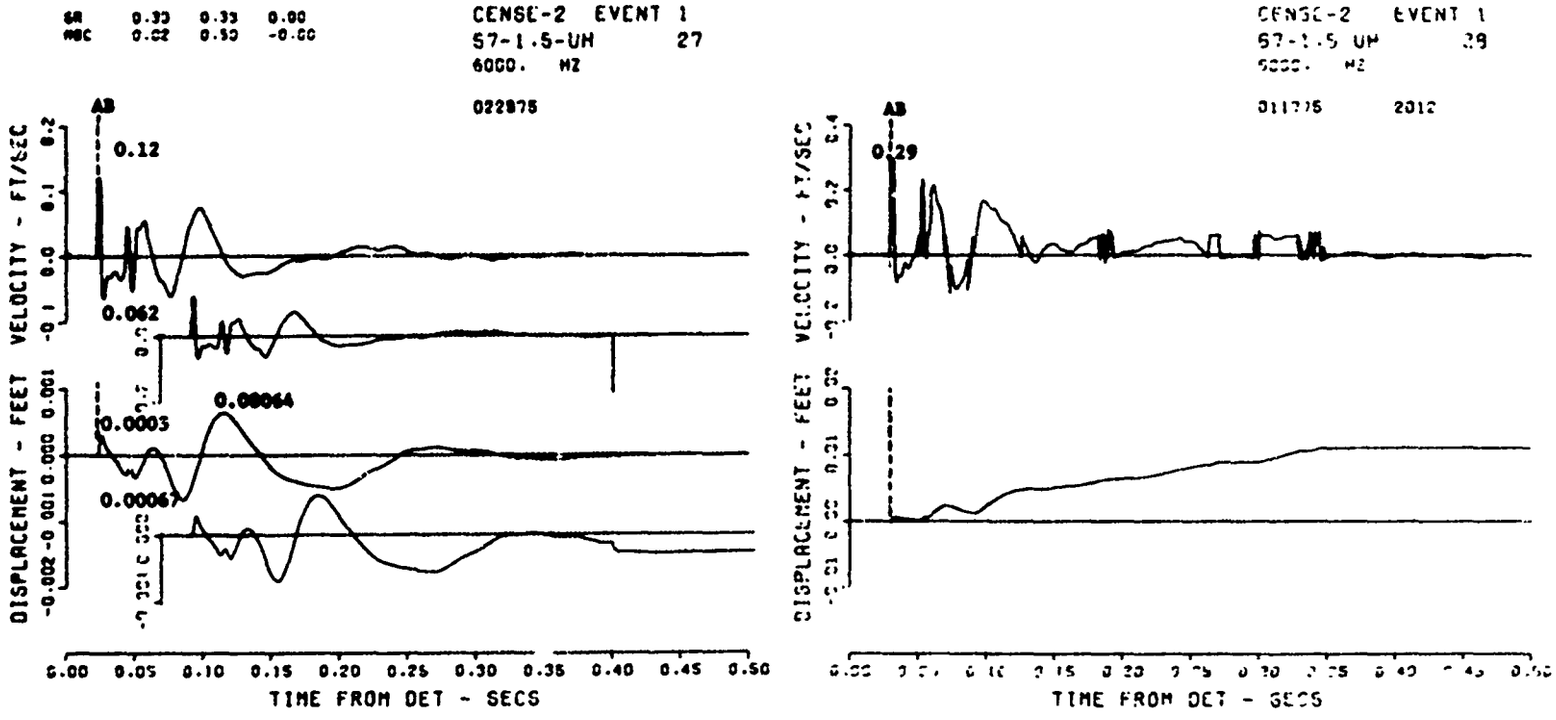

Figure B.4 (sheet 3 of 6).

CENSE-2 EVENT 1
13.4-1.5-UV 1

NO DATA RECOVERED

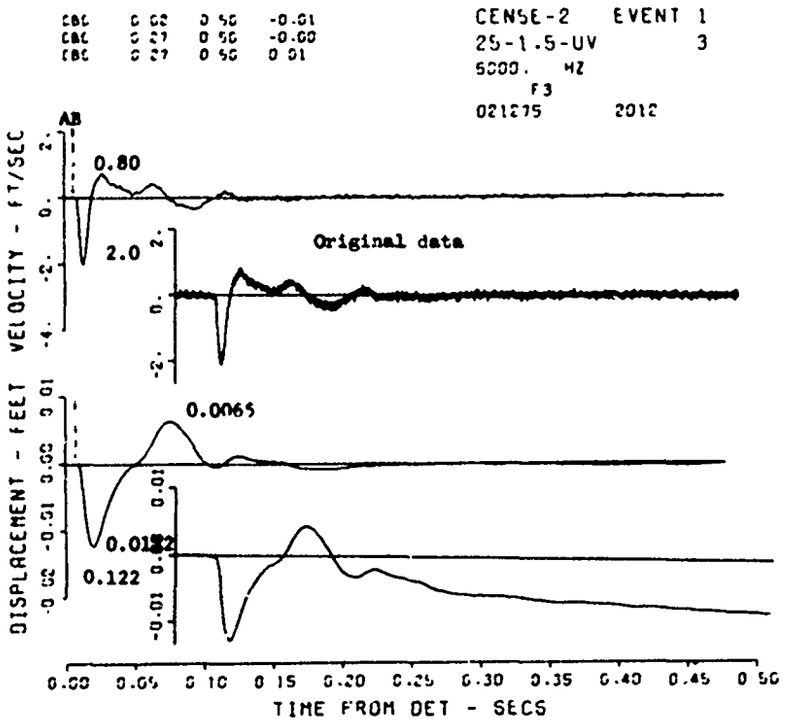

Figure B.4 (sheet 4 of 6).

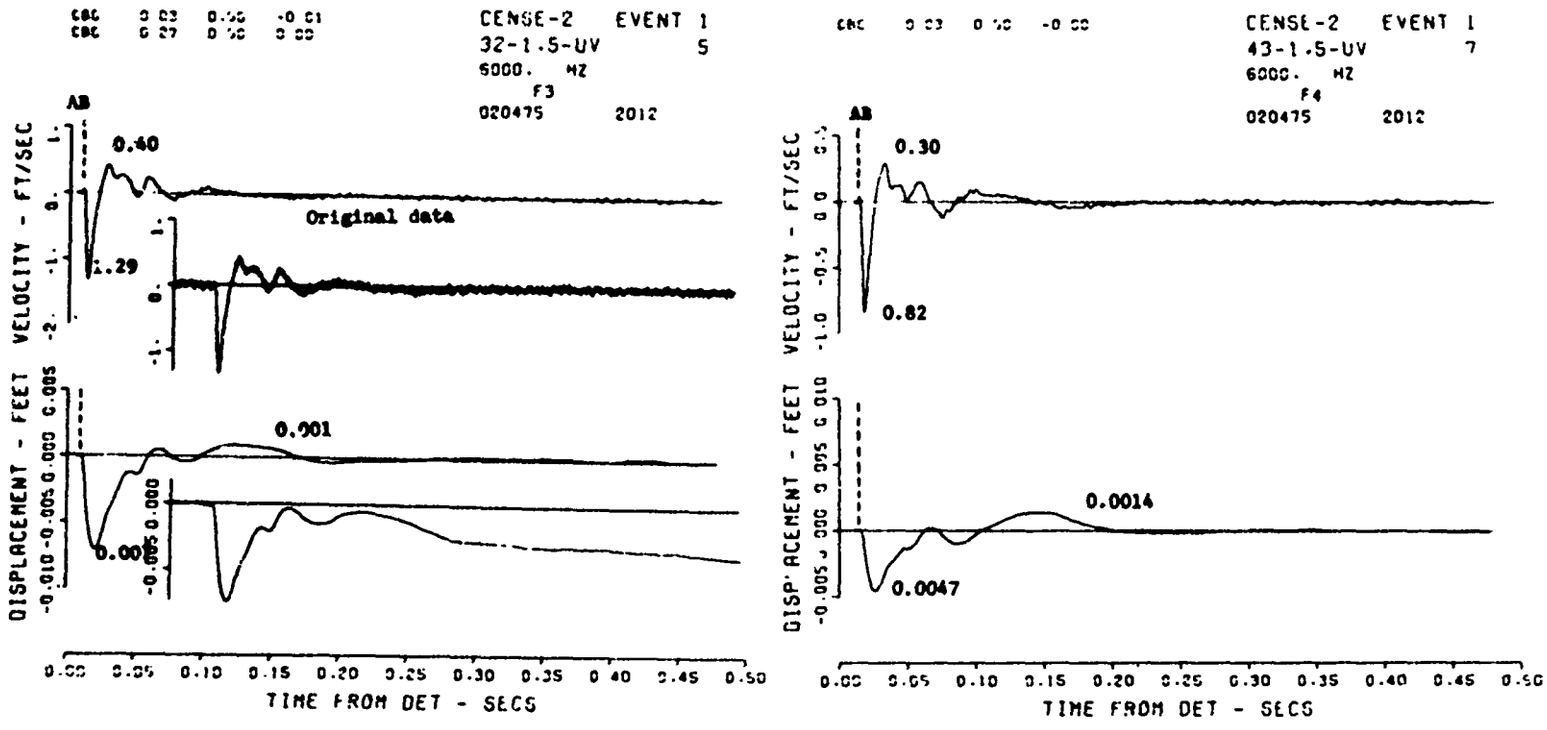

Figure B.4 (sheet 5 of 6).

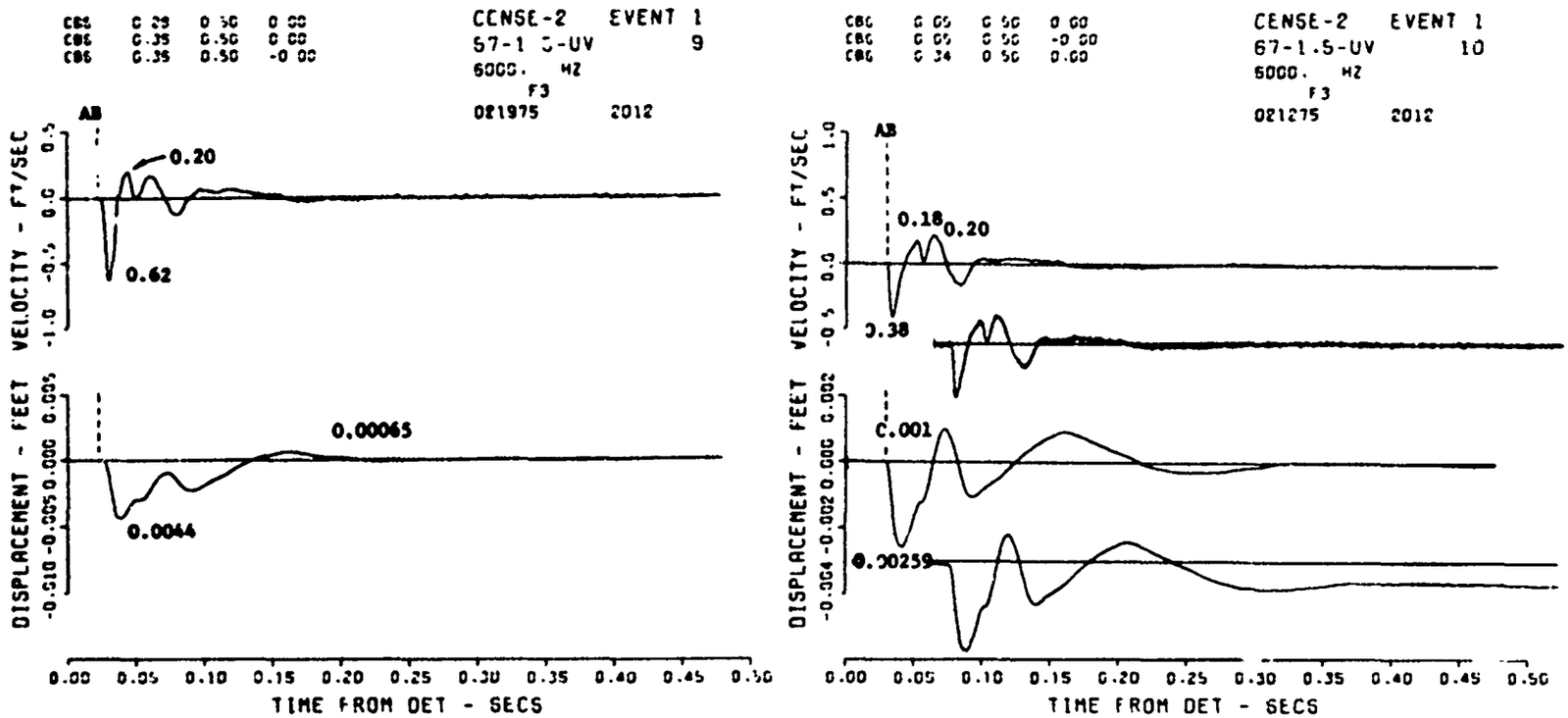

Figure B.4 (sheet 6 of 6).

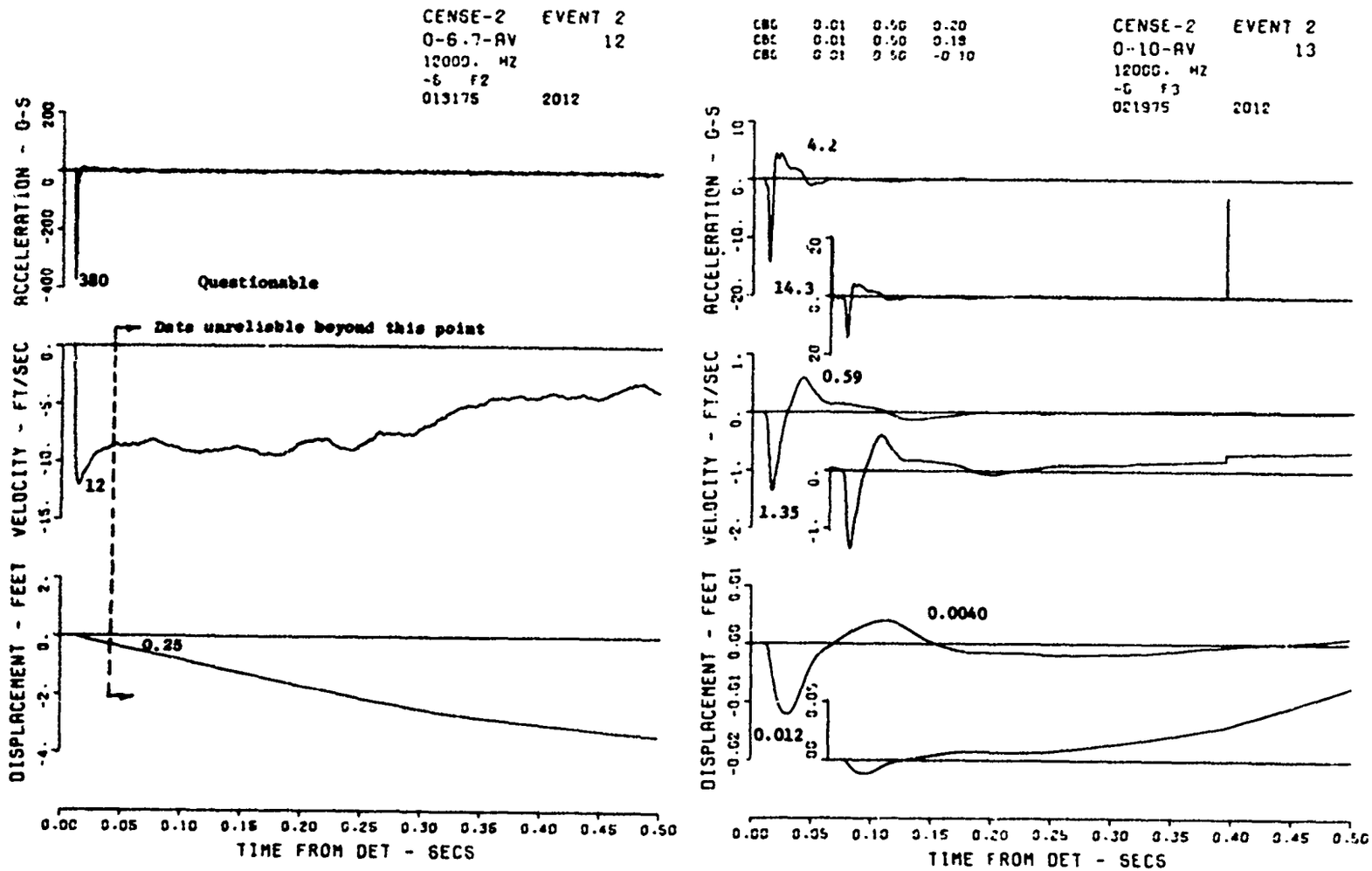

Figure B.5 Event 2, airblast, elevated, $-1.07\ W^{1/3}$ (-7.2 feet); motion- and stress-time histories along the vertical radial directly beneath the explosion (sheet 1 of 6).

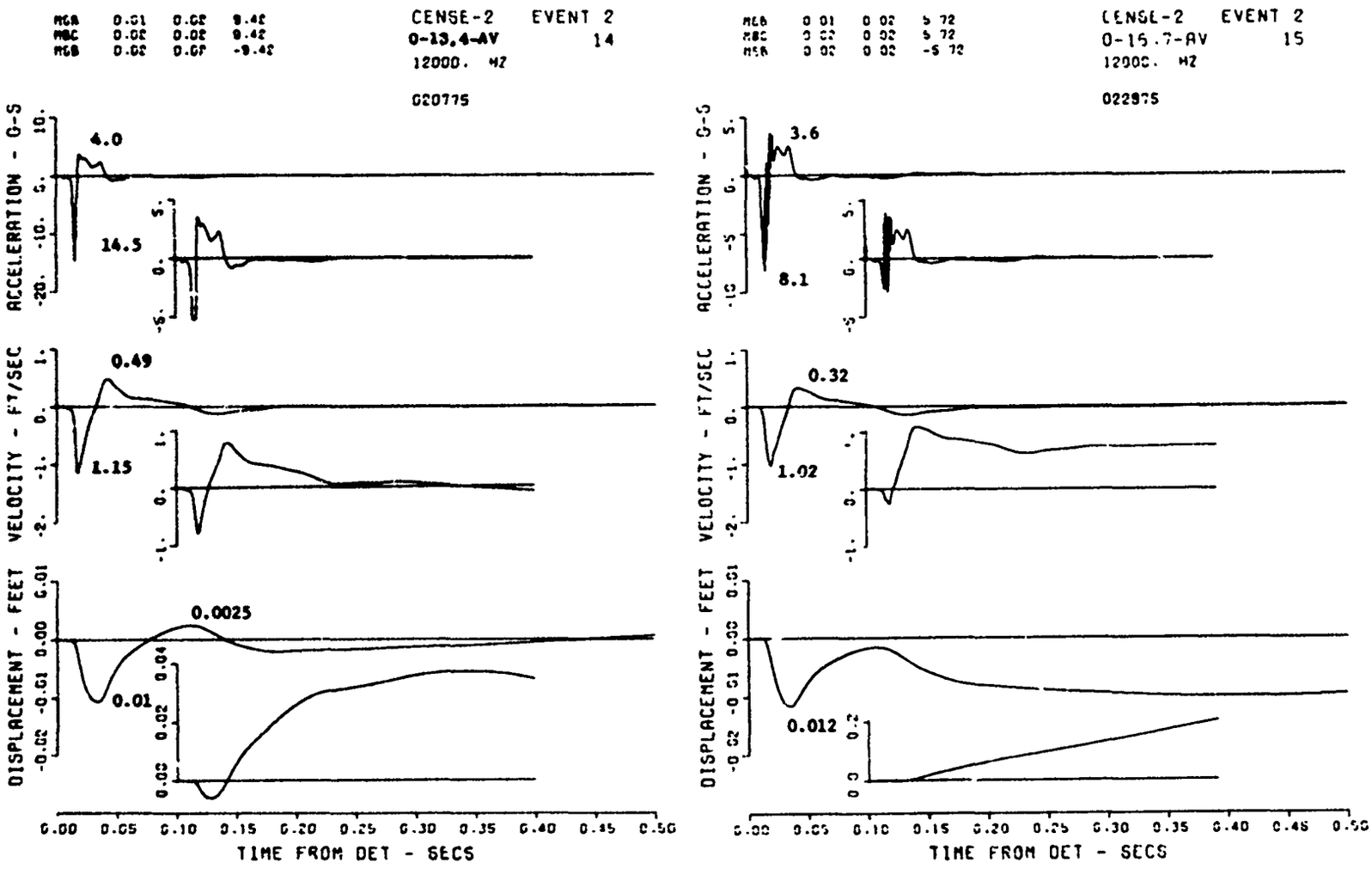

Figure B.5 (sheet 2 of 6).

CEN3E-2 EVENT 2
0-20.1-AV

NO DATA RECOVERED (GAGE SCRATCHED PRESHOT)

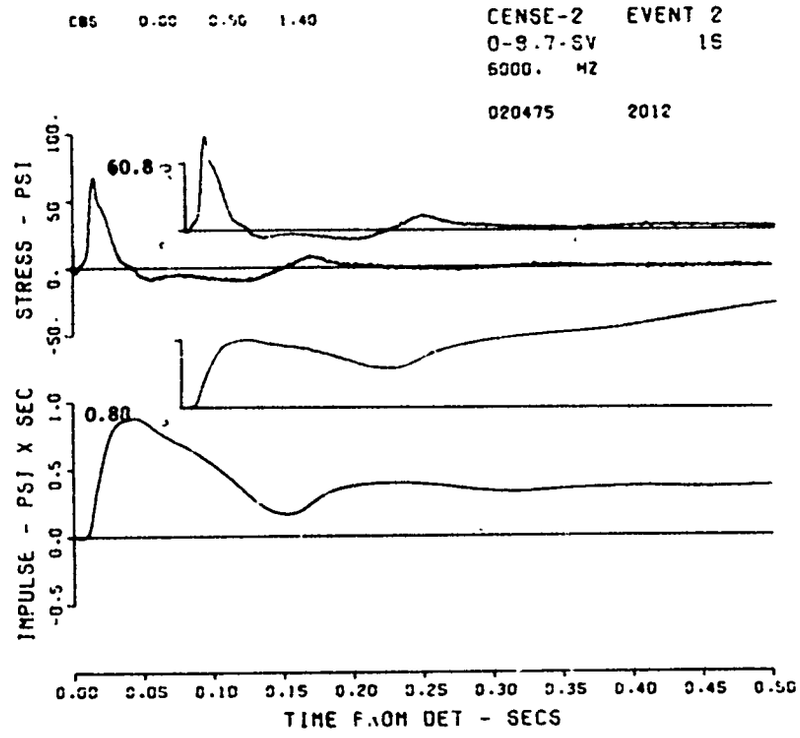

Figure B.5 (sheet 3 of 6).

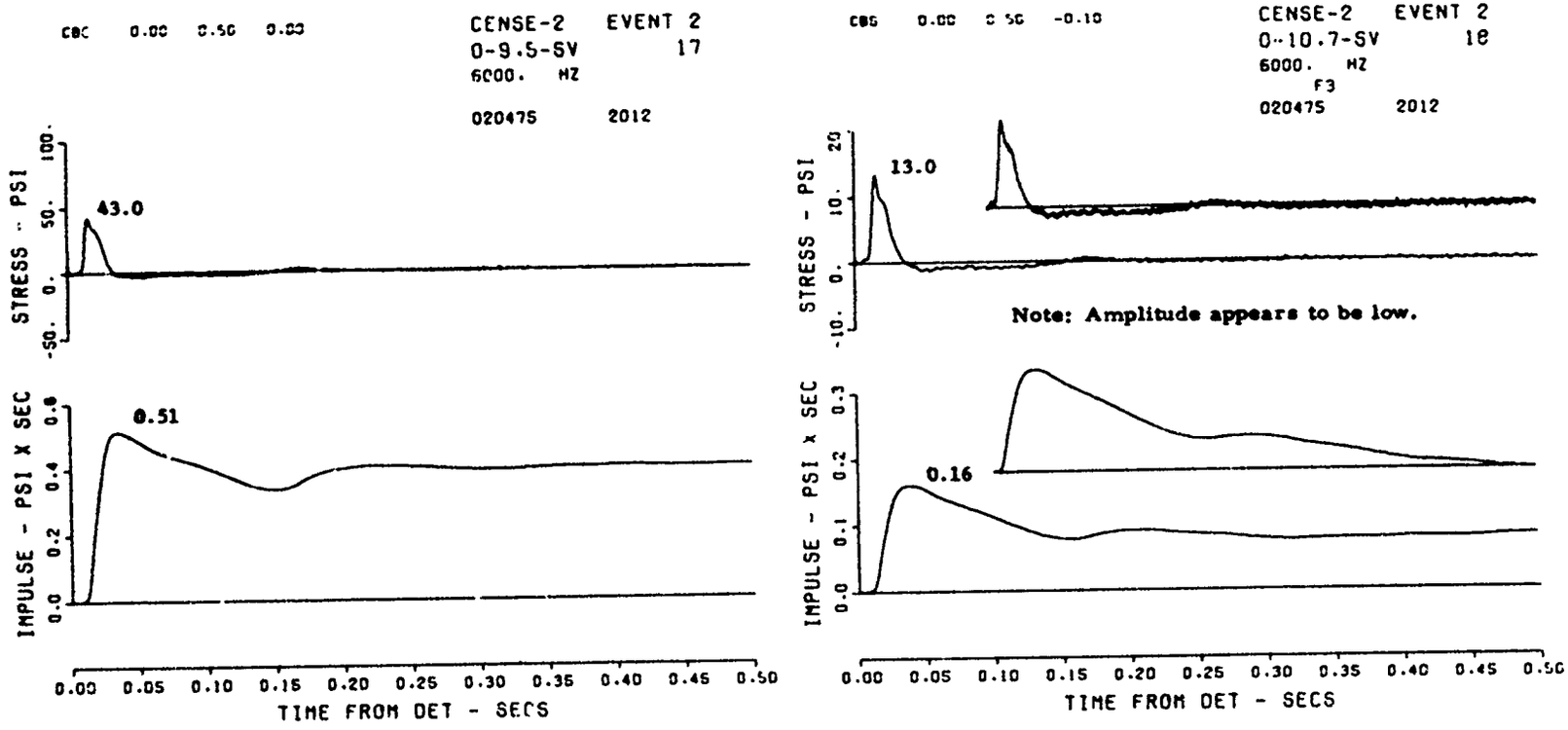

Figure B.5 (sheet 4 of 6).

CENSE-2 EVENT 2
13.4-0-AB

NO DATA RECOVERED (GAGE
SCRATCHED PRESHOT)

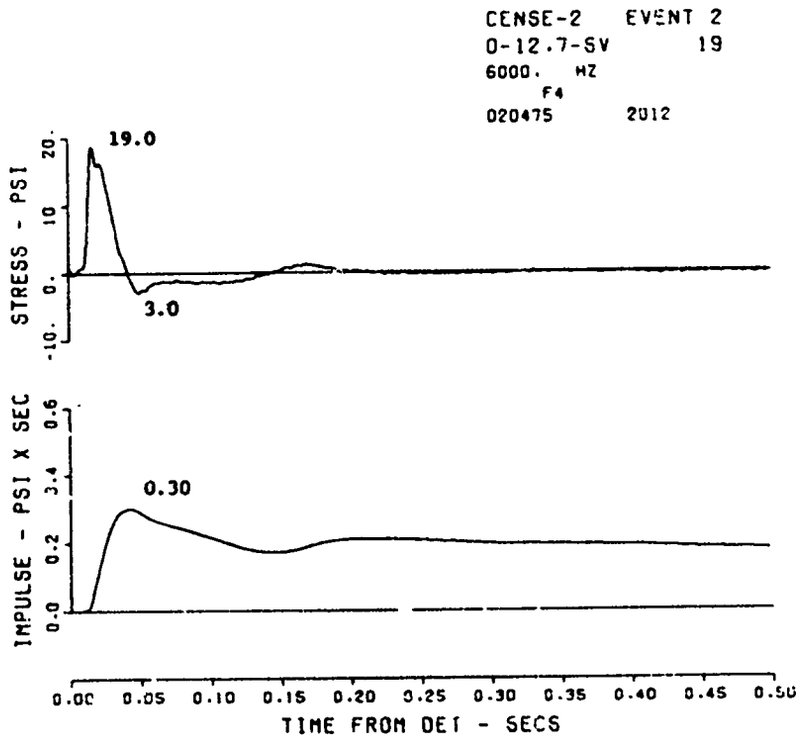

Figure B.5 (sheet 5 of 6).

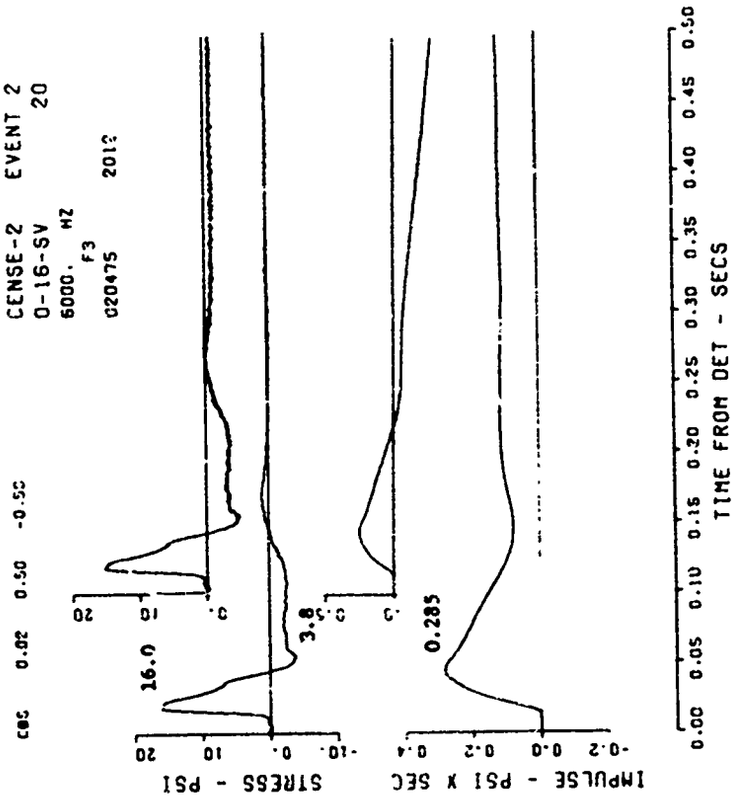

Figure B.5 (sheet 6 of 6).

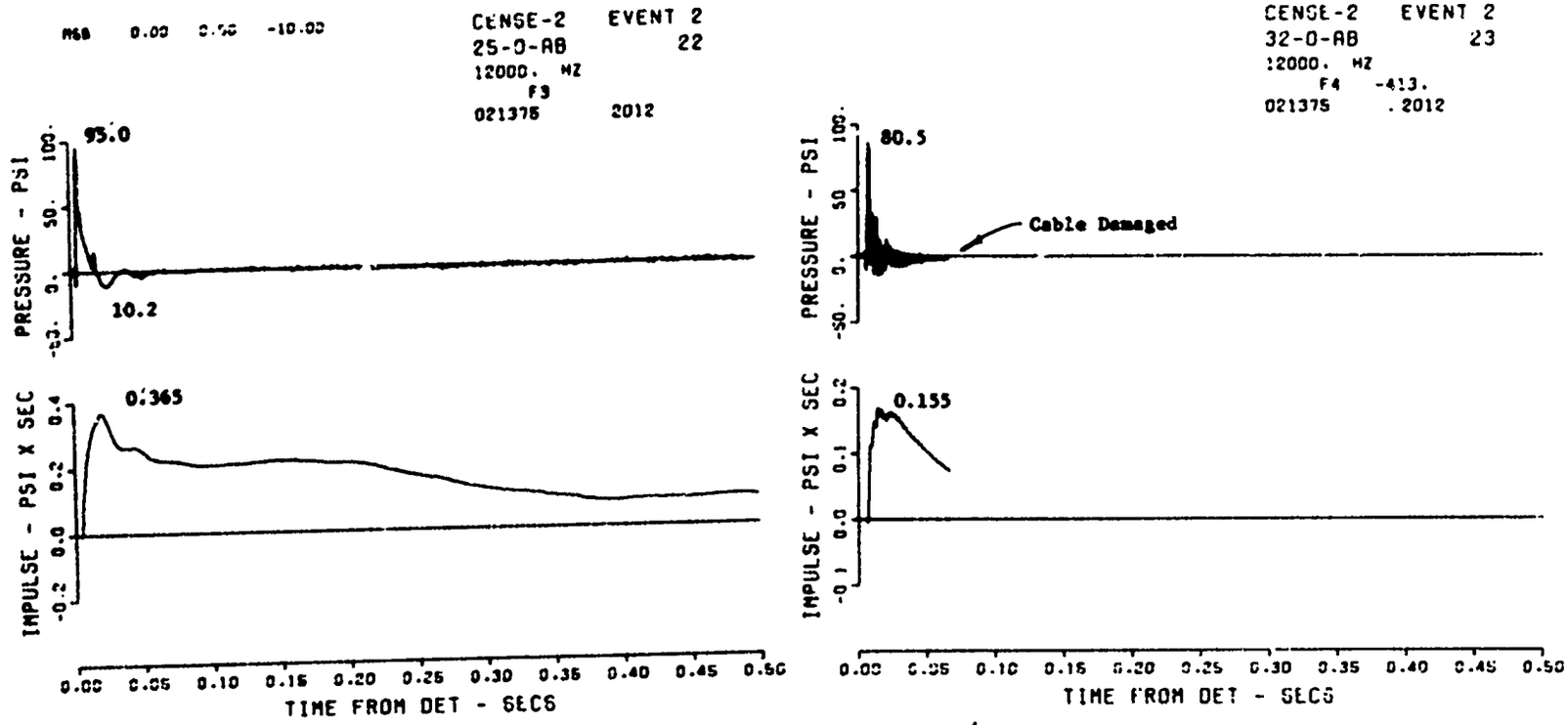

Figure B.6 Event 2, airblast, elevated, $-1.07\ W^{1/3}$ (-7.2 feet); surface-airblast time histories (sheet 1 of 3).

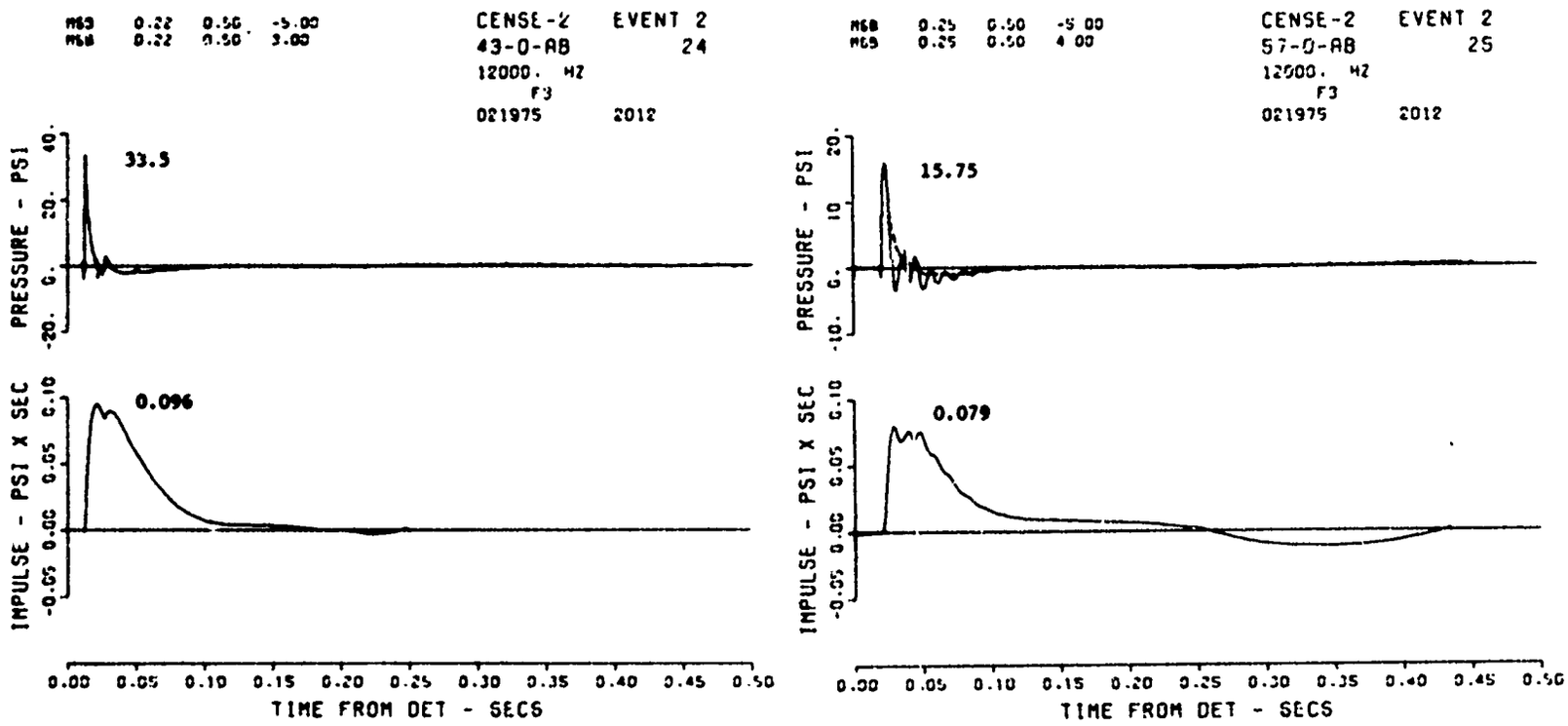

Figure B.6 (sheet 2 of 3).

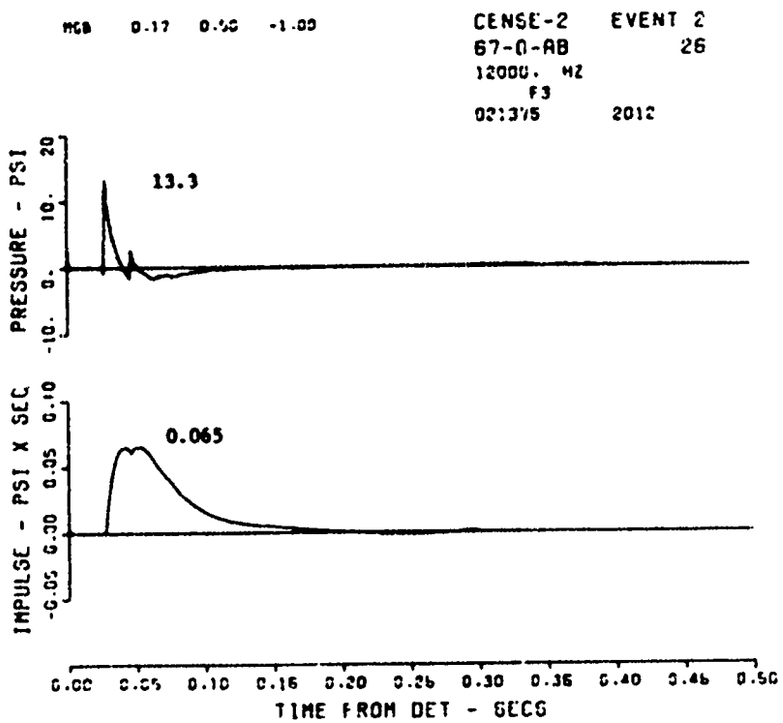

Figure B.6 (sheet 3 of 3).

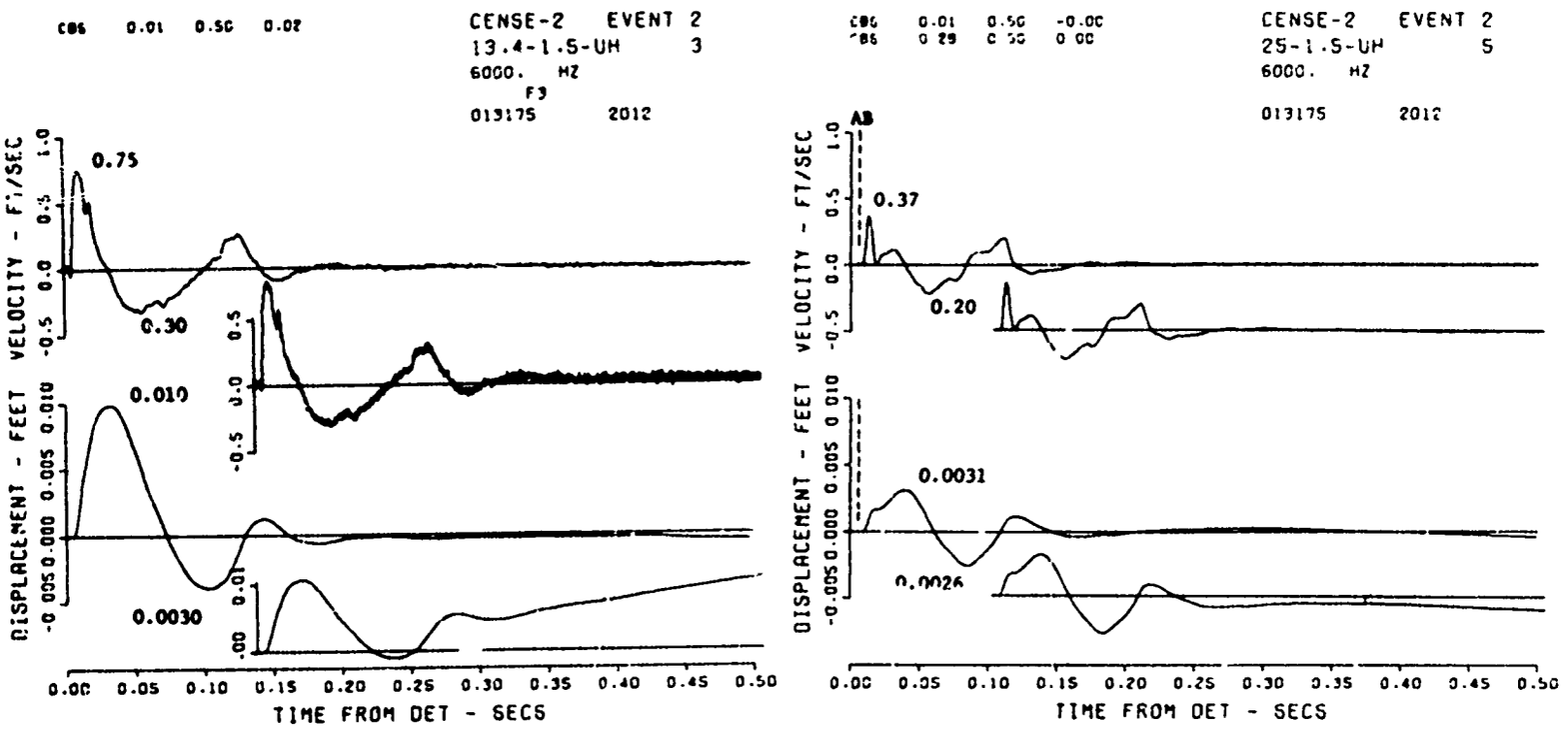

Figure B.7 Event 2, airblast, elevated, $-1.07\ W^{1/3}$ (-7.2 feet); near-surface motion-time histories (sheet 1 of 6).

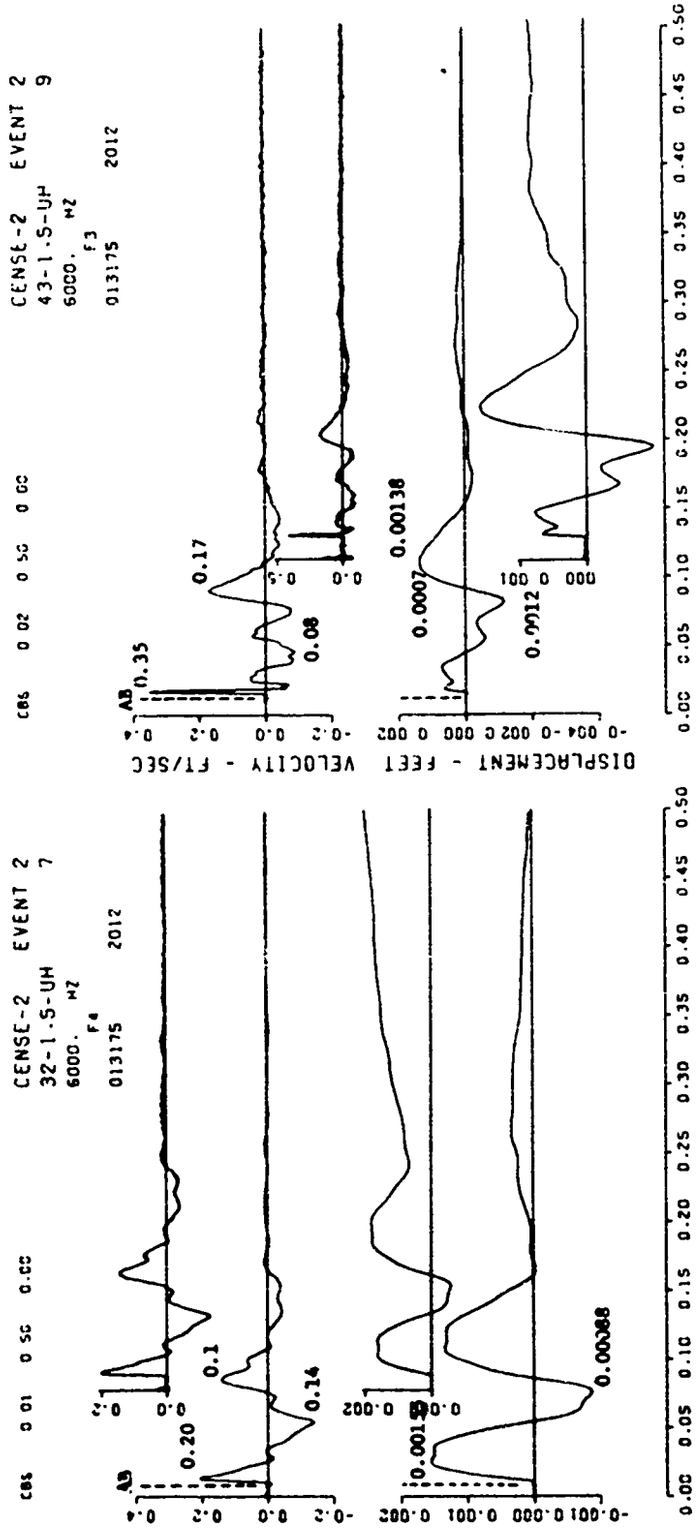

Figure B.7 (sheet 2 of 6).

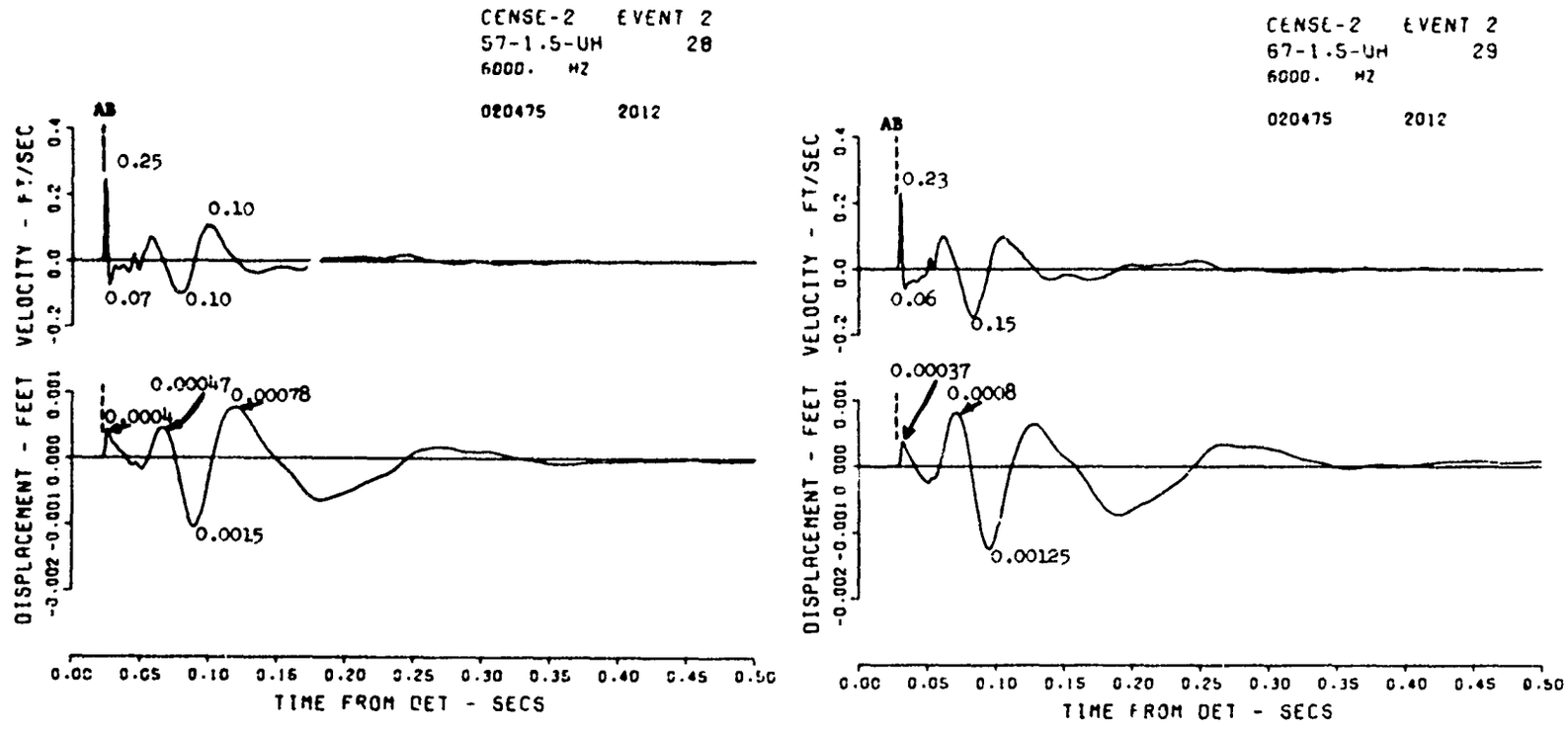

Figure B.7 (sheet 3 of 6).

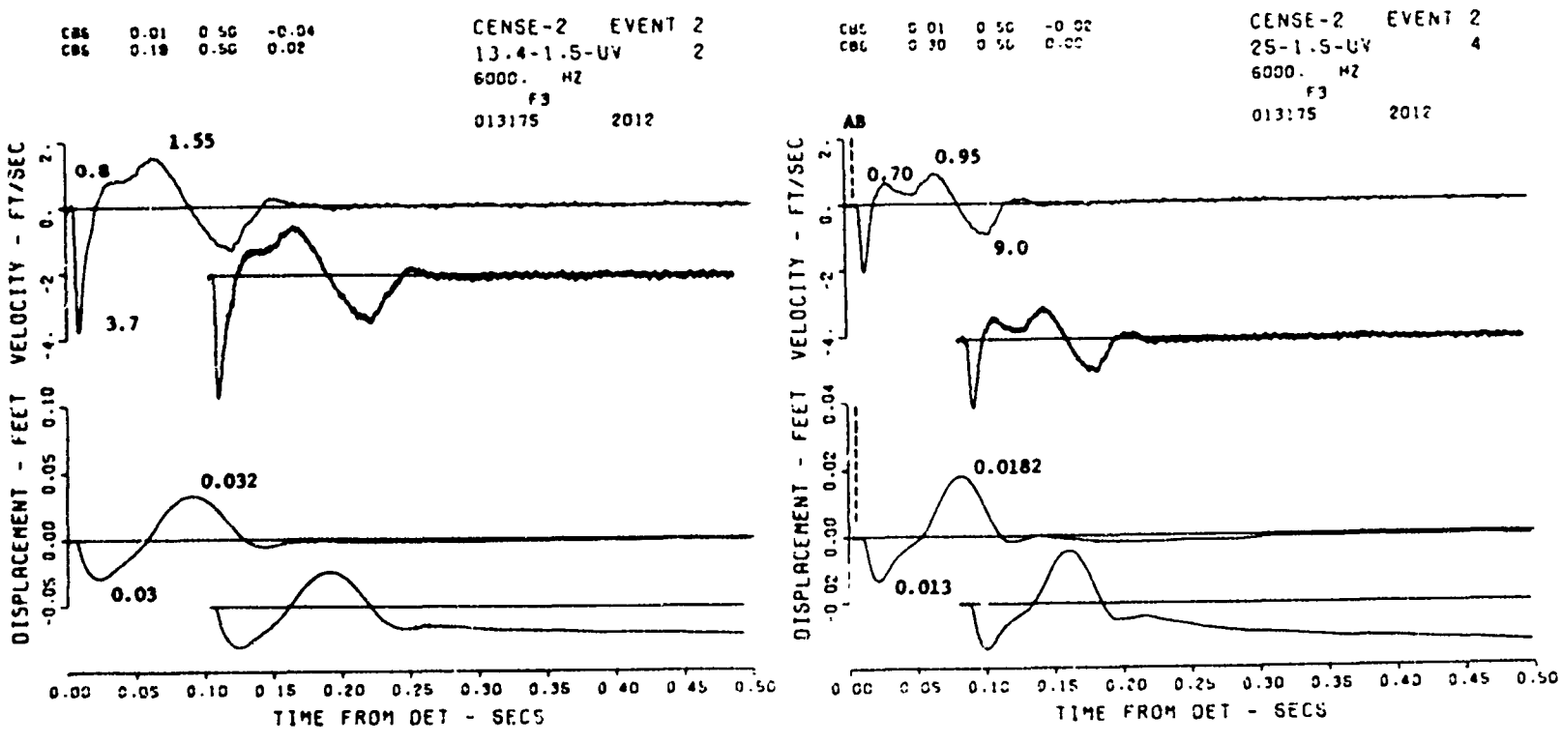

Figure B.7 (sheet 4 of 6).

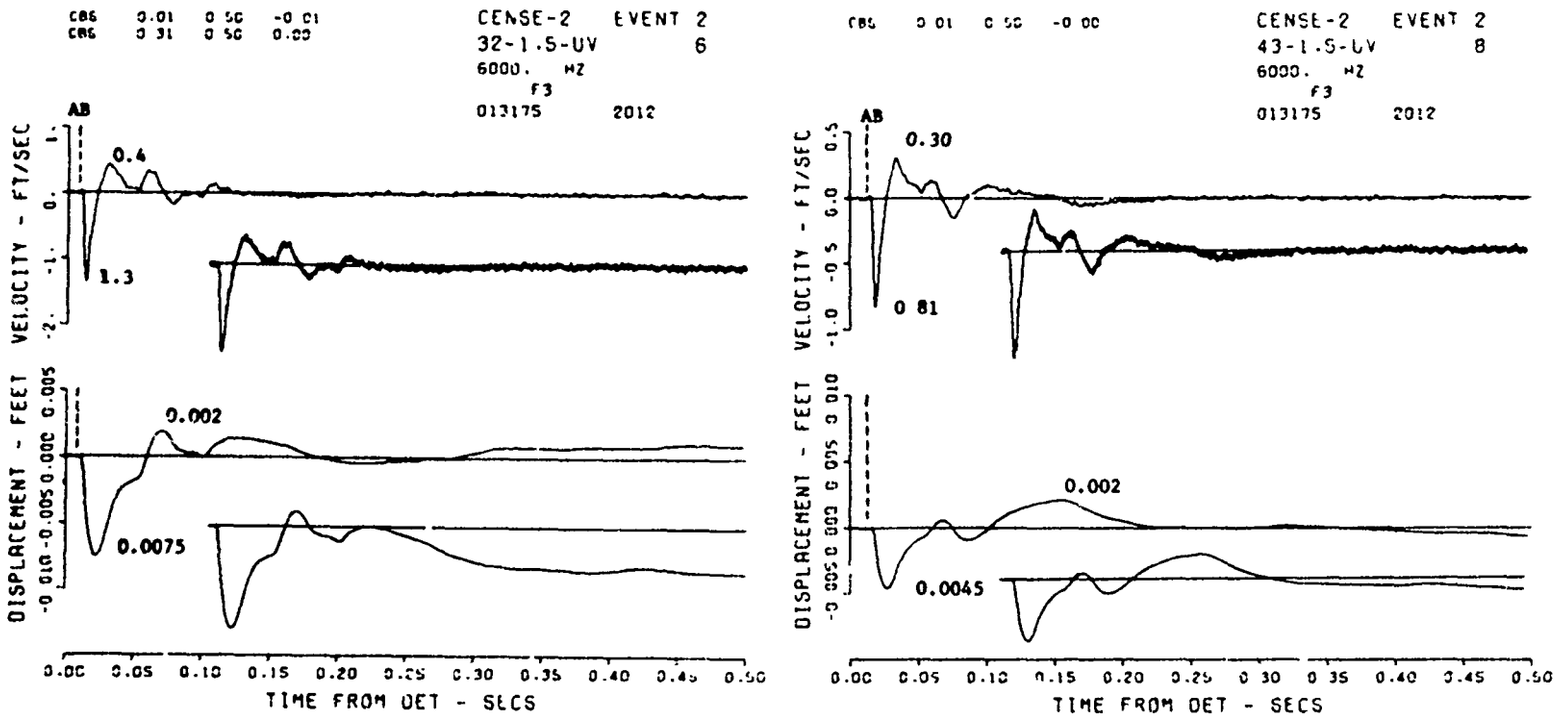

Figure B.7 (sheet 5 of 6).

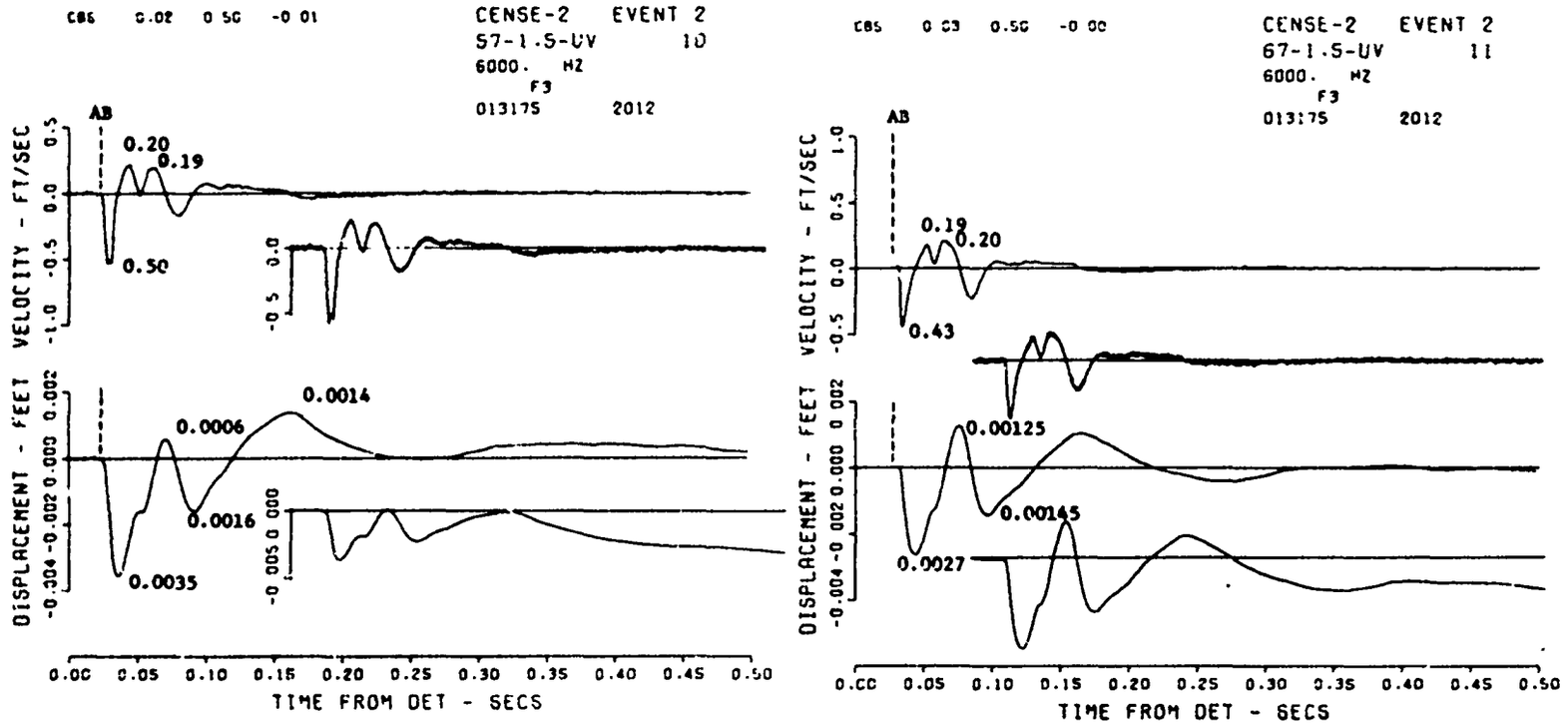

Figure B.7 (sheet 6 of 6).

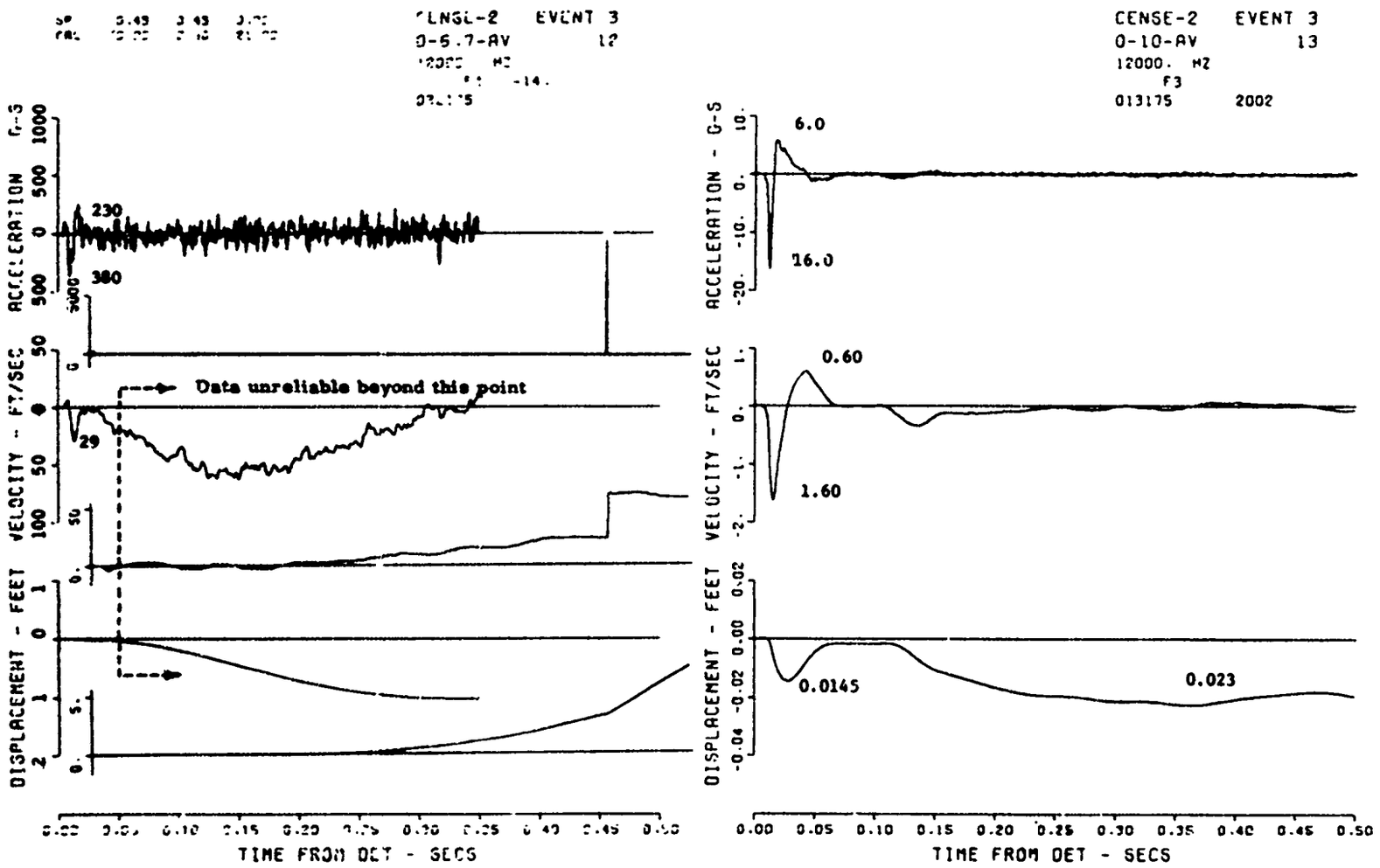

Figure B.8 Event 3, elevated, $-0.54\ W^{1/3}$ (-3.6 feet); motion- and stress-time histories along the vertical radial directly beneath the explosion (sheet 1 of 5).

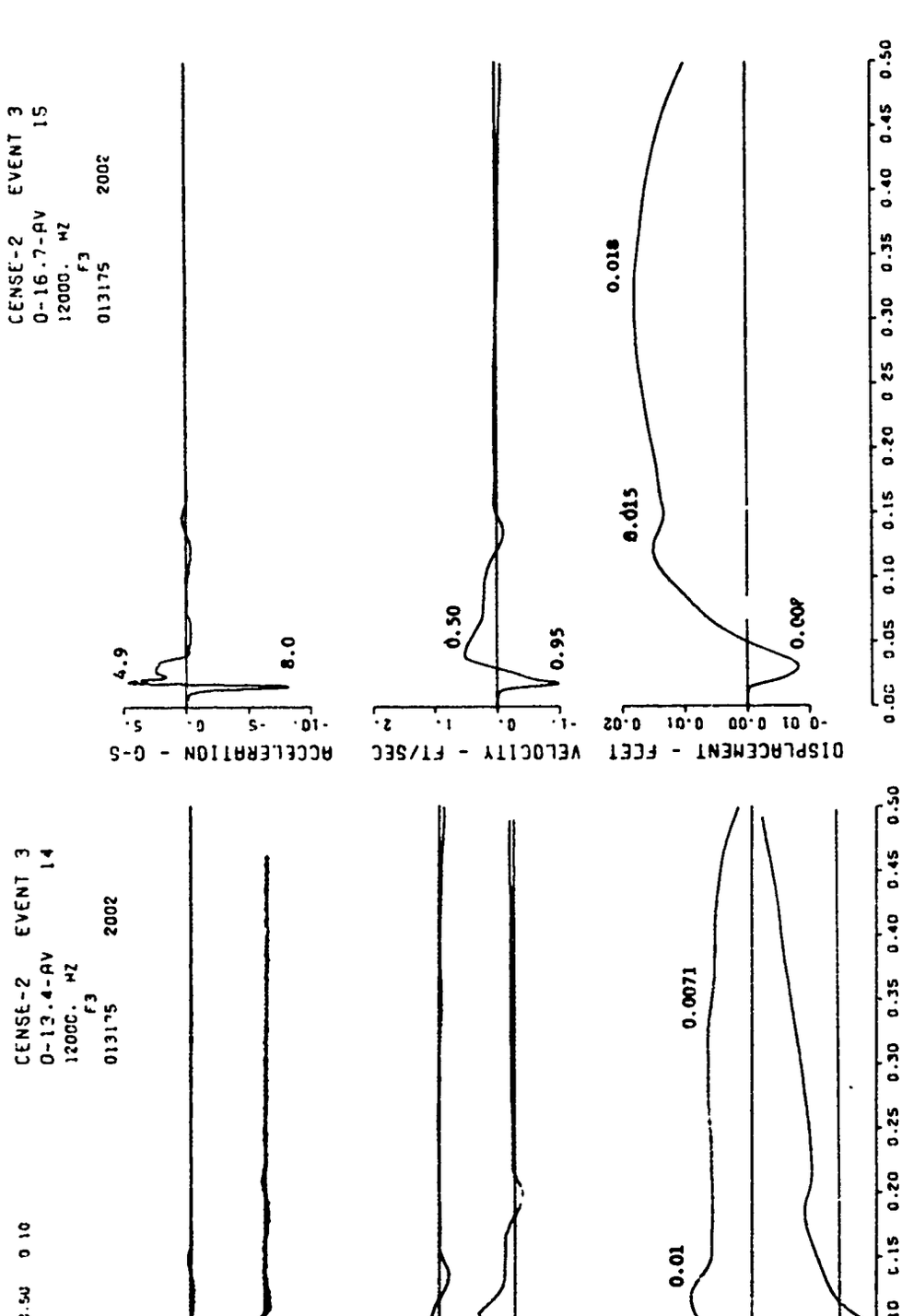

Figure B.8 (sheet 2 of 5).

CENSE-2 EVENT 3
C-20.1-AV

NO DATA RECOVERED (GAGE SCRATCHED PRESHOT)

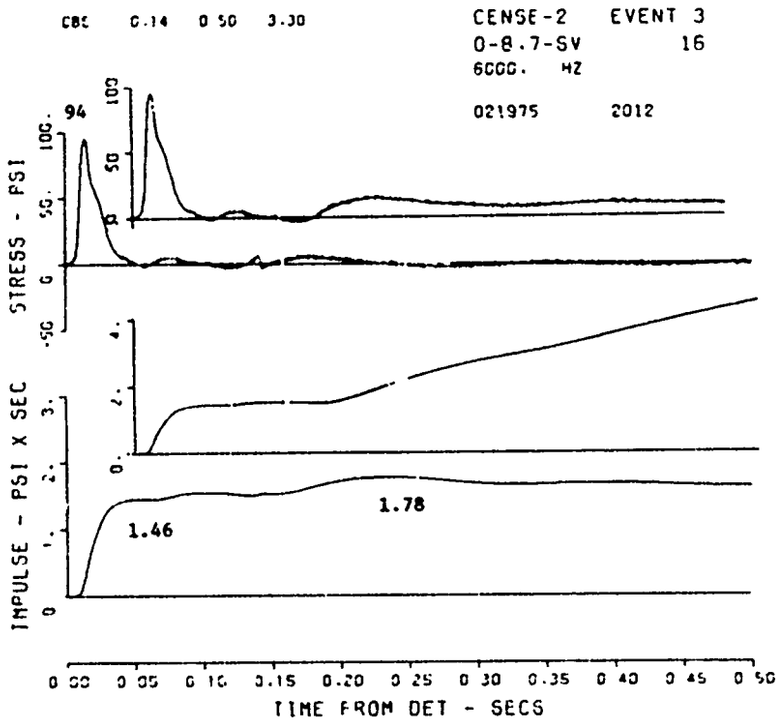

Figure B.8 (sheet 3 of 5).

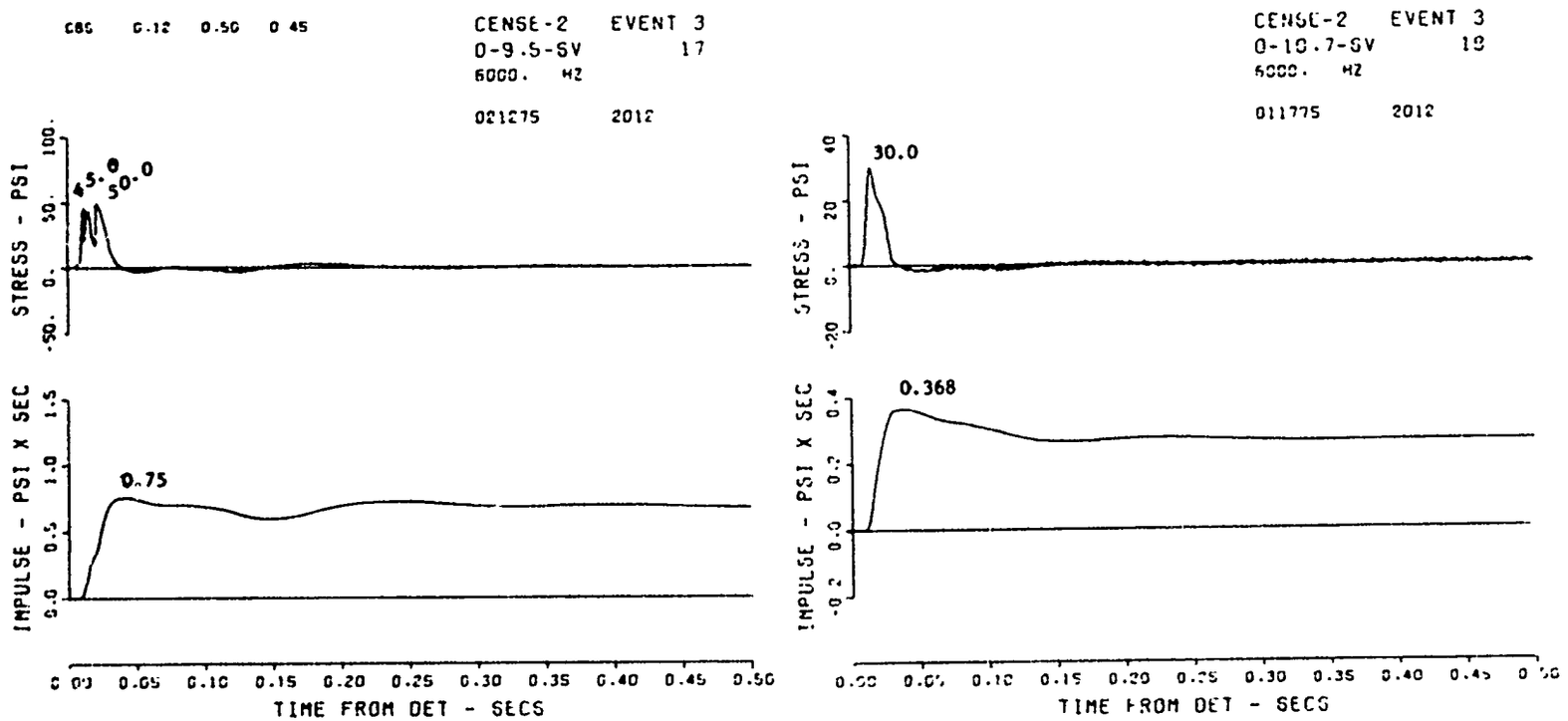

Figure B.8 (sheet 4 of 5).

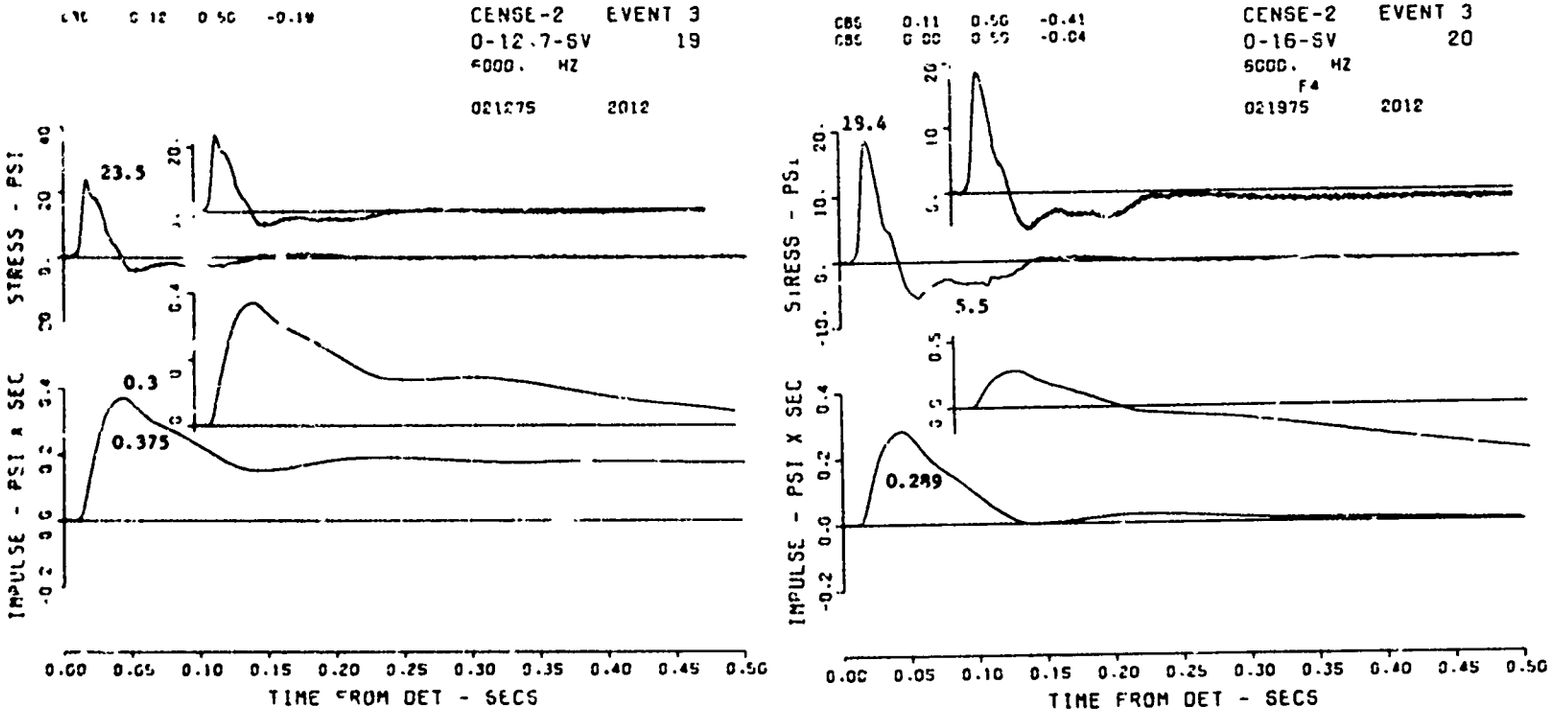

Figure B.8 (sheet 5 of 5).

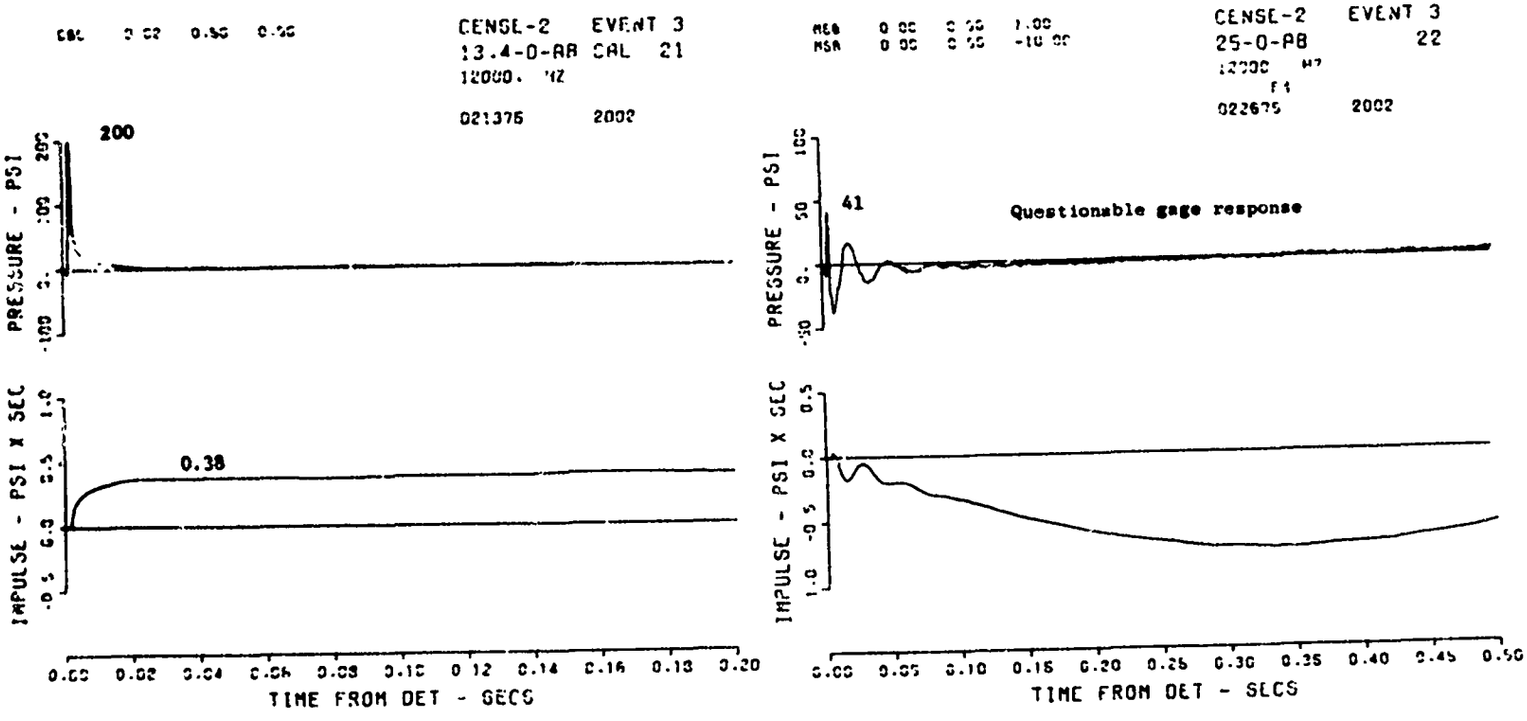

Figure B.9 Event 3, elevated, $-0.54\ W^{1/3}$ (3.6 feet); surface airblast-time histories (sheet 1 of 3).

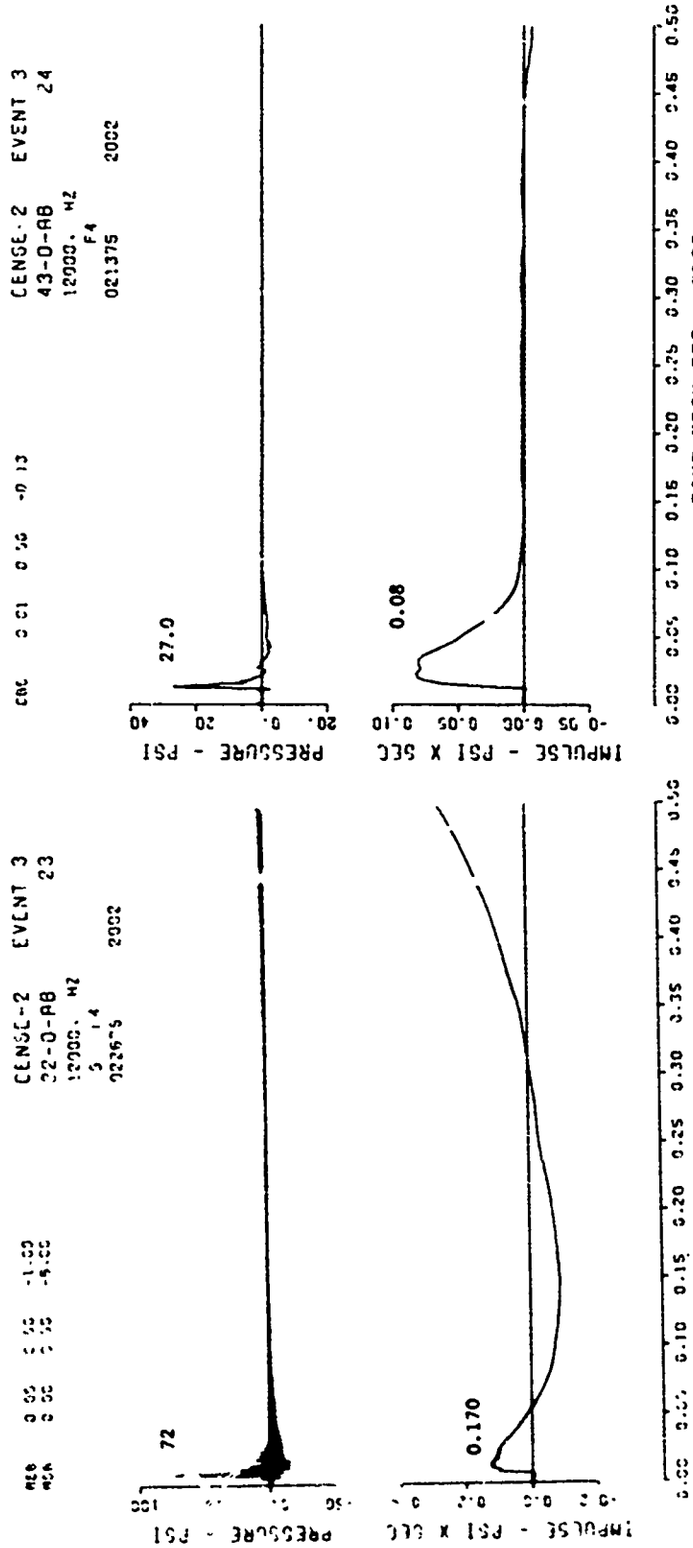

Figure B.9 (sheet 2 of 3).

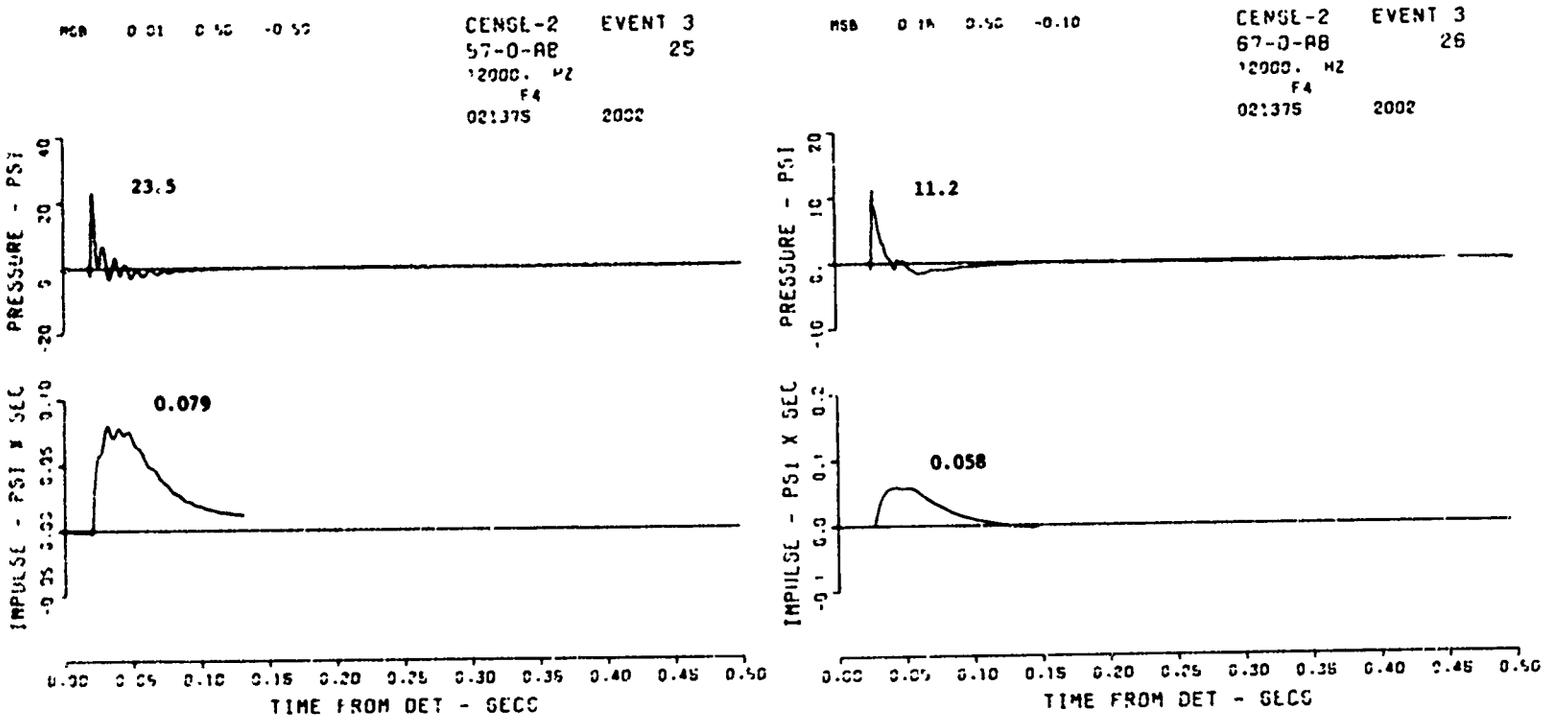

Figure B.9 (sheet 3 of 3).

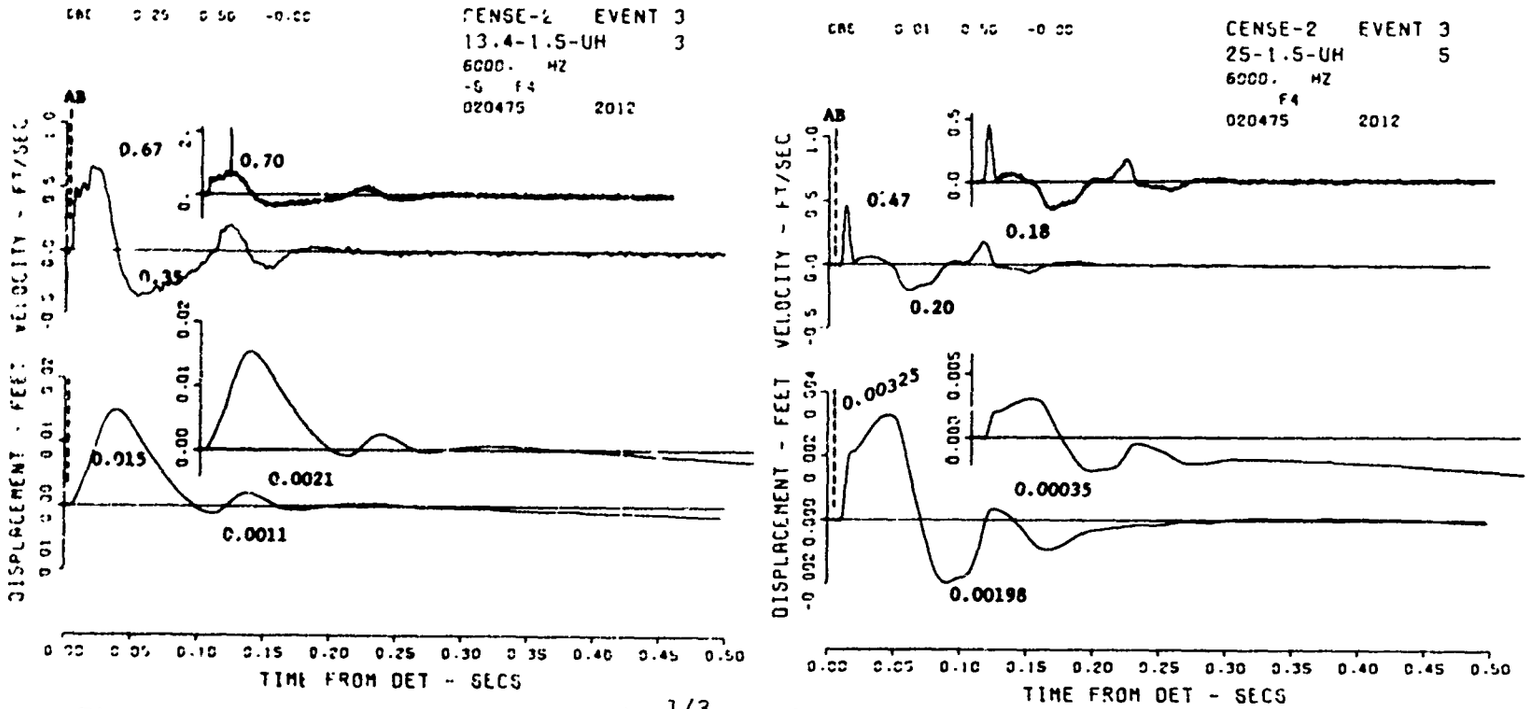

Figure B.10 Event 3, elevated, $-0.54\ W^{1/3}$ (-3.6 feet); near-surface motion-time histories (sheet 1 of 6).

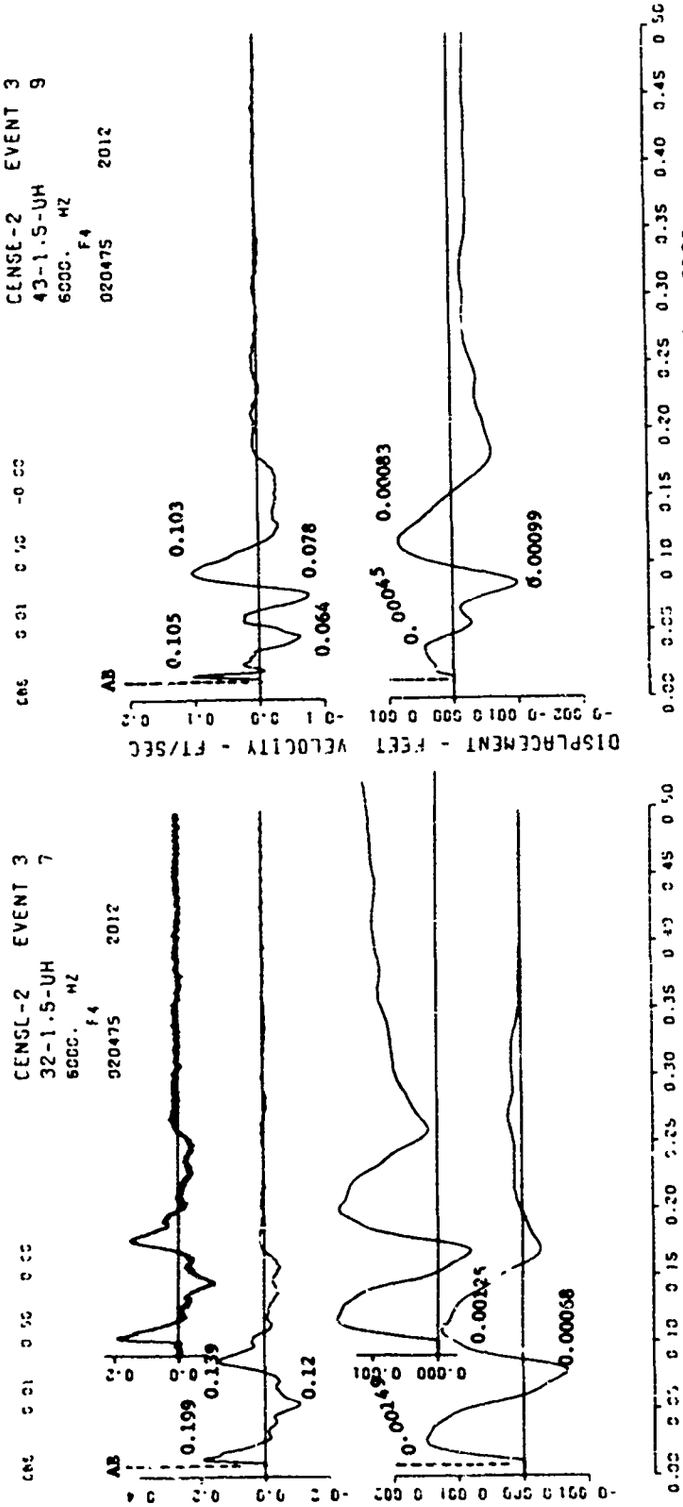

Figure B.10 (sheet 2 of 6).

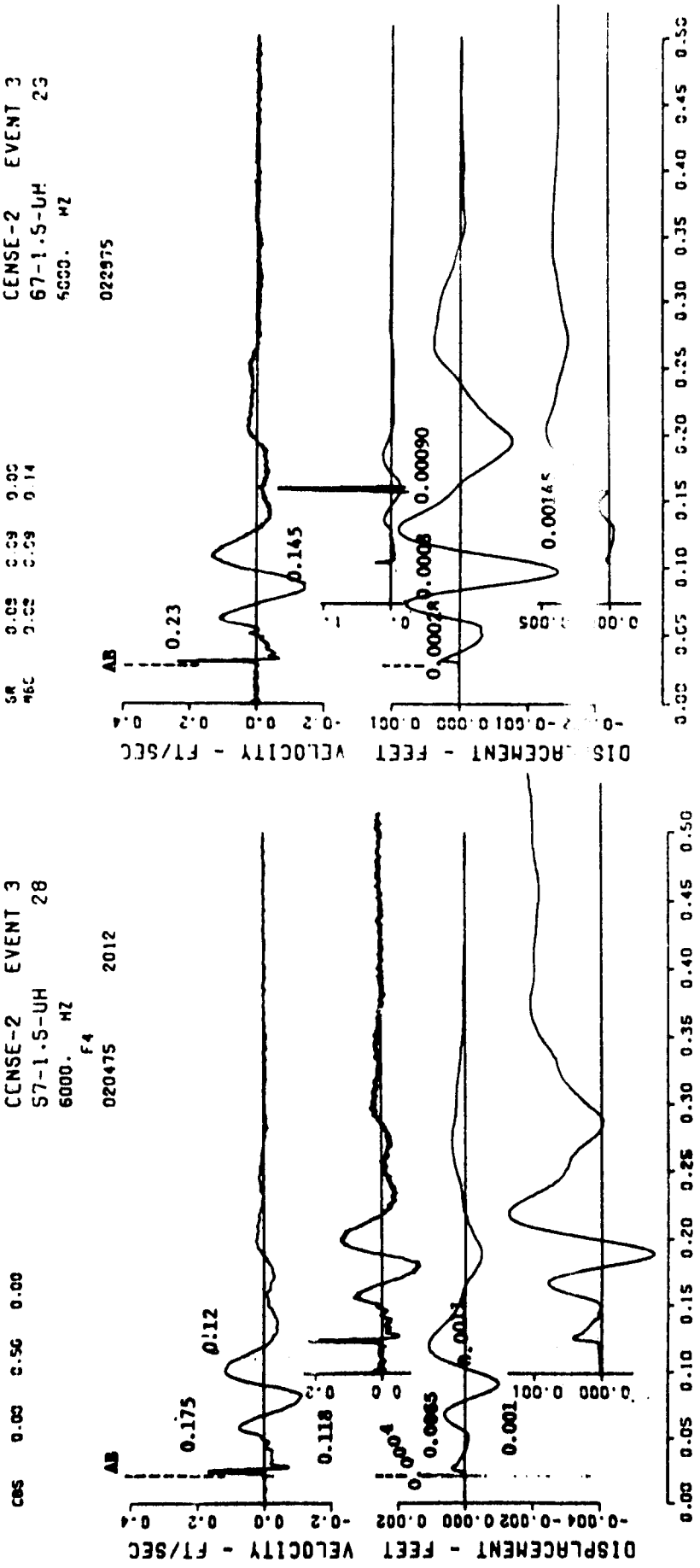

gure B.10 (sheet 3 of 6)

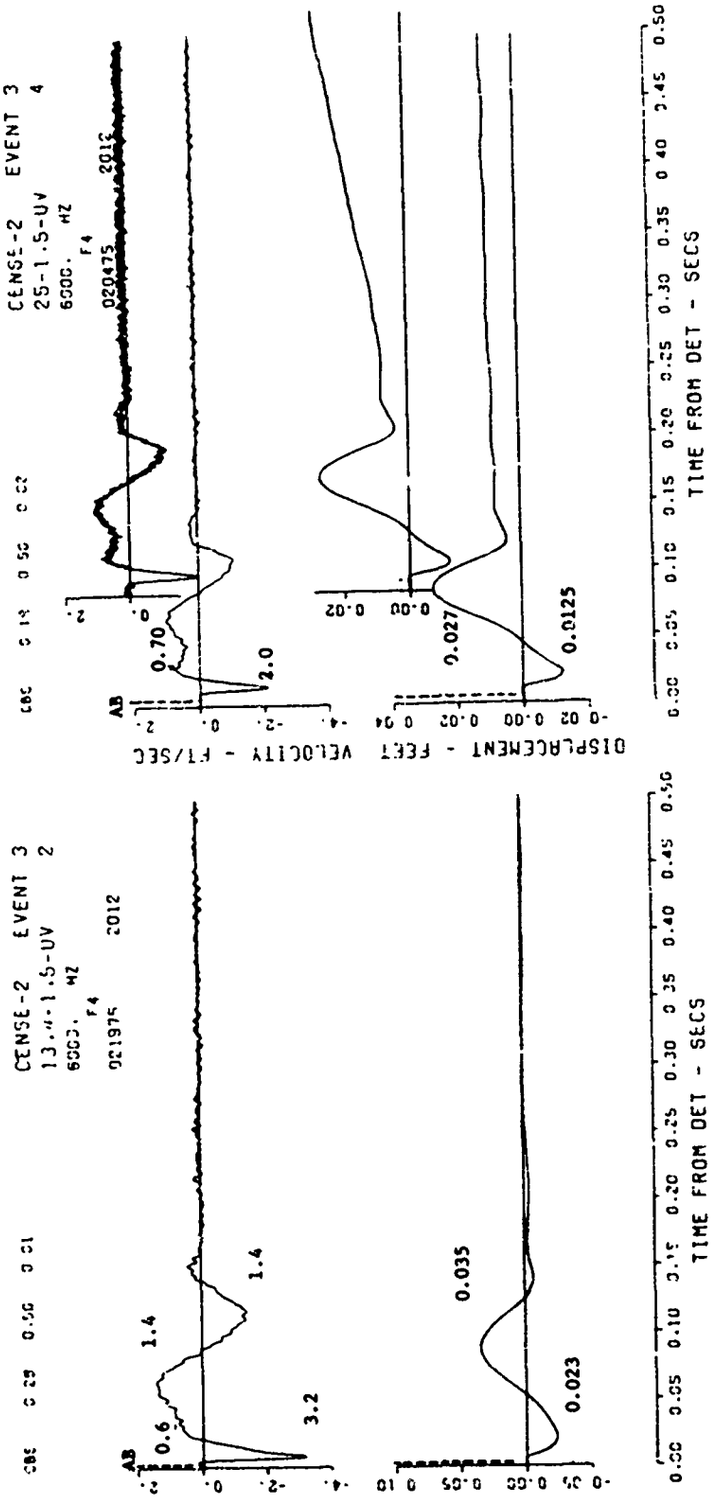

Figure B.10 (sheet 4 of 6).

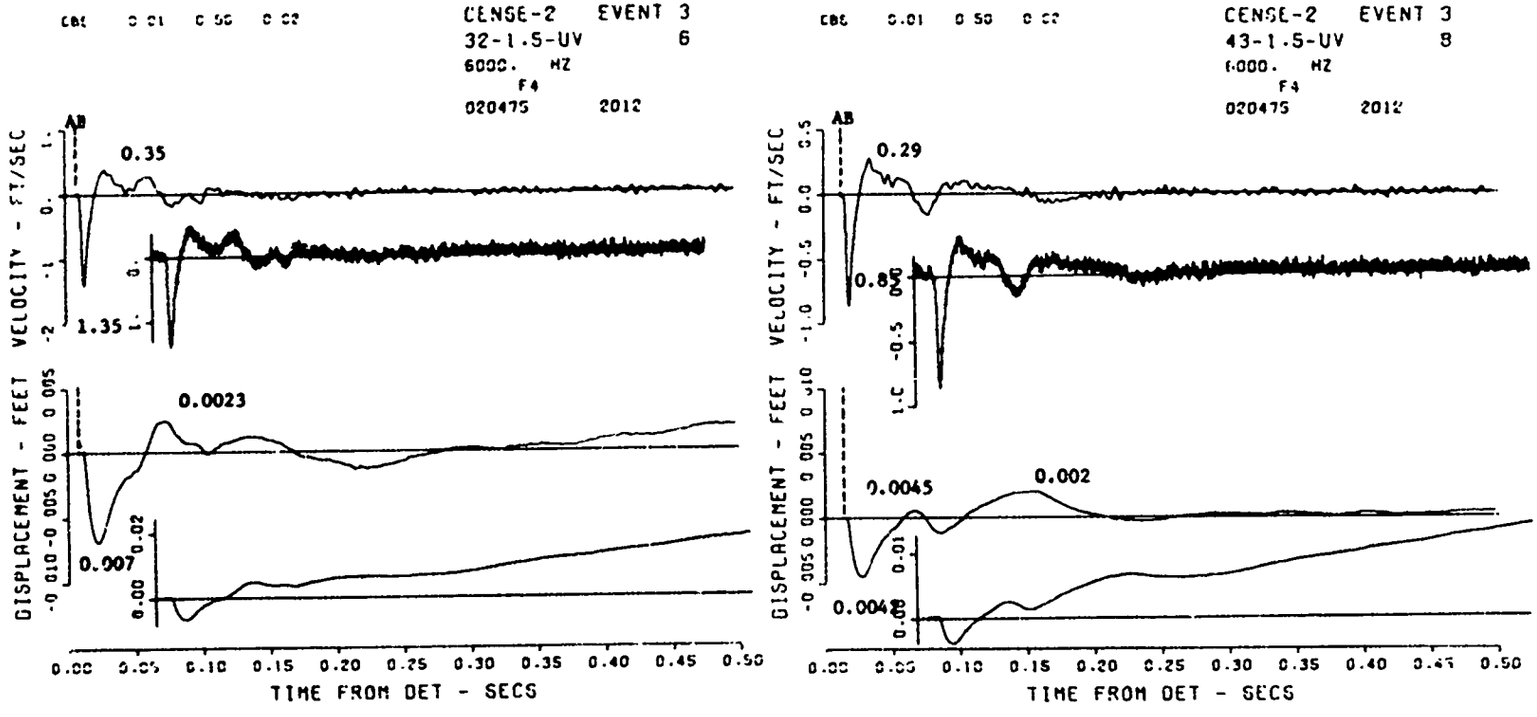

Figure B.10 (sheet 5 of 6).

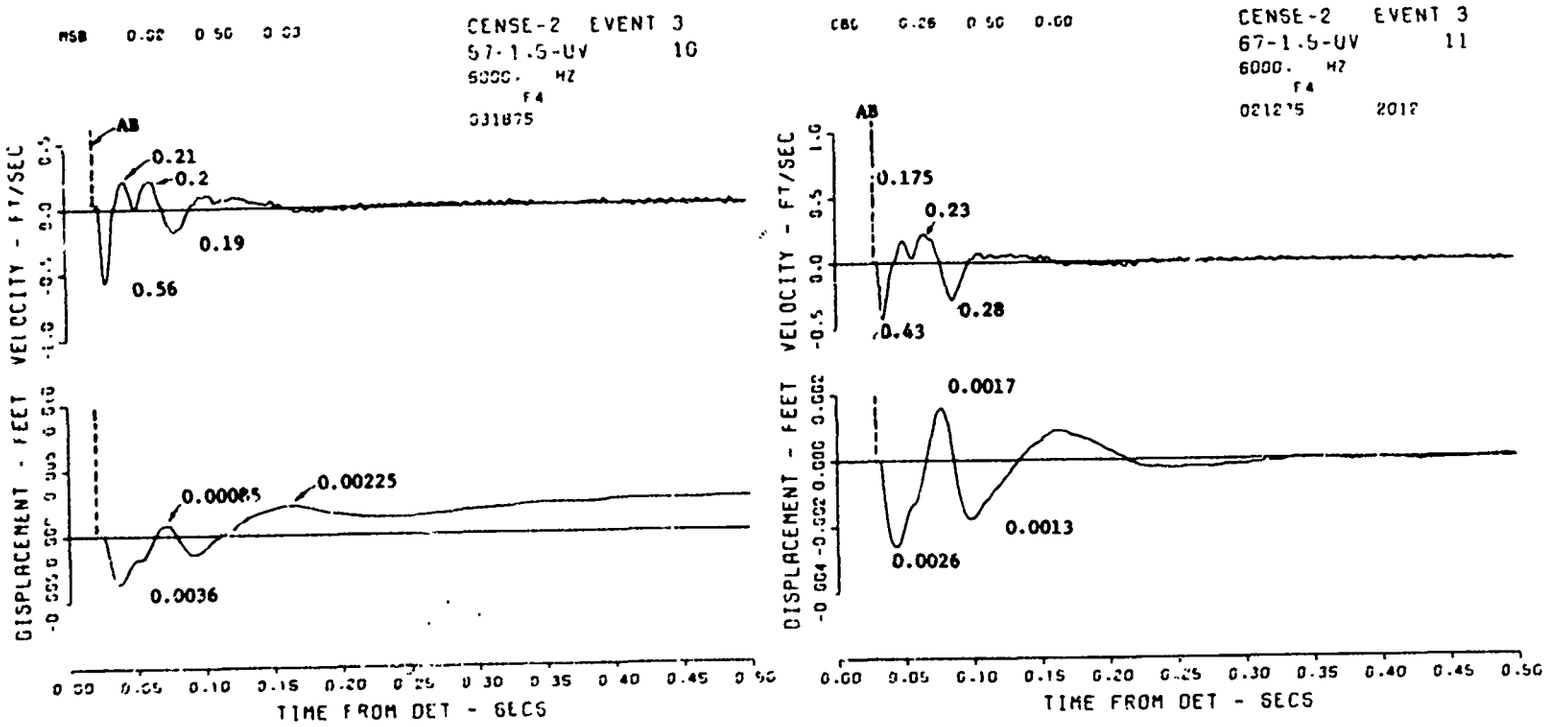

Figure B.10 (sheet 6 of 6).

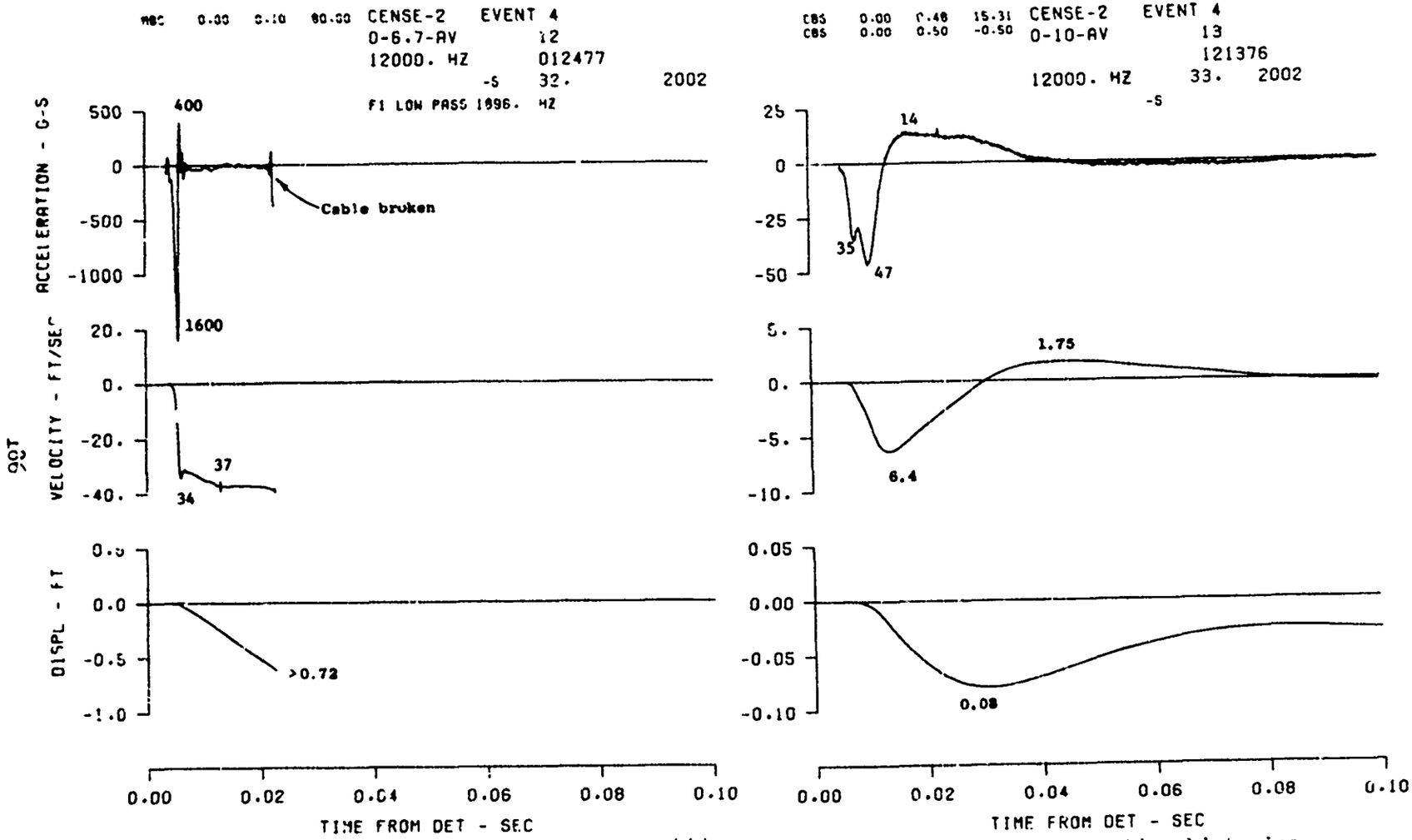

Figure B.11 Event 4, surface tangent, $-0.13\ W^{1/3}$ (-0.9 foot); motion- and stress-time histories along the vertical radial directly beneath the explosion (sheet 1 of 5).

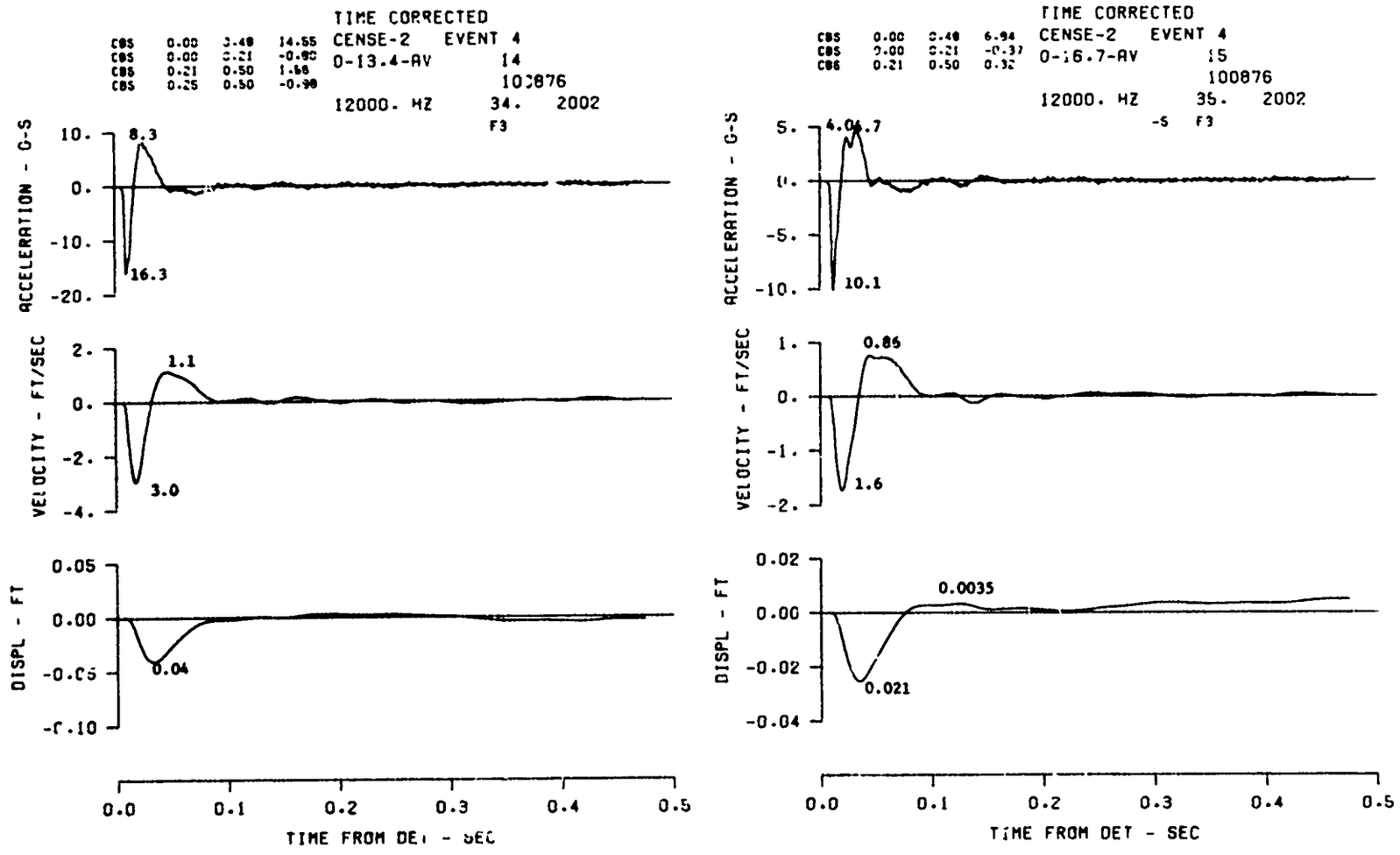

Figure B.11 (sheet 2 of 5).

CENSE-2 EVENT 4
0-20.1-AV

NO DATA RECOVERED
(GAGE SCRATCHED PRESHOT)

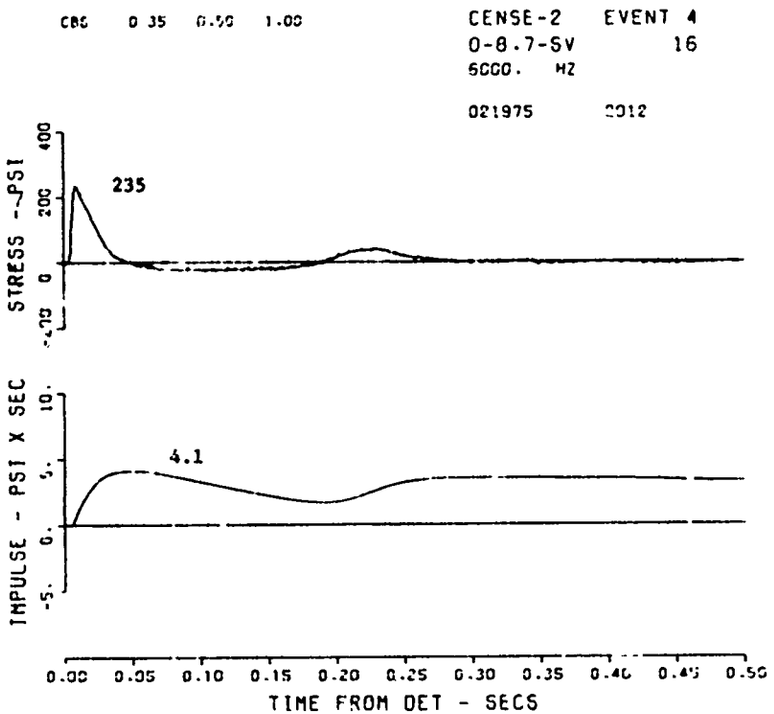

Figure B.11 (sheet 3 of 5).

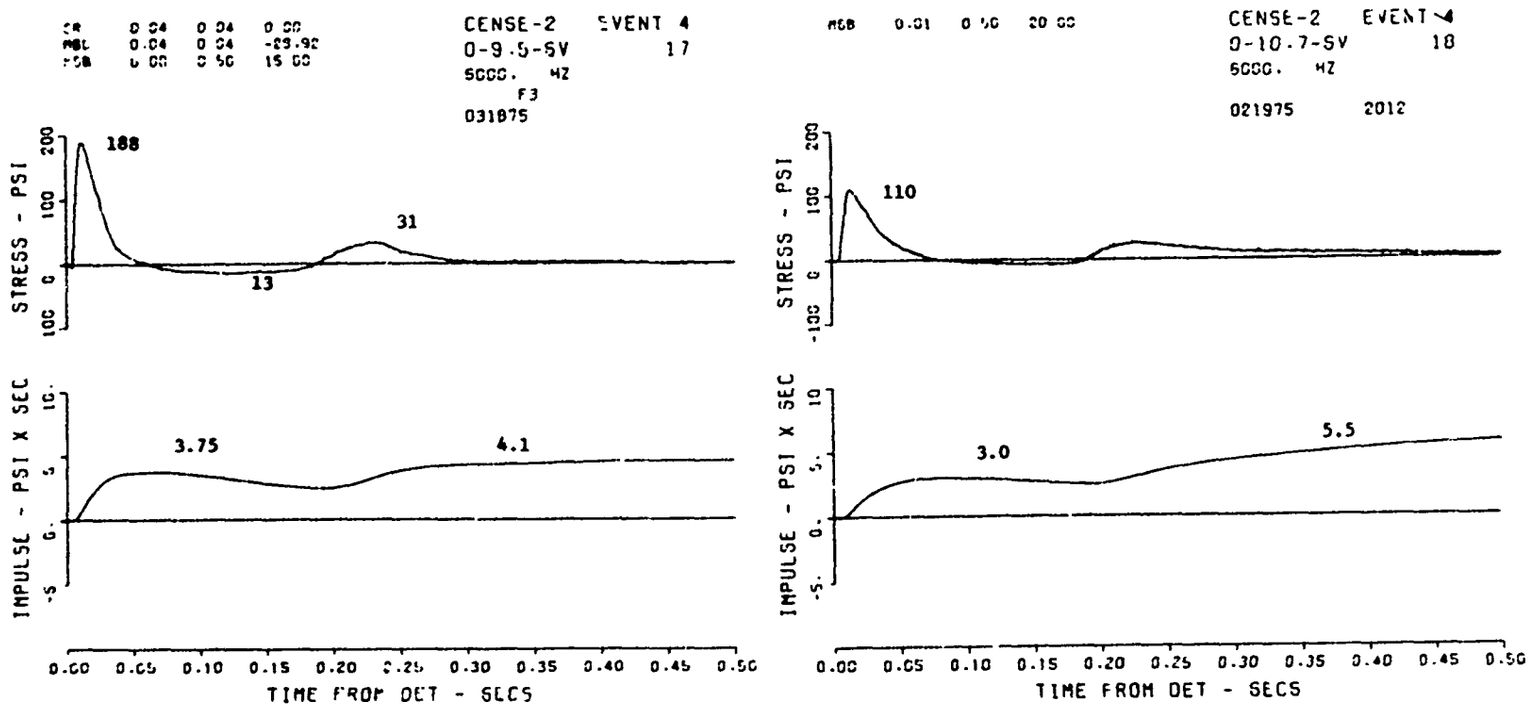

Figure B.11 (sheet 4 of 7).

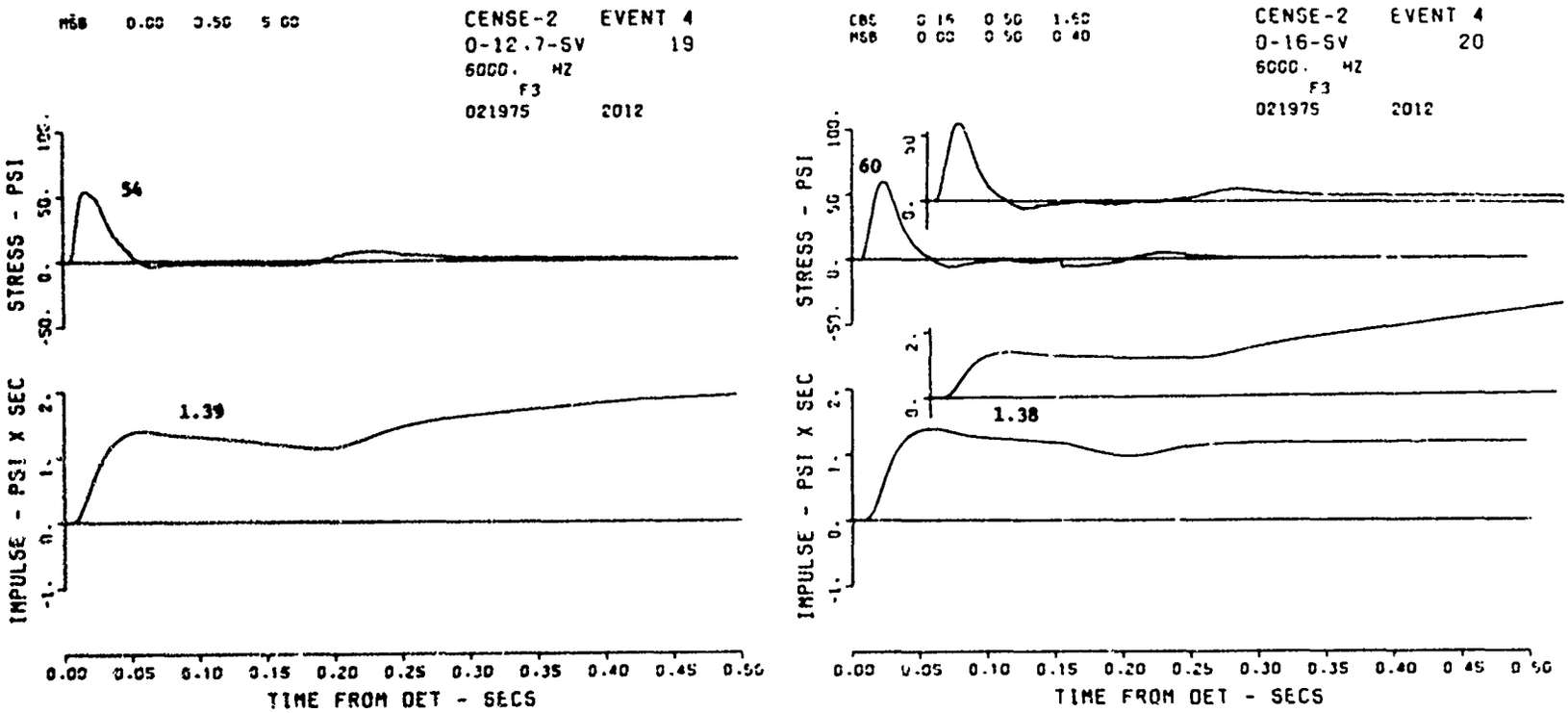

Figure B.11 (sheet 5 of 5).

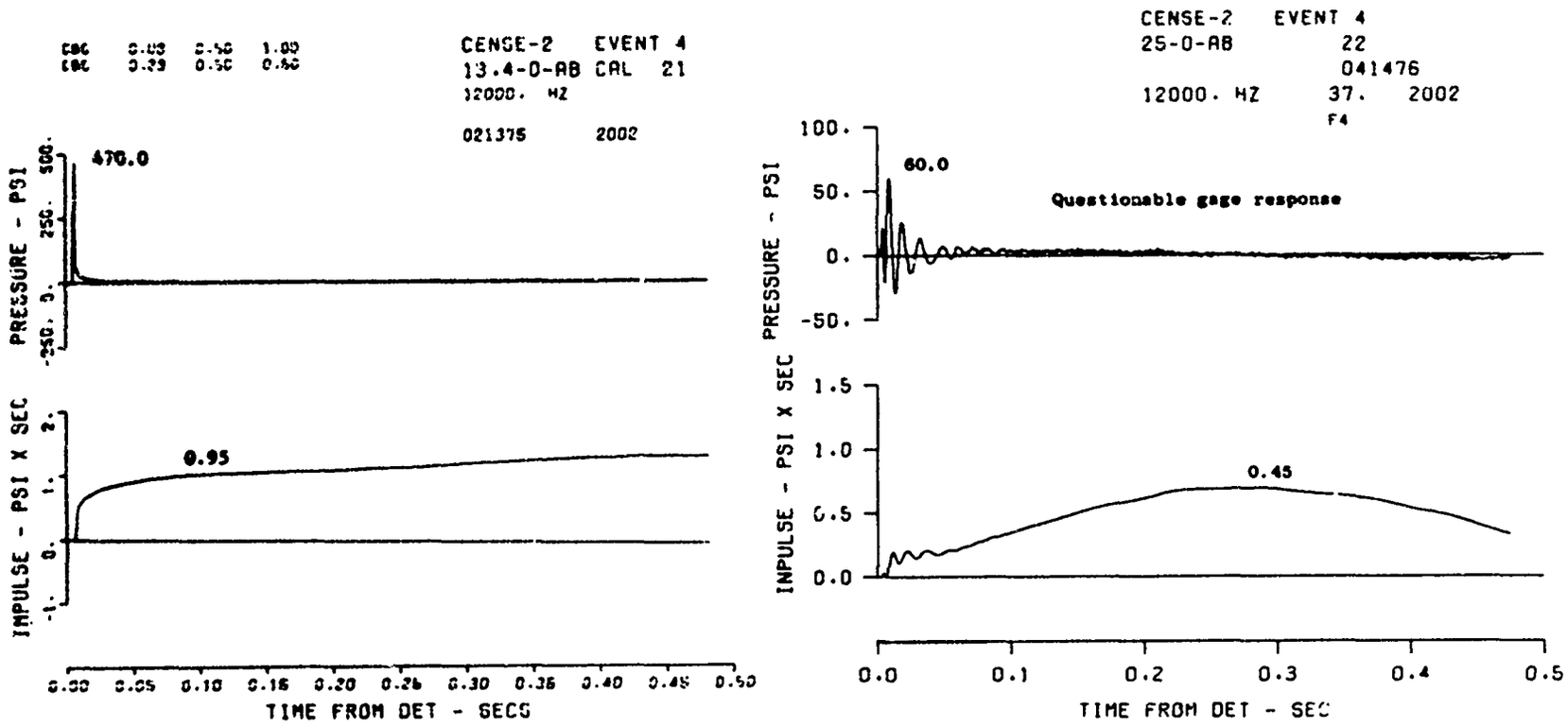

Figure B.12 Event 4, surface tangent, $-0.13\ W^{1/3}$ (-0.9 foot); surface airblast-time histories (sheet 1 of 3).

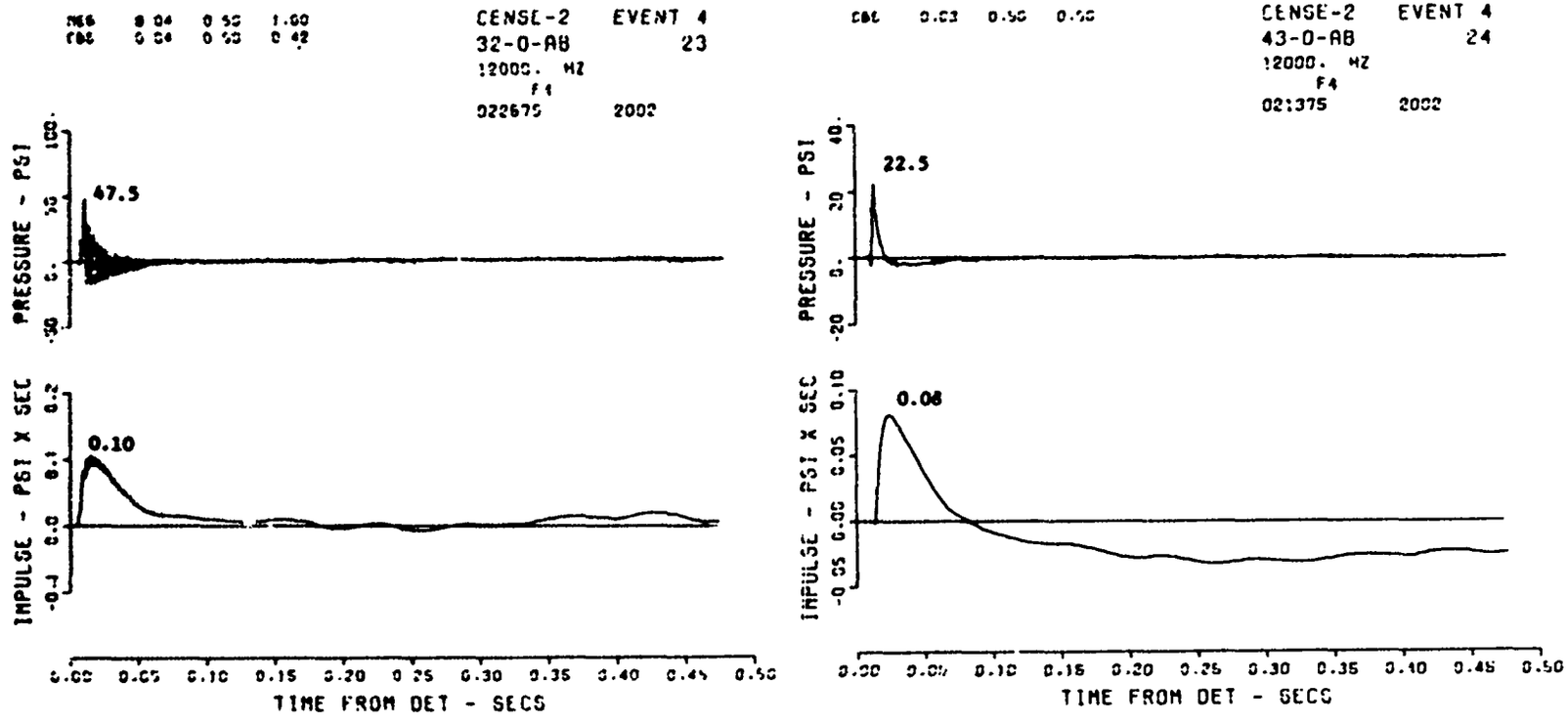

Figure B.12 (sheet 2 of 3).

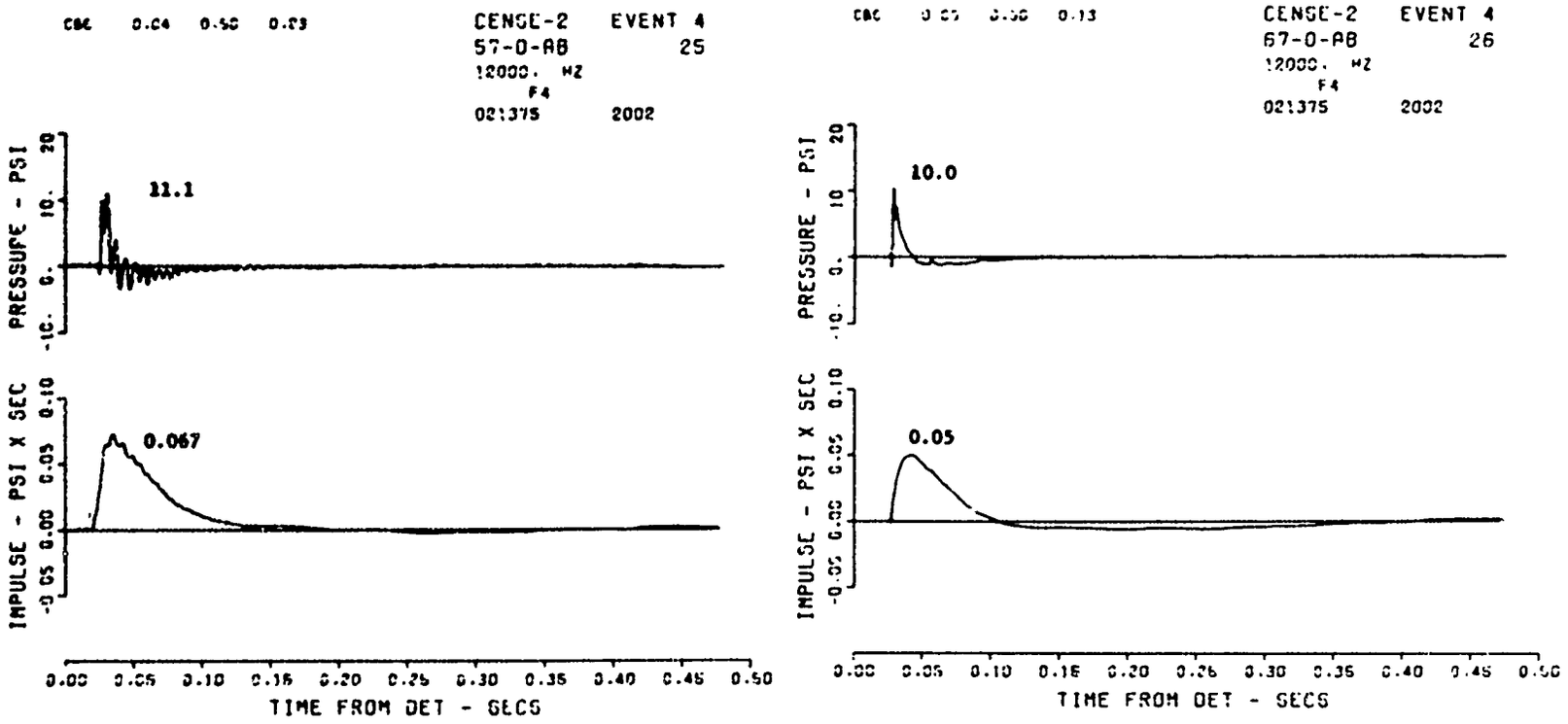

Figure B.12 (sheet 3 of 3).

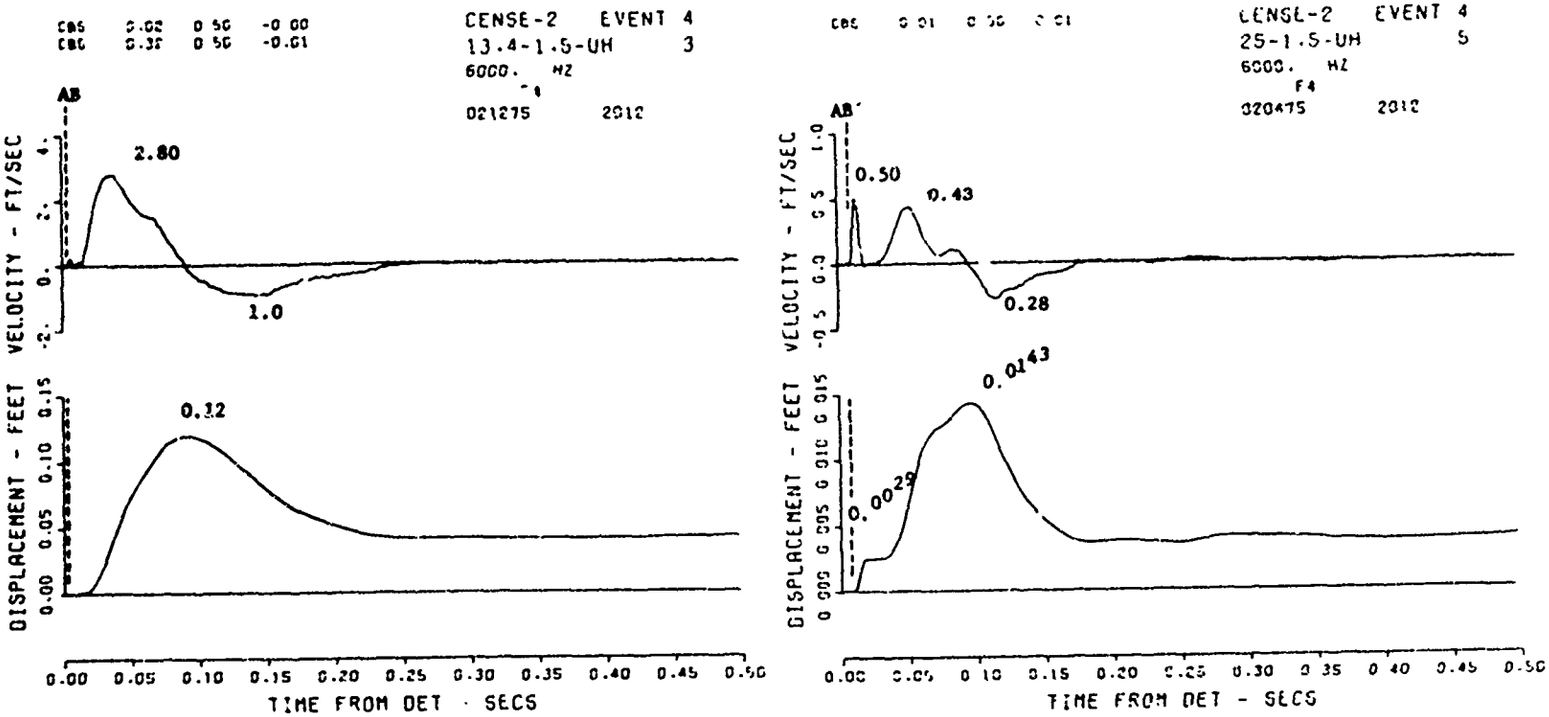

Figure B.13 Event 4, surface tangent, $-0.13\ W^{1/3}$ (-0.9 foot); near-surface motion-time histories (sheet 1 of 6).

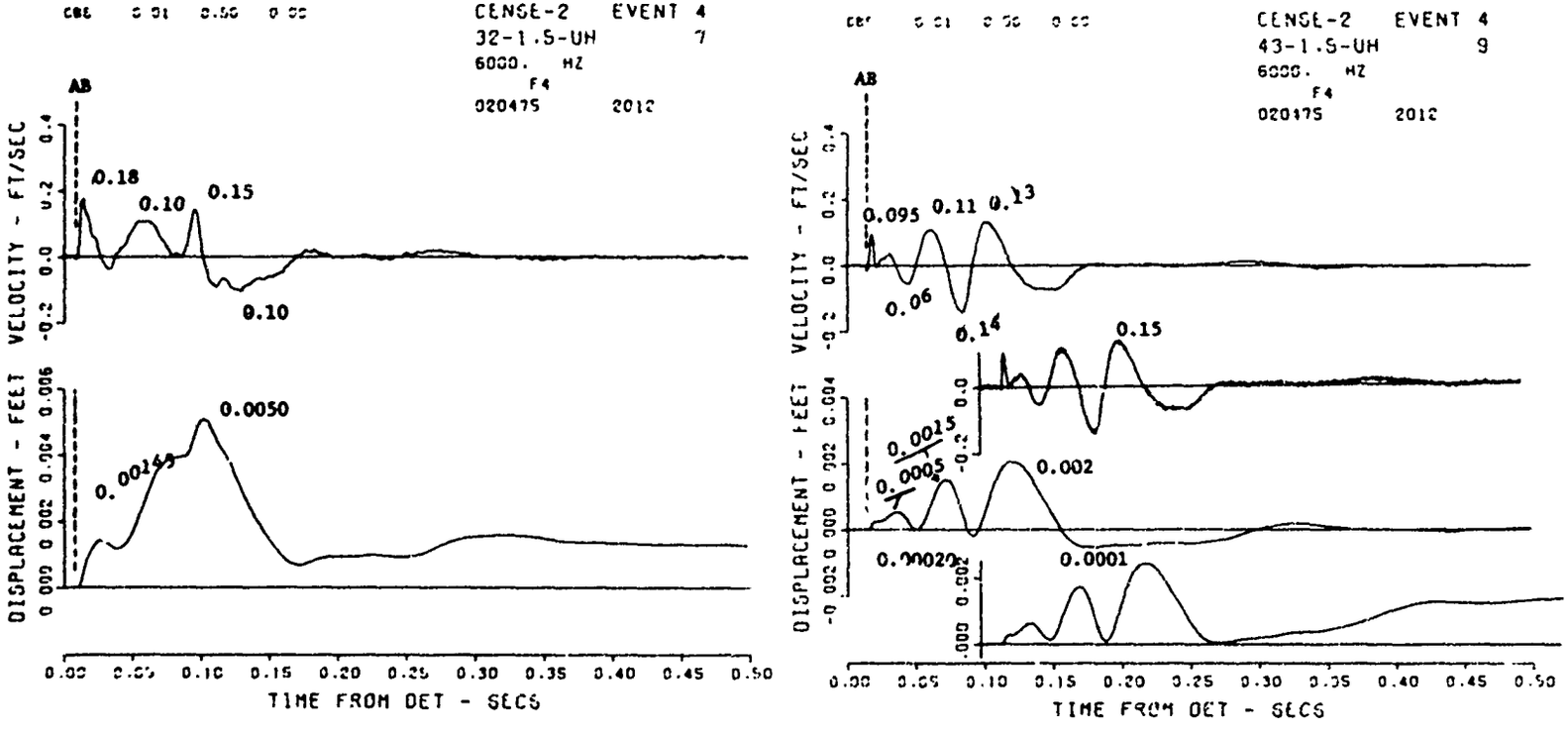

Figure B.13 (sheet 2 of 6).

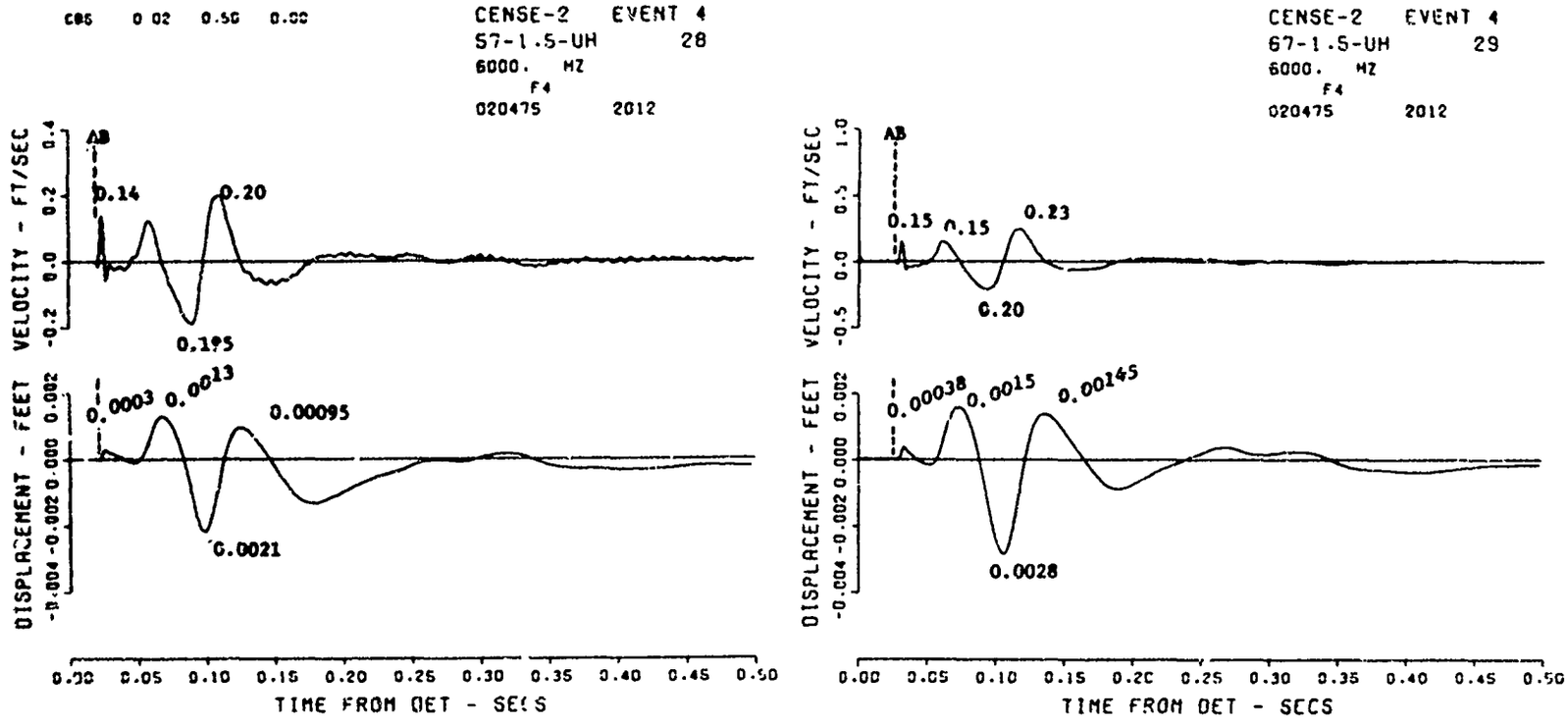

Figure B.13 (sheet 3 of 6).

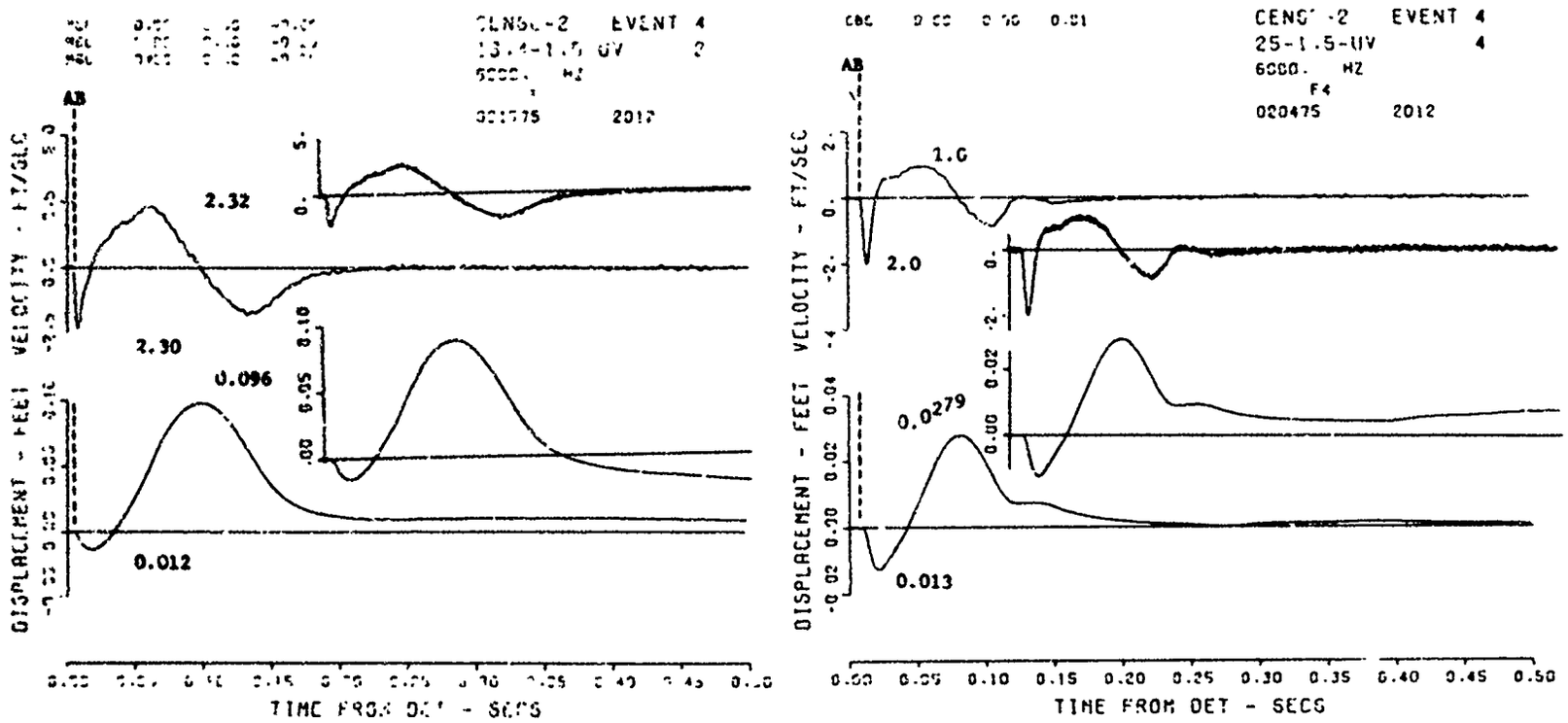

Figure B.13 (sheet 4 of 6).

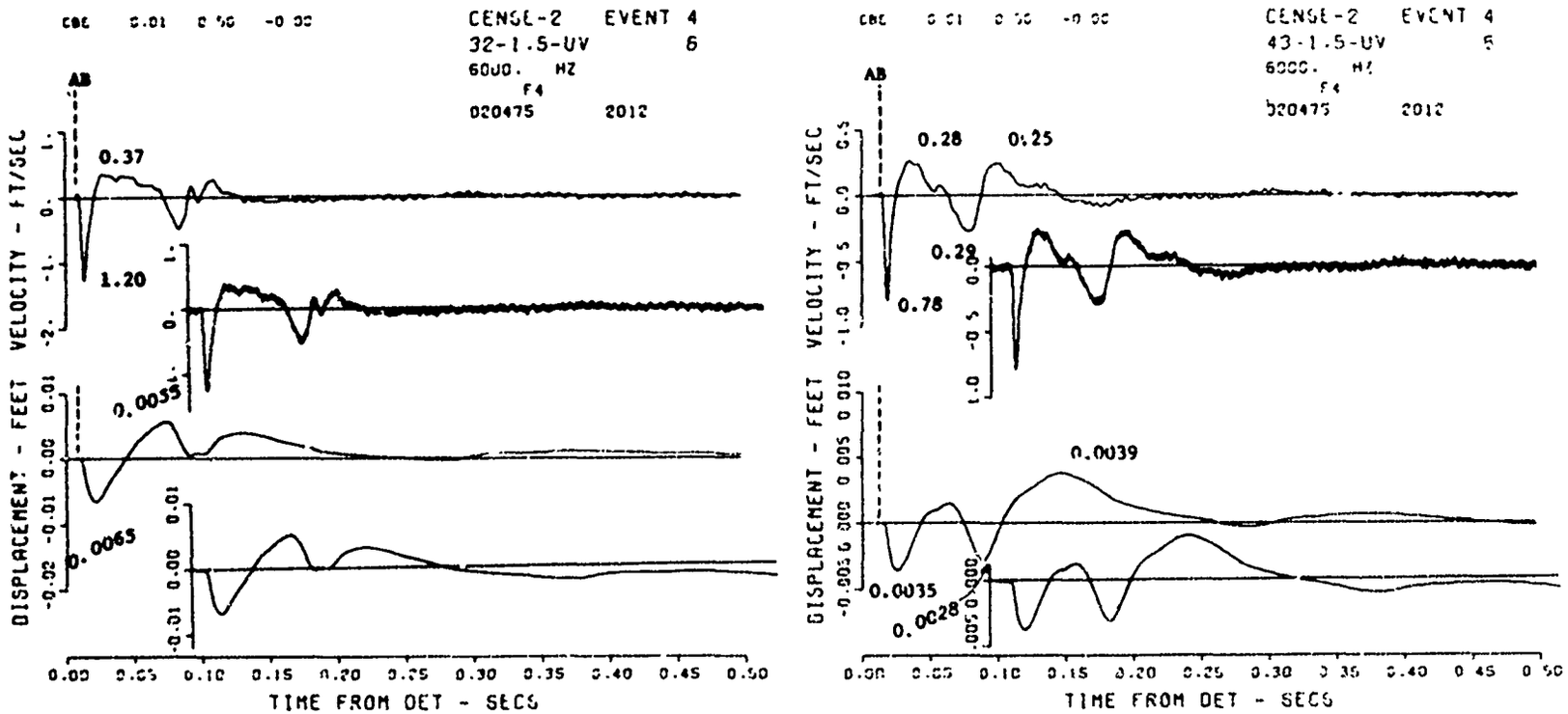

Figure B.13 (sheet 5 of 6).

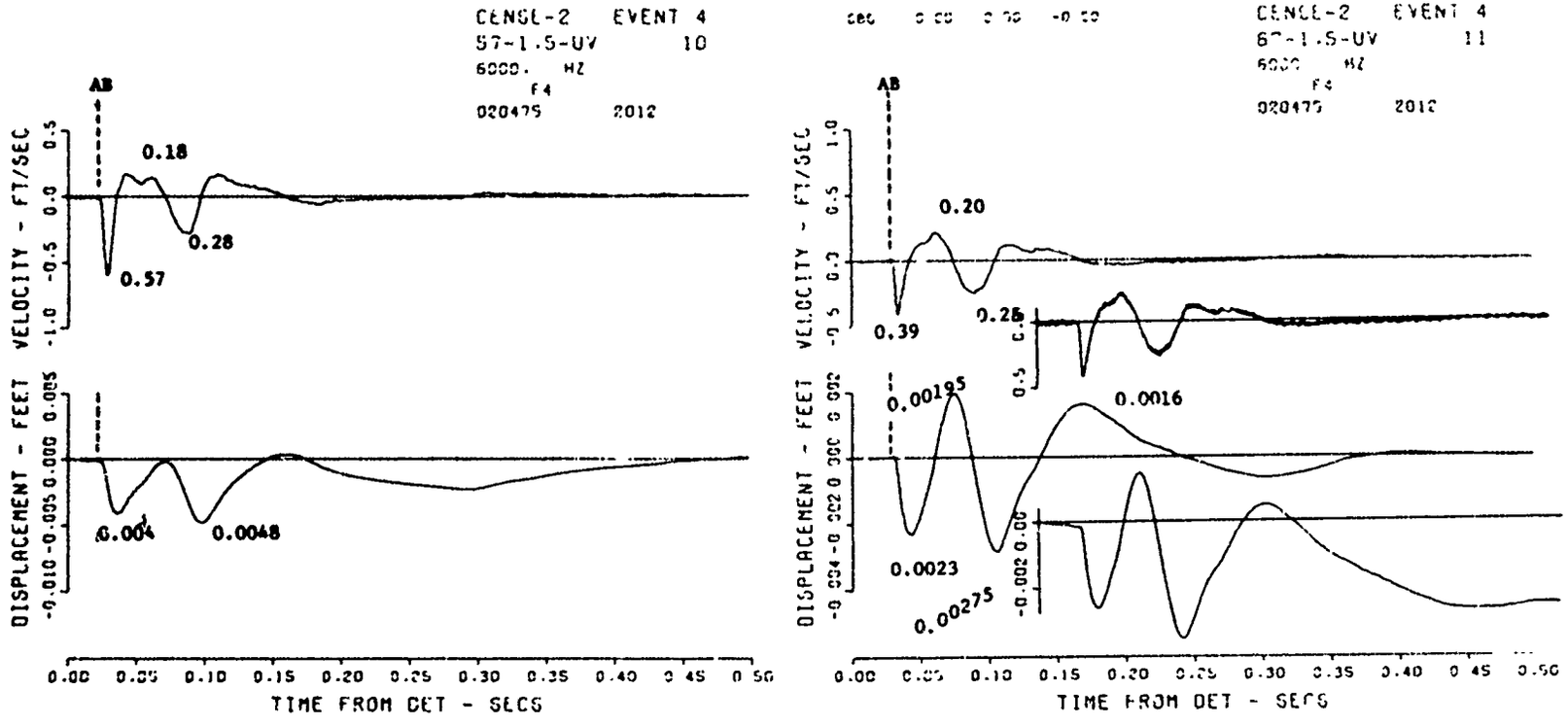

Figure B.13 (sheet 6 of 6).

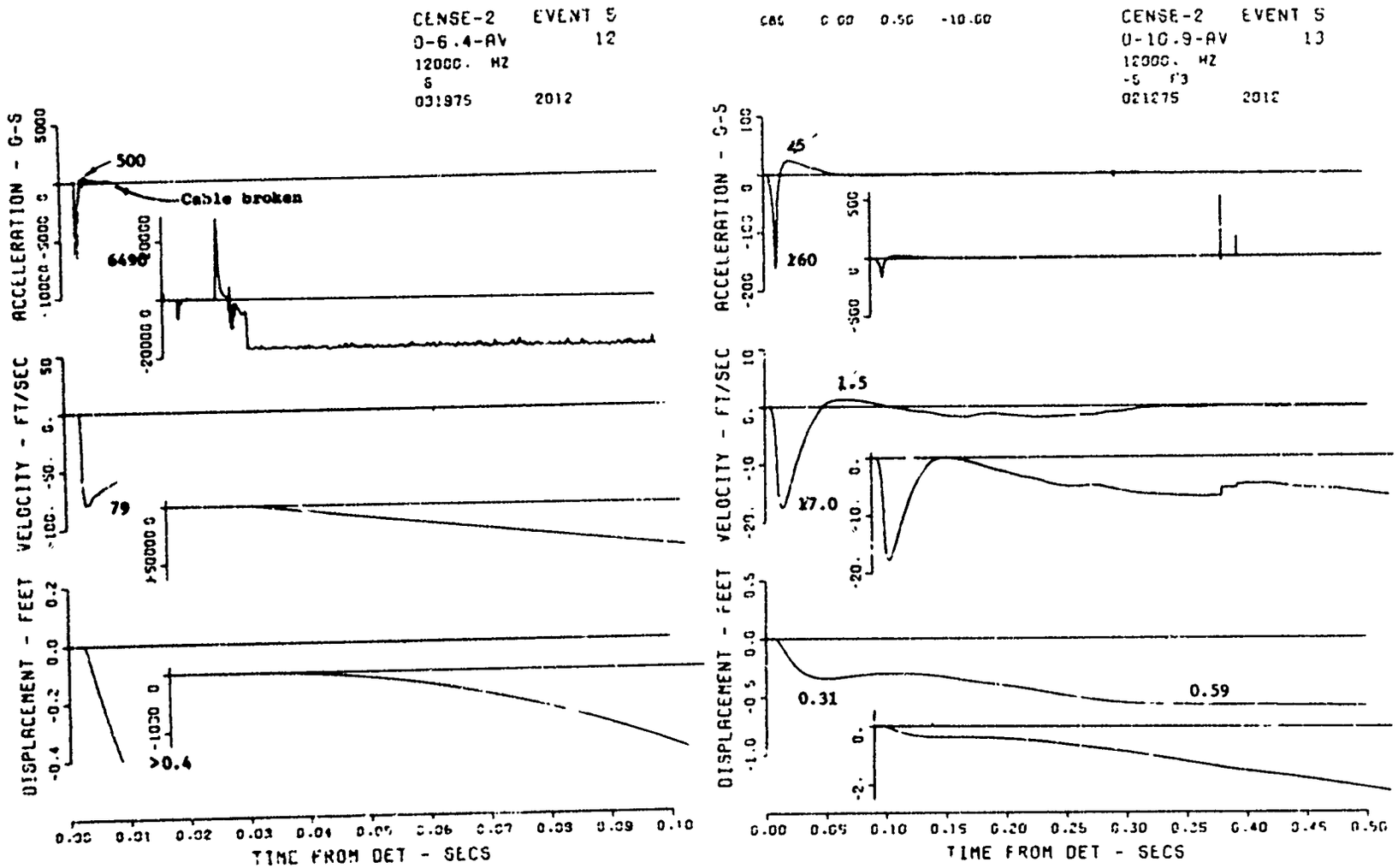

Figure B.14 Event 5, half buried, 0 $W^{1/3}$ (0 foot); motion- and stress-time histories along the vertical radial directly beneath the explosion (sheet 1 of 6).

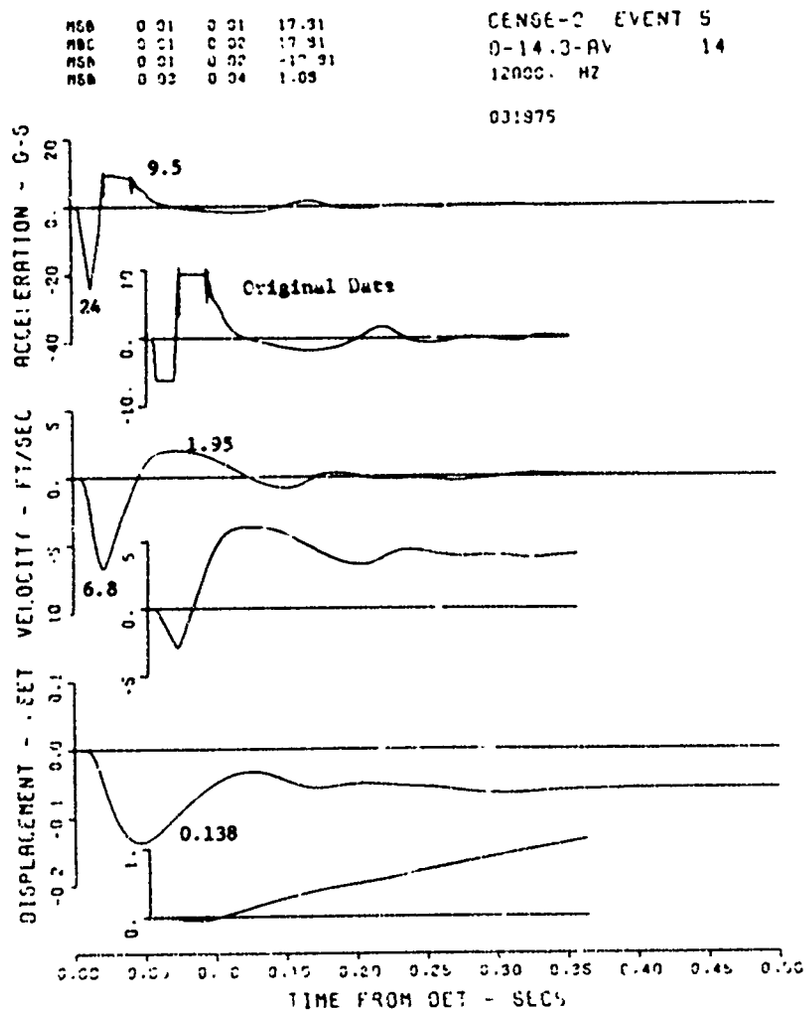

Figure B.14 (sheet 2 of 6).

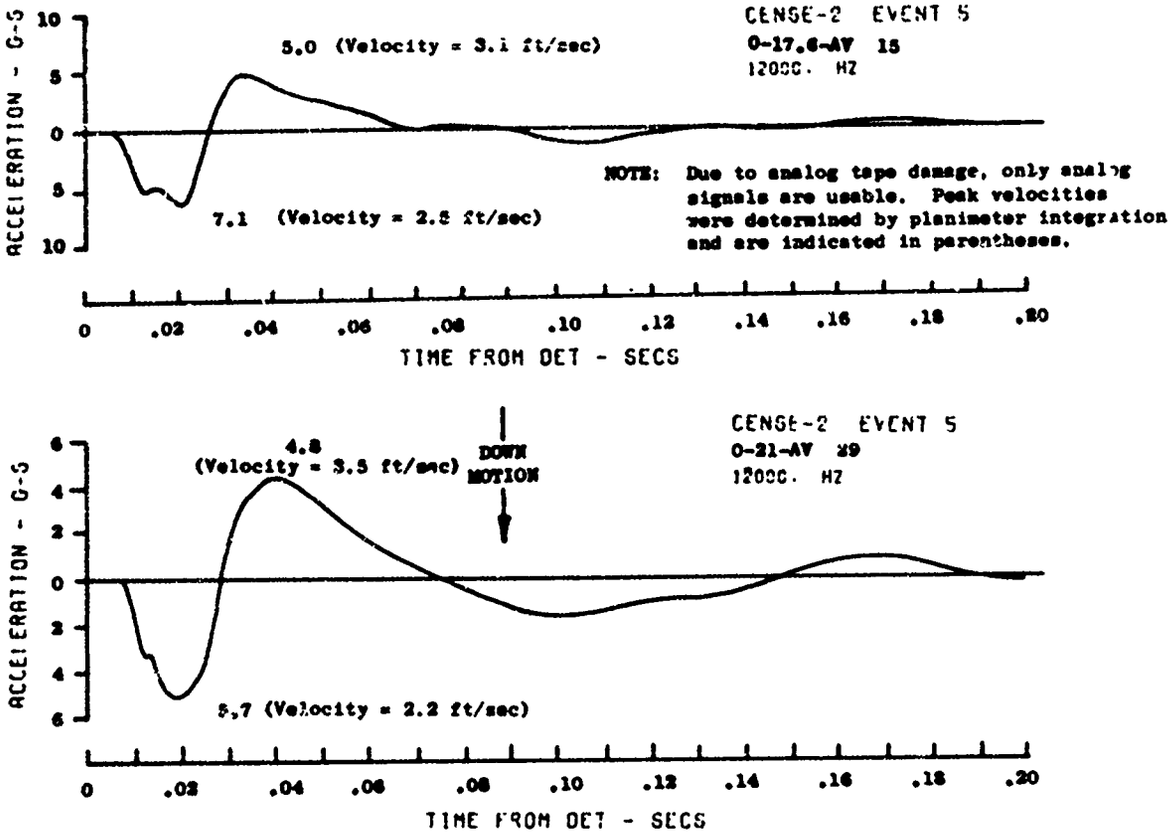

Figure B.14 (sheet 3 of 6).

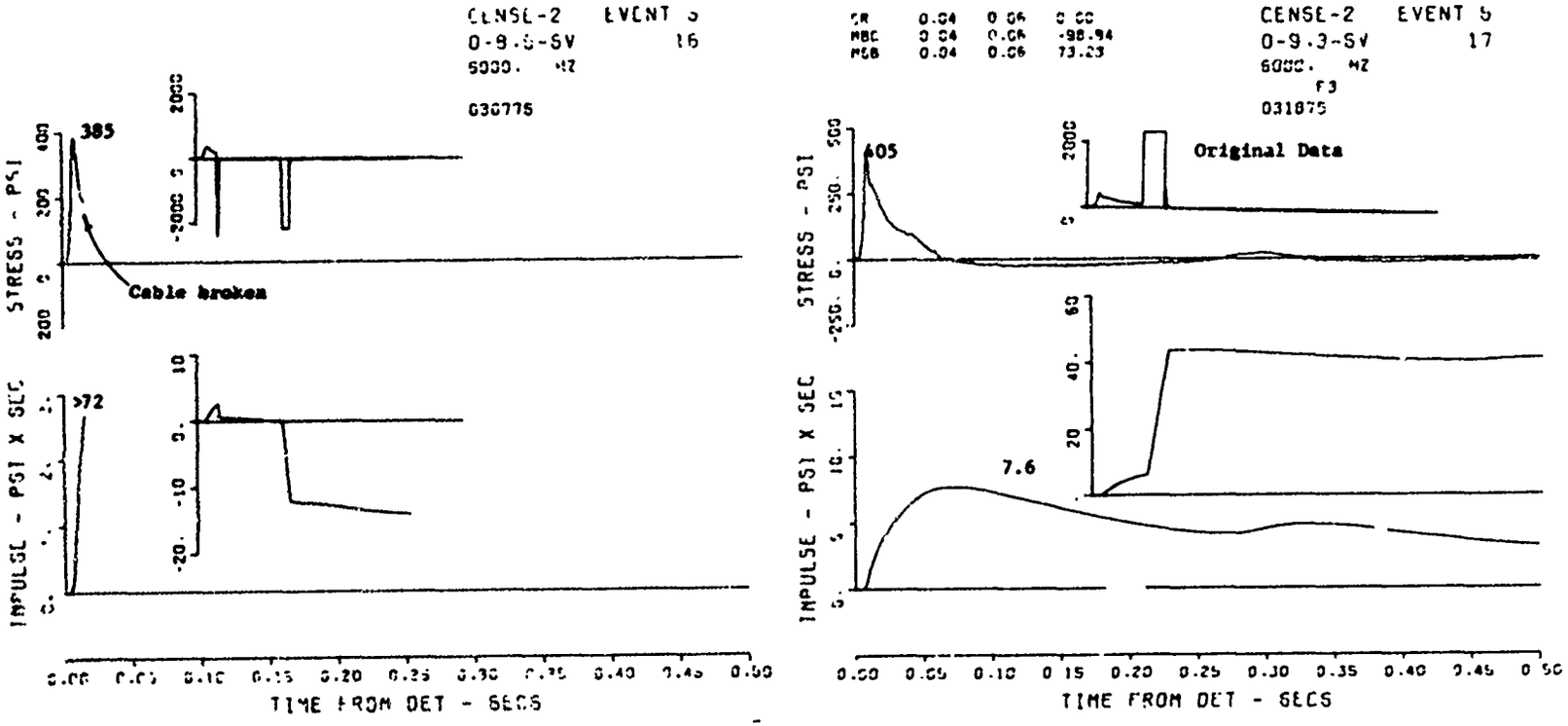

Figure B.14 (sheet 4 of 6).

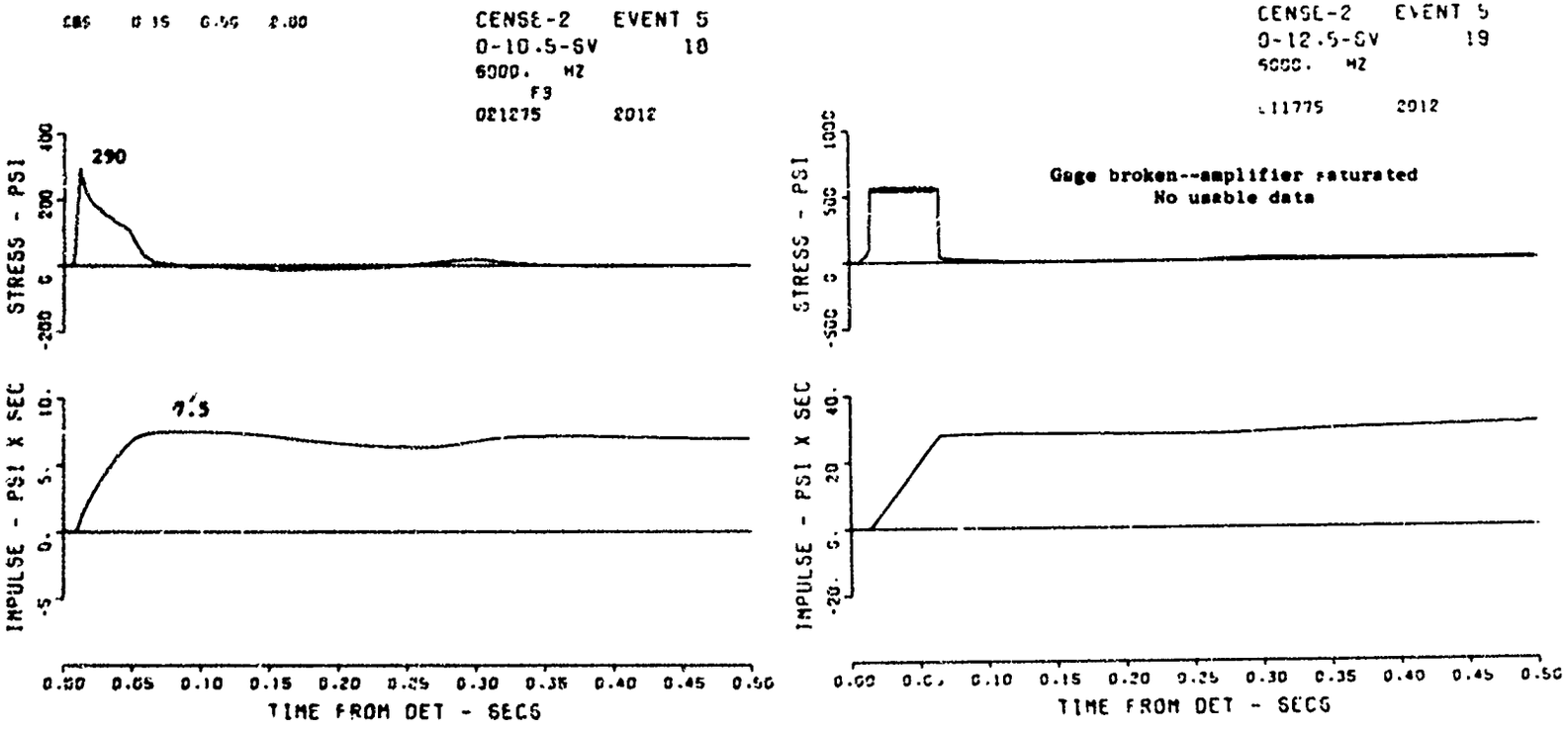

Figure B.14 (sheet 5 of 6).

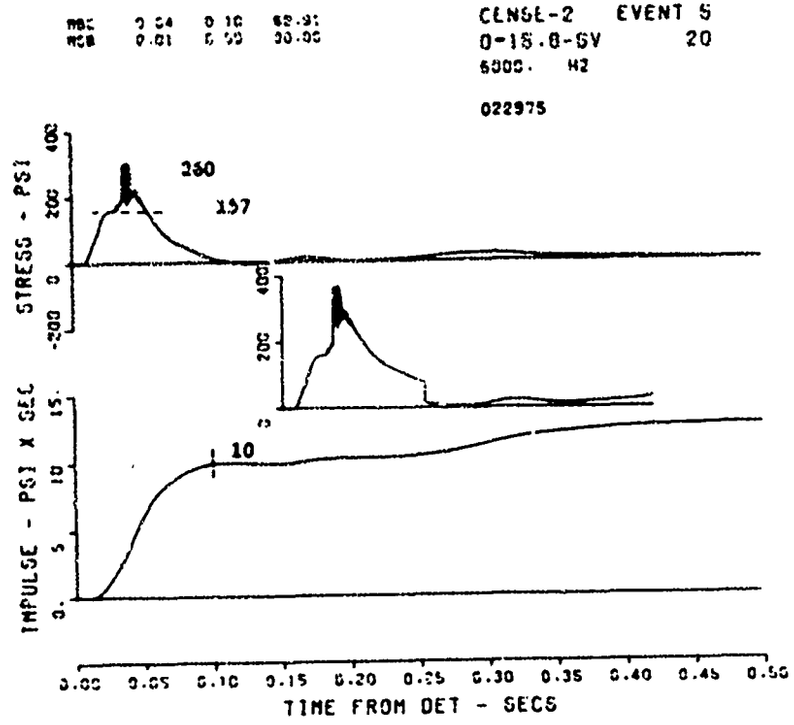

Figure B.14 (sheet 6 of 6).

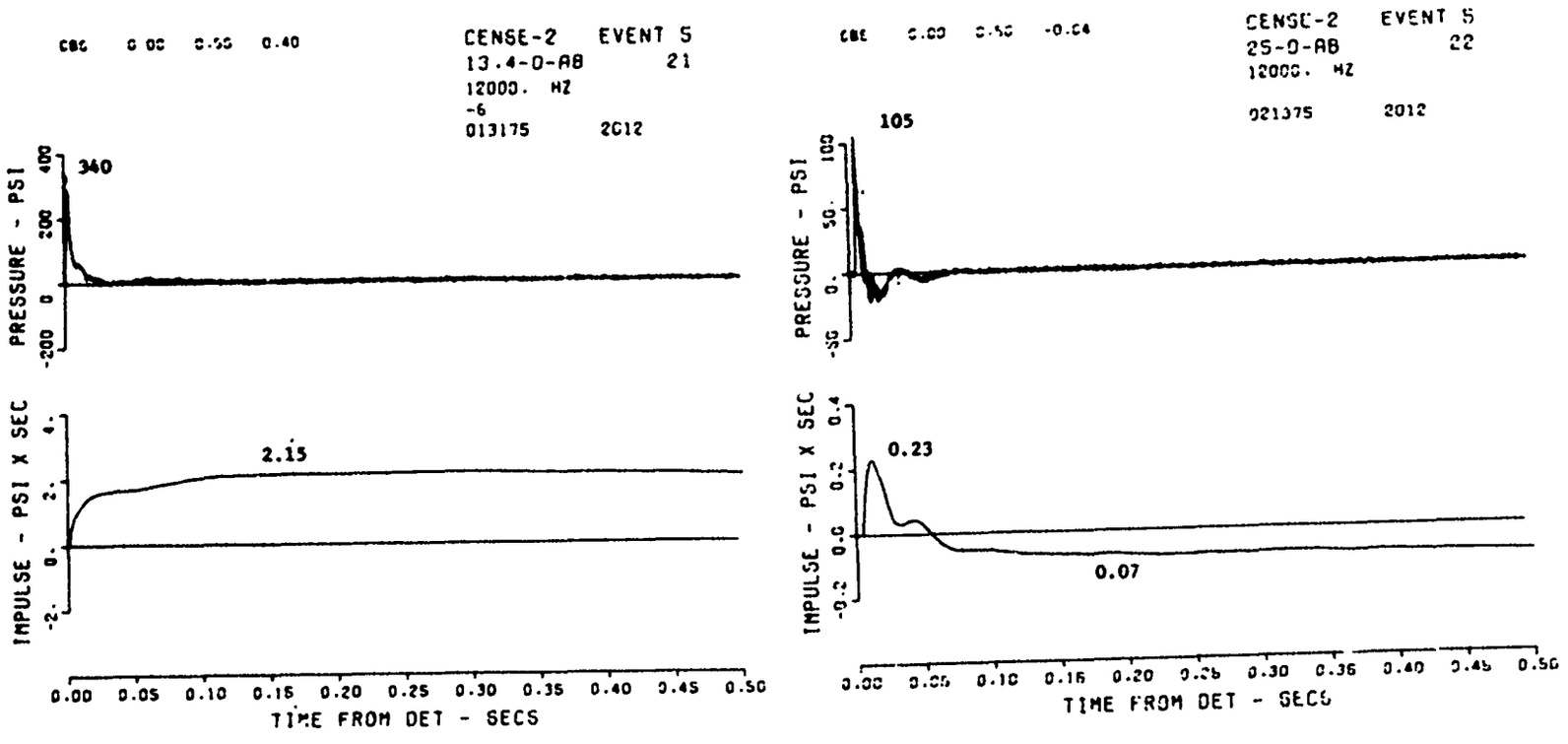

Figure B.15 Event 5, half buried, 0 $W^{1/3}$ (0 foot); surface airblast-time histories (sheet 1 of 3).

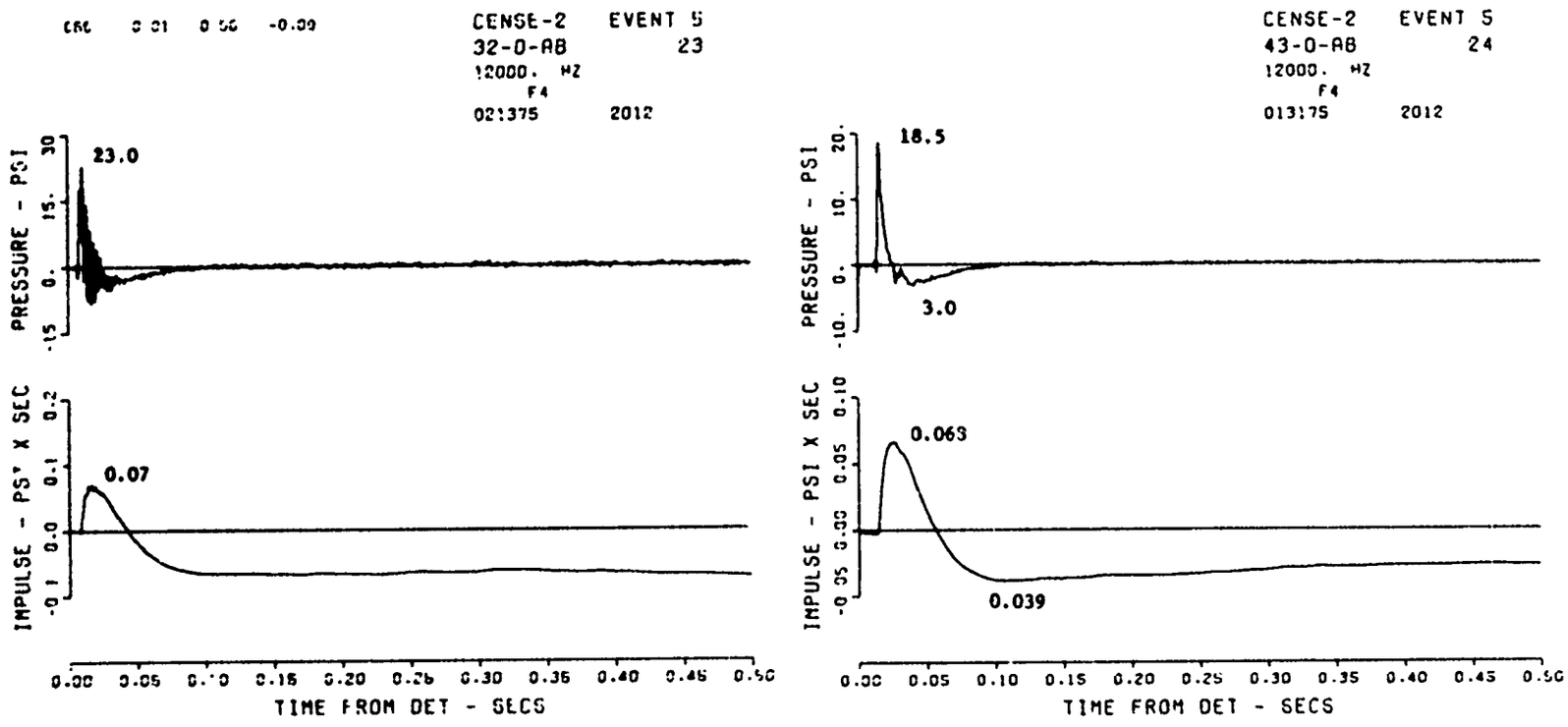

Figure B.15 (sheet 2 of 3).

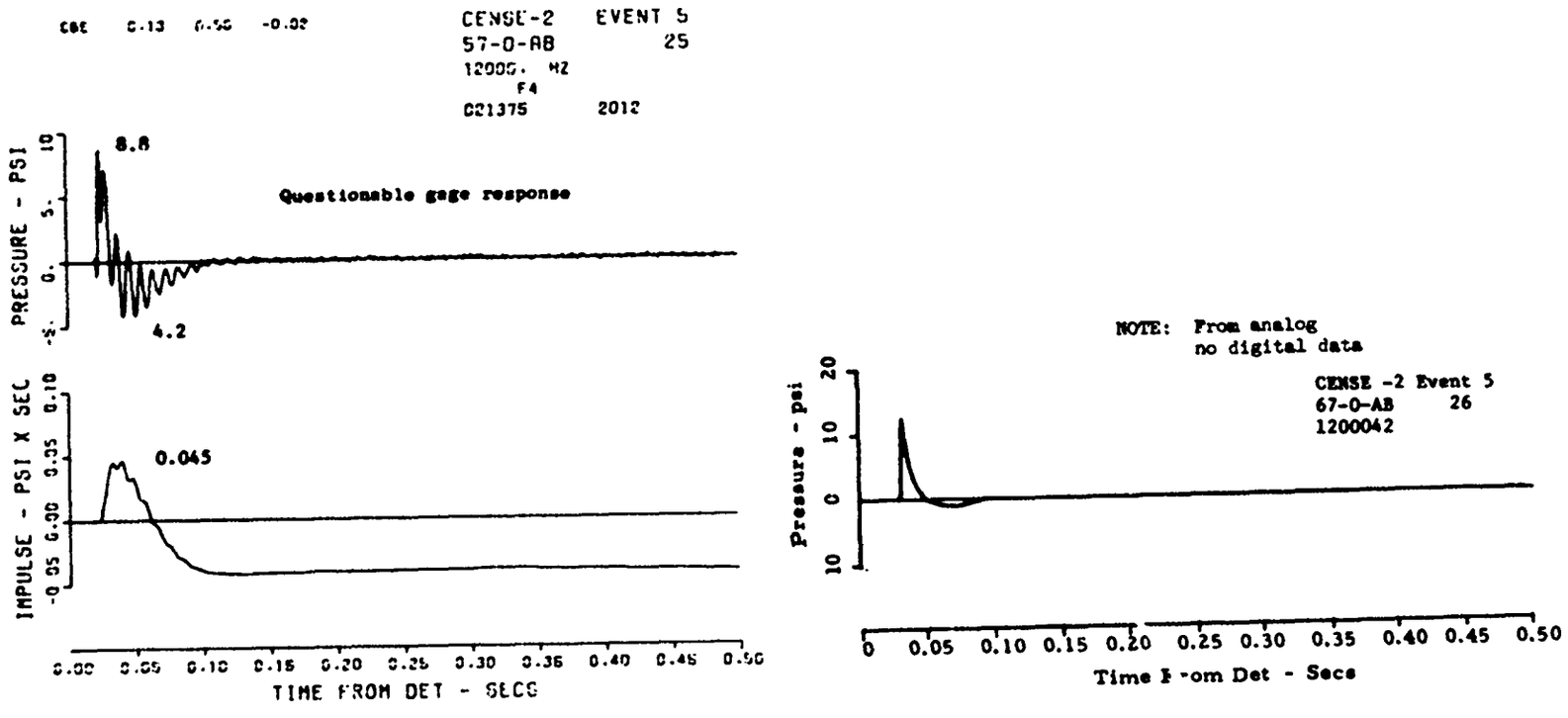

Figure B.15 (sheet 3 of 3).

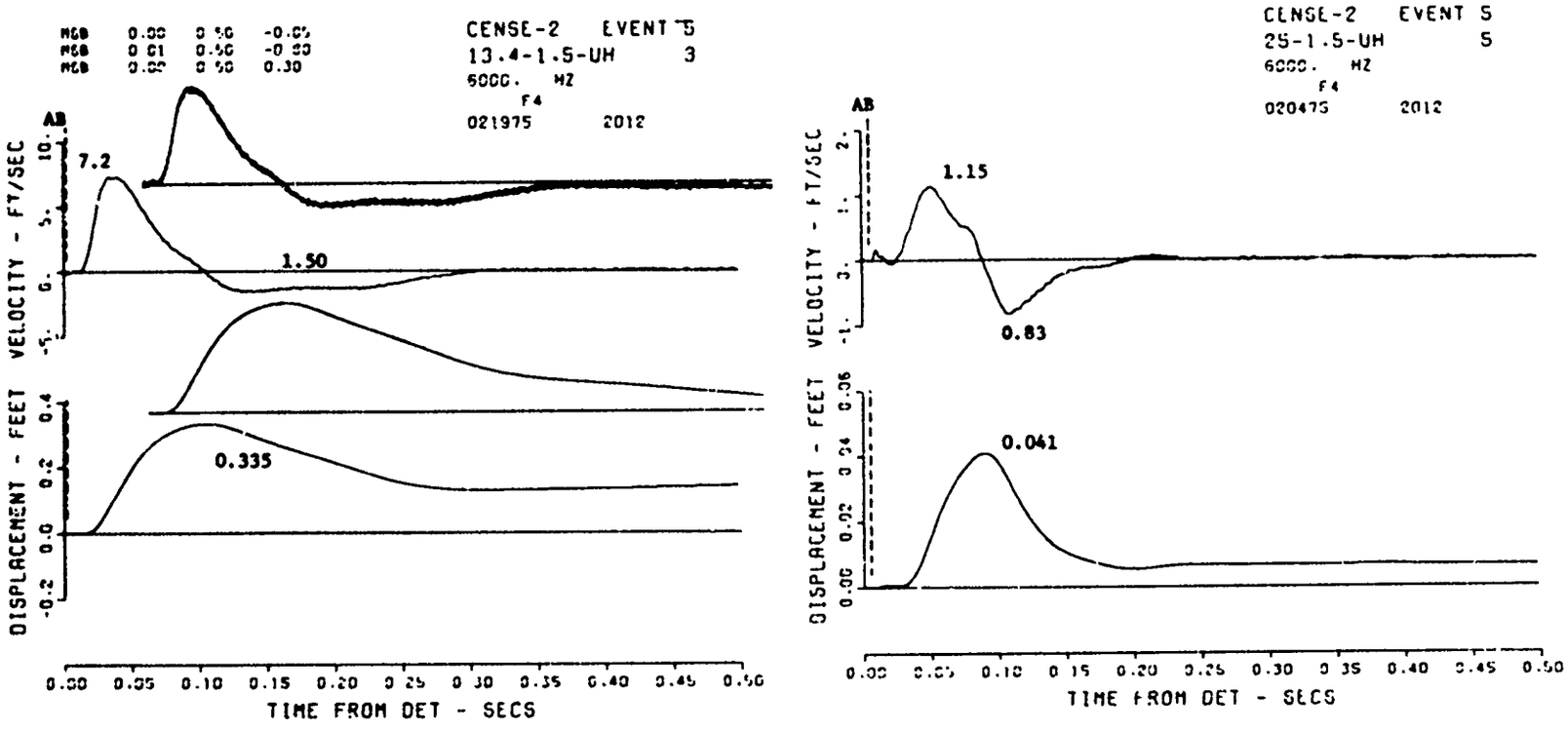

Figure B.16 Event 5, half buried, 0 $W^{1/3}$ (0 foot); near-surface motion-time histories (sheet 1 of 6).

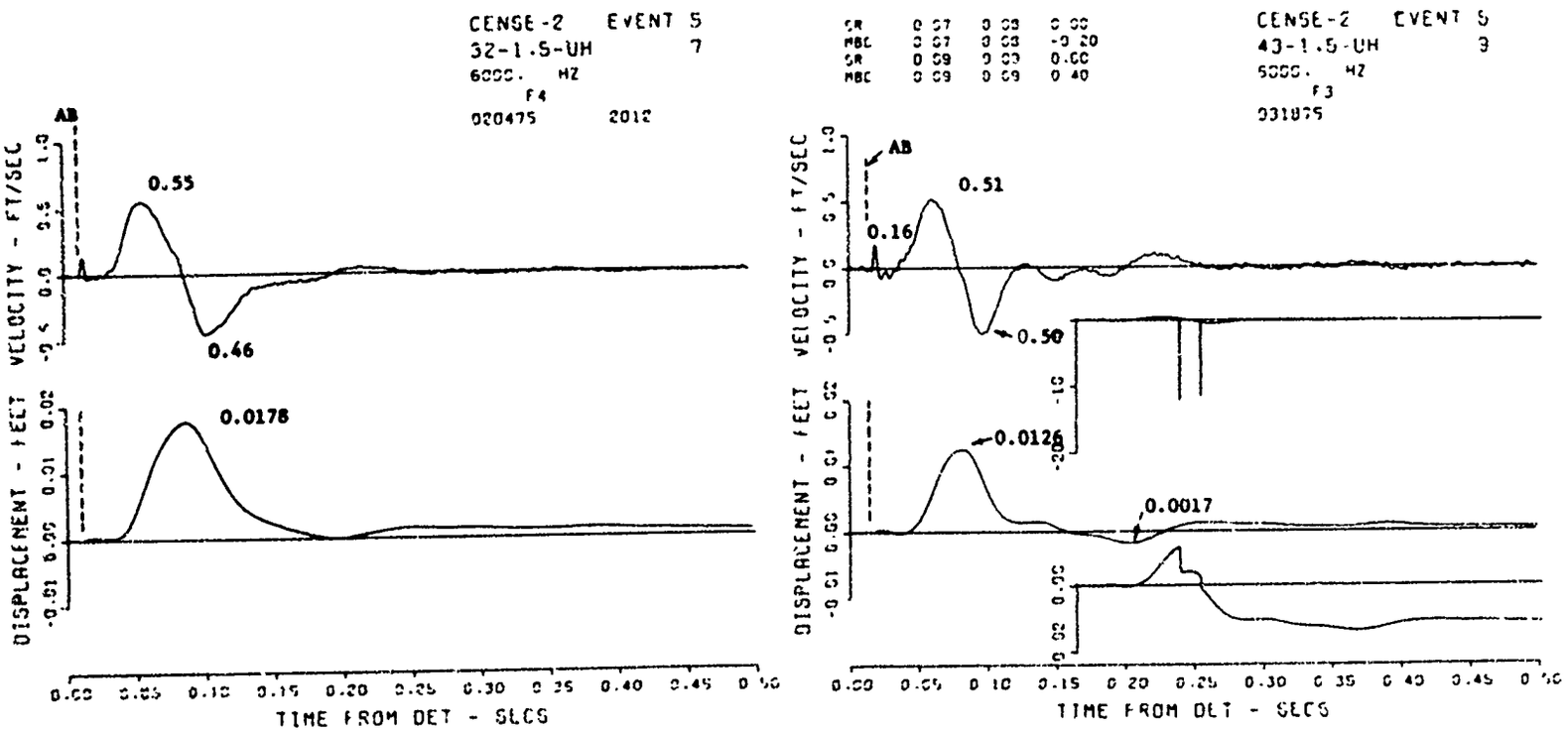

Figure B.16 (sheet 2 of 6).

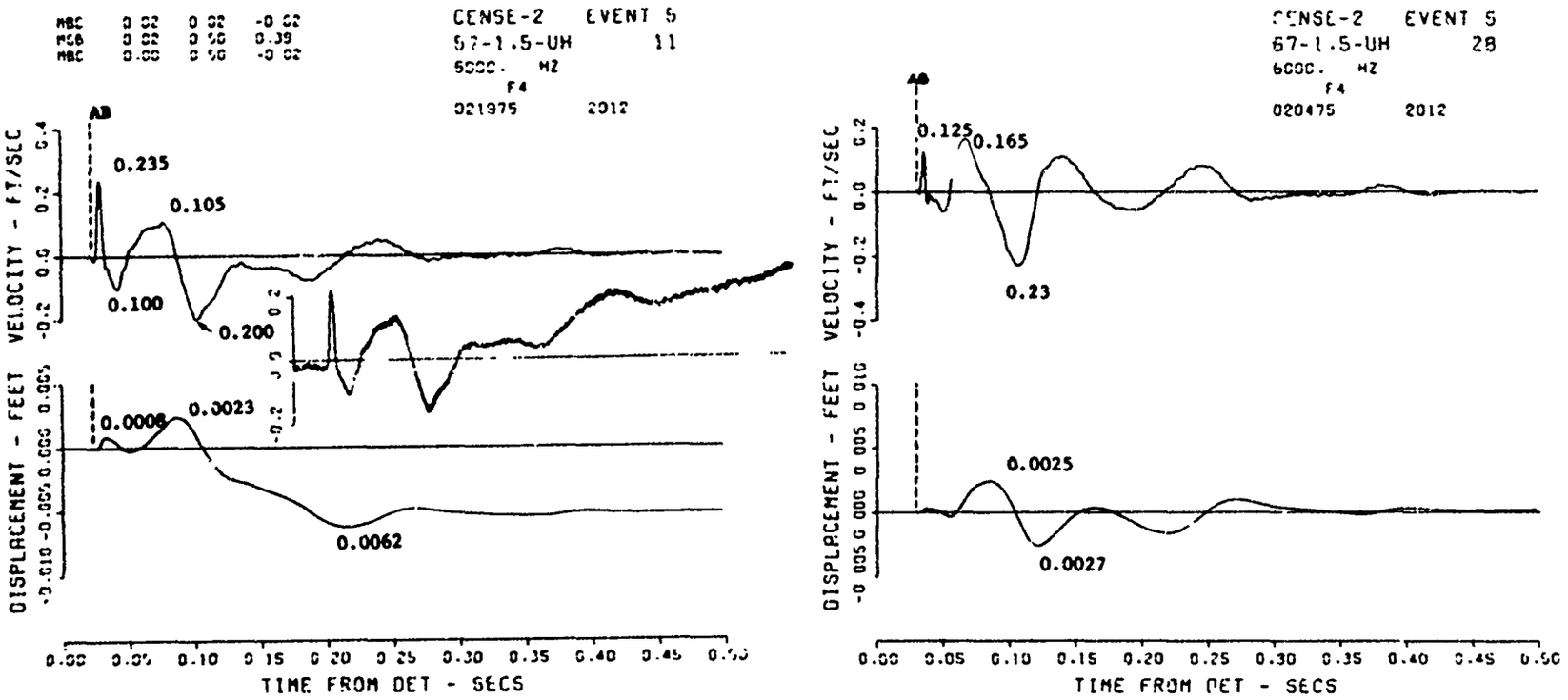

Figure B.16 (sheet 3 of 6).

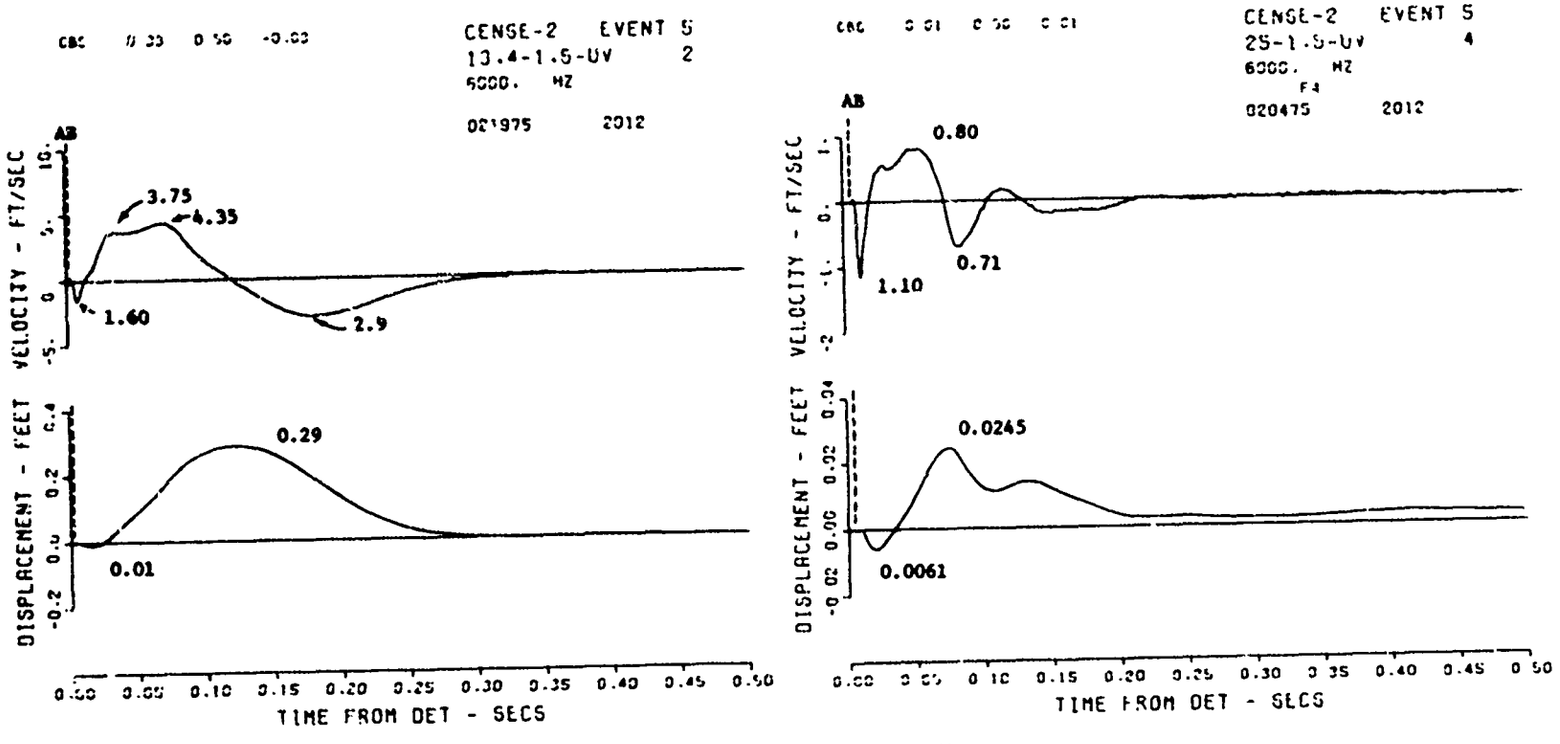

Figure B.16 (sheet 4 of 6).

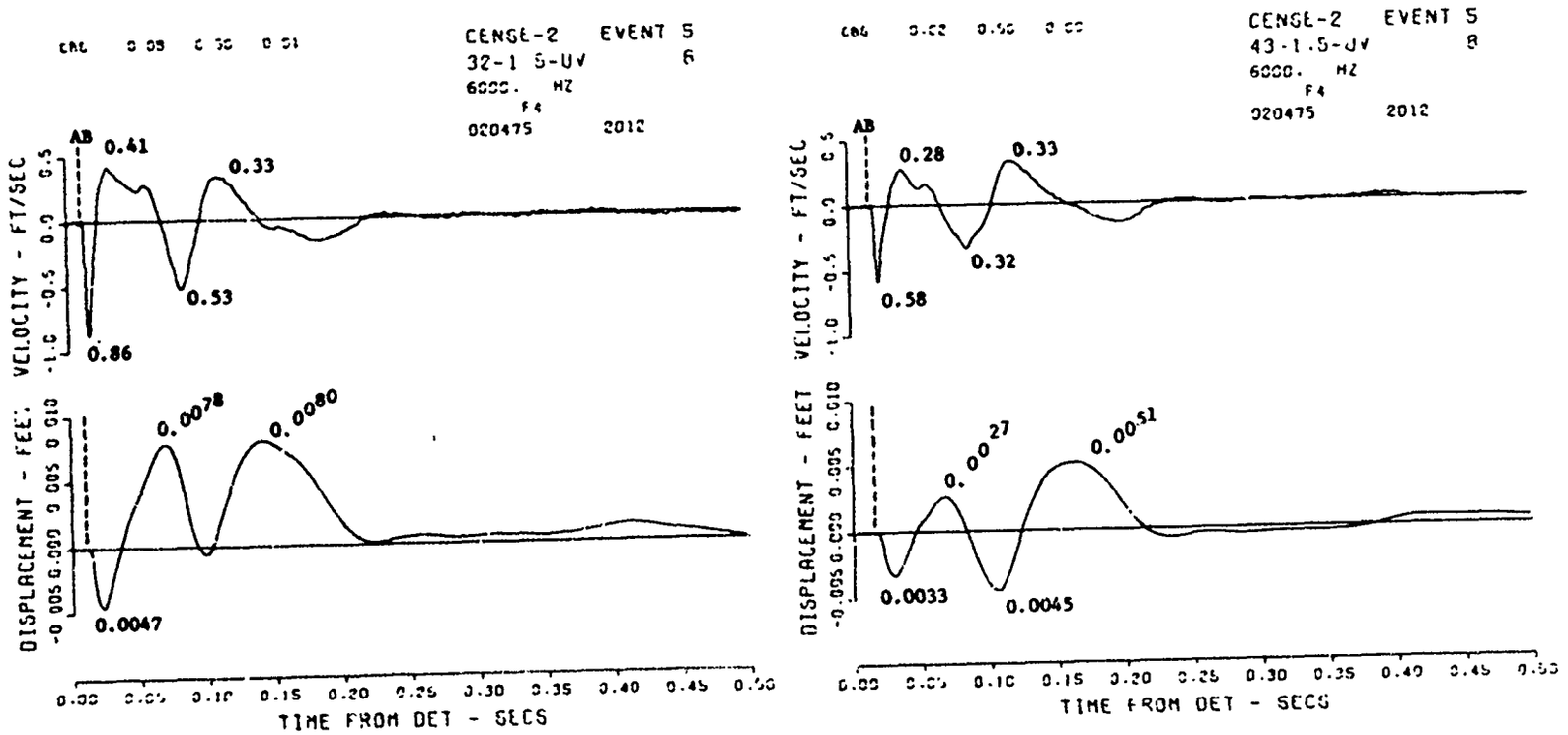

Figure B.16 (sheet 3 of 6).

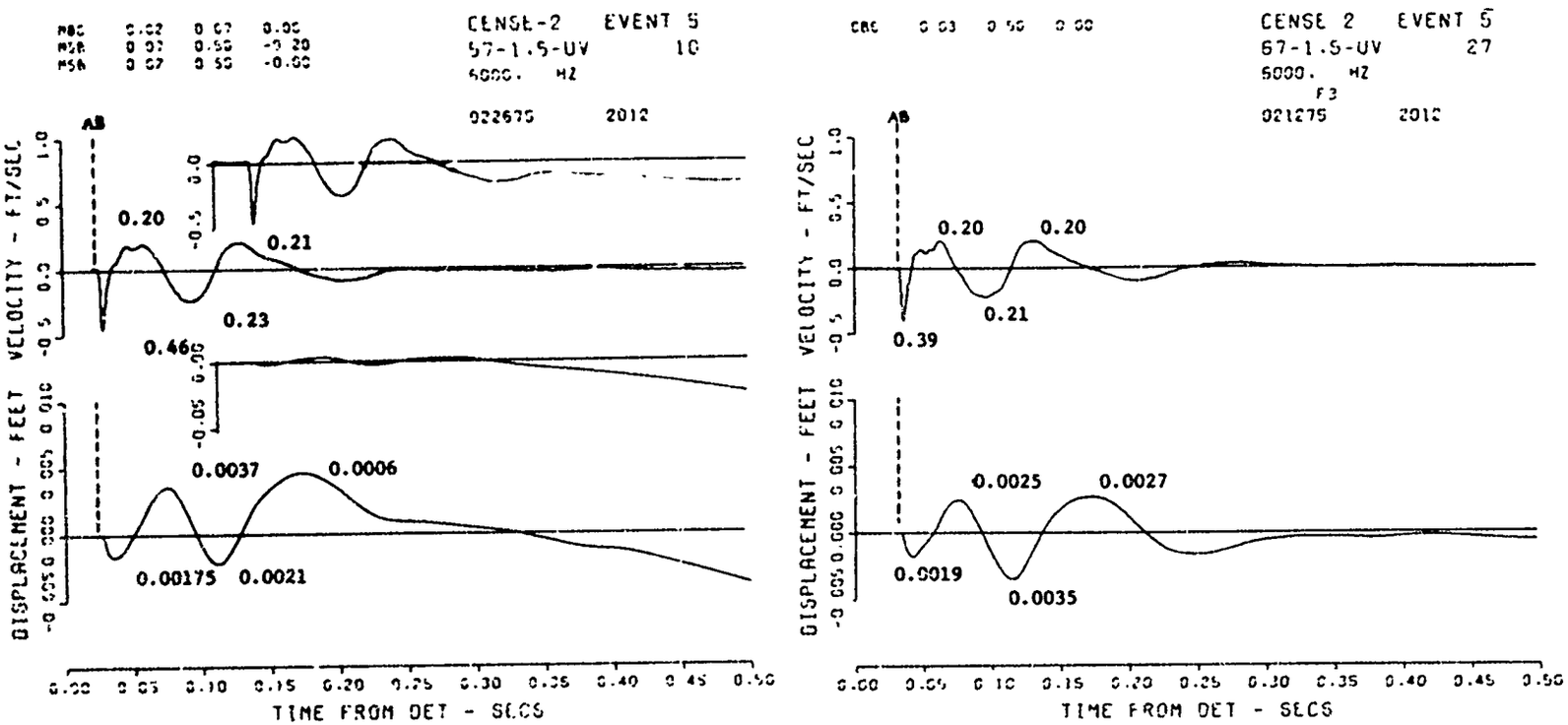

Figure B.16 (sheet 6 of 6).

CENSE-2 EVENT 6
0-7.6-AV

NO DATA RECOVERED (OUTPUT SIGNAL DEVIATED OUT OF TAPE BANDPASS: DEFECTIVE GAGE)

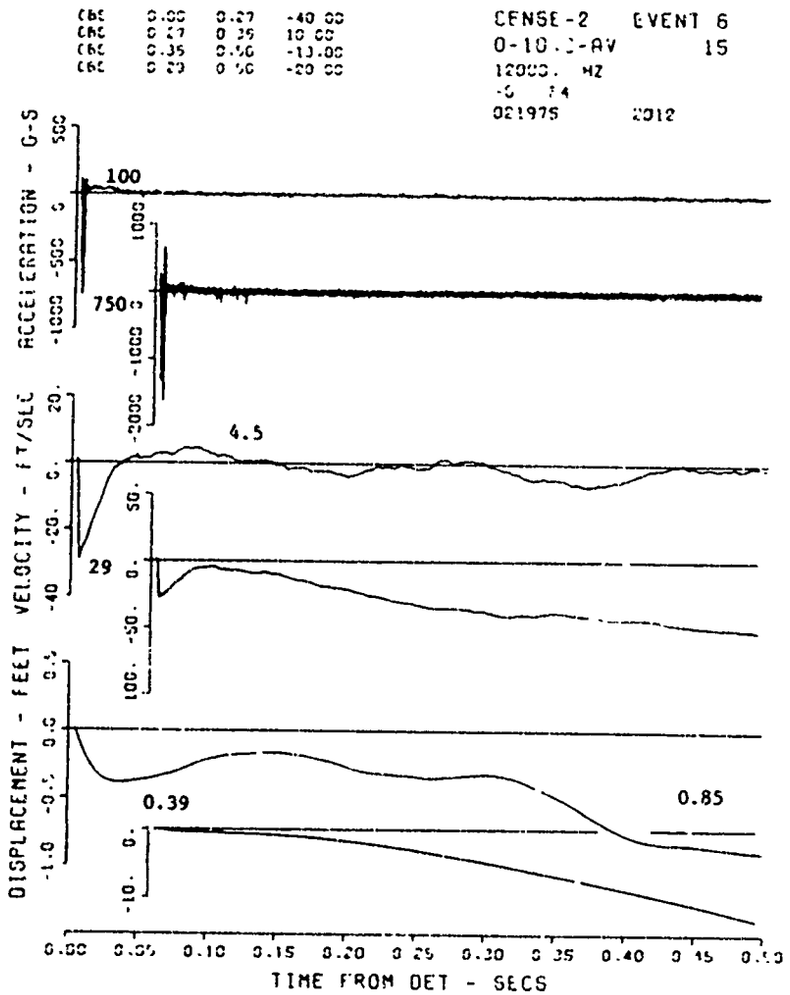

Figure B.17 Event 6, buried tangent, +0.13 $W^{1/3}$ (+0.9 foot); motion- and stress-time histories along the vertical radial directly beneath the explosion (sheet 1 of 5).

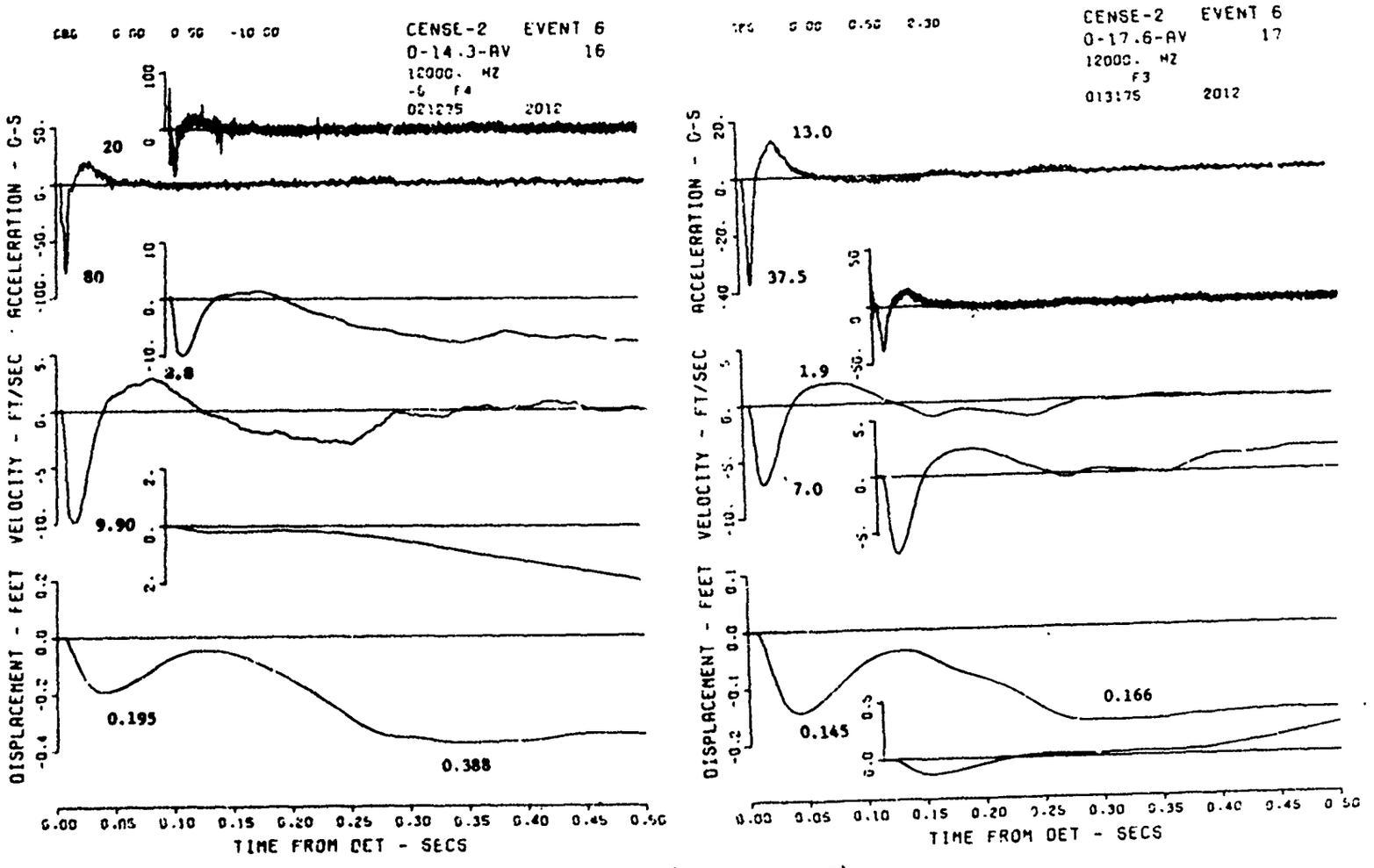

Figure B.17 (sheet 2 of 5).

CENSE-2 EVENT 6
0-2.1-AV

NO DATA RECOVERED (GAGE SCRATCHED PRESHOT)

CENSE-2 EVENT 6
0-3.6-SV

NO DATA RECORED (DEFECTIVE GAGE)

Figure B.17 (sheet 3 of 5).

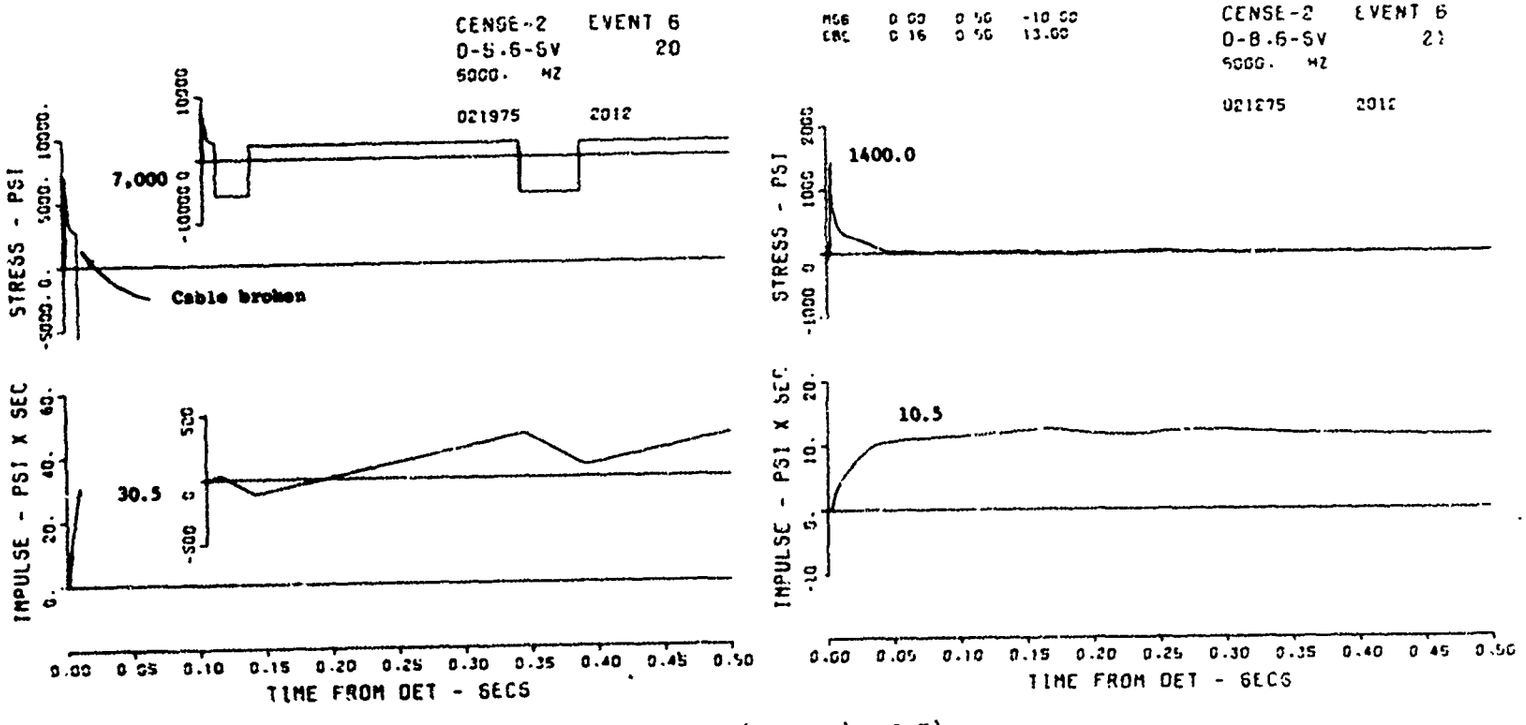

Figure B.17 (sheet 4 of 5).

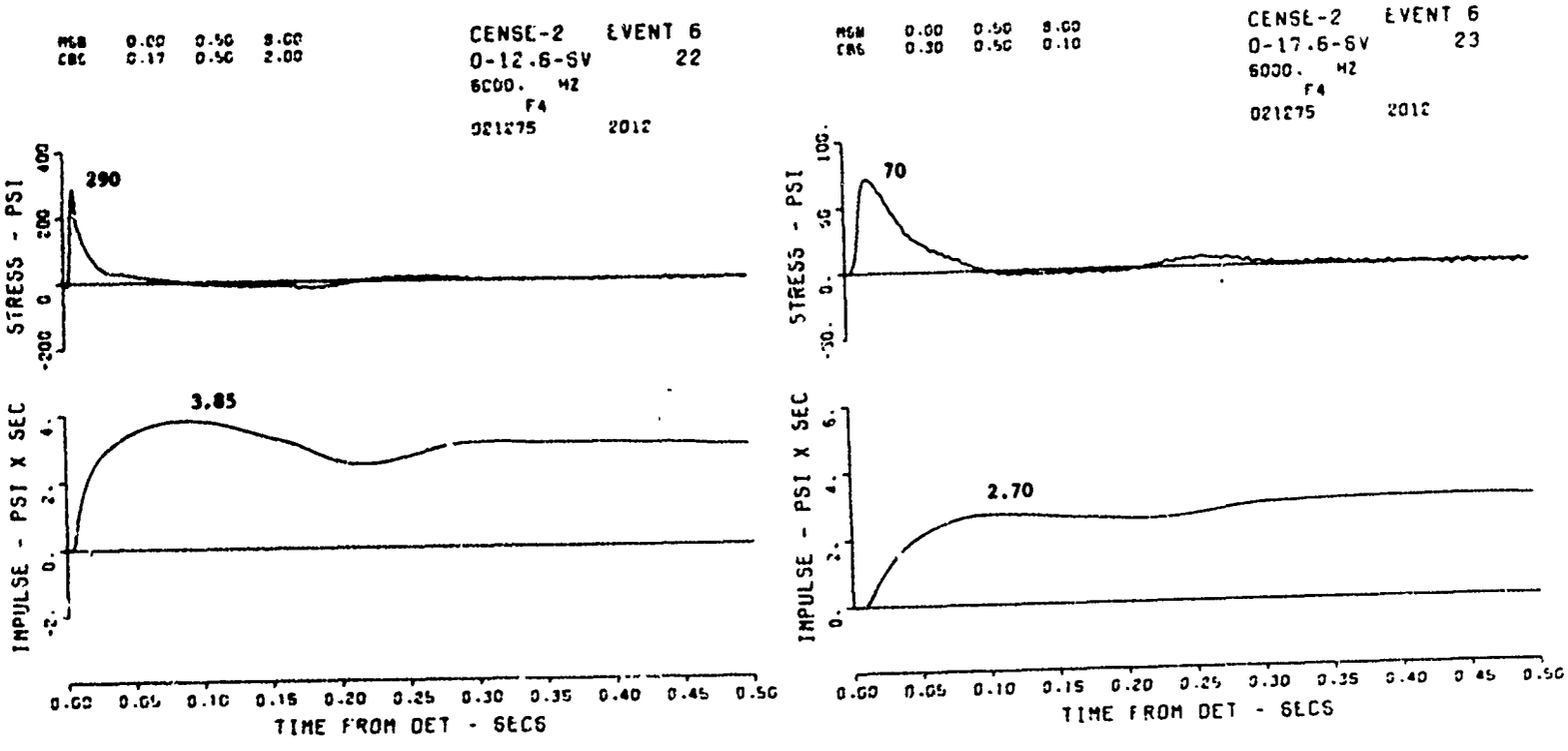

Figure B.17 (sheet 5 of 5).

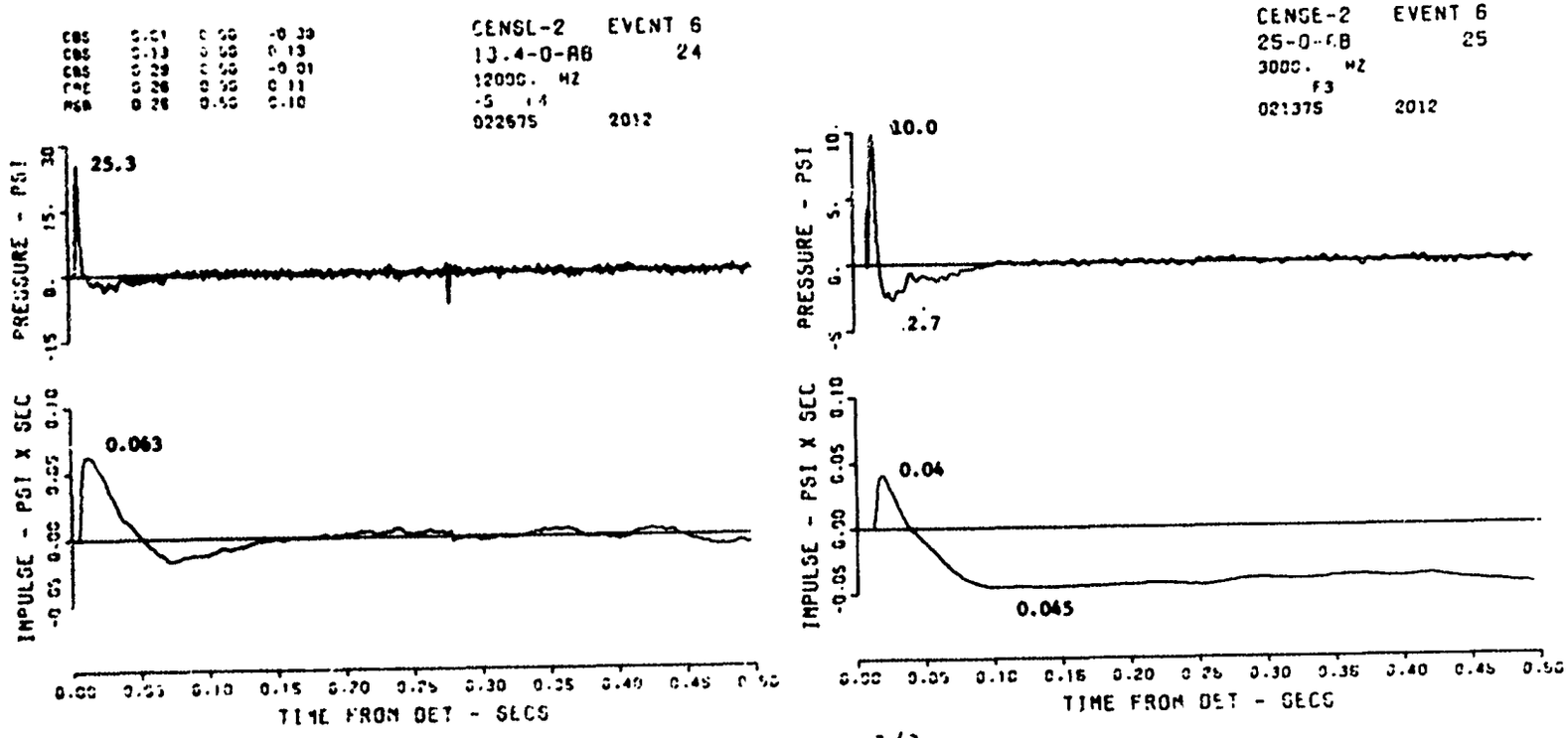

Figure B.18 Event 6, buried tangent, +0.13 $W^{1/3}$ (+0.9 foot); surface airblast-time histories (sheet 1 of 3).

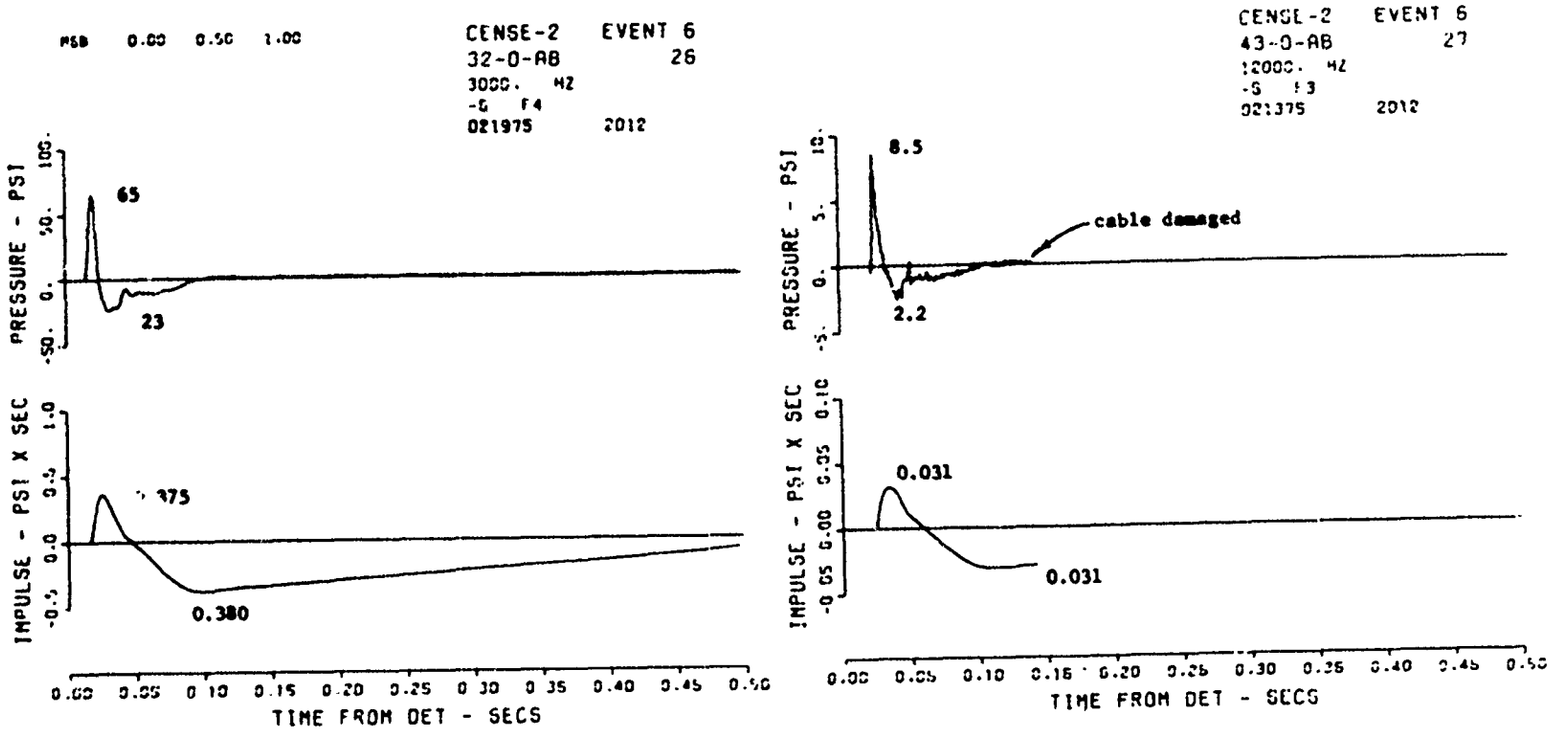

Figure B.18 (sheet 2 of 3).

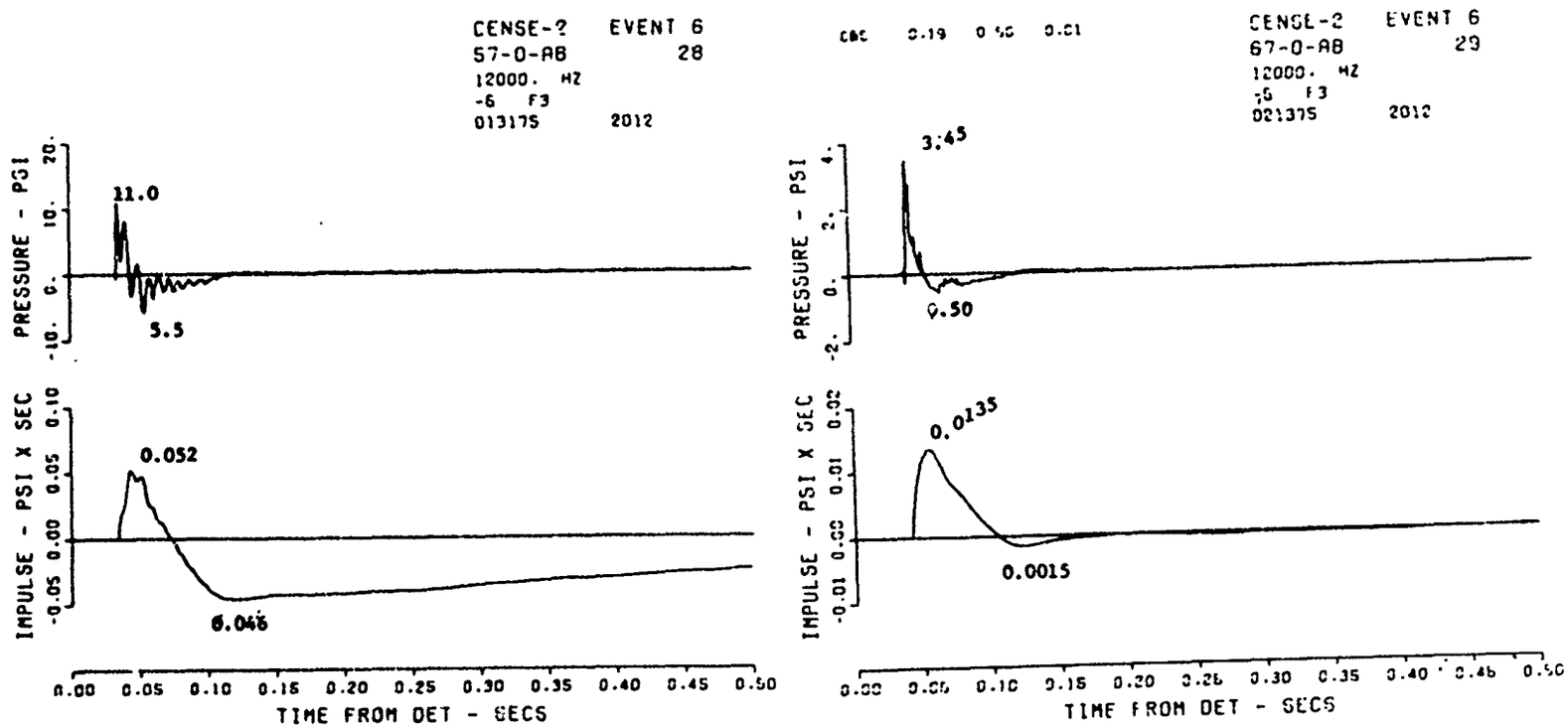

Figure B.18 (sheet 3 of 3).

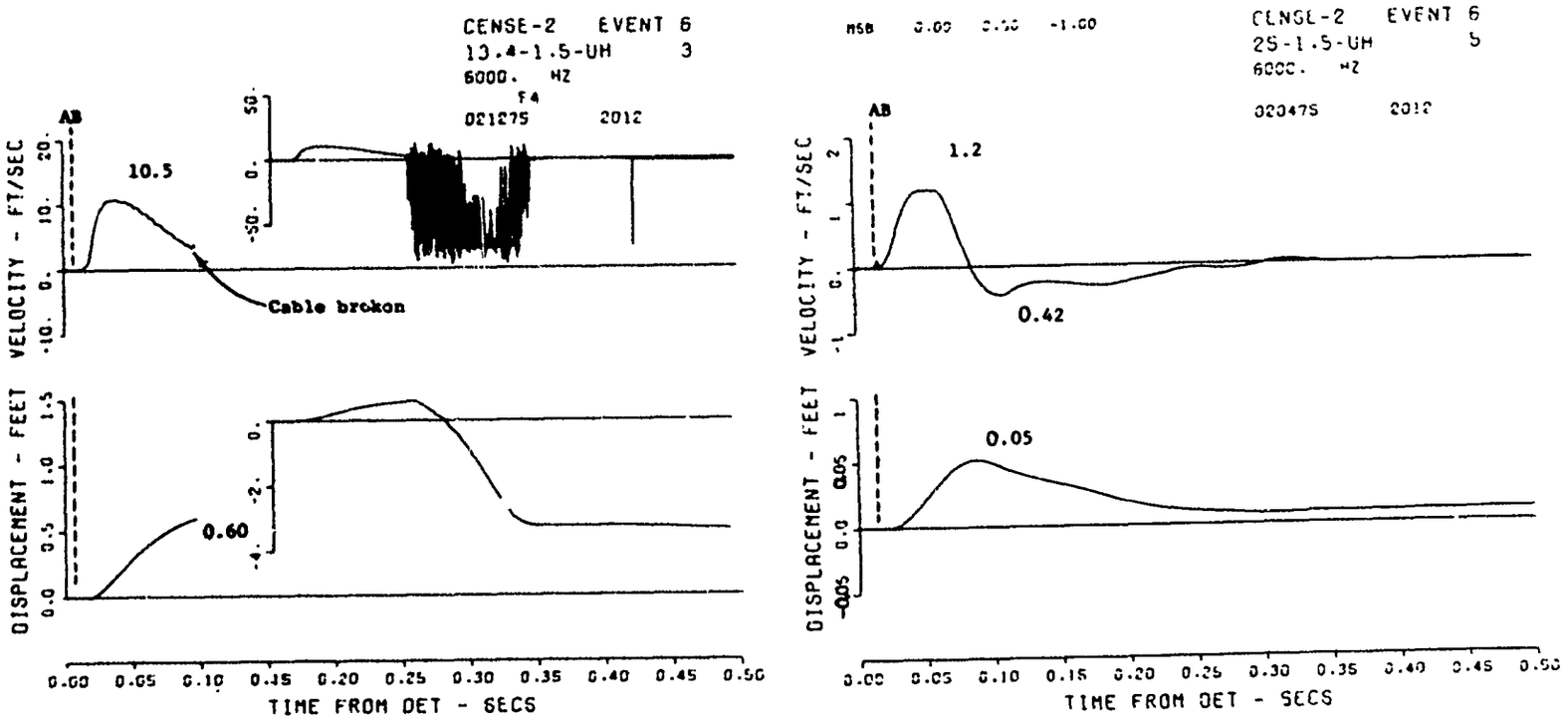

Figure B.19 Event 6, buried tangent, $+0.13\ W^{1/3}$ (+0.9 foot); near-surface motion-time histories (sheet 1 of 6).

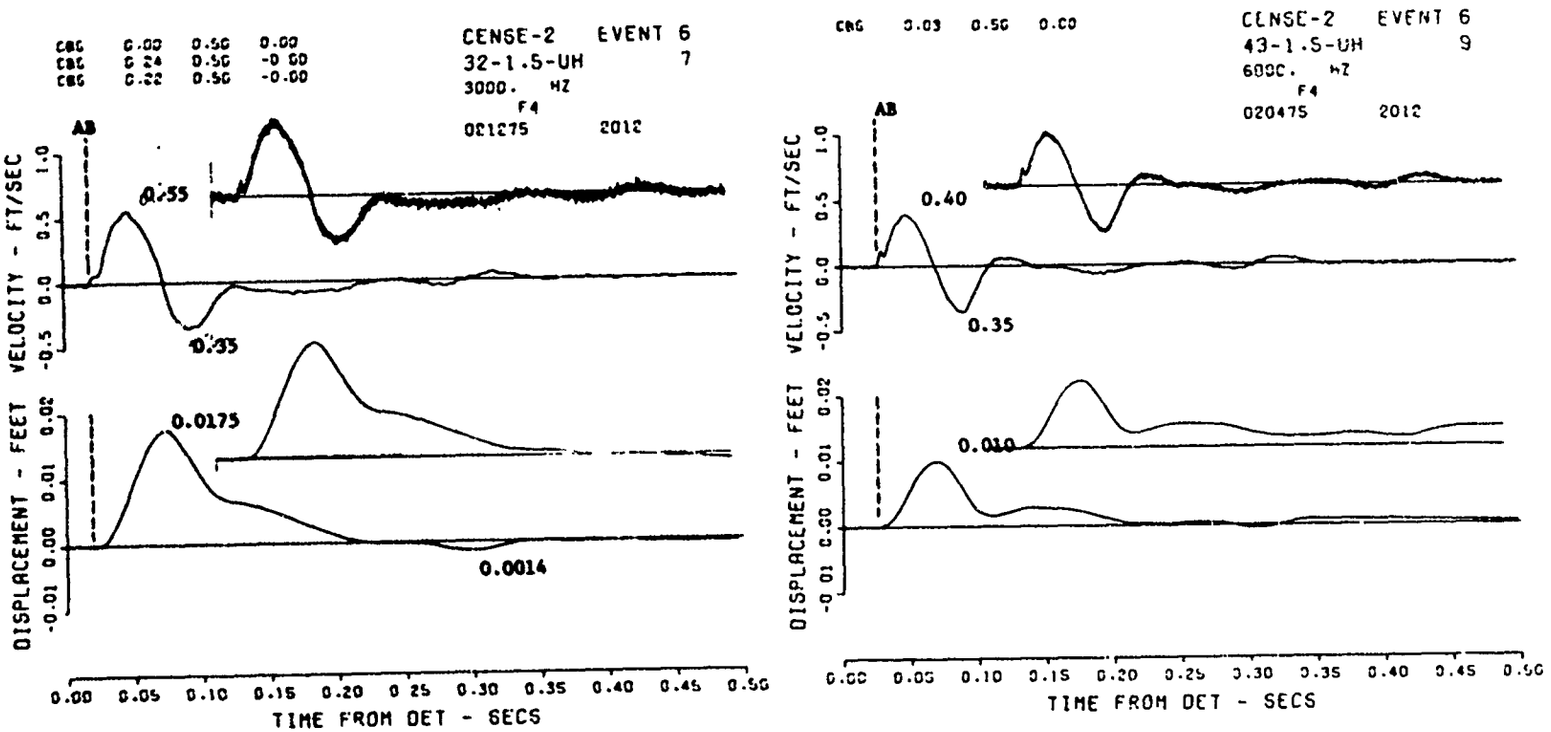

Figure B.19 (sheet 2 of 6).

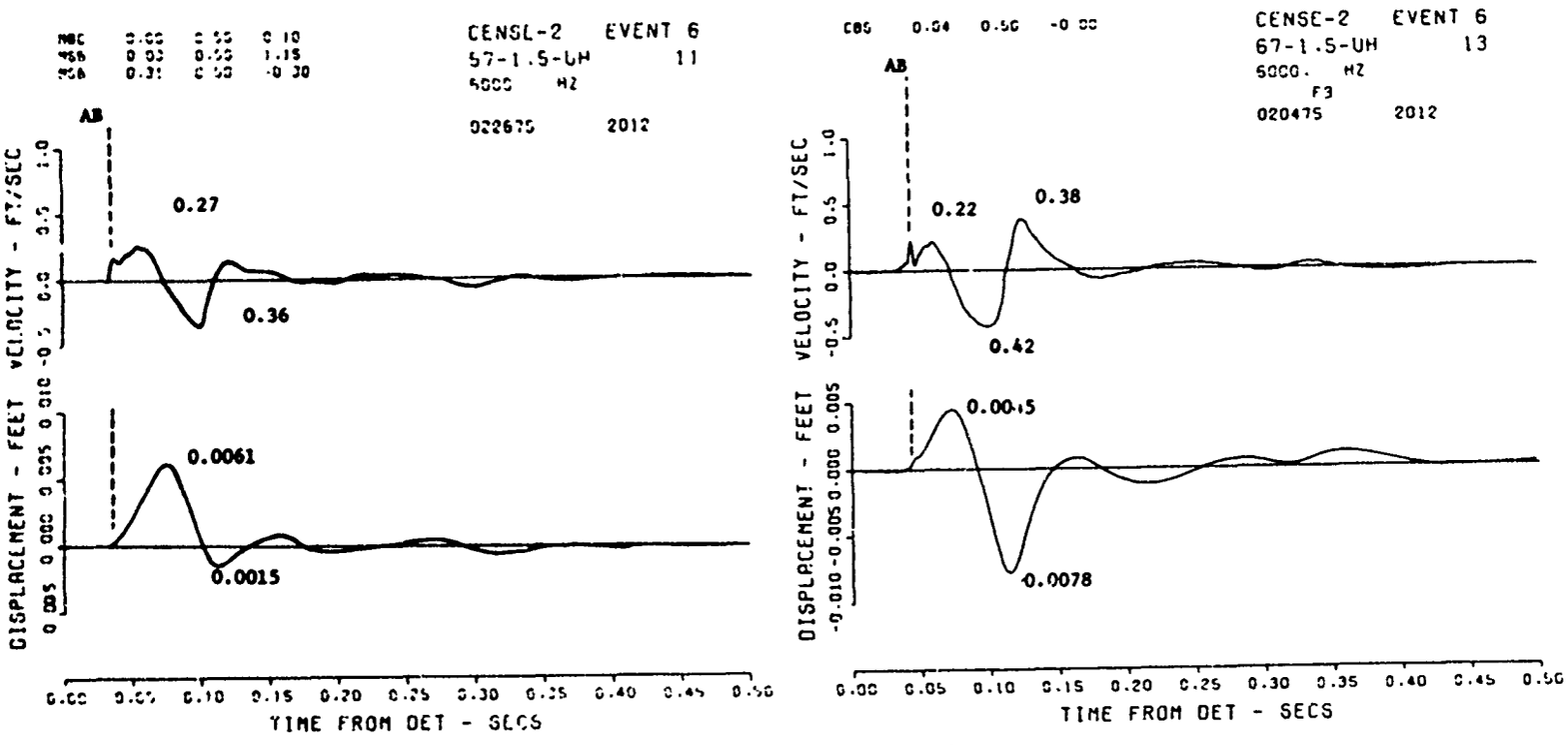

Figure B.19 (sheet 3 of 6).

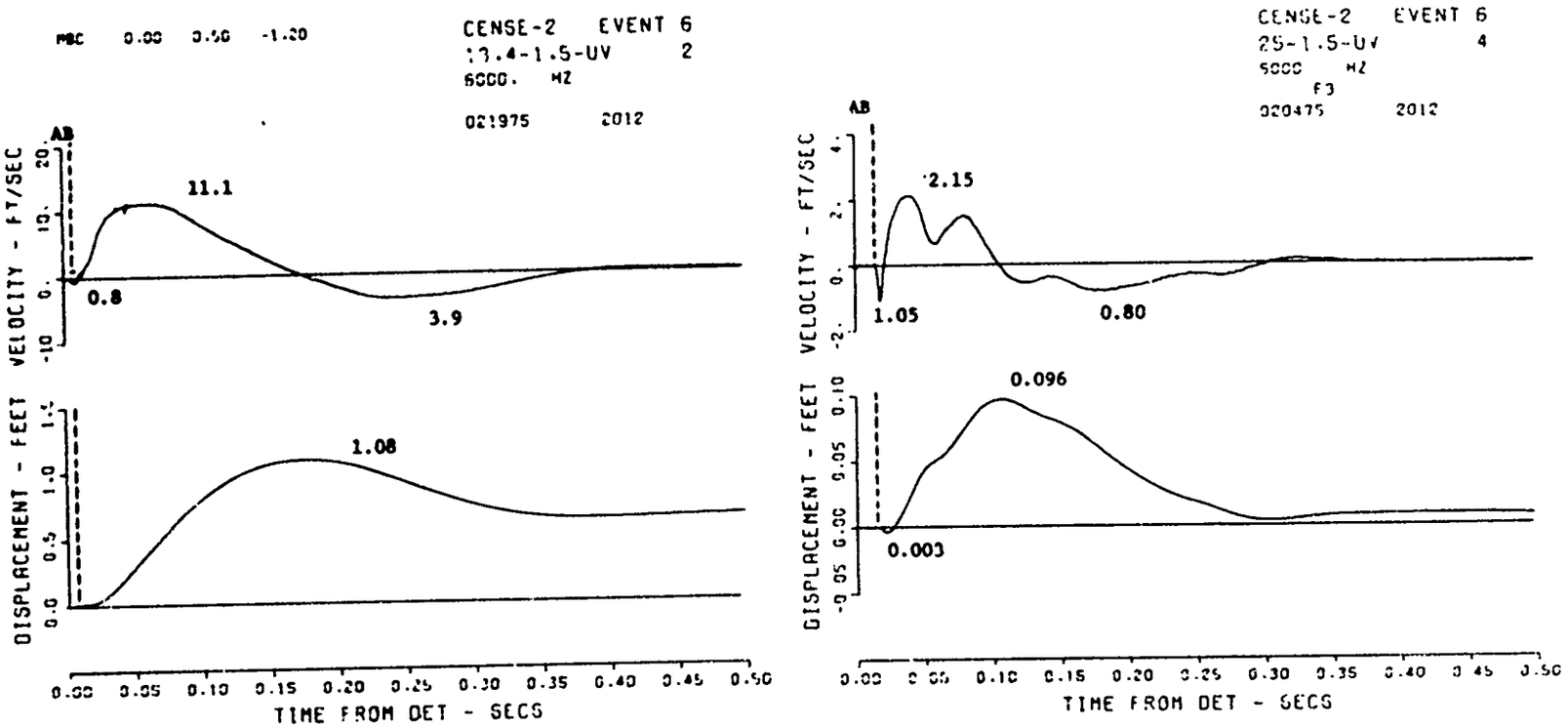

Figure B.19 (sheet 4 of 6).

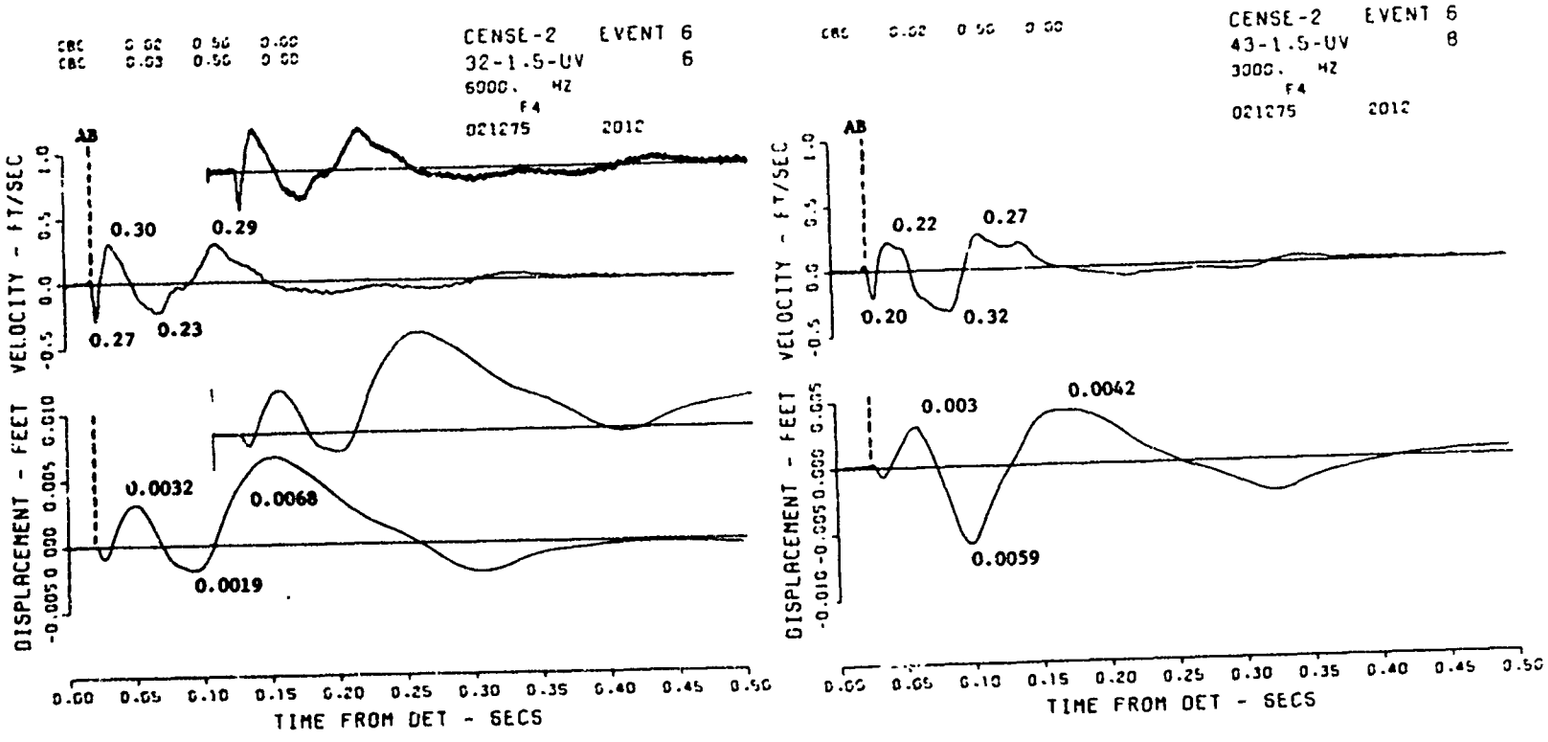

Figure B.19 (sheet 5 of 6).

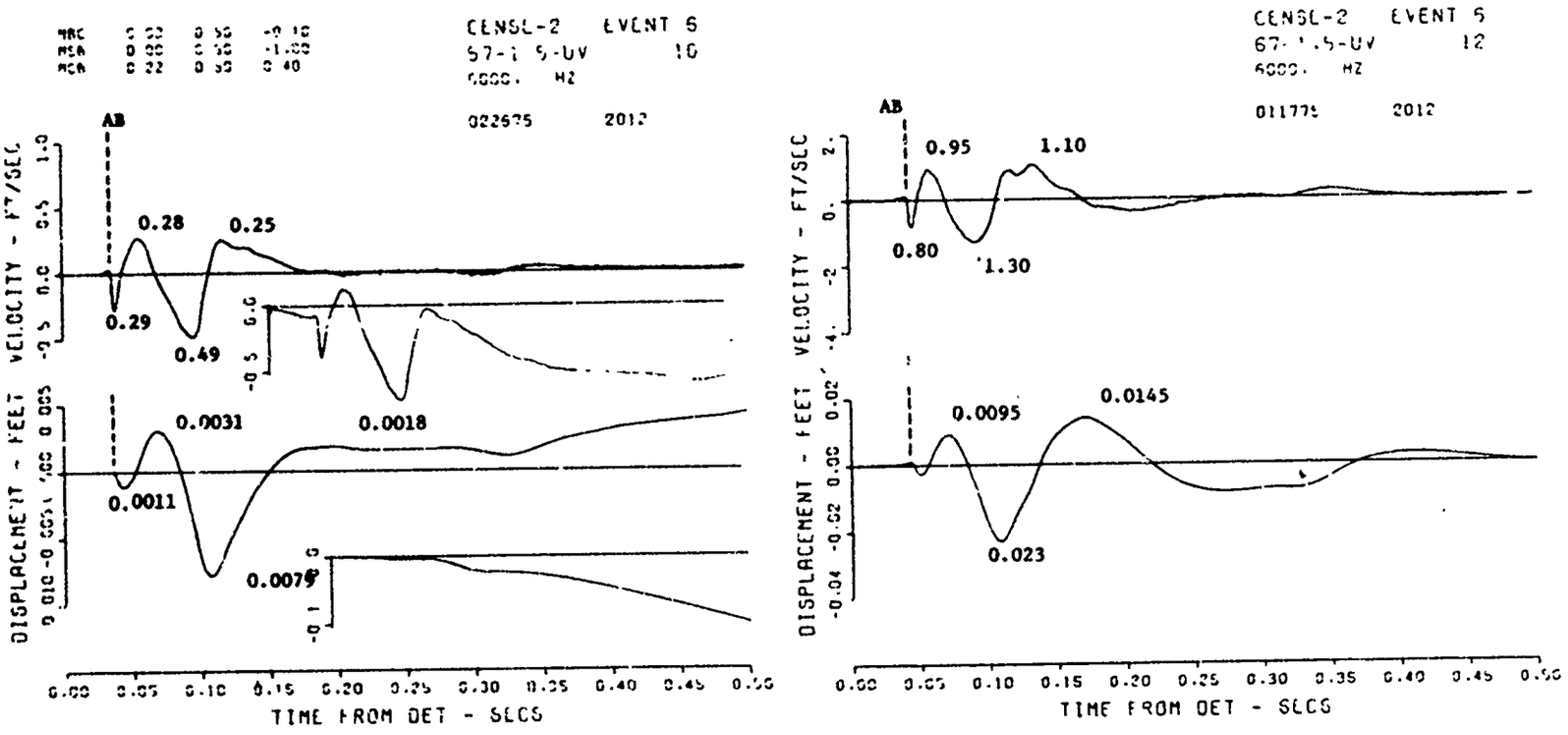

Figure B.19 (sheet 6 of 6).

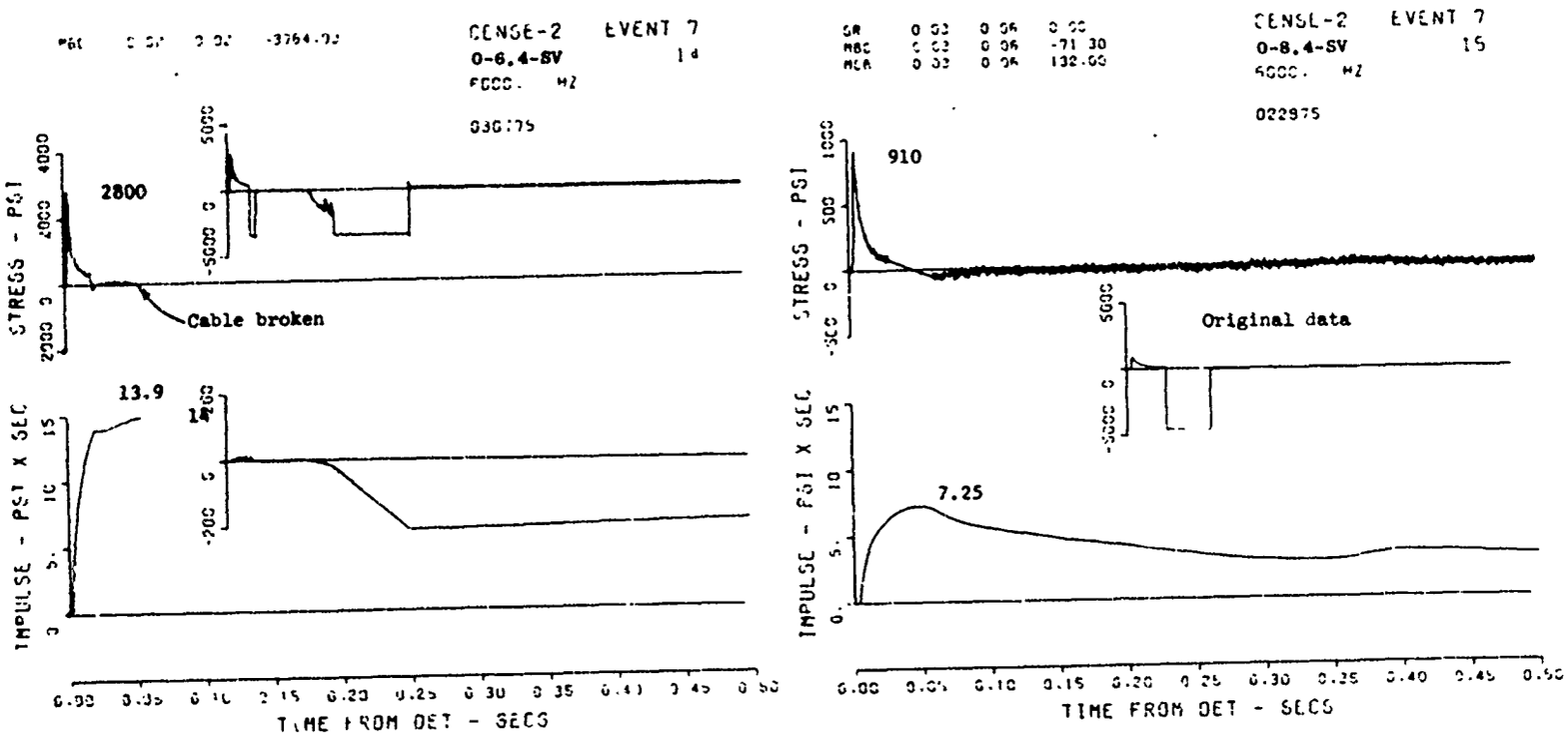

Figure B.20 Event 7, buried, $+0.54\ W^{1/3}$ (+3.6 feet); stress-time histories along the vertical radial directly beneath the explosion (sheet 1 of 3).

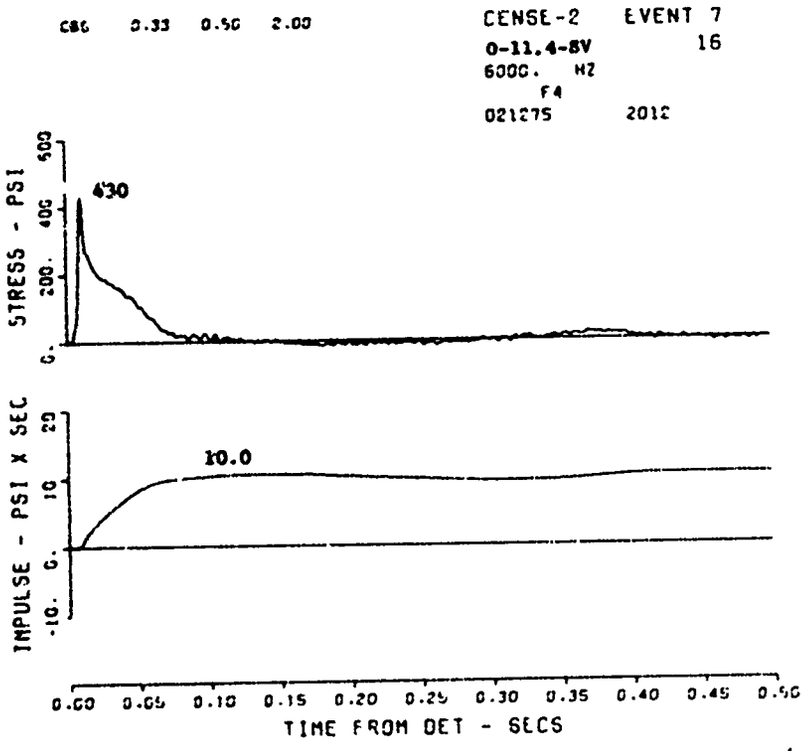

CENSE-2 EVENT 7
0-15.4-SV

NO DATA REVOCERED
(DEFECTIVE GAGE)

Figure B.20 (sheet 2 of 3).

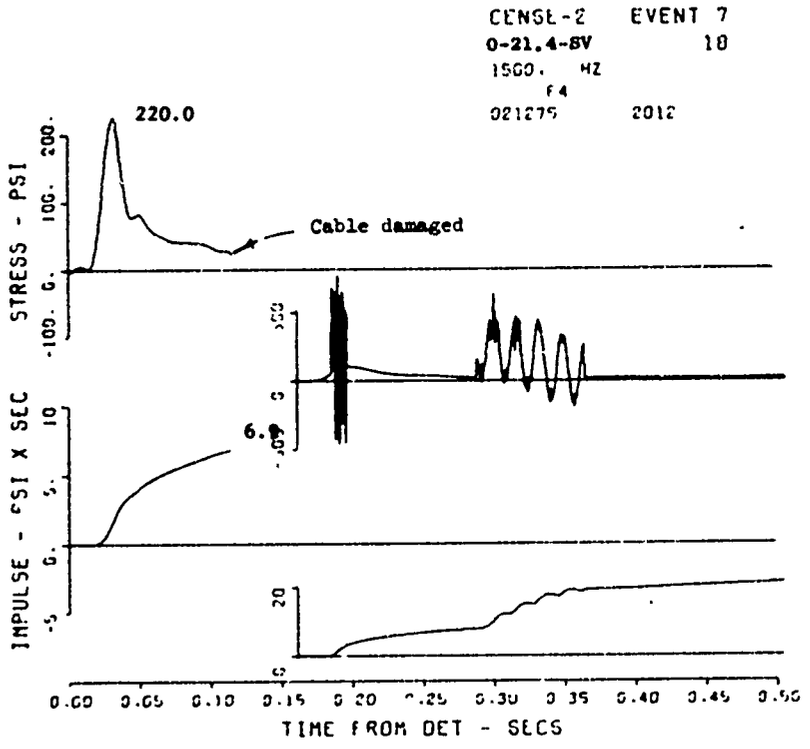

Figure B.20 (sheet 3 of 3).

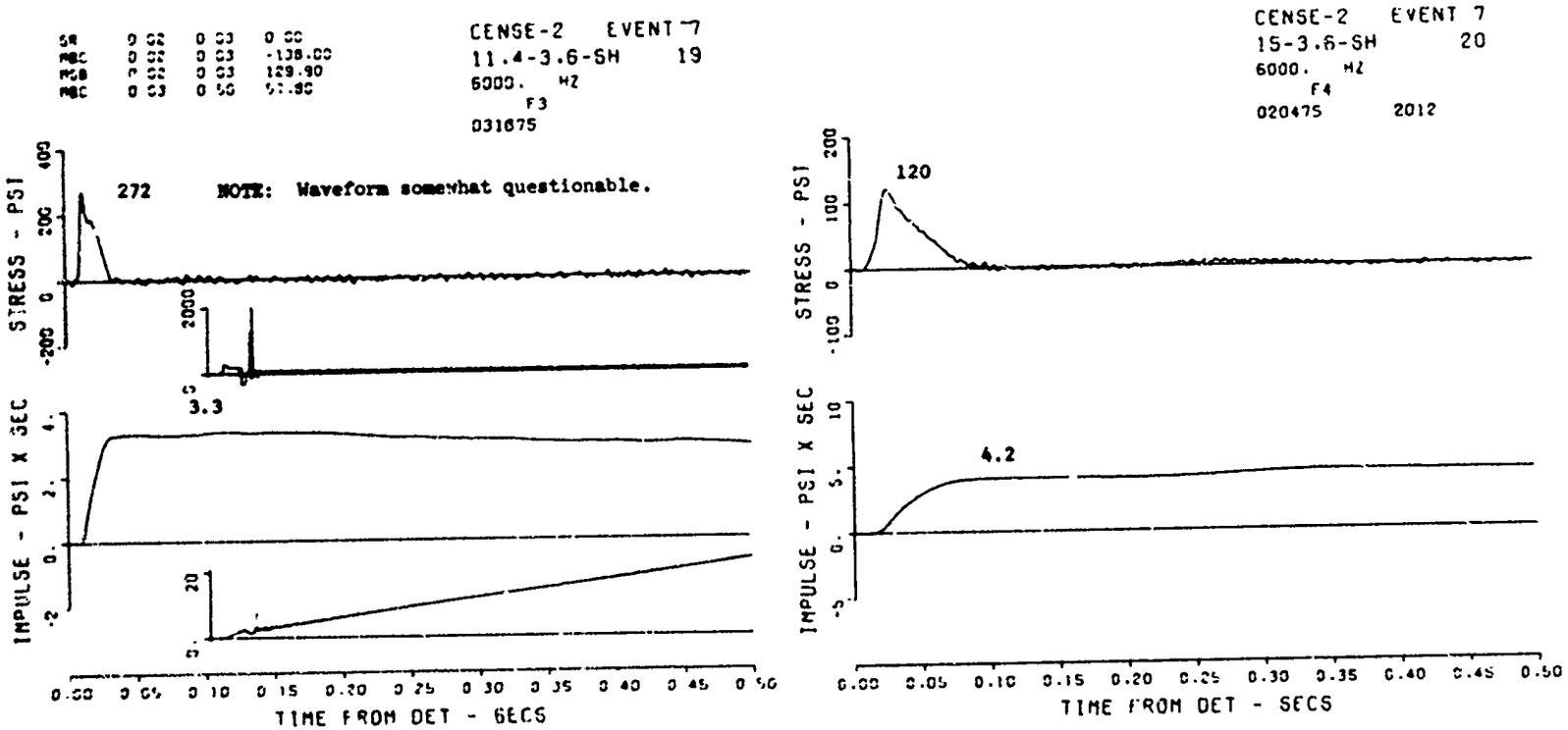

Figure B.21 Event 7, buried, $+0.54\ W^{1/3}$ (+3.6 feet); stress- and motion-time histories along the horizontal radial at charge depth (sheet 1 of 7).

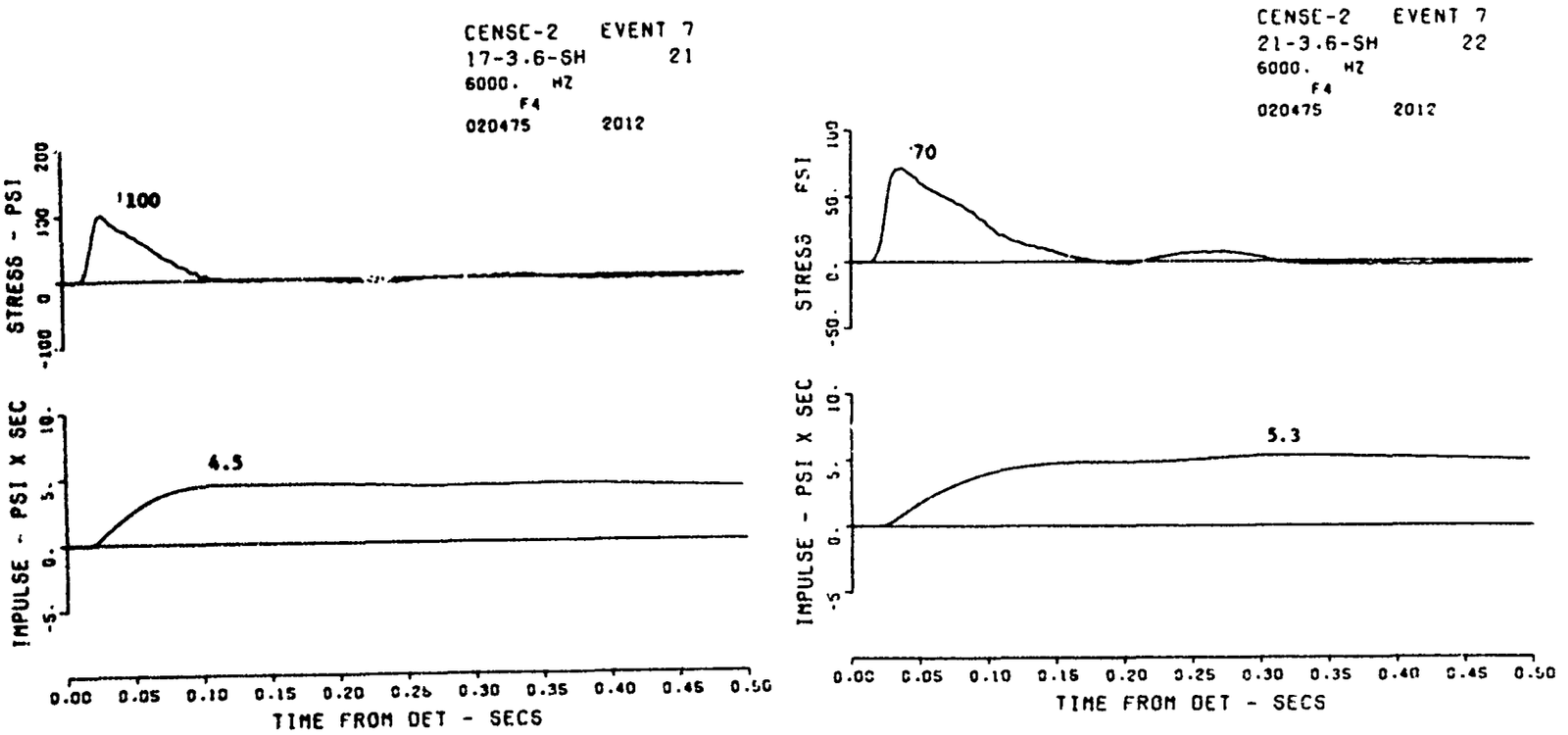

Figure B.21 (sheet 2 of 7).

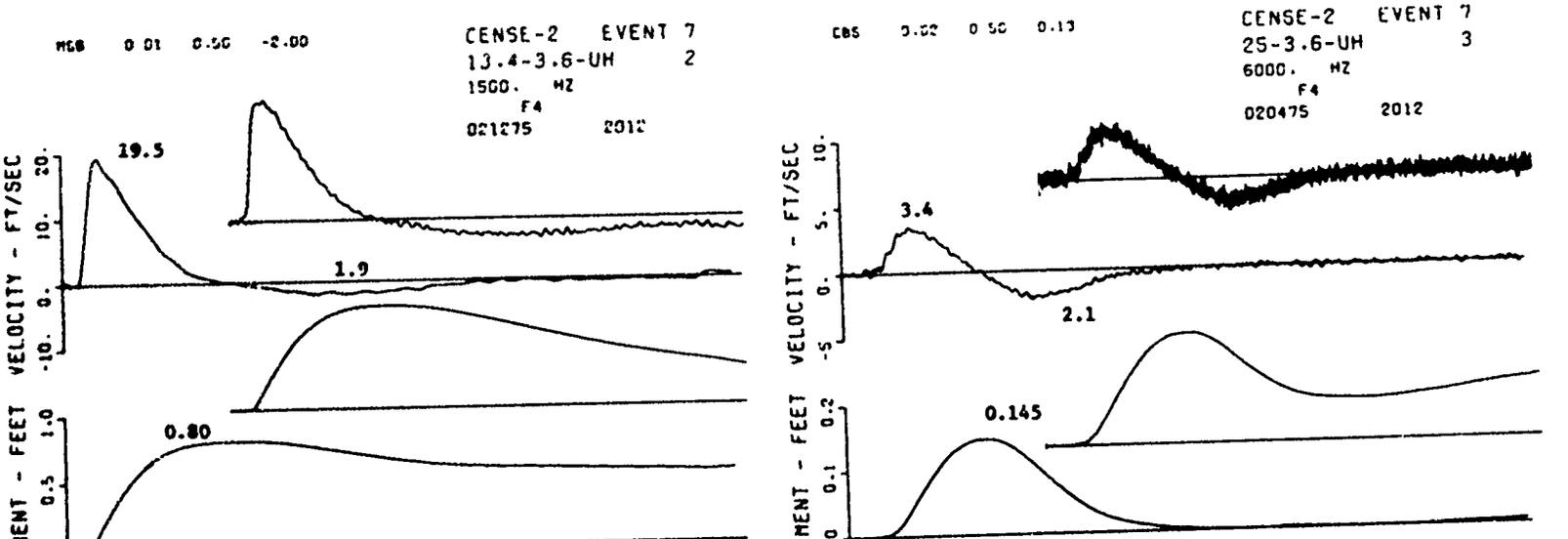

Figure B.21 (sheet 3 of 7).

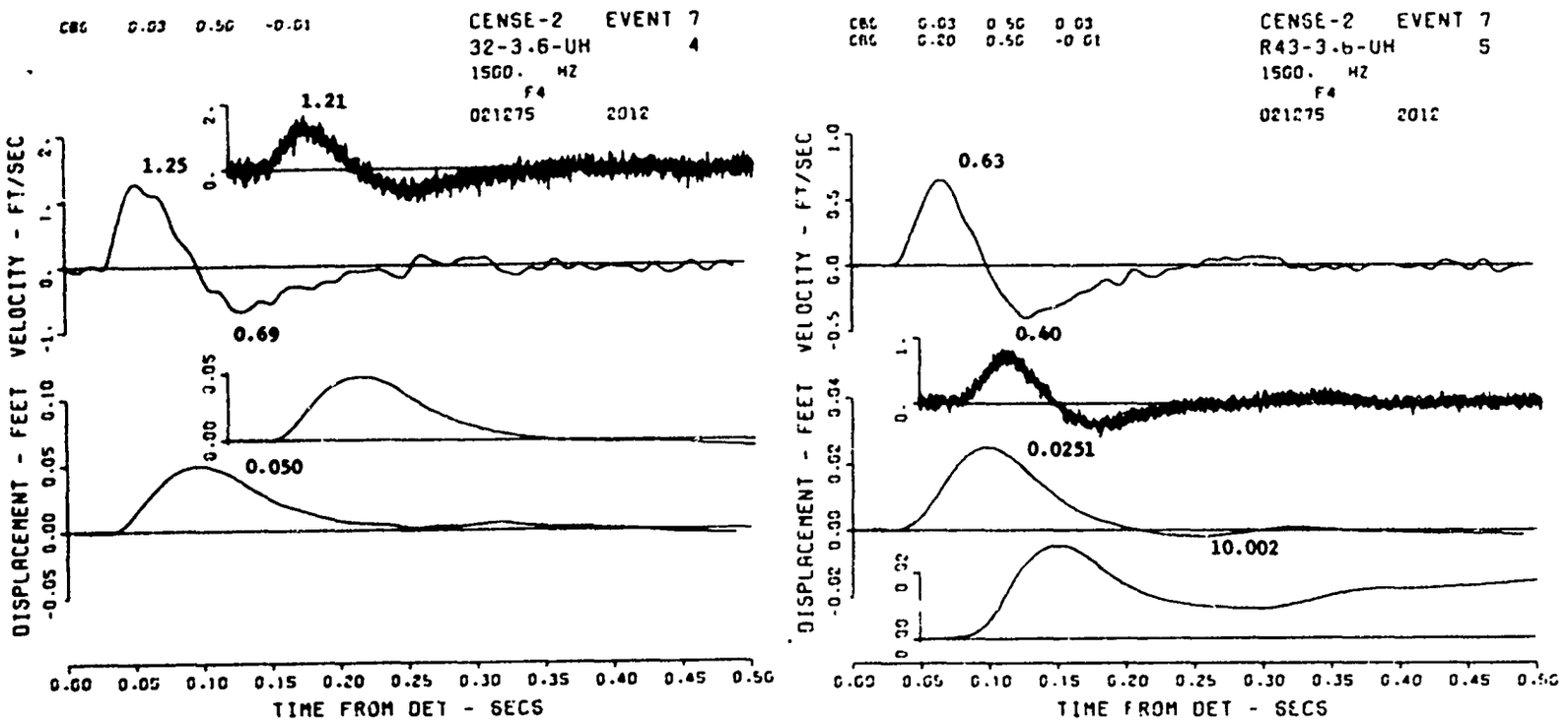

Figure B.21 (sheet 4 of 7).

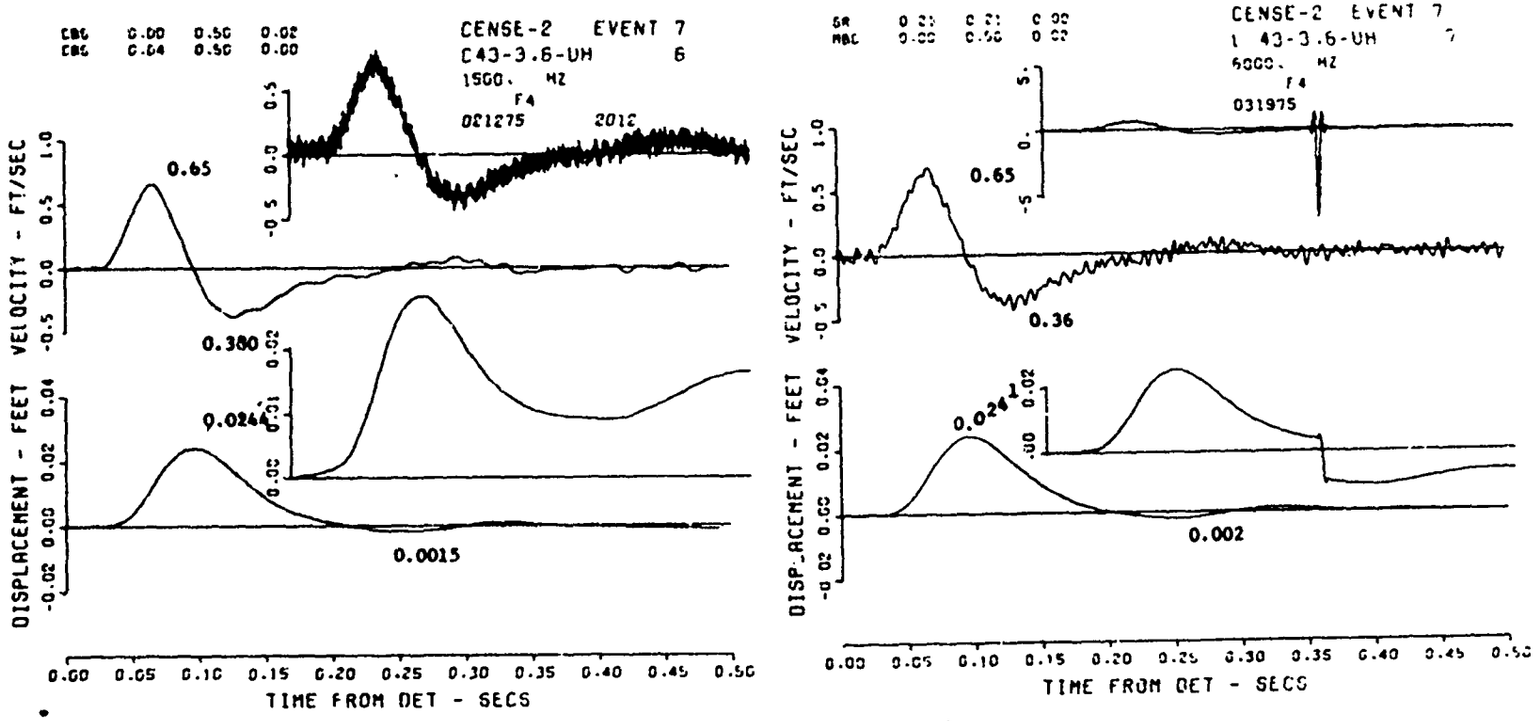

Figure B.21 (sheet 5 of 7).

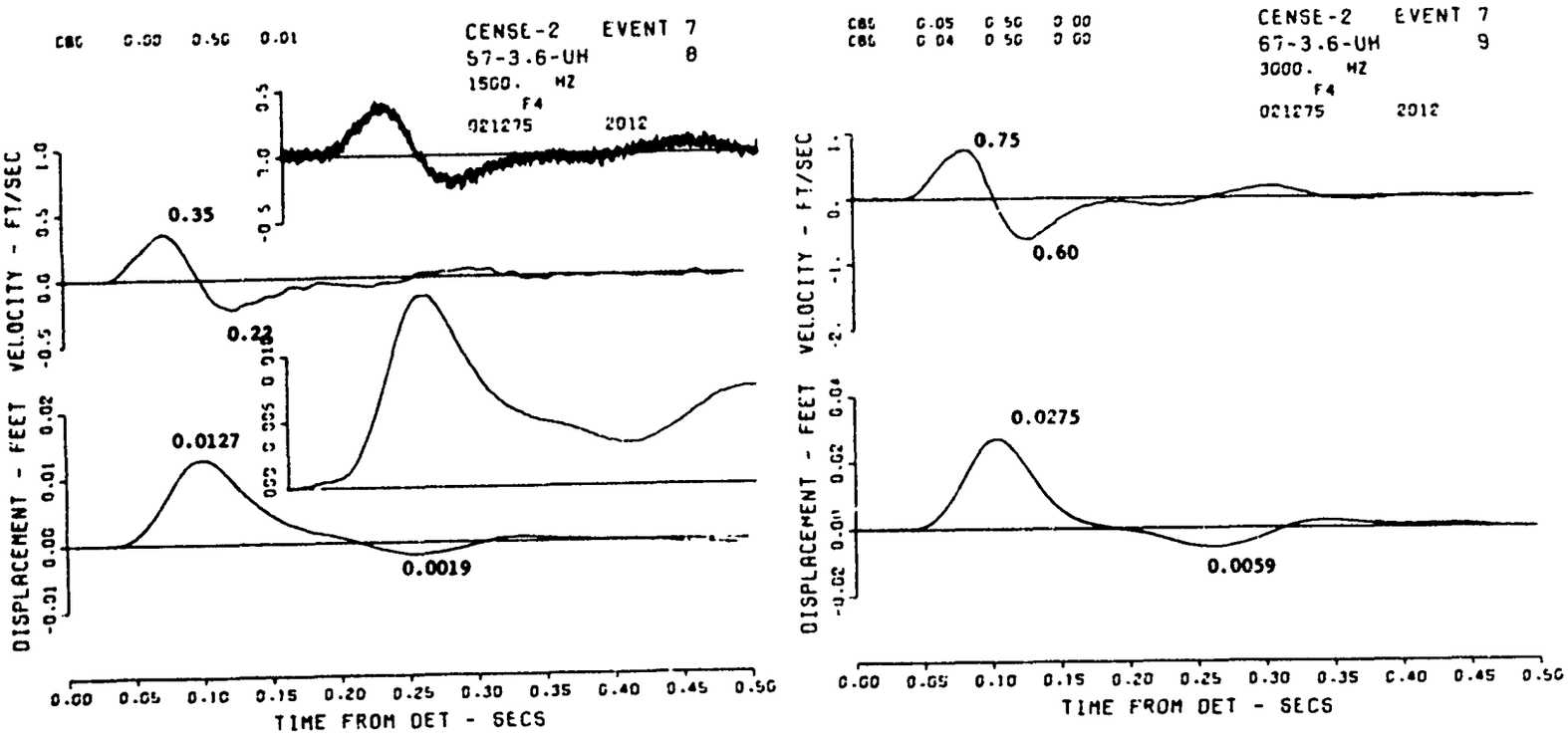

Figure B.21 (sheet 6 of 7).

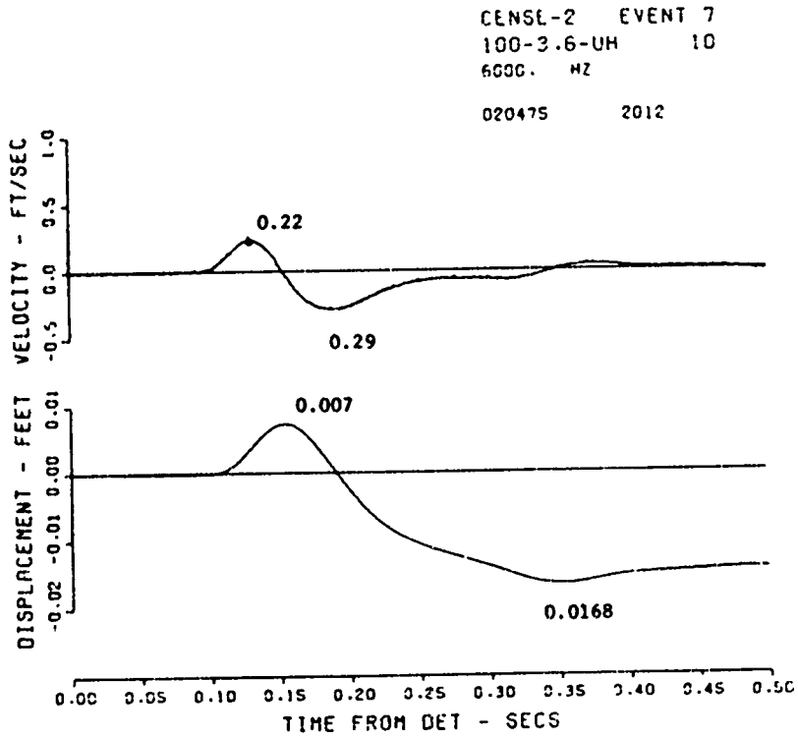

Figure B.21 (sheet 7 of 7).

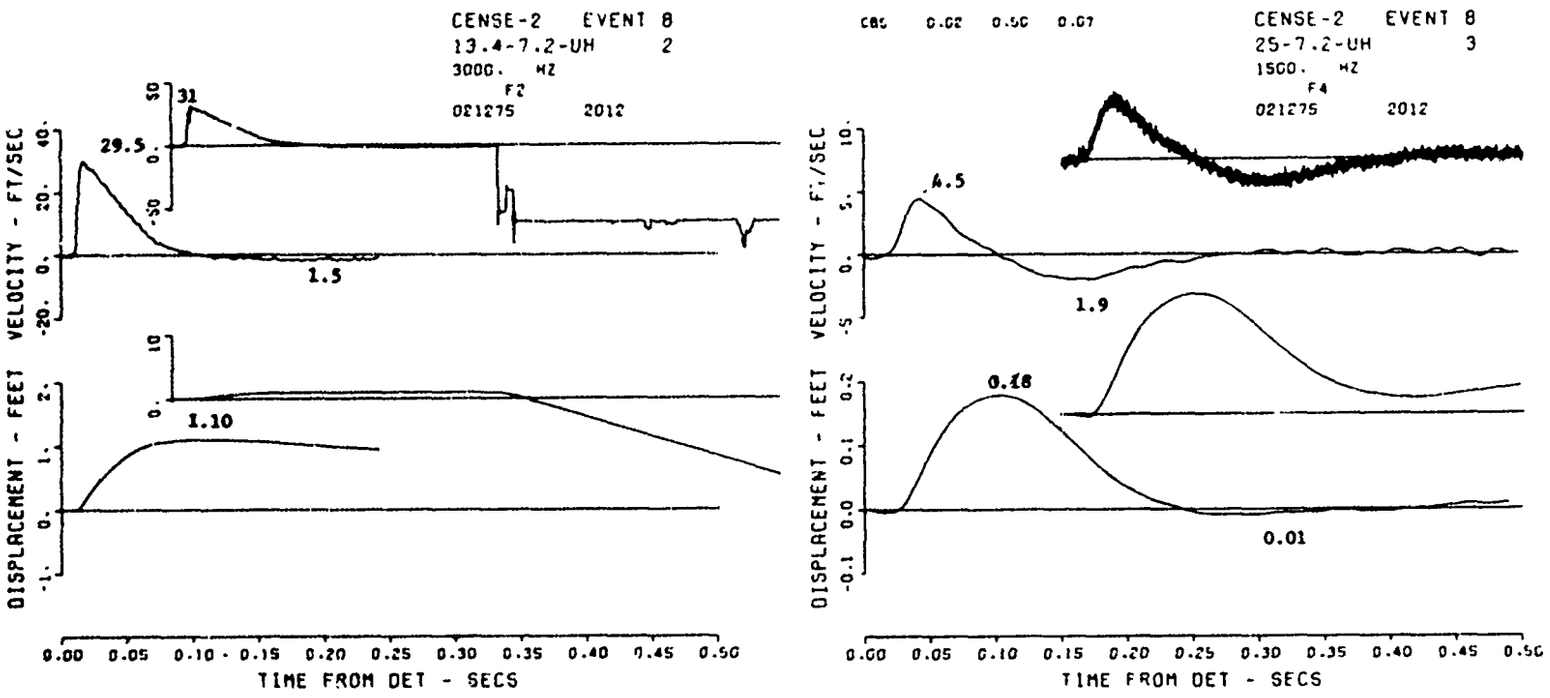

Figure B.22 Event 8, buried, +1.07 $W^{1/3}$ (+7.2 feet); motion- and stress-time histories along the horizontal radial at charge depth (sheet 1 of 8).

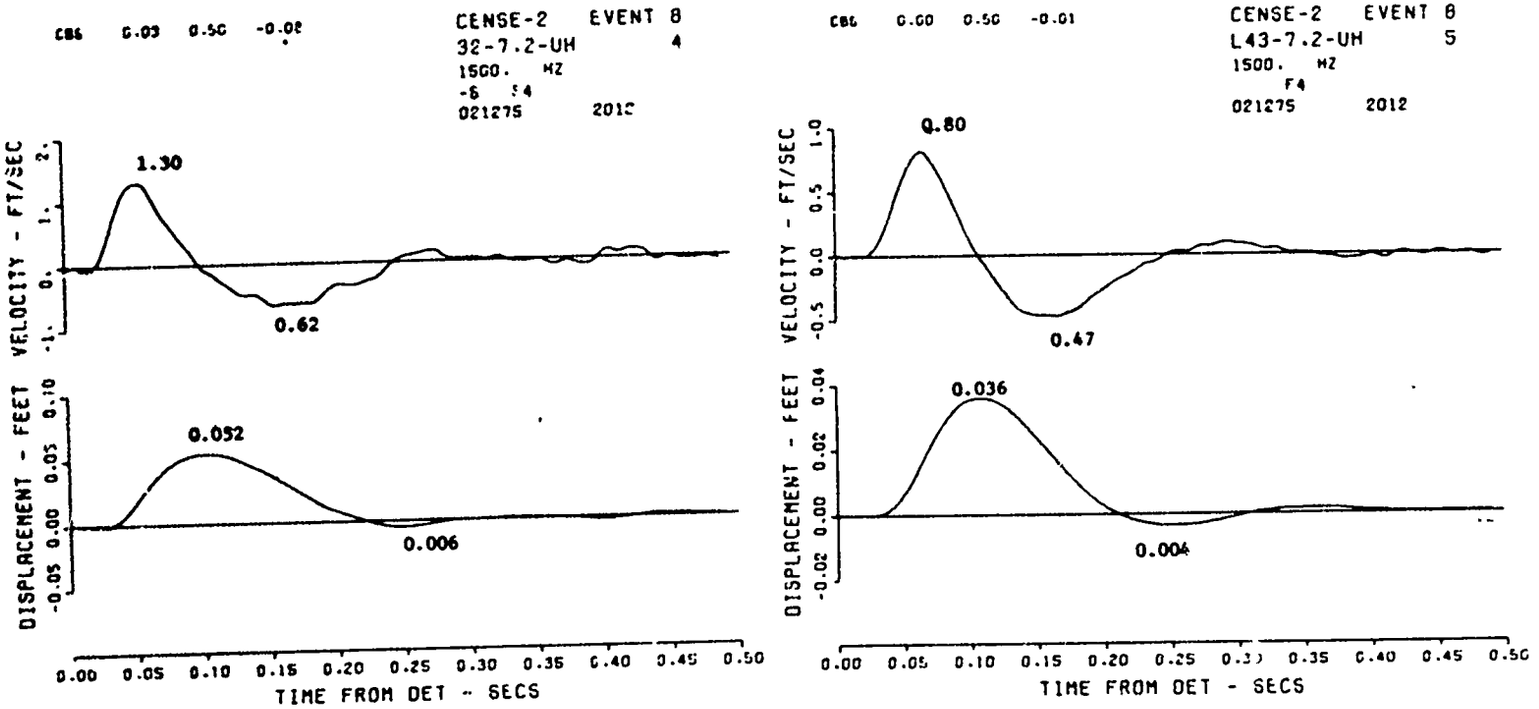

Figure B.22 (sheet 2 of 8).

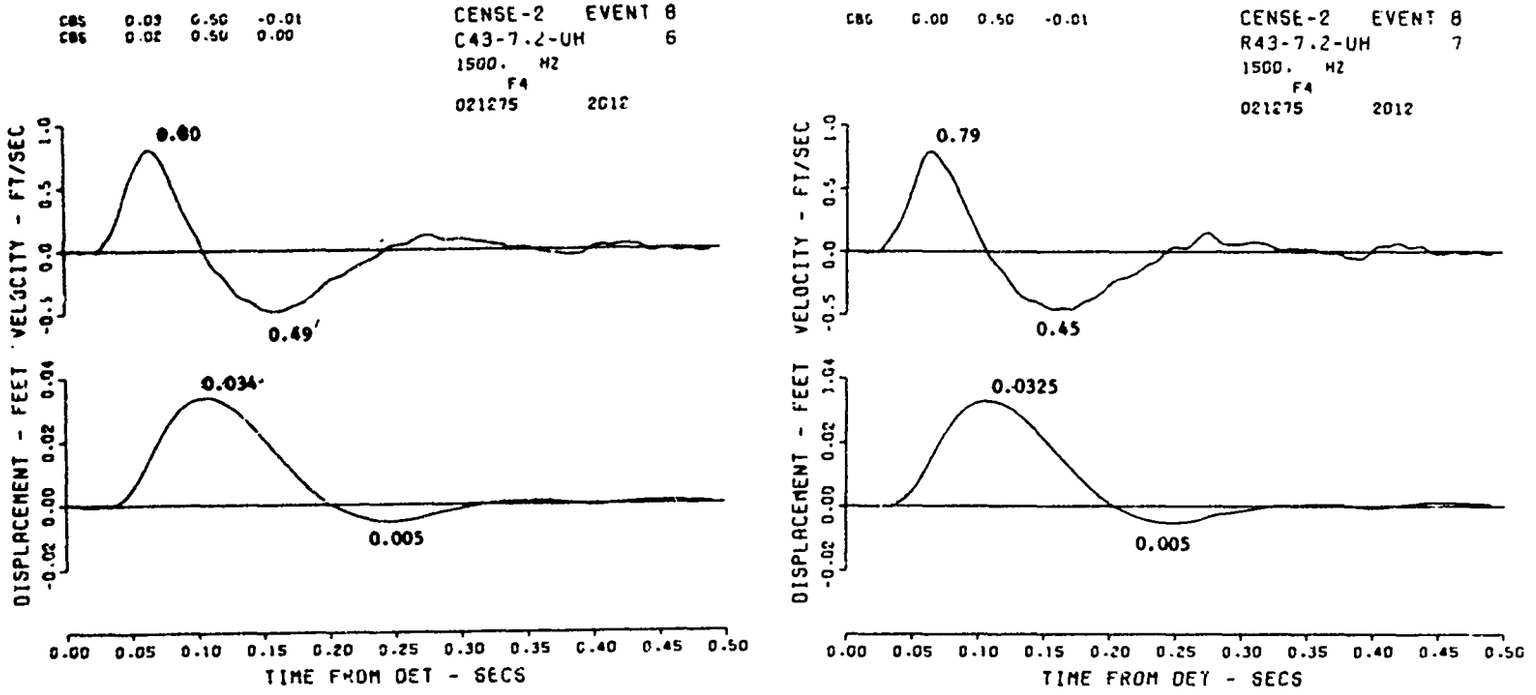

Figure B.22 (sheet 3 of 8).

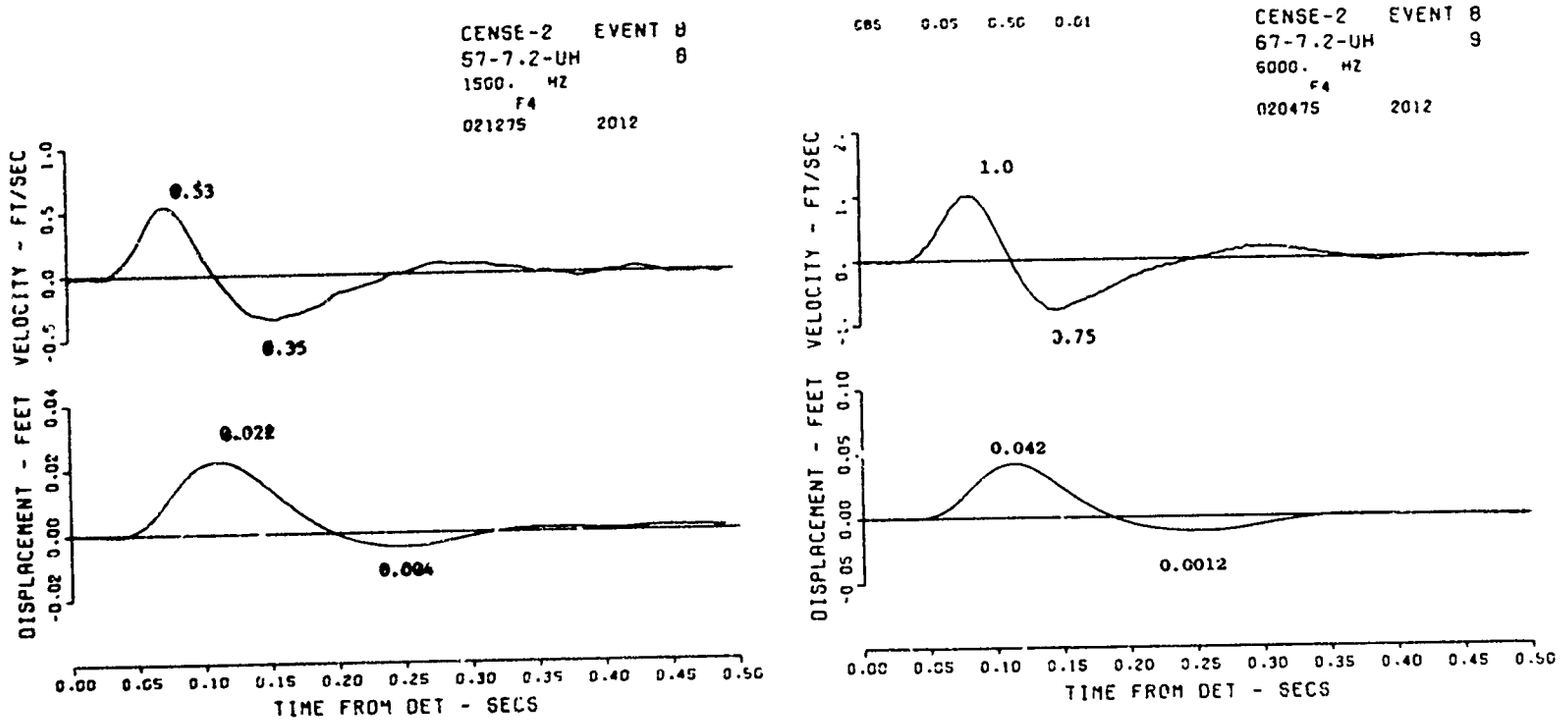

Figure B.22 (sheet 4 of 8).

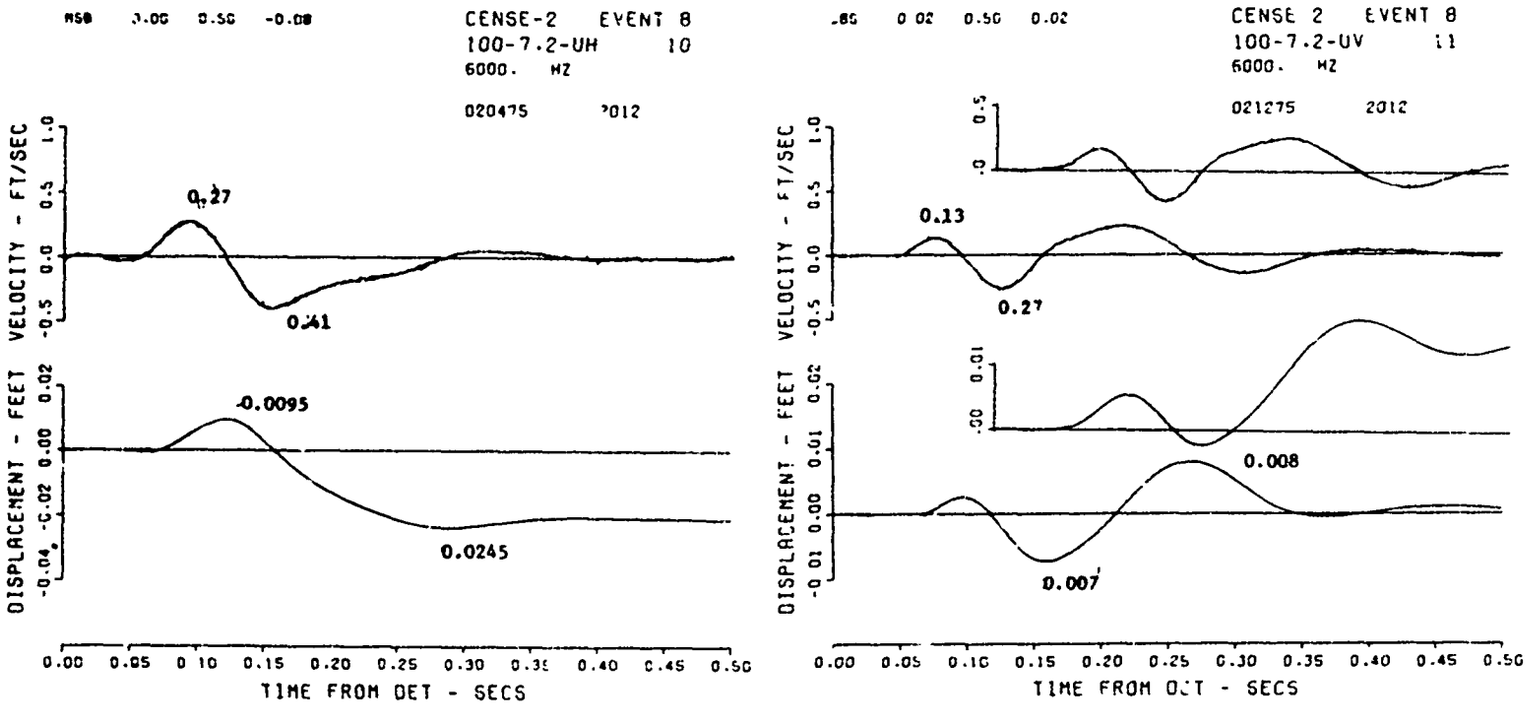

Figure B.22 (sheet 5 of 8).

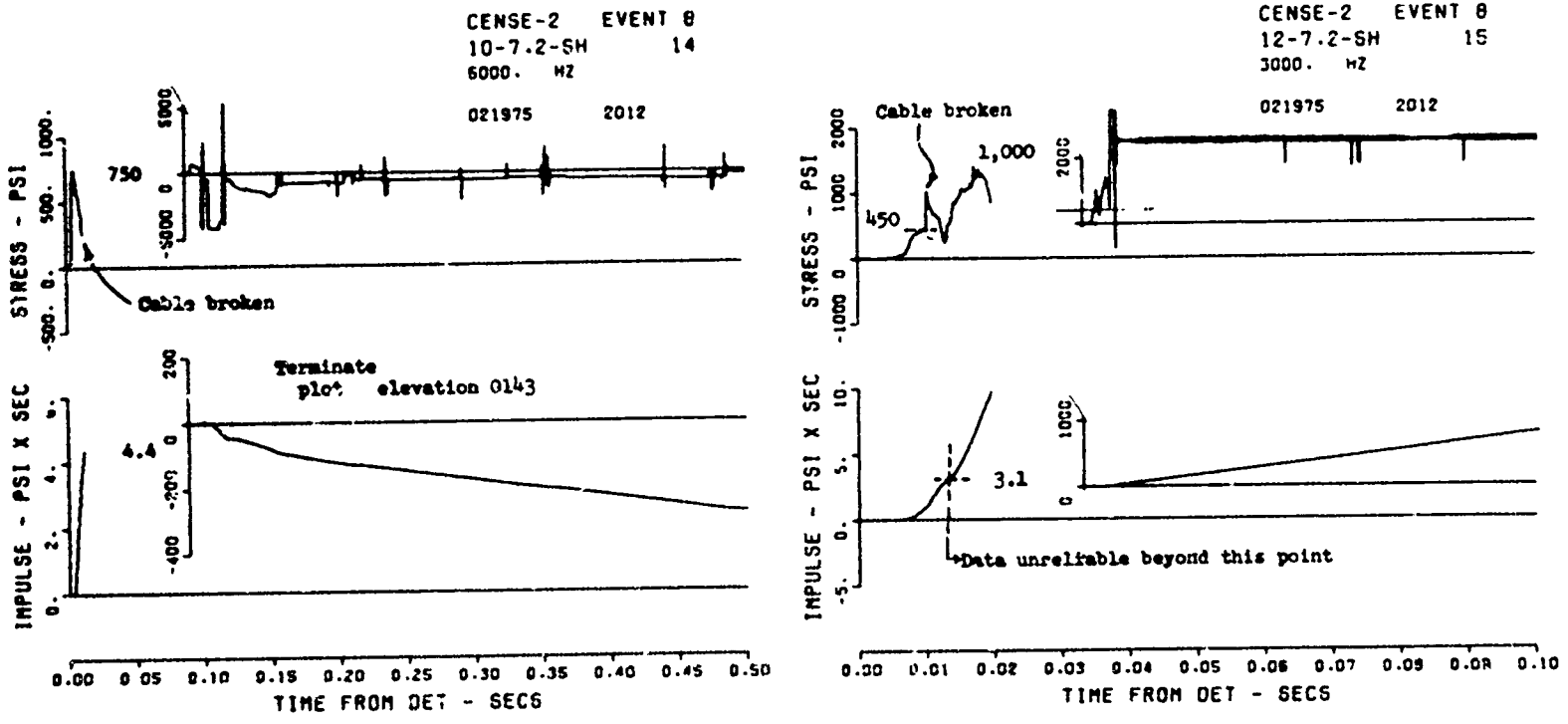

Figure B.22 (sheet 6 of 8).

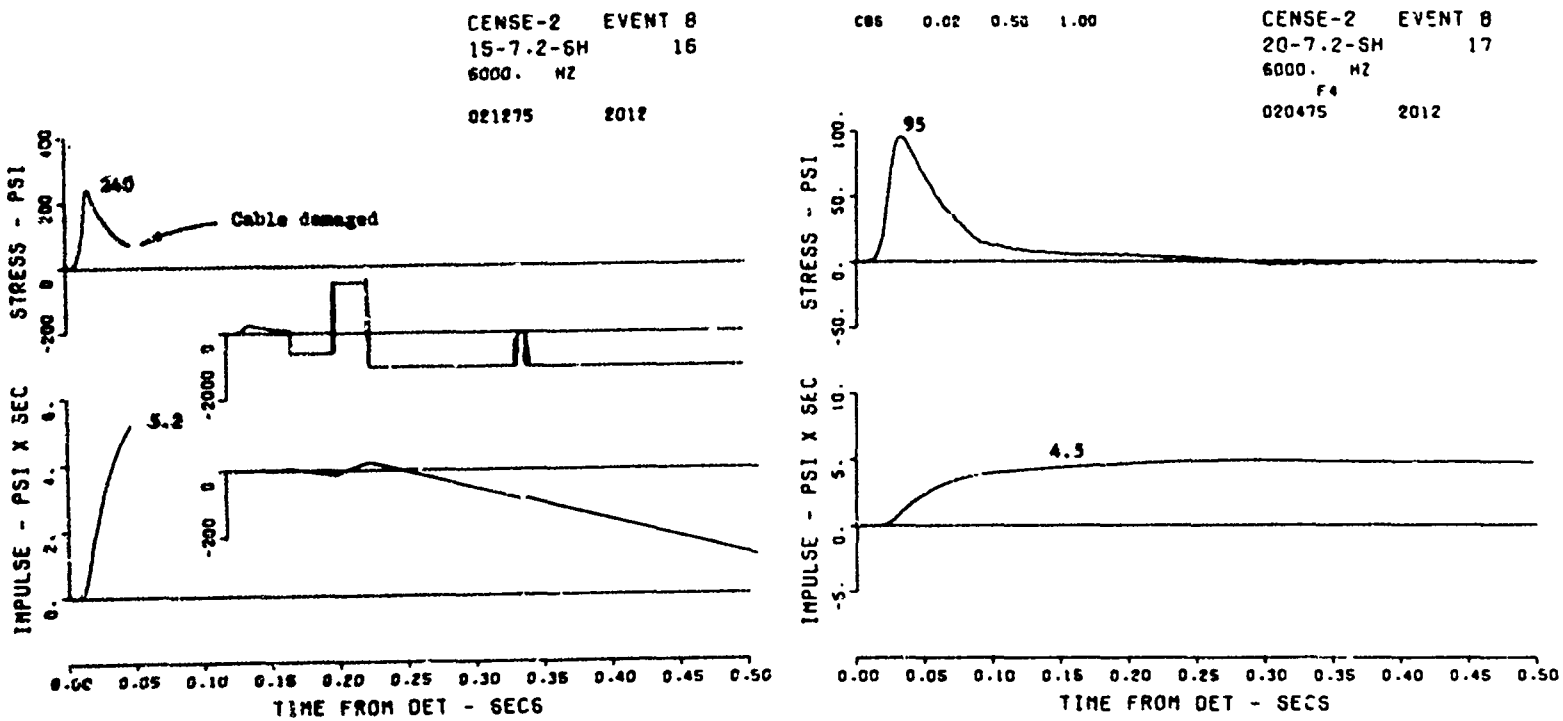

Figure B.22 (sheet 7 of 8).

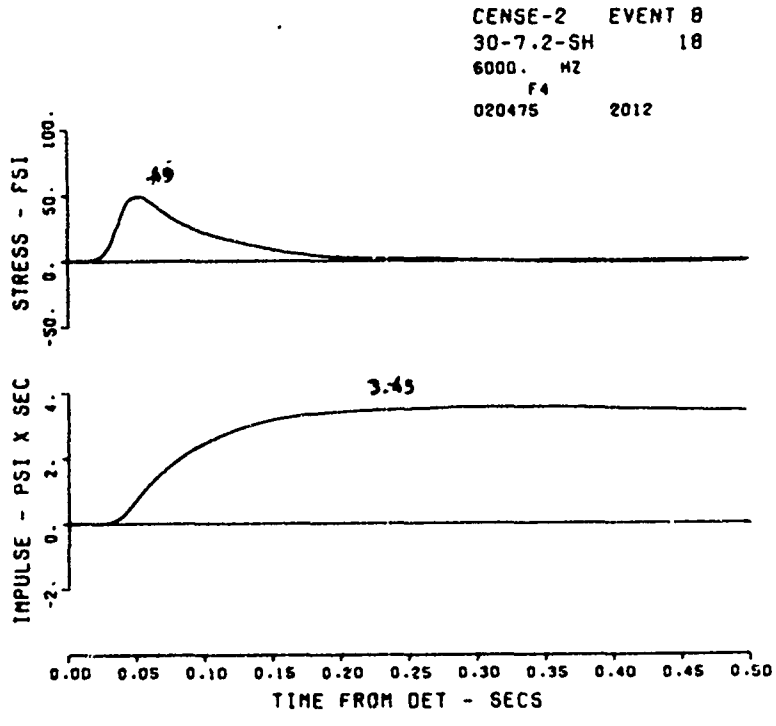

Figure B.22 (sheet 8 of 8).

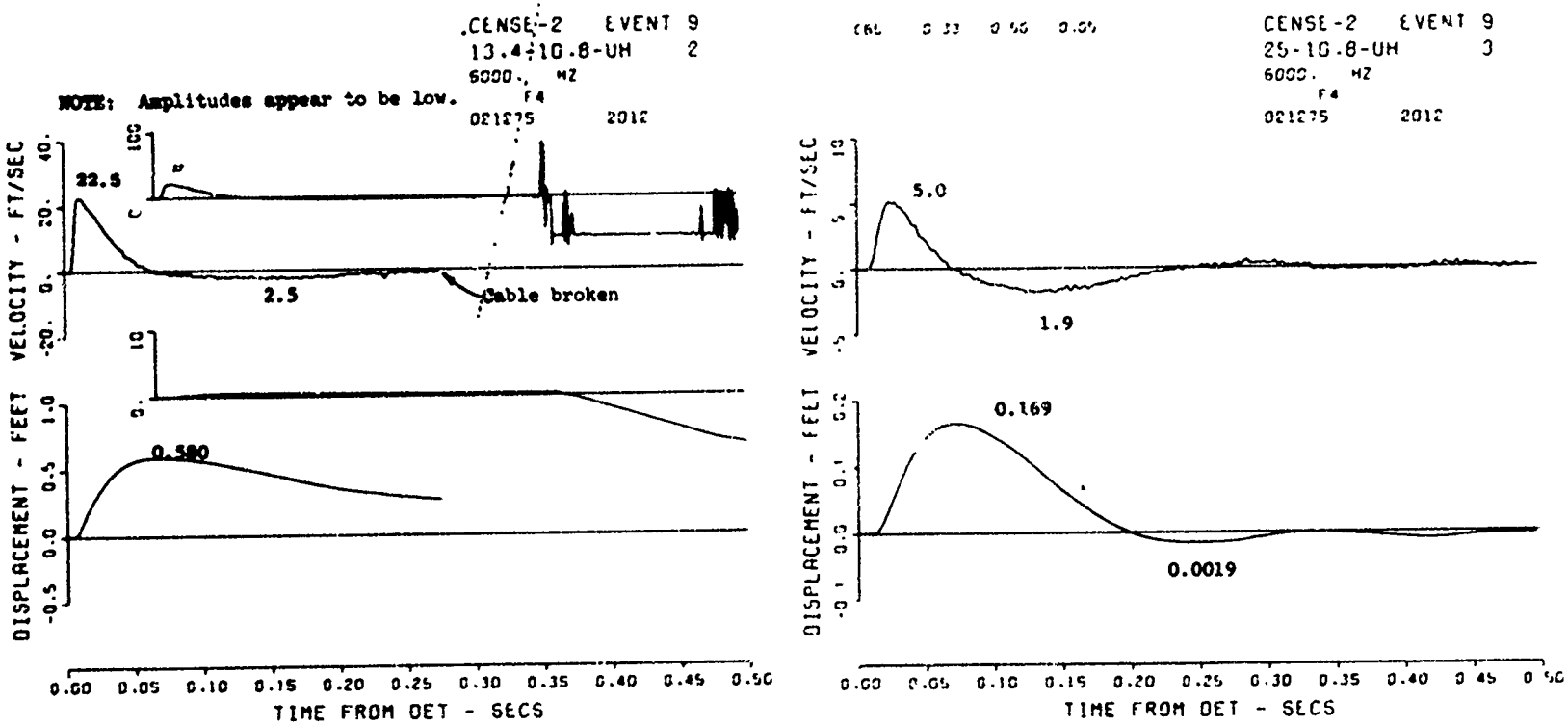

Figure B.23 Event 9, buried, $+1.61\ W^{1/3}$ (+10.8 feet); motion- and stress-time histories along the horizontal radial at charge depth (sheet 1 of 7).

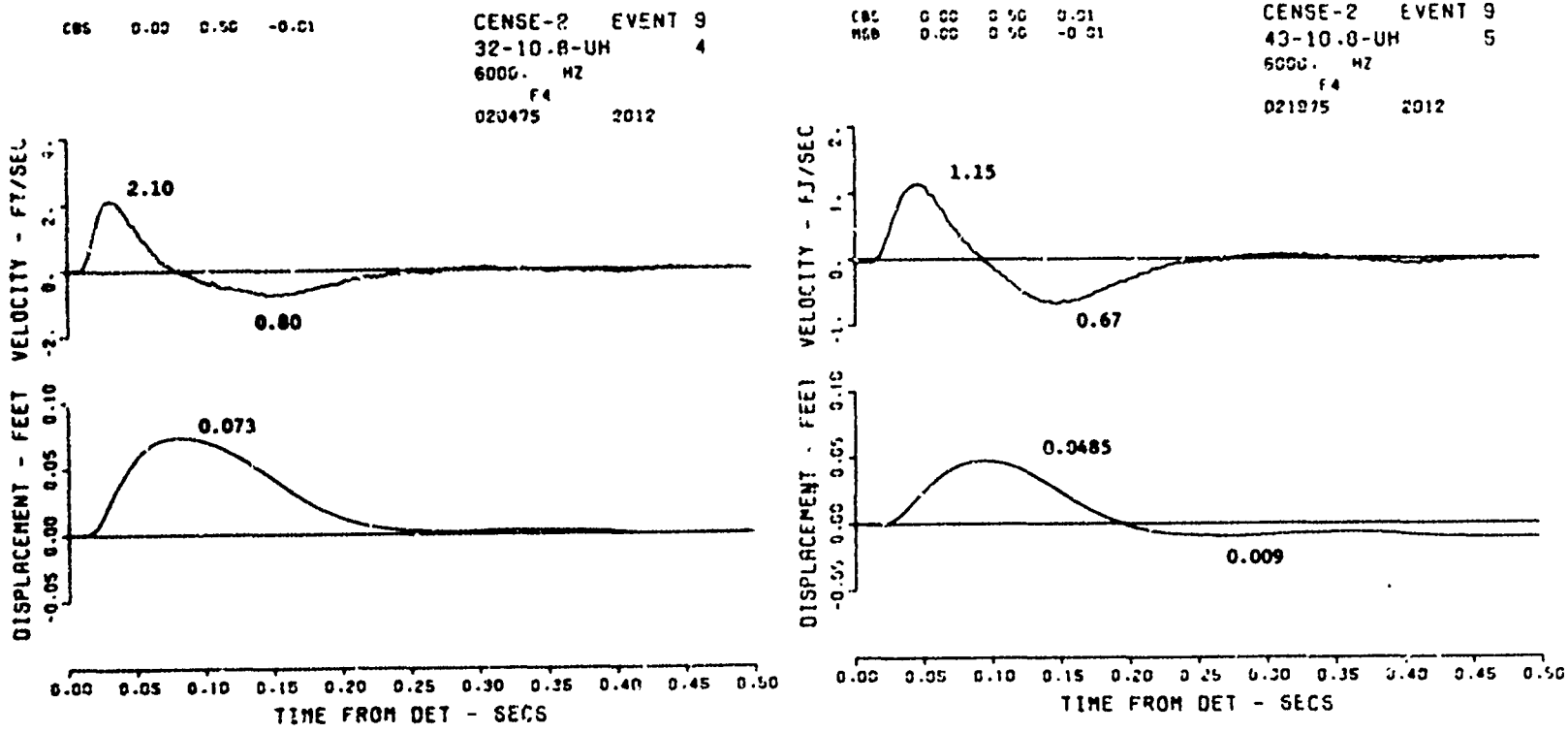

Figure B.23 (sheet 2 of 7).

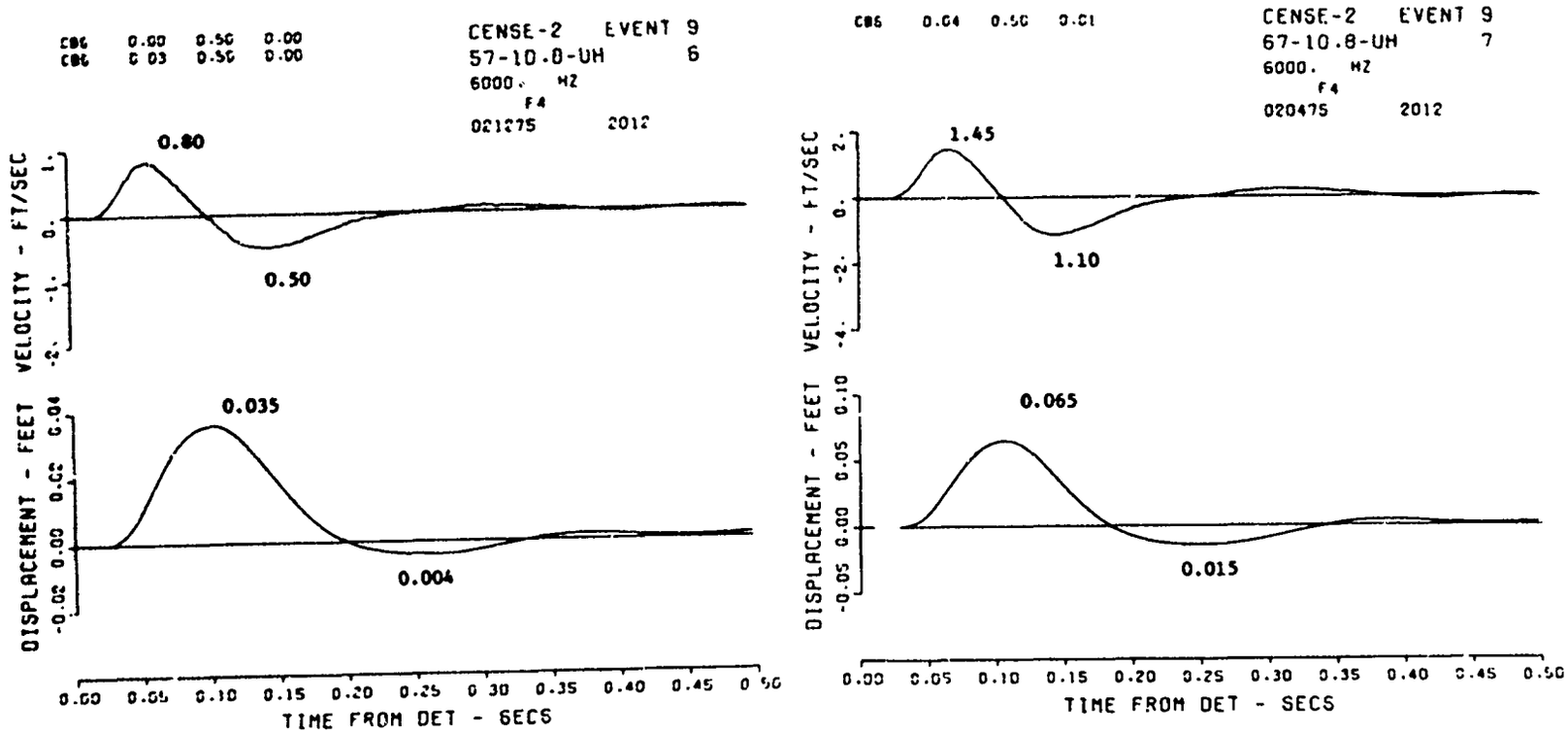

Figure B.23 (sheet 3 of 7).

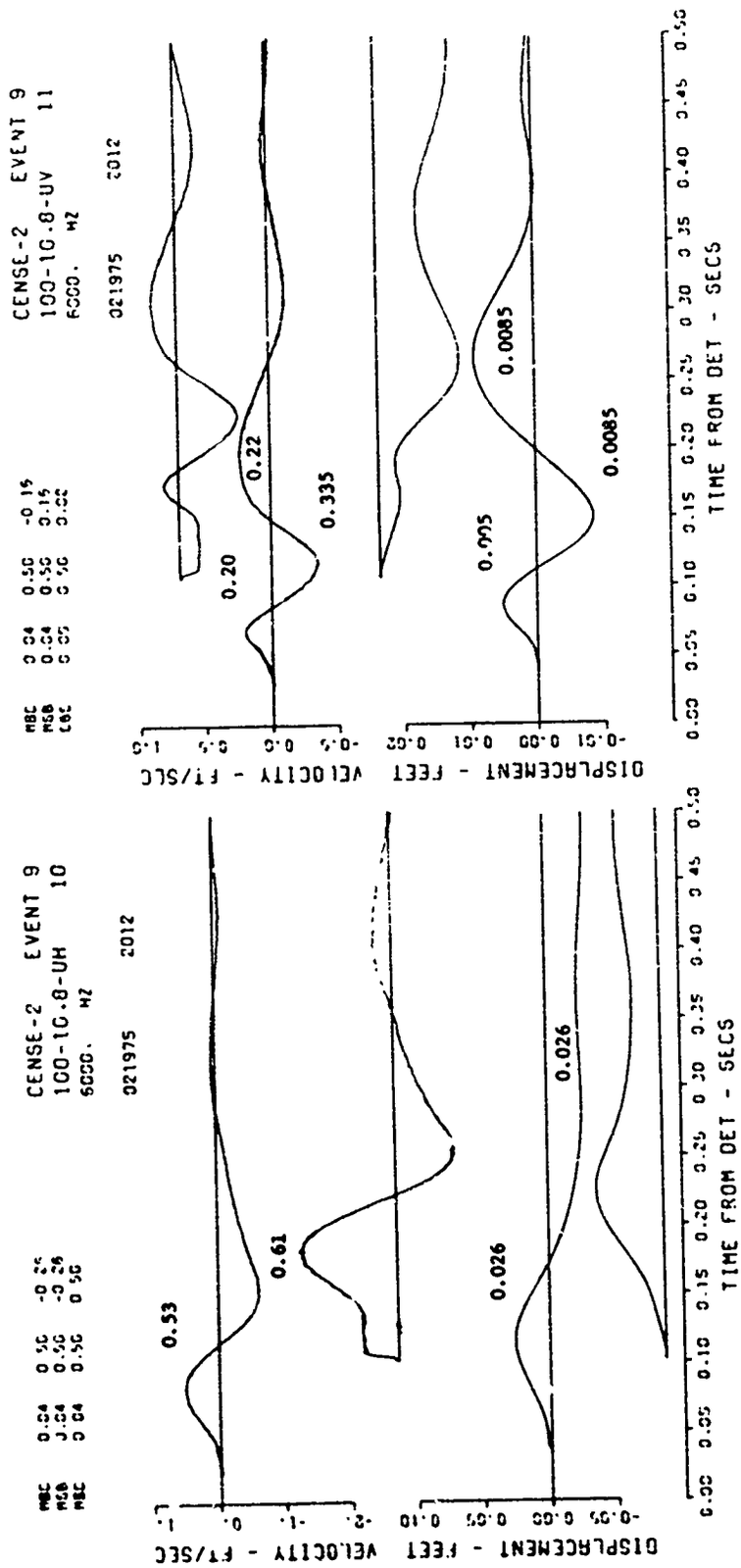

Figure B.23 (sheet 4 of 7).

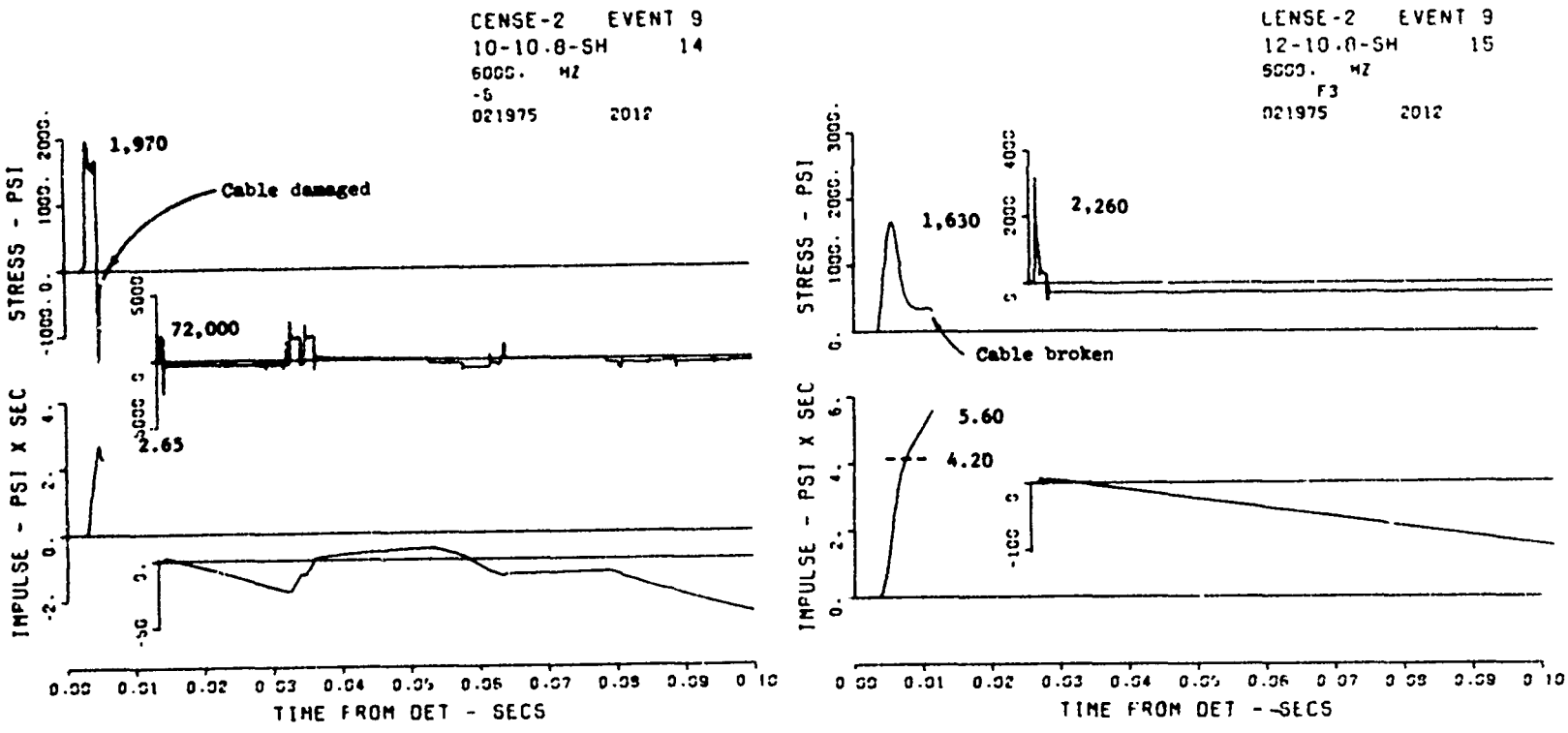

Figure B.23 (sheet 5 of 7).

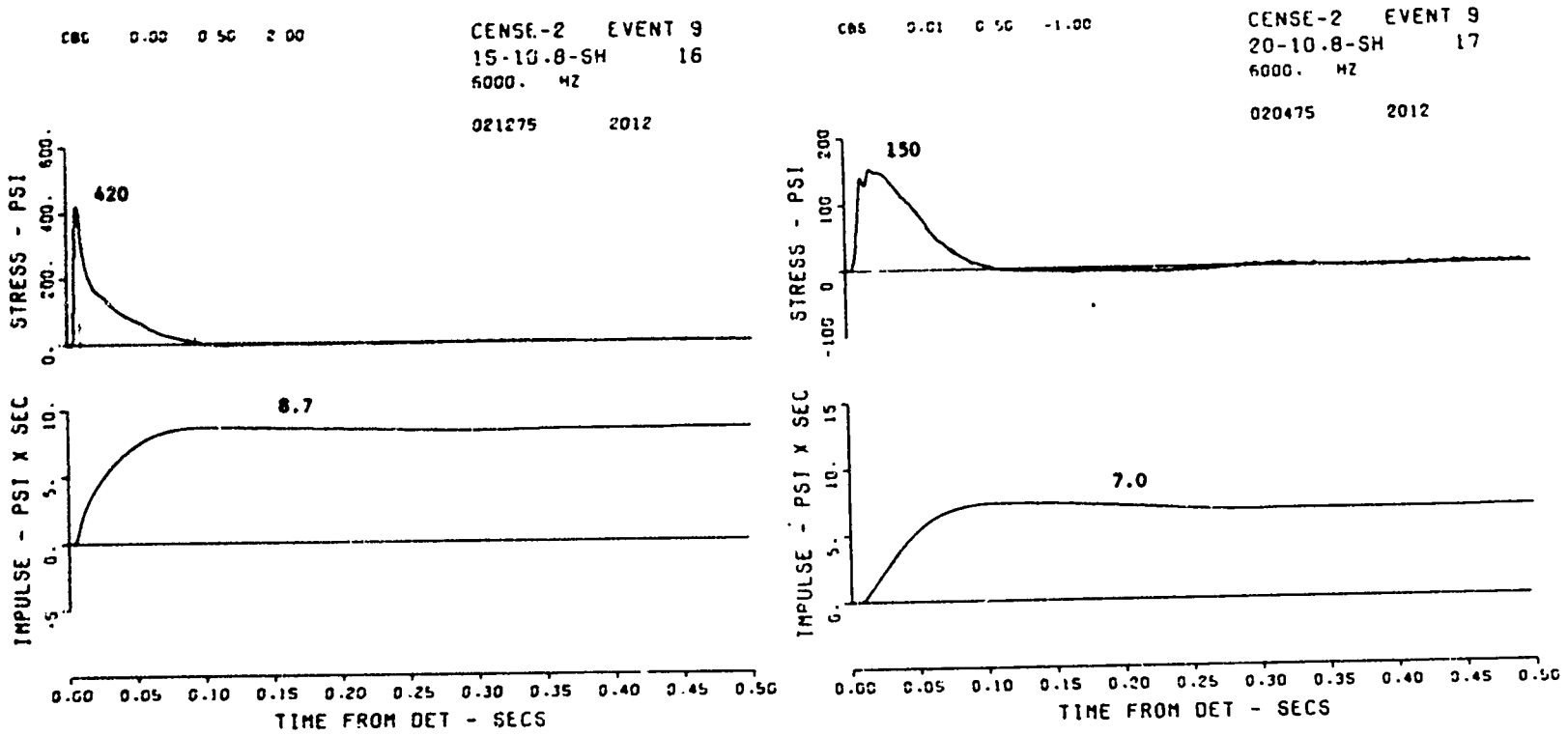

Figure B.23 (sheet 6 of 7).

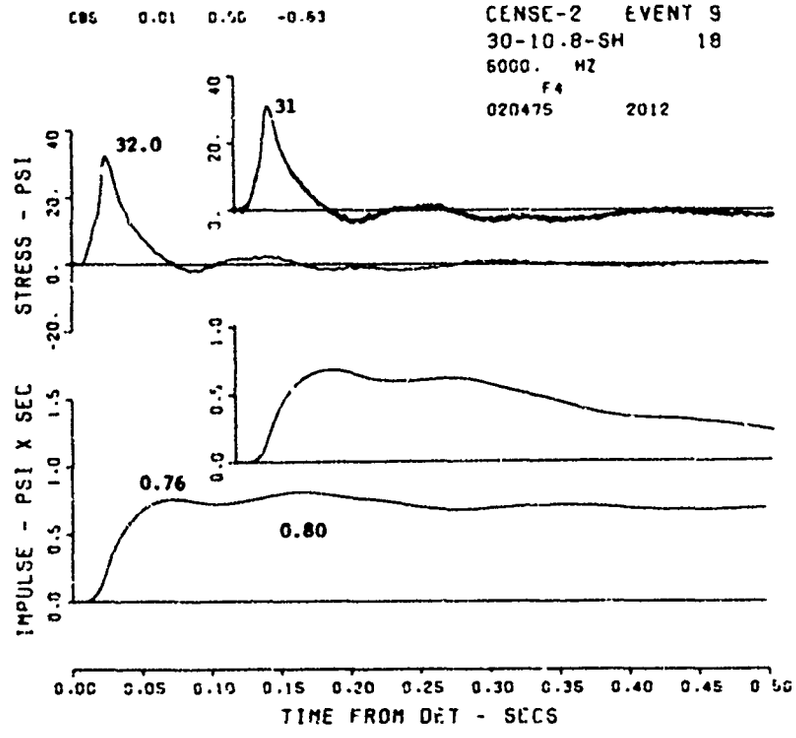

Figure B.23 (sheet 7 of 7).

APPENDIX C

NOTATION

AB	Surface airblast pressure, psi
AV	Vertical acceleration, g's
CG	Center of gravity of explosive charge
C_s	Wave propagation velocity. ft/s
d_a	Apparent crater depth, feet
$d/W^{1/3}$	Scaled distance (cube root scaling), $ft/lb^{1/3}$ Scaled displacement (cube root scaling), $ft/lb^{1/3}$
DOB	Depth of burst beneath ground surface (to center of charge)
g	Acceleration (one gravity unit) = 32.2 ft/s^2
$g \cdot W^{1/3}$	Scaled acceleration (cube root scaling), $g \cdot lb^{1/3}$
GZ	Ground zero
h	Crater lip height, feet
HE	High explosive
HOB	Height of burst above ground surface (to center of charge)
NM	Liquid nitromethane charges
r	Radius, feet
r_a	Apparent crater radius, feet
R	Slope of data with respect to distance
R_c	Charge radius, ft: R_c for 300 lb charge = 0.9 foot R_c for 2 lb charge = 0.158 foot
SH	Horizontal stress, psi
SV	Vertical stress, psi
UH	Horizontal particle velocity, ft/s
UV	Vertical particle velocity, ft/s
va	Apparent crater volume, ft^3
W	Charge weight (TNT equivalent), pound
$W^{1/3}$	Scaled charge weight (cube root scaling), $lb^{1/3}$

In accordance with letter from DAEN-RDC, DAEN-ASI dated 22 July 1977, Subject: Facsimile Catalog Cards for Laboratory Technical Publications, a facsimile catalog card in Library of Congress MARC format is reproduced below.

Ingram, James K
CENSE explosion test program; Report 2: CENSE 2, explosions in soil / by James K. Ingram. Vicksburg, Miss. : U. S. Waterways Experiment Station ; Springfield, Va. : available from National Technical Information Service, 1977.
255 p. : ill. ; 27 cm. (Technical report - U. S. Army Engineer Waterways Experiment Station ; N-77-6, Report 2)
Prepared for Office, Chief of Engineers, U. S. Army, Washington, D. C., under R&D Project 4A762719AT40, Task A1, Work Unit 018, Ground Shock from Multiple Bursts.
References: p. 77-78.

1. Airblast-induced ground motion. 2. Airblast waves. 3. Bursting charges. 4. CENSE (Test program). 5. Cratering. 6. Explosion effects. 7. Explosions. 8. Explosives. 9. Ground shock. 10. Stresses. I. United States. Army. Corps of Engineers. II. Series: United States. Waterways Experiment Station, Vicksburg, Miss. Technical report ; N-77-6, Report 2.
TA7.W34 no.N-77-6 Report 2